CRANFIELD UNIVERSITY

Centre for Photonics and Optical Engineering

School of Mechanical Engineering

PhD Thesis

Academic Year 2001-2002

Roger Michael Groves

Development of Shearography for Surface Strain Measurement of Non-Planar Objects

Supervisor: Professor R. P. Tatam

December 2001

This thesis is submitted in partial fulfillment of the requirements for the degree of Doctor of Philosophy

ABSTRACT

The subject of this thesis is the development of optical instrumentation for surface strain measurement of non-planar objects. The speckle interferometry technique of shearography is used to perform quantitative measurements of surface strain on non-planar objects and to compensate these measurements for the errors that are due to the shape and slope of the object.

Shearography is an optical technique that is usually used for defect location and for qualitative strain characterisation. In this thesis a multi-component shearography system is described that can measure the six components of displacement gradient. From these measurements the surface strain can be fully characterised. For non-planar objects an error is introduced into the displacement gradient measurement due to the variation of the sensitivity vector across the field of view and the variation in the magnitude of applied shear due to the curvature of the object surface. To correct for these errors requires a knowledge of the slope and shape of the object.

Shearography may also be used to measure object slope and shape by a source displacement technique. Therefore slope, shape and surface strain may be measured using the same optical system.

The thesis describes a method of multiplexing the shear direction using polarisation switching, a method of measuring the source position using shadow Moiré and the shearography source displacement technique for measuring the surface slope and shape of objects. The multi-component shearography system is used to perform measurements of the six components of surface strain, on an industrial component, with a correction applied for errors due to the shape and slope of the object.

We shall not cease from exploration

And the end of all our exploring

Will be to arrive where we started

And know the place for the first time.

Eliot T S, Four Quartets, Little Gidding, pt. 5, 1942

ACKNOWLEDGEMENTS

I would like to thank Professor Ralph P. Tatam for his supervision and guidance throughout the PhD project. I would also like to thank Dr Stephen W. James for his assistance.

Of my fellow PhD students I would like to thank Dr Itziar Balboa for many discussions of the phenomena of speckle and Gerald D. Byrne for technical assistance on aspects of optics and support through the difficulties encountered during the PhD process.

I would also like to thank Chun Yue Chan for reminding me of the importance of life outside my PhD studies.

LIST OF CONTENTS

LIST OF FIGURES

LIST OF TABLES

NOTATION

a	Diameter of the viewing aperture, arbitrary length
C	Constant
$C(x,y)$	zero slope constant at point (x,y) in the field of view
d	Displacement between the grating and the shadow
d_{osx}	Average objective speckle size in the x direction
d_{osy}	Average objective speckle size in the y direction
d_{ss}	Diameter of subjective speckle
$\boldsymbol{ds}$	Applied Shear with components $[dx, dy, dz]$
dx	Magnitude of applied shear in the x direction
dc_C	Corrected applied shear
dx_M	Measured applied shear
dy	Magnitude of applied shear in the y direction
dz	Magnitude of applied shear in the z direction
D	First minima of the diffraction pattern, distance from the optical source to the object
$\boldsymbol{DD}$	Source displacement with components $[DX, DY, DZ]$
D_i	Internal diameter of a cylinder
D_o	External diameter of a cylinder
DU	Source displacement in the u direction
DV	Source displacement in the v direction
DW	Source displacement in the w direction
DX	Source displacement in the x direction
DY	Source displacement in the y direction

DZ	Source displacement in the z direction
E	Young's Modulus
F_j	Camera frame j
g_F	Gauge factor
G	Geometric factor
G_F	Gain Factor
h	Plate thickness
$\boldsymbol{H}$	The position of the principal plane of the imaging system
i	$i = 1, 2, 3 \ldots$
$I_{CORRECTED}$	Corrected intensity
$I_{MOIRÉFRINGE}$	Intensity of frame containing Moiré fringes
$I_{REFERENCE}$	Intensity of reference frame
I_j	Intensity of frame j
I_0	Average Intensity
j	$j = A, B, C \ldots$
k	Constant
k_{xi}, k_{yi}, k_{zi}	Sensitivity vectors for x, y and z components respectively for channel i
K	Slope sensitivity constant
L	Length
L_B	Beat length of highly-birefringent optical fibre
m	Integer
M	Transformation matrix
M_V, M_H	Wrapped phase maps
n_1, n_2	Refractive indices

N	Fringe order
N_b	Refractive index of the block
p	Pitch of grating
p_l	Pitch of linear grating
p_c	Pitch of circular grating
P	Optical power
P_i	Internal pressure
P_o	External pressure
$\boldsymbol{P_i}$	Point (i) on the object surface
Px_i, Py_i, Pz_i	x, y and z components of the point of the object surface i
r_1, r_2	Angles of refraction
$Q(\boldsymbol{r})$	Point within objective speckle pattern
S	Strain tensor, Strain
$\boldsymbol{S_i}$	Source position i
Sx_i, Sy_i, Sz_i	x, y and z components of the source position i
t	thickness
u	Displacement in the x direction, distance in the w direction
$u(x,y)$	Complex amplitude of light incident at (x,y)
$U(\boldsymbol{r})$	Amplitude of light at point $Q(\boldsymbol{r})$
v	Lens to image plane distance, displacement in the y direction, distance in the v direction
V	Voltage
V_0	Initial Voltage
V_B	Bridge voltage

w	Displacement in the z direction, distance in the w direction
W	Source to object distance in the w direction
x	Distance between the object and viewing planes, distance in the x direction
y	Distance in the y direction
z	Distance in the z direction
α	Angle of beam expansion
γ	Visibility
γ_{xy}	Flexural strain component
$\delta u/\delta x$	In-plane displacement gradient component
$\delta v/\delta x$	In-plane displacement gradient component
$\delta w/\delta x$	Out-of-plane displacement gradient component
$\delta u/\delta y$	In-plane displacement gradient component
$\delta v/\delta y$	In-plane displacement gradient component
$\delta w/\delta y$	Out-of-plane displacement gradient component
$\delta^2 w/\delta x^2$	Second derivative of displacement component
$\delta^2 w/\delta y^2$	Second derivative of displacement component
$\delta^2 w/\delta x dy$	Second derivative of displacement component
Δ_C	Pitch of carrier fringes
Δd	Physical pathlength imbalance
ΔD	Optical pathlength imbalance
ΔL	Distance between grating and shadow
Δn	Difference in effective refractive index

Δ_{SL}	Phase of slope fringes
Δx	x displacement when the viewing direction is changed
Δy	y displacement when the viewing direction is changed
Δz	Change in surface height
$\Delta\theta$	Change in polarisation phase
$\Delta\lambda$	Change in optical wavelength
$\Delta\phi$	Change in optical phase
ε	Angle of rotation
ε_A	Axial strain
ε_{AR}, ε_{AS}, ε_{AT}	Axial strain determined by resistance gauges, shearography and theoretical calculation respectively
ε_H	Hoop Strain
ε_{HR}, ε_{HS}, ε_{HT}	Hoop strain determined by resistance gauges, shearography and theoretical calculation respectively
ε_N	Angle of radial fringes of order N
ε_R	Radial Strain
ε_{xx}	Flexural strain component
ε_{yy}	Flexural strain component
θ	Angle of rotation, angle of illumination, optical phase
θ_0	Initial phase
θ_A	Azmuithal angle
θ_E	Elevation angle
θ_i	Angle of illumination from direction i

θ_I	Angle of illumination
θ_N	Angle of fringe of order N
θ_r	Angle of rotation of object
θ_V	Angle of viewing
κ	Conditioning number of a matrix
λ	Optical wavelength
λ_1, λ_2	Optical wavelengths
Λ_{REF}	Optical pathlength difference in reference frame
Λ_i	Optical pathlength difference in frame i
Λ_Δ	Optical pathlength difference between frames
μ_F	Microstrain factor
ν	Poisson's ratio
ξ	Surface height
σ_A	Axial stress
σ_H	Hoop stress
σ_R	Radial stress
ϕ	Optical phase
ϕ_C	Phase of carrier fringes
ϕ_{dq}	Phase of correlation fringes
ϕ_{dqi}	Phase of correlation fringes for channel i
ϕ_{dqdxi}	Phase of displacement gradient sensitive correlation fringes, with shear applied in the x direction, for channel i
ϕ_E	Phase extended to a $-\pi$ to $+\pi$ radian range

ϕ_i	Phase of pixel in camera frame *i*
ϕ_{noise}	Speckle phase noise
ϕ_S	Phase of slope fringes
ϕ_{SH}	Phase of correlation fringes sensitive to shape
ω_x, ω_y	Beam half-width in the *x* and *y* directions respectively

Examples of compound notation

SPH	Pathlength ***S*** to ***H*** via ***P***
SRH	Optical path of reference beam between ***S*** and ***H***

1. INTRODUCTION

1.1. Optical Metrology

Light is an established tool for performing measurements. In general an optical system will consist of light emitted from a source interacting with the object under investigation, possibly with some form of optical processing, and then passing to a detector, the output of which can be processed to yield the measurand. In this thesis the interference of light (Young 1804) is used to perform the measurements using the technique of speckle pattern interferometry (Leendertz 1970). Speckle pattern interferometry is a technique that allows simultaneous measurement across an area of an object, rather than a point measurement, by correlation of interferometric speckle patterns.

1.2. Strain and Shape Measurement

Industrial components and materials increasingly require a more detailed characterisation of their behaviour under different loading circumstances for condition monitoring, reliability assessment, quality assurance and product optimisation. This is usually accomplished by measuring using strain gauges. These gauges are glued to the object surface and perform point measurements of in-plane strain. To fully characterise the surface strain requires the measurement of six displacement gradient components, four in-plane and two out-of-plane components. For non-planar objects the slope and shape of the object are needed to map the measured strain onto the object surface.

A number of optical techniques have been used for full-field surface strain measurement. A full-field measurement is a simultaneous measurement across the surface of the object. The principal techniques that are used are Moiré interferometry (McDonach *et al* 1980), photoelasticity (Frocht 1961), holography (Ennos 1968) and the speckle techniques of speckle pattern interferometry (Leendertz 1970), ESPI (Butters and Leendertz 1971) and shearography (Butters and Leendertz 1973). Moiré interferometry requires the fixing of a grating to the object surface and photoelasticity requires a surface coating with a birefringent material. Holography is experimentally intense and speckle pattern interferometry has been replaced by the ESPI and shearography techniques that use better camera technology. ESPI is sensitive to displacement and to perform strain measurement requires a numerical differentiation. The speckle technique of shearography is a non-contact method sensitive to displacement gradient, a parameter that is closely related to surface strain. It is an interferometic technique offering high sensitivity measurement and may be configured to measure to the in-plane and out-of-plane displacement gradient components.

Shape measurement requires the measurement of the relative location of points on the object surface in three-dimensional space. In this thesis, in order to simplify the instrumentation required, the shearography technique is used to perform *both* the strain measurement and the slope and shape measurement.

1.3. Speckle Interferometry

Speckle interferometry is a technique that can measure optical pathlength differences of the order of the optical wavelength, or below, in full-field across the surface of the object under investigation. The full-field aspect of the measurement is due to the recording of the intensity of the interferometric speckle pattern across the field of view of the camera. A speckle pattern is a distribution of intensities formed by the interference of coherent light scattered from different points on an optically rough surface. In speckle pattern interferometry the speckle pattern formed in this way is optically mixed with a reference beam, or reference speckle pattern, originating from the same optical source, to form an interferometric speckle pattern that is recorded by a camera. In the interferometric speckle pattern the intensity of the light contains information on the optical phase and hence on the optical pathlength difference between the two paths through the interferometer. Recording interferometric speckle patterns obtained before and after applying a perturbation to the system and then correlating the interferometric speckle patterns, commonly by subtraction, yields correlation fringes that can be processed to recover the measurand.

The principal speckle interferometry techniques are electronic speckle pattern interferometry (ESPI) and shearography. ESPI utilising a smooth reference beam is a technique sensitive to displacement (Butters and Leendertz 1971) or surface shape (Denby *et al* 1976) depending on the optical configuration used. Shearography is a complimentary technique to ESPI, utilising a close to common path speckle reference formed using a shearing interferometer, and is an optical configuration that is sensitive

to displacement gradient (Butters and Leendertz 1973) or surface slope (Hung *et al* 1978). The sensitivity to displacement gradient, a parameter closely related to surface strain, and a reduced sensitivity to rigid body motion (Butters and Leendertz 1973) are advantages of shearography for surface strain measurement. In comparison with shearography though ESPI, with a smooth (unspeckled) reference beam, has better fringe quality (Jones and Wykes 1981). Both ESPI and shearography have variable sensitivity vectors depending on the illumination and imaging directions. The design of these systems can therefore yield three-dimensional components by measuring three, or more, components and performing a coordinate transformation. Currently *quantitative* measurements may be performed using ESPI (Ettemeyer 2000) and *qualitative* measurements using shearography.

An example of the formation of correlation fringes using shearography is shown in Figure 1.1. To illustrate the sensitivity of shearography to displacement gradient, Figure 1.2 shows shearography and ESPI correlation fringes for an out-of-plane deformation and the corresponding graphs showing the displacement gradient and displacement respectively.

1.4. Shearography

Shearography is the principal technique investigated in this thesis as it can produce correlation fringes that are sensitive to displacement gradient, a parameter that is closely related to the surface strain, and can measure three-dimensional components. The transformation to surface strain is simpler from displacement gradient than it would be

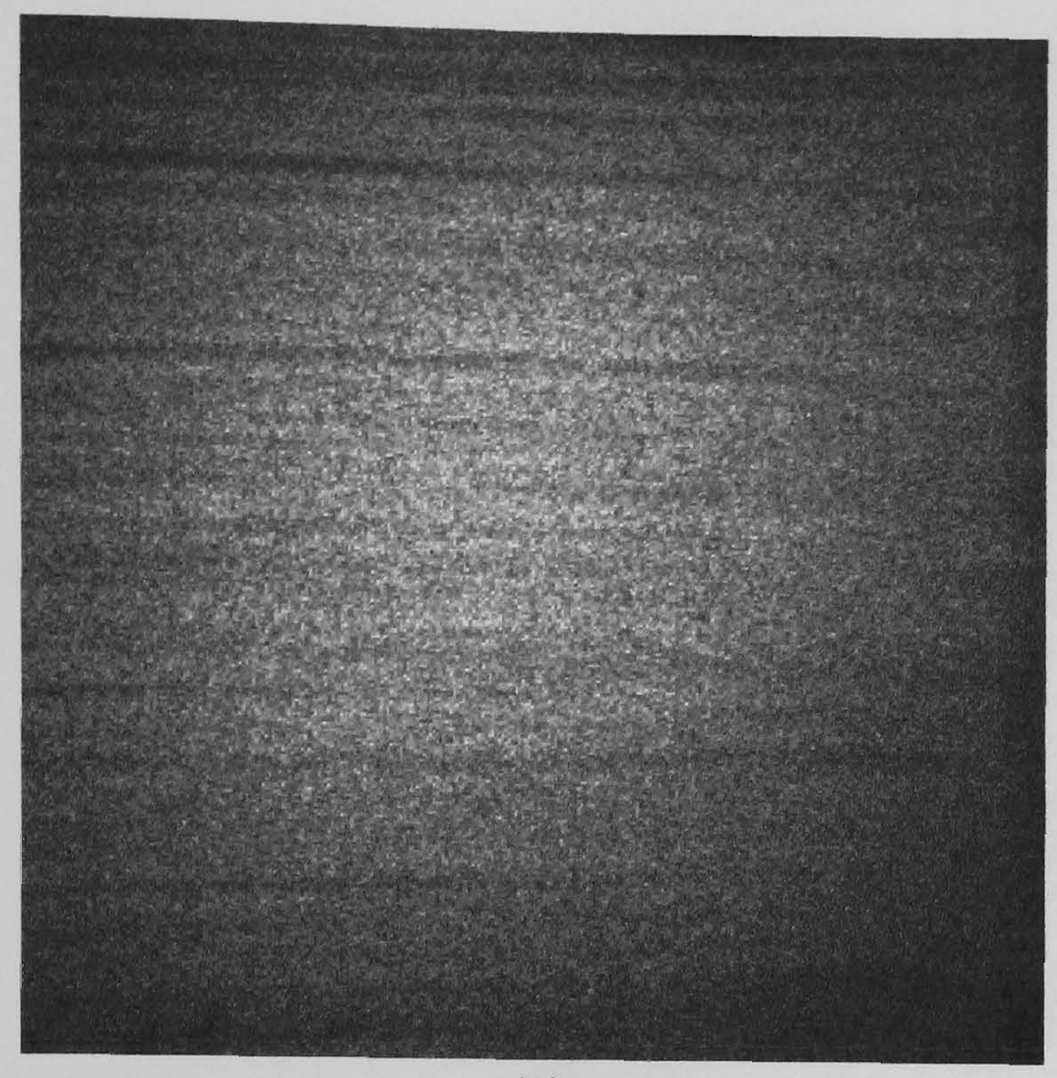

(a)

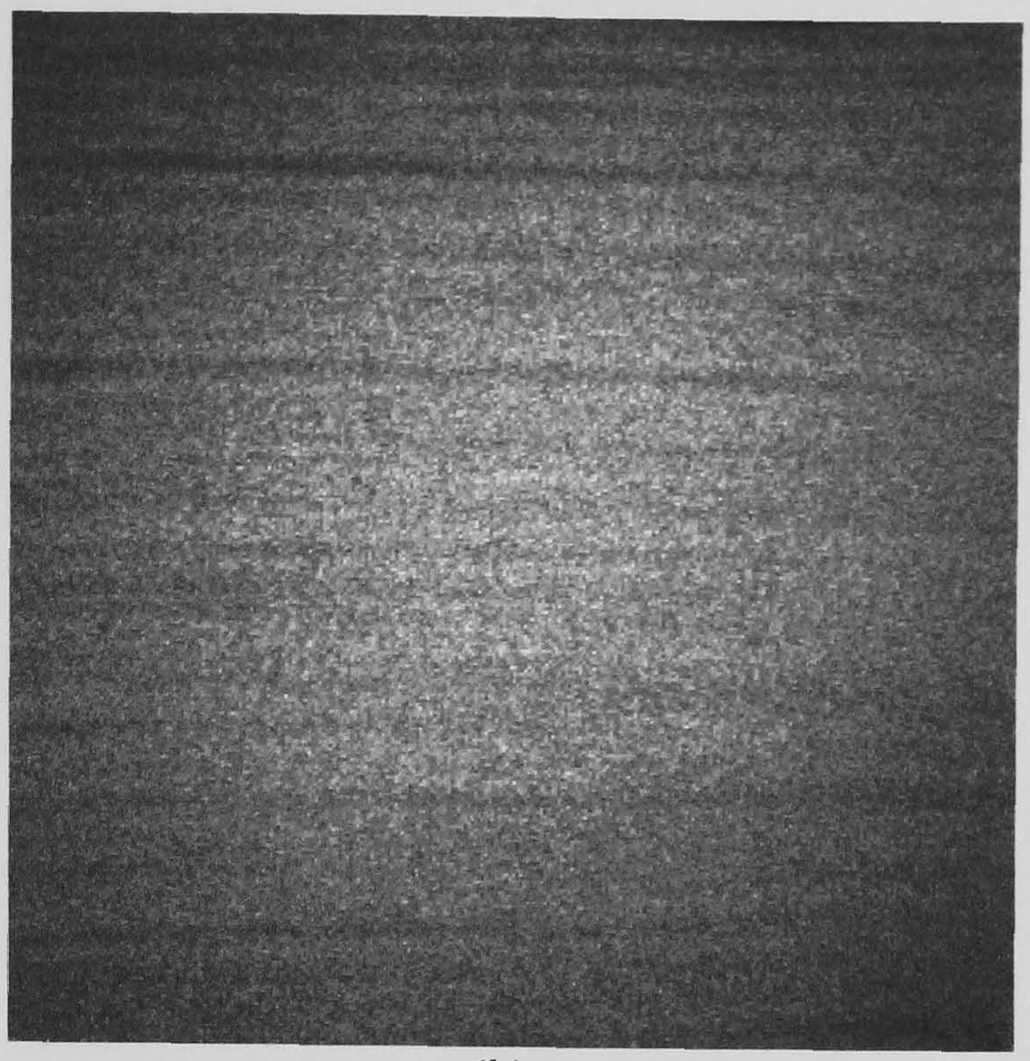

(b)

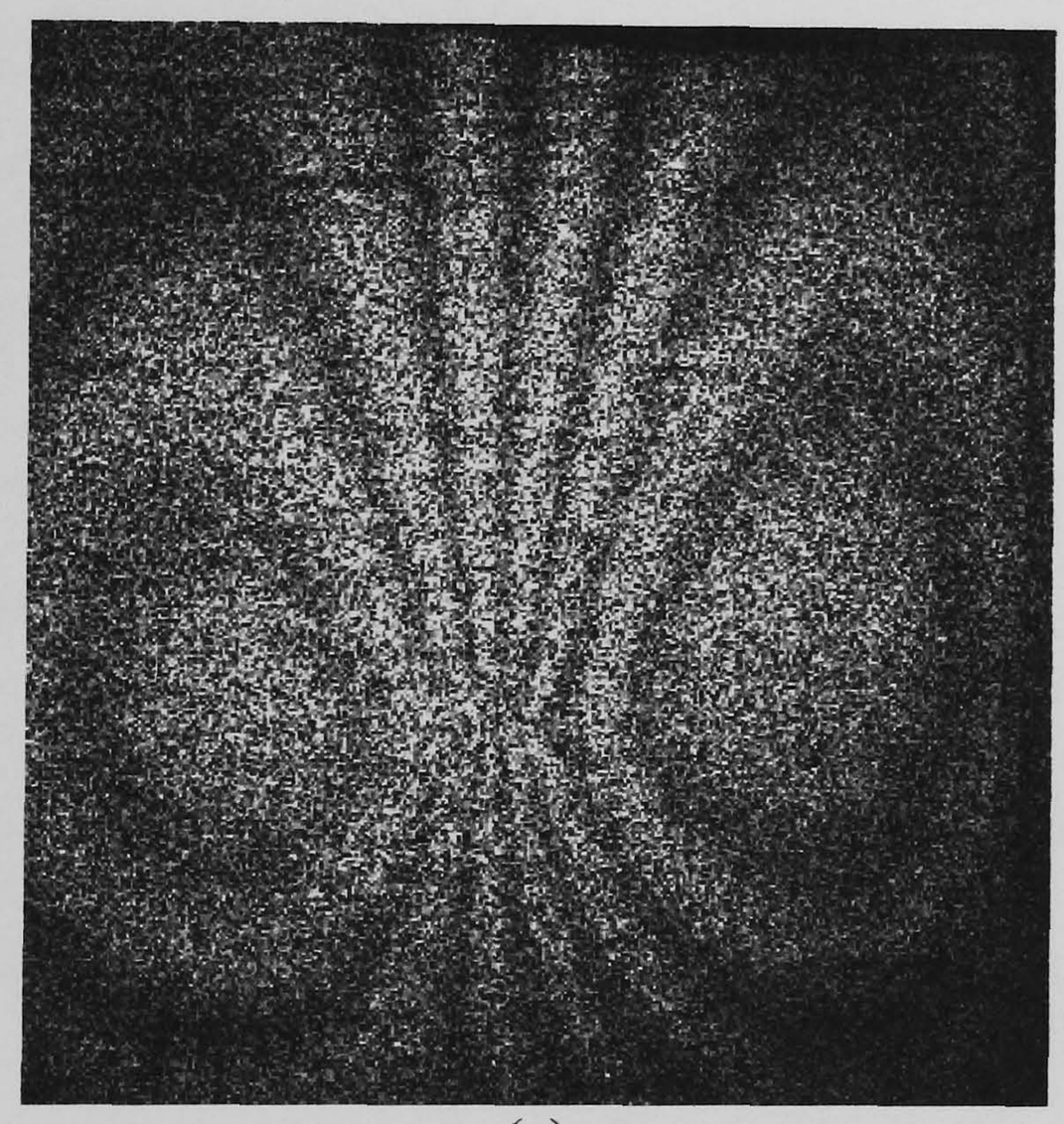

(c)

Figure 1.1 shows interferometric speckle patterns obtained (a) before object deformation and (b) after object deformation from a shearography system. In (c) is the displacement gradient correlation fringes obtained from subtracting image (a) from image (b). The correlation fringes are sensitive to out-of-plane displacement gradient.

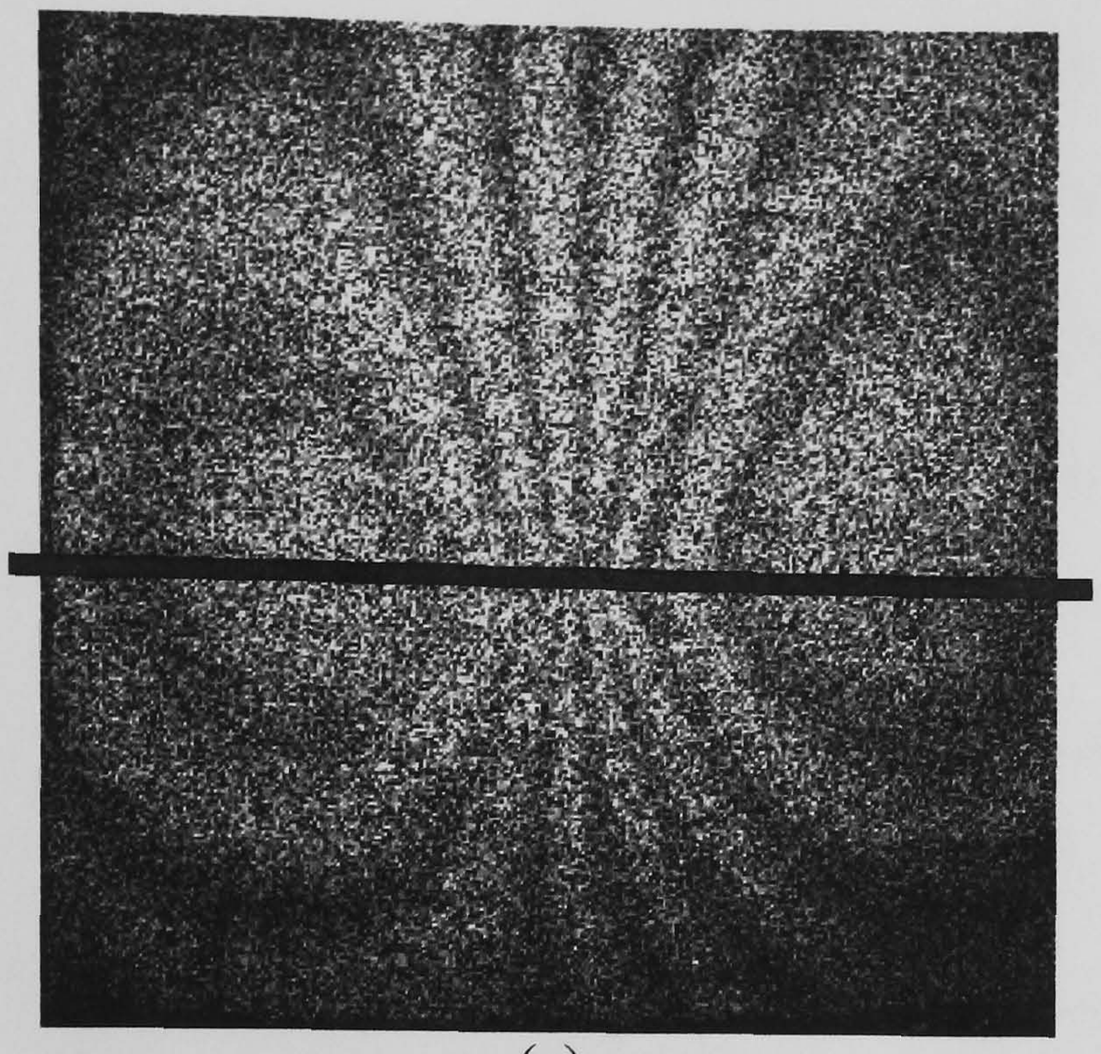

(a)

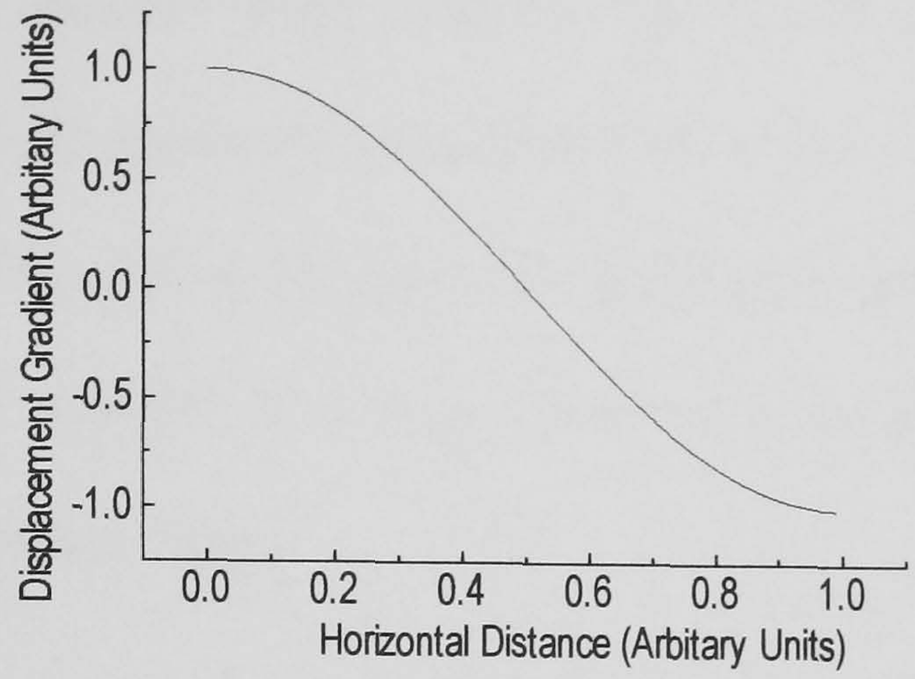

(b)

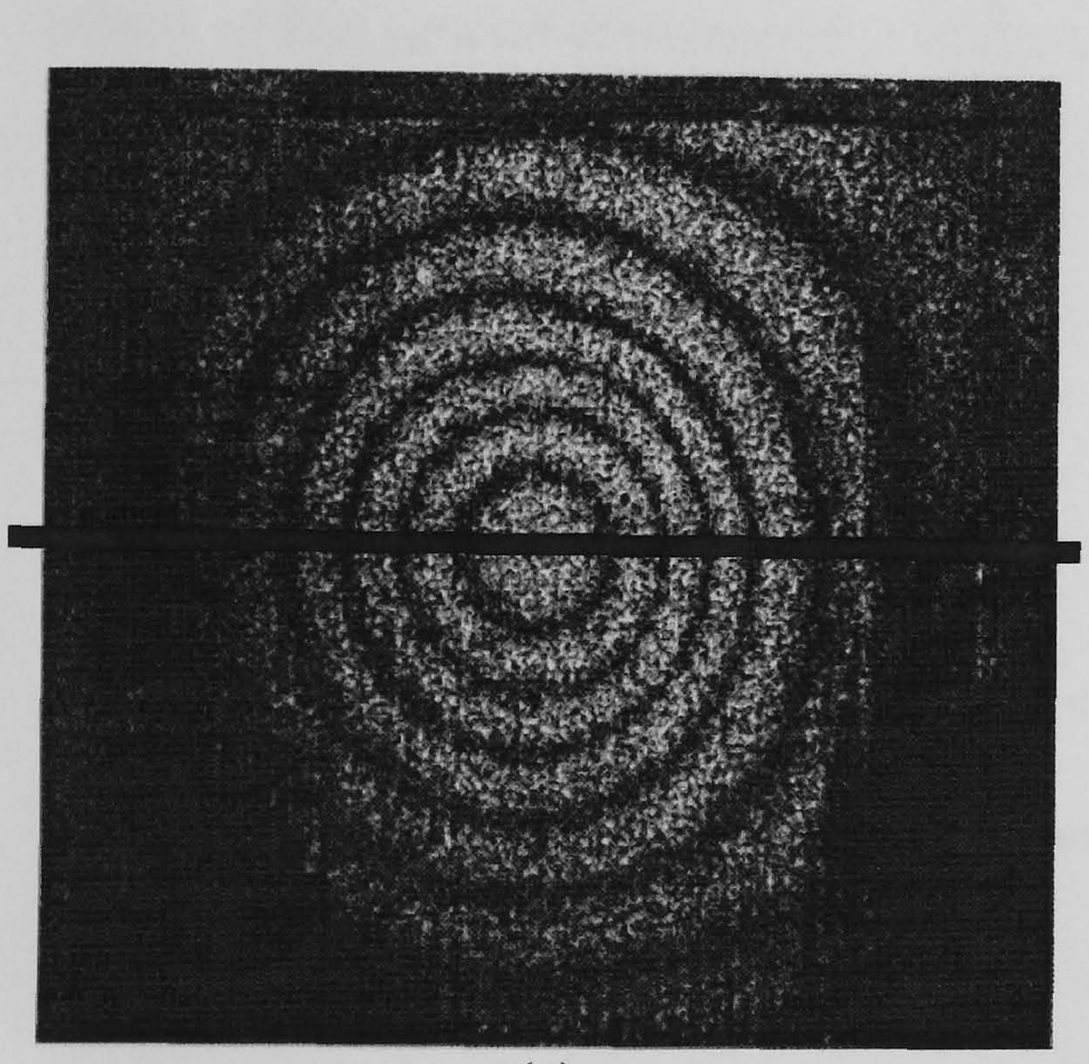

(c)

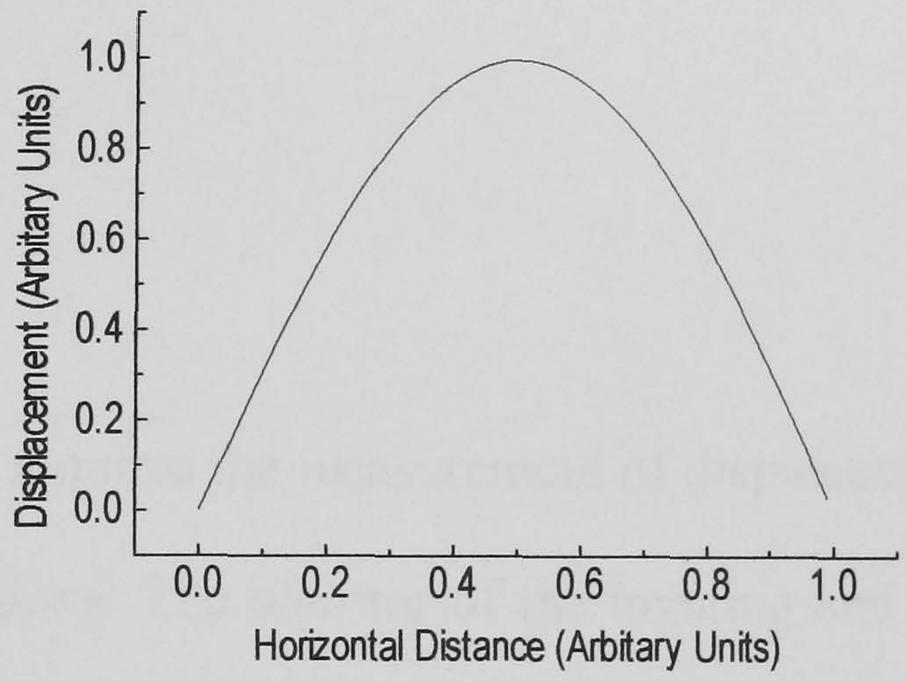

(d)

Figure 1.2 shows (a) shearography correlation fringes with shear applied in the horizontal direction, (b) displacement gradient along a line horizontally through image (a), (c) ESPI correlation fringes and (d) displacement along a line horizontally through image (d). (a) is an optical differentiation of (c). In both the shearography and ESPI images a flat plate test object is subjected to a point deformation, normal to the object surface and approximately in the centre of the field of view.

from displacement, as measured by ESPI, resulting in less error in the final measured surface strain. There is also a requirement to measure shape, and the related parameter surface slope, by the need to correct errors in the displacement gradient when the object is non-planar or tilted. To simplify the instrumentation the same shearography system was used to generate displacement gradient sensitive *and* slope sensitive correlation fringes. Slope can be integrated to yield the surface shape.

The issues in fully characterising the surface strain using shearography are summarised briefly in this section and expanded in detail in individual chapters in the thesis. Figure 1.3 shows a flow chart of the process of fully characterising the surface strain using shearography.

1.5. Multi-Component Shearography

To measure the six surface strain components requires the measurement of displacement gradient using six different optical configurations. The bisector of the imaging and the illumination directions is the sensitivity direction of the shearography system. To measure in three-dimensions a minimum of three sensitivity directions, and therefore three illumination, or imaging, directions are required. To fully characterise the surface strain, measurements of displacement gradient using two applied shear directions, usually orthogonal, are required.

An implementation of three-dimensional shearography is contained in Chapter 7, along with a discussion of the major issues.

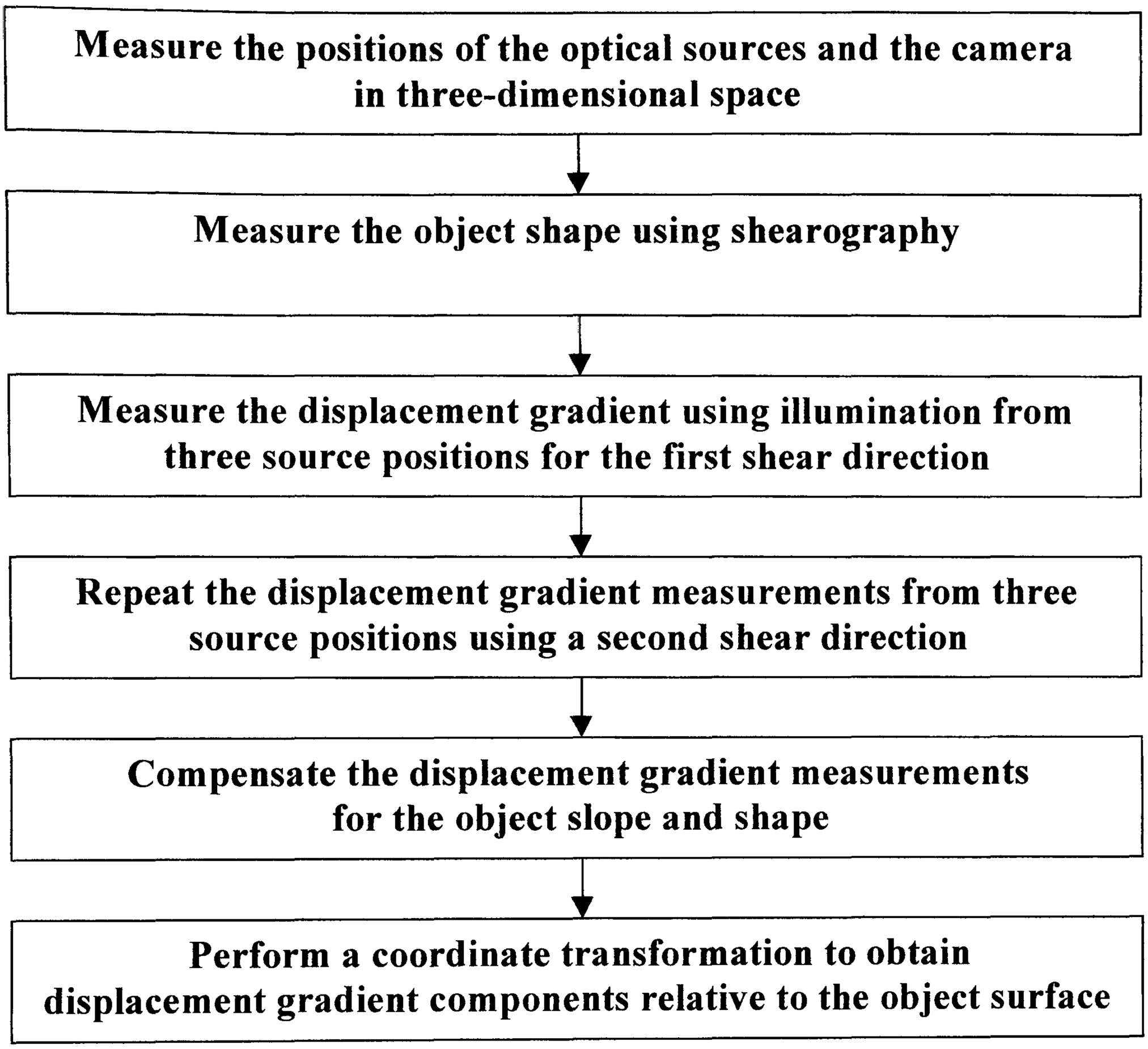

Figure 1.3 Flow chart of the process for full surface strain characterisation of non-planar objects using multi-component shearography

1.6. Shear Direction Multiplexing

The first issue in multi-component shearography to be discussed in detail is shear direction multiplexing in Chapter 4. The reasons for multiplexing the shear direction are expanded, along with a summary of the different possible methods. A new method of implementation of one of the possible shear multiplexing methods, polarisation multiplexing by wavelength tuning, is described in detail and experimental results are presented. The method implemented utilises laser diode wavelength tuning and highly linearly birefringent optical fibre to sequentially illuminate the object with s- and p-polarisation. The scattered light, from the object, is switched between different paths in the shearing interferometer, depending on polarisation, allowing different directions of shear to be applied for light of different polarisation. The interferometer head *also* incorporates a pathlength imbalance allowing phase-stepping by the same wavelength tuning.

This chapter discusses the merits of this and other methods for shear multiplexing and discusses which method is most appropriate when implementing a three-dimensional shearography system.

1.7. Source Position Measurement using Shadow Moiré

Chapter 5 describes possible methods for the measurement of the direction of the sensitivity vectors. An accurate knowledge of the direction of the sensitivity vector is required to perform the coordinate transformation to the orthogonal coordinate system based on the in-plane and out-of-plane directions, relative to the object surface. Three

possible methods were investigated; shadow Moiré, a beam profile technique and a carrier fringe technique. The shadow Moiré method was chosen as it was the simplest to implement and the most accurate. Shadow Moiré is extended to perform the measurement of the source position in the horizontal and vertical directions, with enhanced sensitivity, when the source to camera distance is known. A circular Moiré grating provides a coarse measurement of the source position, by counting the number of radial Moiré fringes generated and from the line of symmetry of the fringe pattern. This approximate measurement is refined using possible source positions measured with vertically and horizontally orientated linear Moiré gratings. An appraisal of the merits of the different methods is given.

1.8. Shape and Slope Measurement

A further issue in the measurement of surface strain is the errors introduced by the shape of the object. Conventionally ESPI would be the most appropriate choice for a speckle interferometry system which measures shape. As the three-dimensional shearography system already contains a shearing interferometer for the surface strain measurement the decision was made to use the existing components for a shape and surface slope measurement system. Chapter 6 describes the problem of shape and slope measurement and discusses different shape measurement methods using shearography. A full theoretical treatment of the generation of slope sensitive correlation fringes and the results from the experimental system are presented. An appraisal of the merits of the different approaches are presented.

1.9. Full Surface Strain Measurement Applying a Correction for Object Slope and Shape.

In Chapter 7 of this thesis the results from the three-dimensional shearography system for a real industrial component, a gas main pipe are presented and the system as a whole is discussed. The target specification for the shearography system is to view an area of 0.1 m by 0.1 m with a spatial resolution of 200 με and for static events. The target strain range is –75 με to +75 με.

1.10. Summary

In summary this thesis describes a quantitative full-field strain measurement instrument which incorporates a correction for object surface slope and shape. The issues of shear direction multiplexing, source position measurement, shape measurement using shearography and the application of the system to a full-field strain measurement are presented.

1.11. References

Butters J N and Leendertz J A, "Holographic and Video Techniques applied to Engineering Measurement", *J. Meas. Control*, **4**, pp. 349-354, 1971.

Butters J N and Leendertz J A, "An image-shearing speckle-pattern interferometer for measuring bending moments", *J. Phy. E*, **6**, pp.1107-1110, 1973.

Denby D, Quintanilla G E and Butters J N, "Contouring by electronic speckle pattern interferometry", pp. 171-197, in ed. Robertson E R, "*The Engineering Uses of Coherent Optics*", Cambridge University Press, Cambridge, 1976.

Ennos A E, "Measurement of in-plane surface strain by hologram interferometry", *J. Phy. E*, **1**, pp. 731-734, 1968.

Ettemeyer A, "Combination of 3-D deformation and shape measurement by electronic speckle-pattern interferometry for quantitative strain-stress analysis", *Opt. Eng.*, **39**:1, pp. 212-215, 2000.

Frocht M M, "*Photoelasticity*", Volumes 1 and 2, John Wiley, New York, 1961.

Hung Y Y, Turner J L, Tafralian M, Hovanesian J D and Taylor C E, "Optical method for measuring contour slopes of an object", *Appl. Opt.*, **17**:1, pp. 128-131, 1978.

Jones R and Wykes C, "General parameters for the design and optimization of electronic speckle pattern interferometers", *Optica Acta*, **28**:7, pp. 949-972, 1981.

Leendertz J A, "Interferometric displacement measurement on scattering surfaces utilizing speckle effect", *J. Phy. E*, **3**, pp. 214-218, 1970.

McDonach A, McKelvie J and Walker C A, "Stress analysis of fibrous composites using Moiré interferometry", *Opt. Laser. Eng.*, **1**, pp. 85-105, 1980.

Young T, "The Bakerian Lecture. Experiments and Calculations relative to physical Optics", *Phil. Trans. Royal Soc. London*, **94**, pp. 1-16, 1804.

2. SPECKLE INTERFEROMETRY THEORY

2.1. Introduction

Normally the existence of speckle is a problem. Many optical techniques rely on the illumination of surfaces, often with the high powers which only lasers can supply, and in these cases the speckles are an intensity variation across the surface. This intensity variation alters the measurement sensitivity across the surface or has other undesirable effects such as generating 'hotspots' where the laser power is locally higher. However in speckle interferometry the speckles are necessary for the technique to operate.

The speckle formation depends on the form of the surface, which must be rough compared with the laser wavelength. The speckles contain phase information about the object surface added to a speckle noise term, which depends on the object surface in a complex way. Speckle pattern interferometry uses this phase information to perform measurements. To avoid analysis of an individual speckle pattern, two speckle patterns are correlated, often by subtraction, to obtain the optical phase change when a perturbation is applied to the system.

This chapter describes the phenomenon of speckle and the principal speckle pattern interferometry techniques in use today; shearography and electronic speckle pattern interferometry (ESPI).

2.2. Speckle

Laser speckle is the granular appearance of the light intensity, formed by illuminating an optically rough surface with a laser. An optically rough surface has a roughness of the order of, or greater than, the optical wavelength. To be more precise this speckle pattern is an objective speckle pattern as the intensity pattern depends on viewing direction. This type of speckle pattern depends on the optical wavelength and the illumination and viewing parameters. Alternatively a subjective speckle pattern can be obtained by imaging of the speckle pattern. The spatial distribution of the speckles in this type of speckle pattern is limited by the diffraction limit of the imaging system and the optical wavelength.

2.2.1 Objective Speckle

This type of speckle exists in three-dimensional space. Each point on the object surface absorbs incident light and emits spherical light waves. These spherical waves contribute to give the amplitude of the light at each point in space in front of the surface. Mathematically at a point $Q(\boldsymbol{r})$ the amplitude $U(\boldsymbol{r})$ is given by summing the contributions from all the points across the surface (Jones and Wykes 1989):

$$U(\boldsymbol{r}) = k \int_{-\infty}^{+\infty} \int u(x,y) \exp\left[\frac{2\pi i}{\lambda} G\xi(x,y)\right] dxdy \tag{2.1}$$

where k is a constant, $u(x,y)$ represents the complex amplitude of the light incident at a point (x,y) on the surface, λ is the optical wavelength, G is a geometric factor associated with the illumination and viewing directions and ξ is the surface height. As the surface height is varying by λ or more, due to the surface roughness, the phase $G\xi(x,y)$ will also vary by λ or more. The resultant amplitude at Q is dependent on the addition of random

vectors to give a random resultant amplitude. Therefore at the point $Q(\boldsymbol{r})$ the amplitude $U(\boldsymbol{r})$ will vary randomly.

To estimate the size of the speckles the distance at which the intensities are unrelated is used. Goodman (1976) has derived an expression for the autocorrelation function for a surface of size L by L illuminated by a wavelength λ.

$$R(\Delta x, \Delta y) = < I >^2 \left[1 + \sin c^2 \left(\frac{L\Delta x}{\lambda z} \right) \sin c \left(\frac{L\Delta y}{\lambda z} \right) \right] \tag{2.2}$$

where I is the intensity of the light, z is the distance between the object and viewing planes and $(\Delta x, \Delta y)$ are the x and y displacements when the viewing direction is changed. The average speckle size d_{osx}, or d_{osy}, is given by the first zero of the sinc function:

$$d_{osx} = \frac{\lambda x}{L} \qquad \text{and} \qquad d_{osy} = \frac{\lambda y}{L} \tag{2.3}$$

As light scattered from the edge of the illuminated area has the highest spatial frequency the size of the objective speckles is dependent of the size of the illuminated area.

2.2.2 Subjective Speckle

Subjective speckle size is dependent on the imaging system and is important in speckle pattern interferometry. The subjective speckle size can be calculated by considering the diffraction limit of light in the imaging system. The first minima of the diffraction pattern occurs at a distance, D:

$$D = \frac{1.22\lambda v}{a} \tag{2.4}$$

where v is the lens to image plane distance and a is the diameter of the viewing aperture.

The diameter of the subjective speckle, d_{ss}, is therefore:

$$d_{ss} = \frac{2.4\lambda v}{a} \tag{2.5}$$

The speckle diameter has also been calculated using the autocorrelation function technique (Goodman 1976) with agreement between the two methods.

2.3 Shearography

This configuration is sensitive to displacement gradient and is shown in Figure 2.1. Shearography (Leendertz and Butters 1973, Hung 1982), also known as speckle shearing interferometry, is a full-field non-contact optical technique, usually used for the qualitative measurement of changes in the displacement gradient caused by surface and sub-surface defects. A speckle pattern is formed by illuminating an optically rough surface with an expanded laser beam. In shearography this speckle pattern is optically mixed with an identical but displaced, or sheared, speckle pattern using a shearing device, and viewed through a lens, forming a speckle interferogram at the camera surface. Correlating speckle interferograms obtained before and after object deformation, by subtraction, yields correlation fringes sensitive to displacement gradient in the shear direction. Phase-stepping techniques (Creath 1993) are often used to extract the phase information, and therefore the displacement gradient information, from the speckle interferograms.

In an individual interferometric speckle pattern the relative phase between two points on the object surface is recorded at each pixel in the camera image. When the object is deformed the relative phase between two points on the object is correlated with the original recorded phase, commonly by subtraction. The correlation fringes therefore

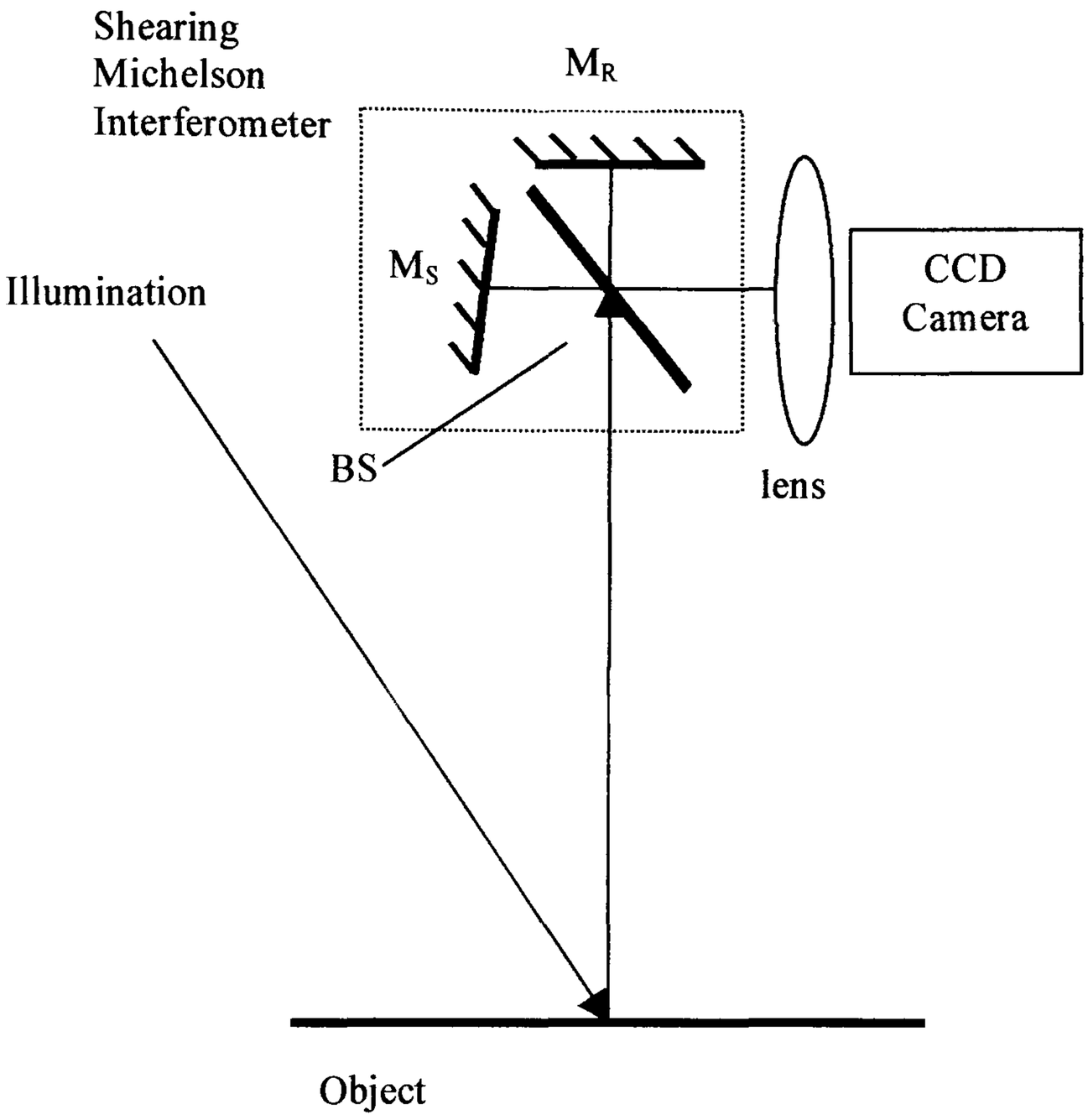

Figure 2.1 This is the shearography configuration for displacement gradient measurement. The shearing Michelson interferometer comprises M_R, reference mirror; M_S, shearing mirror and BS, beamsplitter.

represent displacement gradient as they measure the change in displacement over the fixed distance on the object surface.

This technique uses a shearing interferometer to optically mix light from one point on the object surface with light from another point on the object surface. Shearing devices commonly used for shearography are a Michelson interferometer with a tilt applied to one of the mirrors (Leendertz and Butters 1973) and an image shearing camera (Hung 1982).

In shearography a digital camera (Creath 1984), or in early designs a video camera (Butters and Leendertz 1971), is used to record the images. Subtraction is usually used to generate correlation fringes (Butters and Leendertz 1971). The digital camera replaces the photographic plate used in the speckle pattern correlation interferometry technique (Jones and Wykes 1989). The use of a digital camera allowed the introduction of many of the more complex phase measurement techniques (ed. Robinson and Reid 1993) in use today. There are a few disadvantages though with the use of digital camera, the pixel sizes on the digital cameras are currently larger than the resolution obtained from a photographic plate, the dynamic range is reduced and the data is quantised. A typical silver halide photographic film has a resolution of 2000 lines/mm (Parker 1993) and currently available high resolution CCD cameras have a resolution of 16.8 megapixels, 4000 by 4000 pixels (Benamati 2001). Within a few years however the digital camera should have a resolution approaching photographic film and be available with increased dynamic range.

The technique of phase-stepping in speckle pattern interferometry (Creath 1985, Nakadate and Saito 1985) may be used to recover information from the correlation fringes. In this technique a number of frames are recorded of the object, when static, with a phase shift optically introduced into the optical system between frames. These camera frames are combined using phase-stepping algorithms to yield a wrapped phase map. They would then undergo a phase unwrapping procedure to remove discontinuities, due to the bounded nature of the phase between $-\pi$ and $+\pi$ radians. Alternative phase analysis techniques such as the use of carrier fringes in shearography (Takezaki and Hung 1986) may also be used. In both cases the images from the system can be obtained in reasonably close to real time, the limitation being the speed of the image processing. However image processing algorithms also tend to increase in complexity, to allow processing of data containing more noise, as computer power increases.

2.3.1. *Optical Pathlength Imbalance*

To mathematically describe the sensitivity of the shearography and ESPI configurations to displacement gradient for shearography, and to displacement for ESPI, the optical pathlengths of the object and reference beams in the interferometer, before and after deformation of the object, are considered. For the general case the calculation is performed here.

This thesis uses an orthogonal coordinate system, *XYZ*, with the *x* direction horizontal and the *y* direction vertical. The *z* direction is out-of-plane and normal to the surface of

the object. Displacements are u in the x direction, v in the y direction and w in the z direction. Figure 2.2 shows the coordinate system.

The first camera frame records the initial interferometric speckle pattern, F_A, which contains information on the pathlength difference between the object and reference beams:

$$F_A = [SPH_A - SRH_A]\frac{2\pi}{\lambda} + \phi_{noise} \tag{2.6}$$

where SPH_A is the initial pathlength, between the source and the principal plane of the imaging system, via the object, for the object beam and SRH_A is the pathlength of the reference beam. λ is the optical wavelength and ϕ_{noise} is a speckle phase noise term. After applying a perturbation to the system a second interferometric speckle pattern, F_B, is recorded:

$$F_B = [SPH_B - SRH_B]\frac{2\pi}{\lambda} + \phi_{noise} \tag{2.7}$$

where SPH_B and SRH_B are the optical pathlengths after the system is perturbed, for the object and reference beams respectively. Correlating these two frames, by subtraction in this example, yields correlation fringes which have a phase, ϕ_{dq}, determined by:

$$\phi_{dq} = F_B - F_A \tag{2.8}$$

The sensitivity of the correlation fringes to a measurand depends on the optical configuration and typical configurations are described in the following sections. In shearography two orthogonal directions of the applied shear are required to fully characterise the displacement gradient components so the denominator in the displacement gradient term can most simply be either dx or dy.

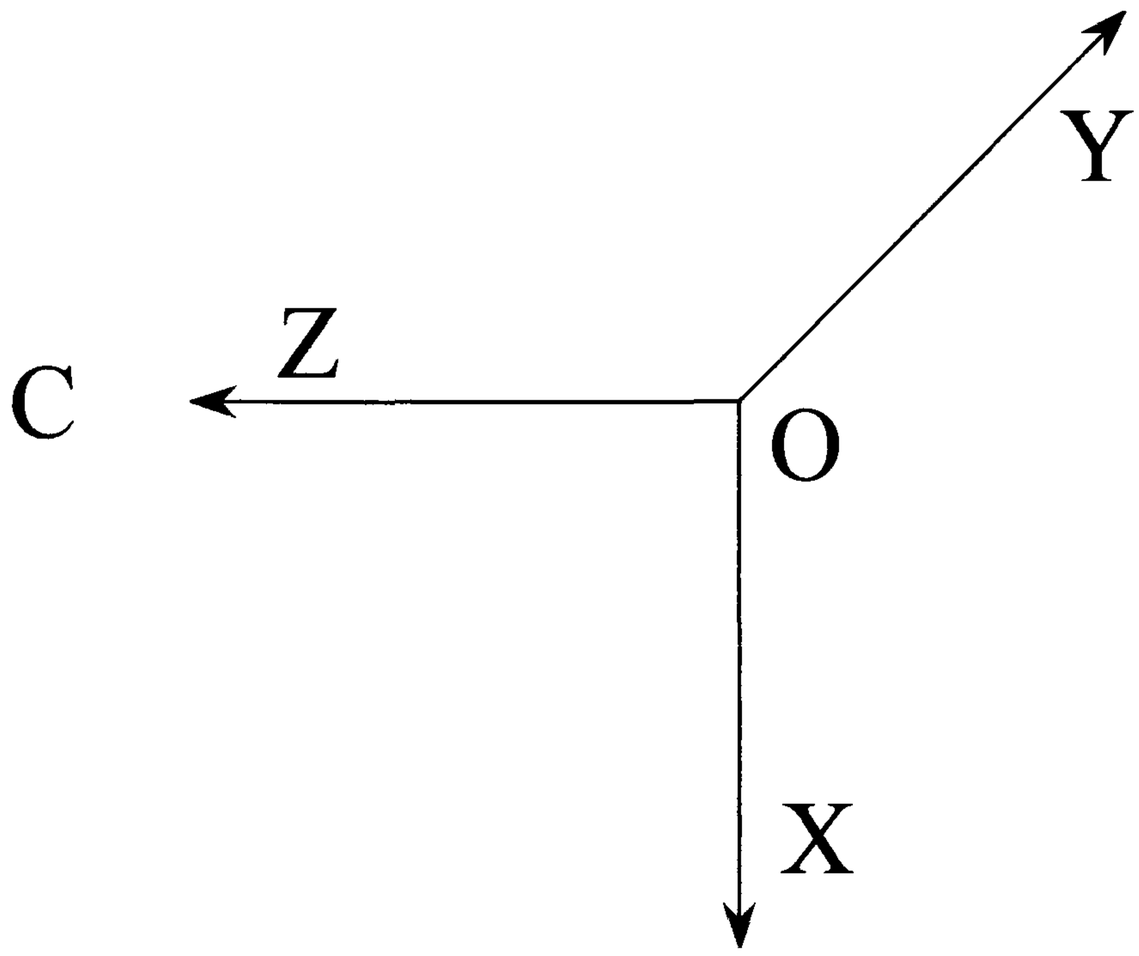

Figure 2.2 The coordinate system used in this thesis. The *z* direction is from object to camera. The *x* and *y* directions are orthogonal horizontally and vertically respectively. O, object position; C, camera position.

2.3.2. Out-of-Plane Displacement Gradient Sensitive Shearography

An out-of-plane displacement gradient sensitive shearography system is shown in Figure 2.3. The illumination and imaging directions are close to collinear and normal to the object surface. An out-of-plane displacement changes both pathlengths through the interferometer equally so there is no sensitivity to displacement. Shearography is sensitive to the difference in the out-of-plane displacement between the sheared images, making the technique sensitive to the displacement gradient over a fixed length, the magnitude of the applied shear.

For more complex illumination and imaging geometries the direction of the sensitivity vector is used to locate the component of displacement gradient the system is sensitive to. The sensitivity vector is the bisector of the illumination direction and the imaging direction. The sensitivity vector can then be resolved into components of the in-plane and the out-of-plane directions relative to the object surface. For small angles of illumination and imaging, relative to the normal to the object surface, the out-of-plane component is dominant and the interferometer can still be used to measure, to a good approximation, the out-of-plane displacement gradient. For large angles of illumination, away from the normal, the in-plane components become more important and with modifications the system can be used to measure in-plane displacement gradient. This is described in Section 2.3.3.

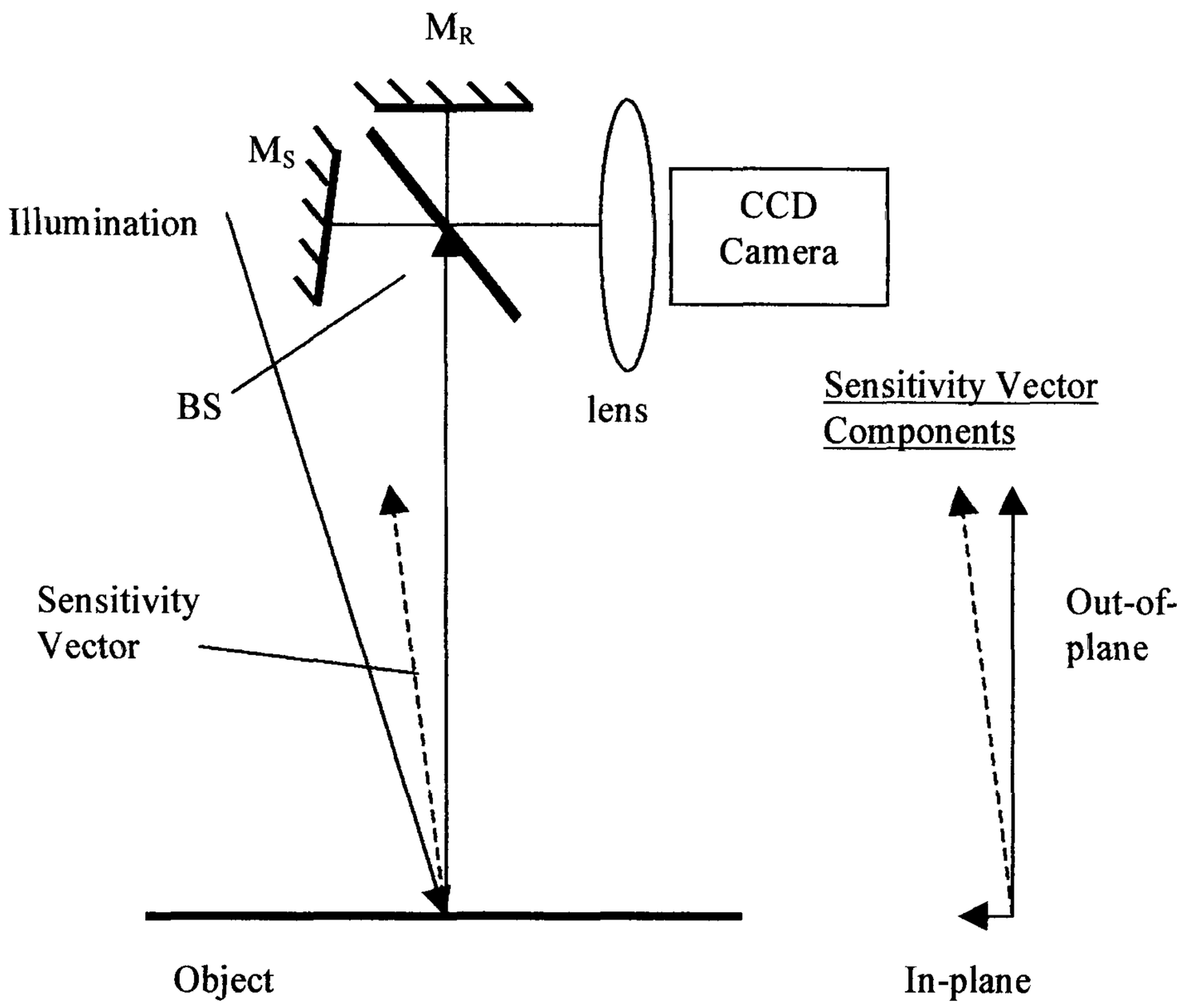

Figure 2.3 This is the shearography configuration predominantly sensitive to out-of-plane displacement gradient. The contribution from the in-plane displacement gradient component is small for angles of illumination of a few degrees from the normal to the object surface. M_R, reference mirror; M_S, shearing mirror and BS, beamsplitter.

Mathematically the sensitivity to out-of-plane displacement gradient can be shown as follows. The reference path is from source to object, via the reference mirror, to the principal plane of the imaging system. Assuming the illumination and imaging directions to be collinear gives:

$$\left(SP_1H\right)_A = \left(SP_1\right)_{AZ} + \left(P_1H\right)_{AZ} \tag{2.9}$$

where S is the source position, P_1 is a point on the object surface and H is the principal plane of the imaging system. The sheared path is via point, P_2, on the object surface:

$$\left(SP_2H\right)_A = \left(SP_2\right)_{AZ} + \left(P_2H\right)_{AZ} \tag{2.10}$$

The phase recorded by frame A is the pathlength difference between $(SP_1H)_A$ and $(SP_2H)_A$:

$$\phi_A = \left[\left\{\left(SP_1\right)_{AZ} + \left(P_1H\right)_{AZ}\right\} - \left\{\left(SP_2\right)_{AZ} + \left(P_2H\right)_{AZ}\right\}\right]\frac{2\pi}{\lambda}dx + \Delta\phi_{noise} \tag{2.11}$$

where dx is the applied shear in the x direction. After deforming the phase recorded by frame B is:

$$\phi_B = \left[\left\{\left(SP_1\right)_{BZ} + \left(P_1H\right)_{BZ}\right\} - \left\{\left(SP_2\right)_{BZ} + \left(P_2H\right)_{BZ}\right\}\right]\frac{2\pi}{\lambda}dx + \Delta\phi_{noise} \tag{2.12}$$

The phase of the correlation fringes, ϕ_{dq}, is given by subtracting Equation 2.11 from Equation 2.12:

$$\phi_{dq} = \phi_B - \phi_A \tag{2.13}$$

For a displacement gradient, $\delta w/\delta x$, with an applied shear, dx:

$$\left[\left\{\left(SP_1\right)_{BZ} - \left(SP_1\right)_{AZ}\right\} - \left\{\left(SP_2\right)_{BZ} - \left(SP_2\right)_{AZ}\right\}\right] = \frac{\delta w}{\delta x} \tag{2.14}$$

$$\left[\left\{\left(P_1H\right)_{BZ} - \left(P_1H\right)_{AZ}\right\} - \left\{\left(P_2H\right)_{BZ} - \left(P_2H\right)_{AZ}\right\}\right] = \frac{\delta w}{\delta x} \tag{2.15}$$

The phase of the correlation fringes simplifies to:

$$\phi_{dq} = 2\frac{\delta w}{\delta x}dx\frac{2\pi}{\lambda} \tag{2.16}$$

This configuration is therefore directly sensitive to out-of-plane displacement gradient. However illumination and imaging from the same direction requires a complicated optical system, so the illumination, or imaging, are not usually normal but close to normal.

Tilting the shearing mirror to apply a shear in an orthogonal direction yields:

$$\phi_{dq} = 2\frac{\delta w}{\delta y}dy\frac{2\pi}{\lambda} \tag{2.17}$$

2.3.3. Out-of-Plane and In-Plane Displacement Gradient Sensitive Shearography

This configuration is sensitive to a mixture of in-plane and out-of-plane components depending on the angles of illumination and imaging. The optical configuration is shown in Figure 2.4. It is assumed that the illumination and imaging directions are in the *x*-*z* plane, although the analysis could be extended to three-dimensions if required. The angle θ is the angle to rotate the illumination direction to *z* axis and the angle ε is the angle required to rotate the imaging direction to the *z* axis.

For this illumination geometry the phase recorded by frame *A* the out-of-plane component is:

$$\phi_{AZ} = \left[\left\{\left(SP_2\right)_{AZ} - \left(SP_1\right)_{AZ}\right\}\cos\theta + \left\{\left(P_2H\right)_{AZ} - \left(P_1H\right)_{AZ}\right\}\cos\varepsilon\right]\frac{2\pi}{\lambda}dx + \Delta\phi_{noise} \tag{2.18}$$

and the in-plane component is:

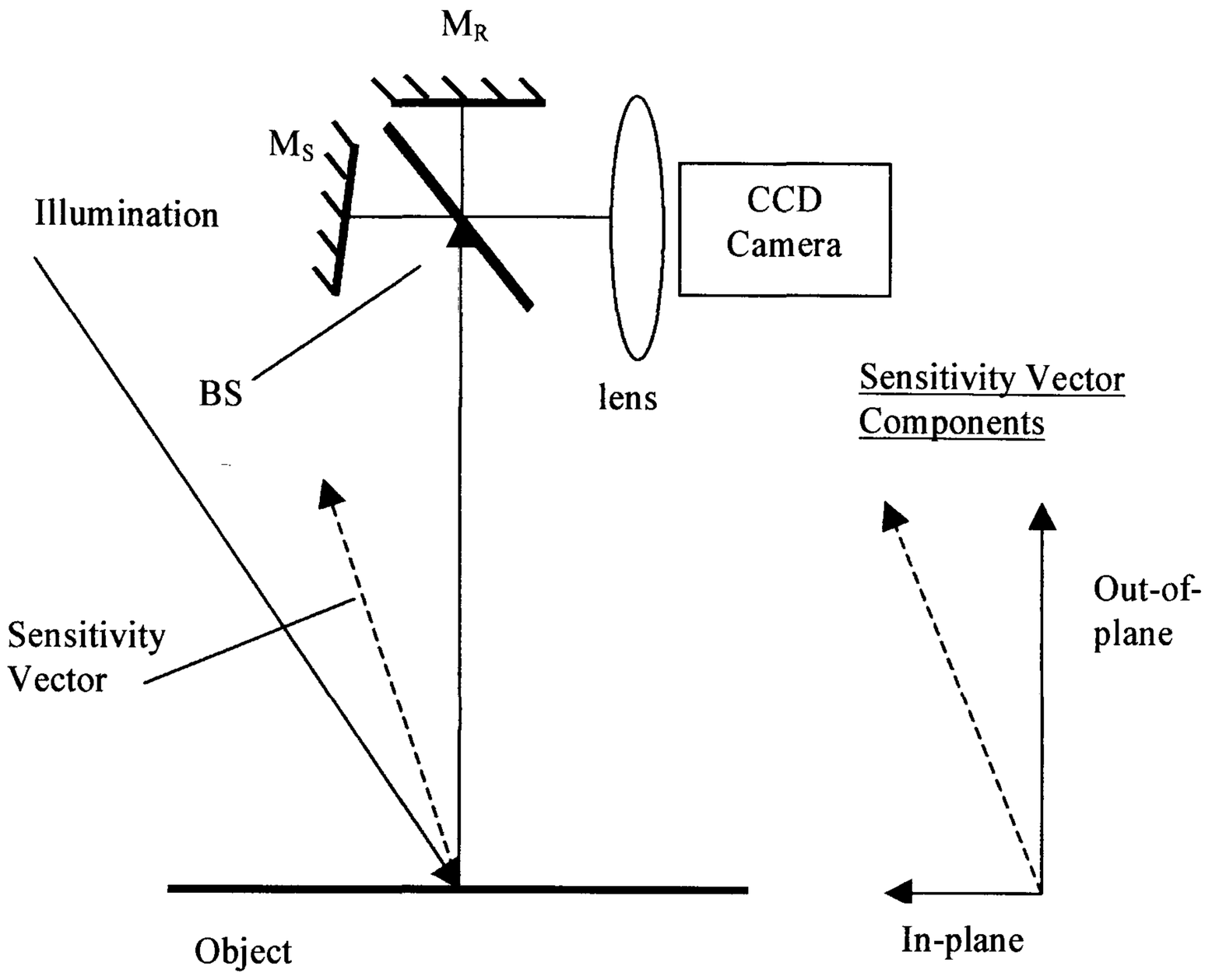

Figure 2.4 This is the shearography configuration for in-plane and out-of-plane displacement gradient measurement. M_R, reference mirror; M_S, shearing mirror and BS, beamsplitter.

$$\phi_{AX} = \left[\left\{\left(SP_2\right)_{AX} - \left(SP_1\right)_{AX}\right\}\sin\theta + \left\{\left(P_2H\right)_{AX} - \left(P_1H\right)_{AX}\right\}\sin\varepsilon\right]\frac{2\pi}{\lambda}dx + \Delta\phi_{noise} \qquad (2.19)$$

and for frame B:

$$\phi_{BZ} = \left[\left\{\left(SP_2\right)_{BZ} - \left(SP_1\right)_{BZ}\right\}\cos\theta + \left\{\left(P_2H\right)_{BZ} - \left(P_1H\right)_{BZ}\right\}\cos\varepsilon\right]\frac{2\pi}{\lambda}dx + \Delta\phi_{noise} \qquad (2.20)$$

$$\phi_{BX} = \left[\left\{\left(SP_2\right)_{BX} - \left(SP_1\right)_{BX}\right\}\sin\theta + \left\{\left(P_2H\right)_{BX} - \left(P_1H\right)_{BX}\right\}\sin\varepsilon\right]\frac{2\pi}{\lambda}dx + \Delta\phi_{noise} \qquad (2.21)$$

For an out-of-plane displacement gradient, $\delta w/\delta x$, and an in-plane displacement gradient, $\delta u/\delta x$, with an applied shear, dx, this simplifies to:

$$\phi_{dq} = \left[\left(\cos\theta + \cos\varepsilon\right)\frac{dw}{dx} + \left(\sin\theta + \sin\varepsilon\right)\frac{du}{dx}\right]dx\frac{2\pi}{\lambda} \qquad (2.22)$$

For small angles of θ and ε the system is predominantly sensitive to $\delta w/\delta x$. For example if θ and ϕ are equal to 5° the error in measuring $\delta w/\delta x$ is 1 % (assuming the magnitude of $\delta w/\delta x$ is comparable with the magnitude of $\delta u/\delta x$).

Referring to Equation 2.22, for applied shears of dy the sensitivities to displacement gradient are:

$$\phi_{dq} = \left[\left(\cos\theta + \cos\varepsilon\right)\frac{dw}{dy} + \left(\sin\theta + \sin\varepsilon\right)\frac{du}{dy}\right]dy\frac{2\pi}{\lambda} \qquad (2.23)$$

2.3.4. Multi-Component Displacement Gradient Sensitive Shearography

The three-dimensional components of displacement gradient, $\delta u/\delta x$, $\delta v/\delta x$ and $\delta w/\delta x$ for dx applied shear can be measured by performing three measurements of displacement

gradient from different illumination (or viewing) directions, followed by a coordinate transformation. Figure 2.5 shows a multi-component shearography system.

Consider three illumination positions, S_1, S_2 and S_3, at three of the four corners of a square. For shearography James and Tatam (1999) have shown this to be the optimum practical configuration. The vector normal to the object surface passes through the centre of this square. In three-dimensional space the source positions are at:

$$S_1 = [+a,-a,+D] \qquad S_2 = [+a,+a,+D] \qquad S_3 = [-a,+a,+D] \tag{2.24}$$

where D is the distance from the optical source to the object in the z direction and $2a$ is the length of the side of the square. The imaging is normal to the object surface and the angles of illumination are θ in the x-z plane, and θ in the x-y plane:

$$\theta = \tan^{-1}\left(\frac{a}{D}\right) \tag{2.25}$$

By measuring using a minimum of three directions of sensitivity vector, and two directions of applied shear, the out-of-plane displacement gradient components $\delta w/\delta x$ and $\delta w/\delta y$, and the in-plane components, $\delta u/\delta x$, $\delta u/\delta y$, $\delta v/\delta x$ and $\delta v/\delta y$, may be determined. Three displacement gradient components are measured and then transformed into the in-plane and out-of-plane displacement gradient components for each shear direction.

Illuminating from these three source positions yields three measured components:

$$\phi_{dq1} = \left[+\frac{\delta u}{\delta x}\sin\theta\cos\theta - \frac{\delta v}{\delta x}\cos\theta\sin\theta + \frac{\delta w}{\delta x}\cos\theta\cos\theta\right]dx\frac{2\pi}{\lambda} \tag{2.26}$$

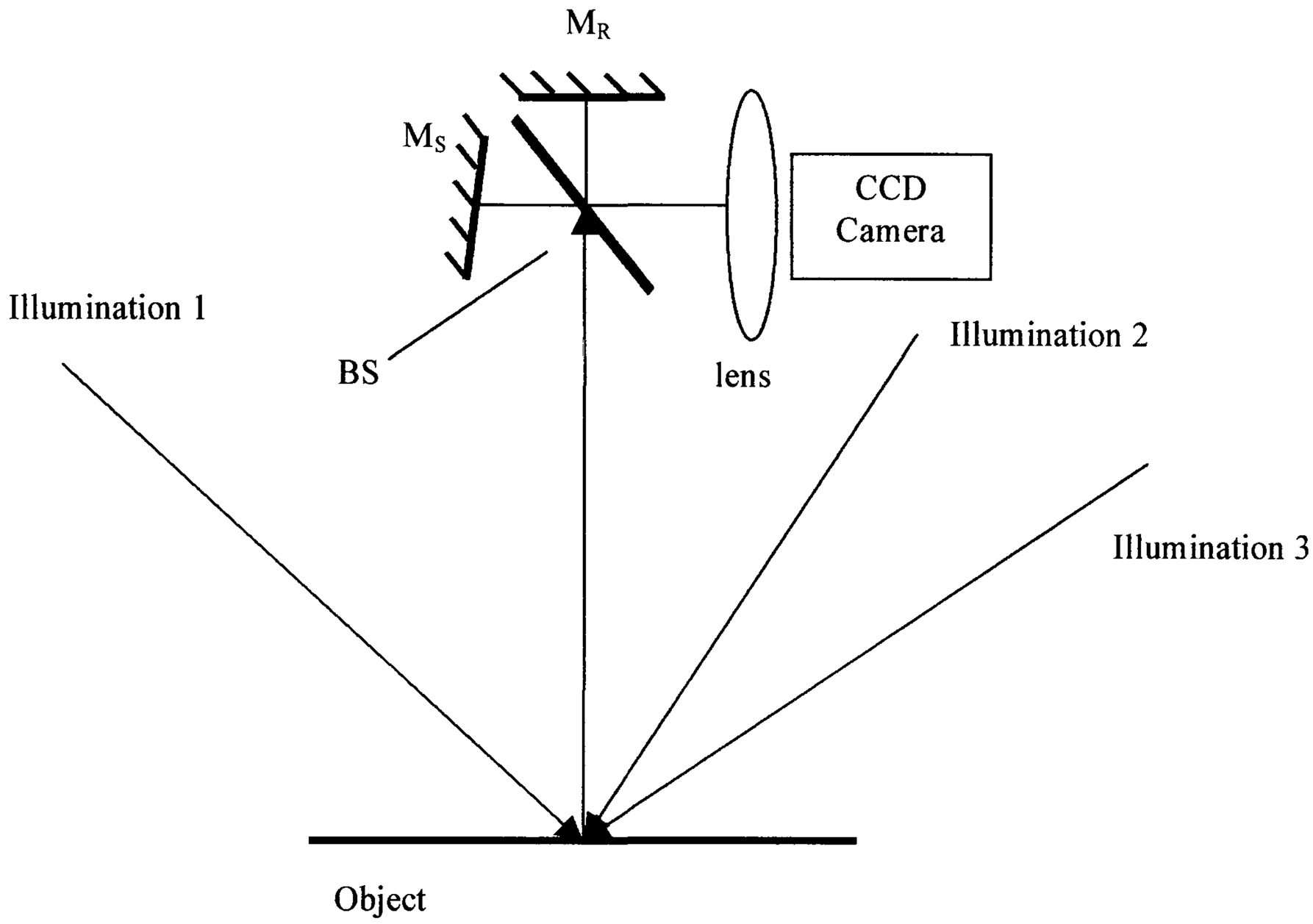

Figure 2.5 This is the shearography configuration for multi-component displacement gradient measurement. M_R, reference mirror; M_S, shearing mirror and BS, beamsplitter. Illumination is from three directions, utilising a multiplexing technique.

$$\phi_{dq2} = \left[+ \frac{\delta u}{\delta x} \sin\theta\cos\theta + \frac{\delta v}{\delta x} \cos\theta\sin\theta + \frac{\delta w}{\delta x} \cos\theta\cos\theta \right] dx \frac{2\pi}{\lambda} \tag{2.27}$$

$$\phi_{dq3} = \left[- \frac{\delta u}{\delta x} \sin\theta\cos\theta + \frac{\delta v}{\delta x} \cos\theta\sin\theta + \frac{\delta w}{\delta x} \cos\theta\cos\theta \right] dx \frac{2\pi}{\lambda} \tag{2.28}$$

where ϕ_{dq1}, ϕ_{dq2} and ϕ_{dq3} are the phase of the correlation fringes obtained from the different sensitivity directions.

In vector notation the measured components of displacement gradient for an applied shear in dx are:

$$\phi_{dqdx1} = \left[k_{x1} \frac{\delta u}{\delta x} + k_{y1} \frac{\delta v}{\delta x} + k_{z1} \frac{\delta w}{\delta x} \right] dx \frac{2\pi}{\lambda} \tag{2.29}$$

$$\phi_{dqdx2} = \left[k_{x2} \frac{\delta u}{\delta x} + k_{y2} \frac{\delta v}{\delta x} + k_{z2} \frac{\delta w}{\delta x} \right] dx \frac{2\pi}{\lambda} \tag{2.30}$$

$$\phi_{dqdx3} = \left[k_{x3} \frac{\delta u}{\delta x} + k_{y3} \frac{\delta v}{\delta x} + k_{z3} \frac{\delta w}{\delta x} \right] dx \frac{2\pi}{\lambda} \tag{2.31}$$

And for an applied shear in dy are:

$$\phi_{dqdy1} = \left[k_{x1} \frac{\delta u}{\delta y} + k_{y1} \frac{\delta v}{\delta y} + k_{z1} \frac{\delta w}{\delta y} \right] dy \frac{2\pi}{\lambda} \tag{2.32}$$

$$\phi_{dqdy2} = \left[k_{x2} \frac{\delta u}{\delta y} + k_{y2} \frac{\delta v}{\delta y} + k_{z2} \frac{\delta w}{\delta y} \right] dy \frac{2\pi}{\lambda} \tag{2.33}$$

$$\phi_{dqdy3} = \left[k_{x3} \frac{\delta u}{\delta y} + k_{y3} \frac{\delta v}{\delta y} + k_{z3} \frac{\delta w}{\delta y} \right] dy \frac{2\pi}{\lambda} \tag{2.34}$$

The phase changes for an applied shear of *dx* are:

$$\begin{pmatrix} \phi_{dqdx1} \\ \phi_{dqdx2} \\ \phi_{dqdx3} \end{pmatrix} = \begin{pmatrix} k_{x1} & k_{x2} & k_{x3} \\ k_{y1} & k_{y2} & k_{y3} \\ k_{z1} & k_{z2} & k_{z3} \end{pmatrix} \begin{pmatrix} \frac{\delta u}{\delta x} \\ \frac{\delta v}{\delta x} \\ \frac{\delta w}{\delta x} \end{pmatrix} dx = M \begin{pmatrix} \frac{\delta u}{\delta x} \\ \frac{\delta v}{\delta x} \\ \frac{\delta w}{\delta x} \end{pmatrix} dx \tag{2.35}$$

and an applied shear of *dy* are:

$$\begin{pmatrix} \phi_{dqdy1} \\ \phi_{dqdy2} \\ \phi_{dqdy3} \end{pmatrix} = \begin{pmatrix} k_{x1} & k_{x2} & k_{x3} \\ k_{y1} & k_{y2} & k_{y3} \\ k_{z1} & k_{z2} & k_{z3} \end{pmatrix} \begin{pmatrix} \frac{\delta u}{\delta y} \\ \frac{\delta v}{\delta y} \\ \frac{\delta w}{\delta y} \end{pmatrix} dy = M \begin{pmatrix} \frac{\delta u}{\delta y} \\ \frac{\delta v}{\delta y} \\ \frac{\delta w}{\delta y} \end{pmatrix} dy \tag{2.36}$$

The coordinate transformation using the inverse of the matrix gives:

$$\begin{pmatrix} \frac{\delta u}{\delta x} \\ \frac{\delta v}{\delta x} \\ \frac{\delta w}{\delta x} \end{pmatrix} = M^{-1} \begin{pmatrix} \phi_{dqdx1} \\ \phi_{dqdx2} \\ \phi_{dqdx3} \end{pmatrix} \tag{2.37}$$

$$\begin{pmatrix} \frac{\delta u}{\delta y} \\ \frac{\delta v}{\delta y} \\ \frac{\delta w}{\delta y} \end{pmatrix} = M^{-1} \begin{pmatrix} \phi_{dqdy1} \\ \phi_{dqdy2} \\ \phi_{dqdy3} \end{pmatrix} \tag{2.38}$$

A shearography system in which the direction of applied shear can be switched between the *dx* and the *dy* directions is required to fully characterise the surface strain. A shear direction multiplexing system that can measure both the out-of-plane displacement gradient components is described in Chapter 4.

2.3.5. *Strain Tensor*

The strain tensor is:

$$S = \begin{pmatrix} \dfrac{\delta u}{\delta x} & \dfrac{1}{2}\left(\dfrac{\delta u}{\delta y}+\dfrac{\delta v}{\delta x}\right) & \dfrac{1}{2}\left(\dfrac{\delta u}{\delta z}+\dfrac{\delta w}{\delta x}\right) \\ \dfrac{1}{2}\left(\dfrac{\delta v}{\delta x}+\dfrac{\delta u}{\delta y}\right) & \dfrac{\delta v}{\delta y} & \dfrac{1}{2}\left(\dfrac{\delta v}{\delta z}+\dfrac{\delta w}{\delta y}\right) \\ \dfrac{1}{2}\left(\dfrac{\delta w}{\delta x}+\dfrac{\delta u}{\delta z}\right) & \dfrac{1}{2}\left(\dfrac{\delta w}{\delta y}+\dfrac{\delta v}{\delta z}\right) & \dfrac{\delta w}{\delta z} \end{pmatrix} \tag{2.39}$$

Shearography is only able to measure the components where the denominator is δx or δy as the shear can only be applied in the plane of the camera image. These are shown in bold in Equation 2.39. This is sufficient however to fully characterise the surface strain. The components that cannot be measured using shearography are the bulk strain components.

2.3.6. *Measurement of Flexural Strains*

For a thin plate the flexural strains are related to the second derivatives of the plate displacement. The components of flexural strains that can be determined using shearography are ε_{xx}, ε_{yy} and γ_{xy} (Takezaki and Hung 1986):

$$\varepsilon_{xx} = -\frac{h}{2}\frac{\delta^2 w}{\delta x^2} \tag{2.40}$$

$$\varepsilon_{yy} = -\frac{h}{2}\frac{\delta^2 w}{\delta y^2} \tag{2.41}$$

$$\gamma_{xy} = -h\frac{\delta^2 w}{\delta x \delta y} \tag{2.42}$$

where h is the plate thickness, w is the out-of-plane displacement and x and y are the horizontal and vertical directions, respectively, in the camera image plane.

2.3.7. Shape Measurement using Shearography

Shearography can be used to perform object slope and shape measurement by generating correlation fringes sensitive to object slope. This can be done by wavelength contouring (Huang *et al* 1997), object rotation (Rastogi 1997) or by source displacement (Tay *et al* 1991). These techniques are discussed in detail in Chapter 6. The slope fringes are processed to recover object slope in the shear direction and a numerical integration is used to recover the object shape.

2.4 Electronic Speckle Pattern Interferometry

Electronic speckle pattern interferometry is a speckle technique, sensitive to displacement, employing a fixed reference beam. An analysis of the mathematics of the ESPI configurations can be performed in a similar way to that presented for shearography.

In this section the derivation of the sensitivity for out-of-plane displacement is given, then the equations for the sensitivity to the other components is performed by inspection of the equations for shearography.

2.4.1. Out-of-Plane Displacement Sensitive ESPI

The sensitivity to out-of-plane displacement is determined for an ESPI system with collinear illumination and viewing. This configuration is shown in Figure 2.6.

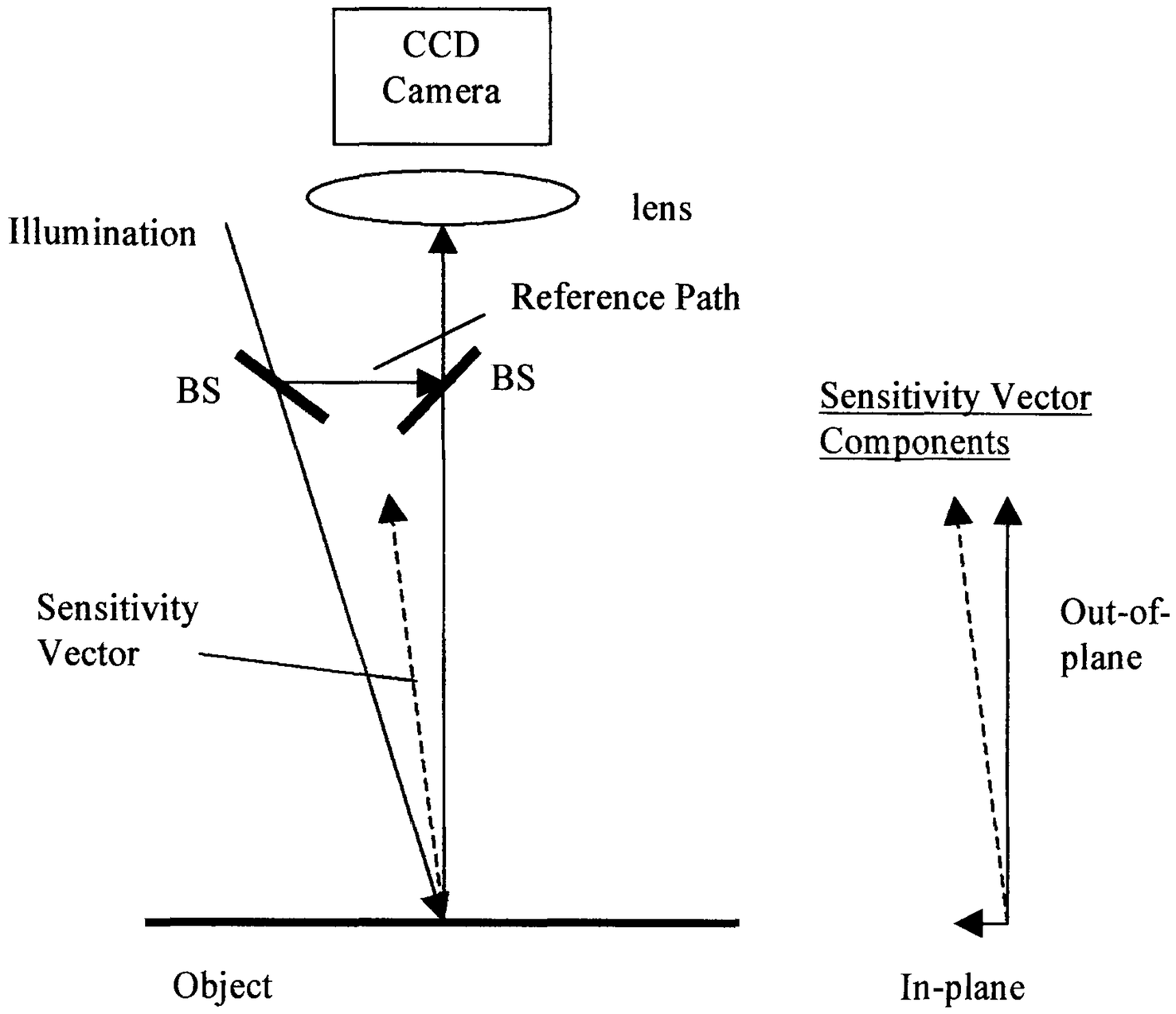

Figure 2.6 This is the ESPI configuration for out-of-plane displacement measurement. The contribution from the in-plane displacement component is small for angles of illumination of less than 5° from the normal to the object surface. BS is a beamsplitter.

Assuming the illumination and imaging directions to be collinear, the path of the object beam, source to object to the principal plane of the imaging system, is:

$$SPH_A = SP_{AZ} + PH_{AZ} \tag{2.43}$$

where S is the source position, P is a point on the object surface and H is the principal plane of the imaging system. The reference beam follows a path, of length L:

$$SRH = L \tag{2.44}$$

After deforming the object surface, the source to object to the principal plane of the imaging system pathlength changes to:

$$SPH_B = SP_{BZ} + PH_{BZ} \tag{2.45}$$

and the reference path SRH is unchanged.

The phase of the correlation fringes, ϕ_{dq}, is given by:

$$\phi_{dq} = [\{SPH_B + SRH_B\} - \{SPH_A - SRH_A\}]\frac{2\pi}{\lambda} \tag{2.46}$$

As: $SP_{BZ} - SP_{AZ} = w$, $PH_{BZ} - PH_{AZ} = w$ and: $SRH_B = SRH_A$ (2.47)

This simplifies to:

$$\phi_{dq} = 2w\frac{2\pi}{\lambda} \tag{2.48}$$

where w is the out-of-plane displacement. This configuration is therefore directly sensitive to out-of-plane displacement.

2.4.2. Out-of-Plane and In-Plane Displacement Sensitive ESPI

The ESPI technique is sensitive to a mixture of the in-plane and out-of-plane displacement if the illumination and imaging are not collinear. Figure 2.7 shows the experimental layout. Referring to Section 2.3.3. the phase change, ϕ_{dq}, is:

$$\phi_{dq} = [(\cos\theta + \cos\varepsilon)w + (\sin\theta + \sin\varepsilon)u]\frac{2\pi}{\lambda} \tag{2.49}$$

where θ is the angle of illumination, ε is the angle of viewing, w is an out-of-plane displacement and u is an in-plane displacement. As for the shearography technique this sensitivity to a mixture of in-plane and out-of-plane components allows the construction of a multi-component system.

2.4.3. Multi-Component Displacement Sensitive ESPI

A multi-component ESPI system is shown in Figure 2.8. In comparison with the multi-component shearography system shown in Figure 2.5 this experimental layout is more complex. A multi-component system with three, or more, channels, which have different sensitivity vectors, may be used to measure the two in-plane and one out-of-plane displacement components. For three channels the sensitivity to optical phase may be written in vector notation as:

$$\phi_{dq1} = k_{x1}u + k_{y1}v + k_{z1}w \tag{2.50}$$

$$\phi_{dq2} = k_{x2}u + k_{y2}v + k_{z2}w \tag{2.51}$$

$$\phi_{dq3} = k_{x3}u + k_{y3}v + k_{z3}w \tag{2.52}$$

where the k terms are components of the sensitivity vector, dependent on geometrical factors. The u, v and w displacement components may be obtained using matrix

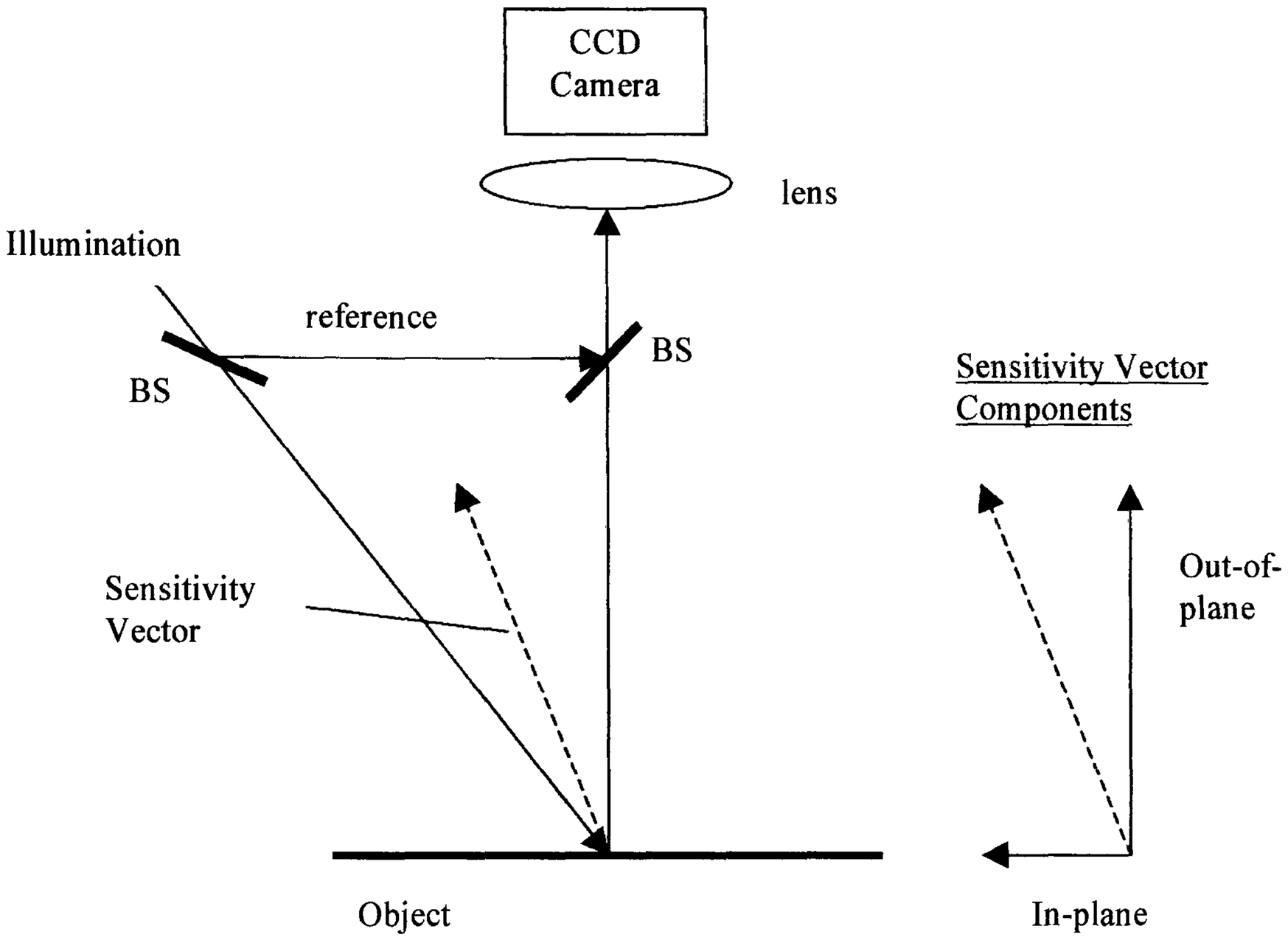

Figure 2.7 This is the ESPI configuration for sensitivity to a mixture of in-plane and out-of-plane displacements. BS is a beamsplitter.

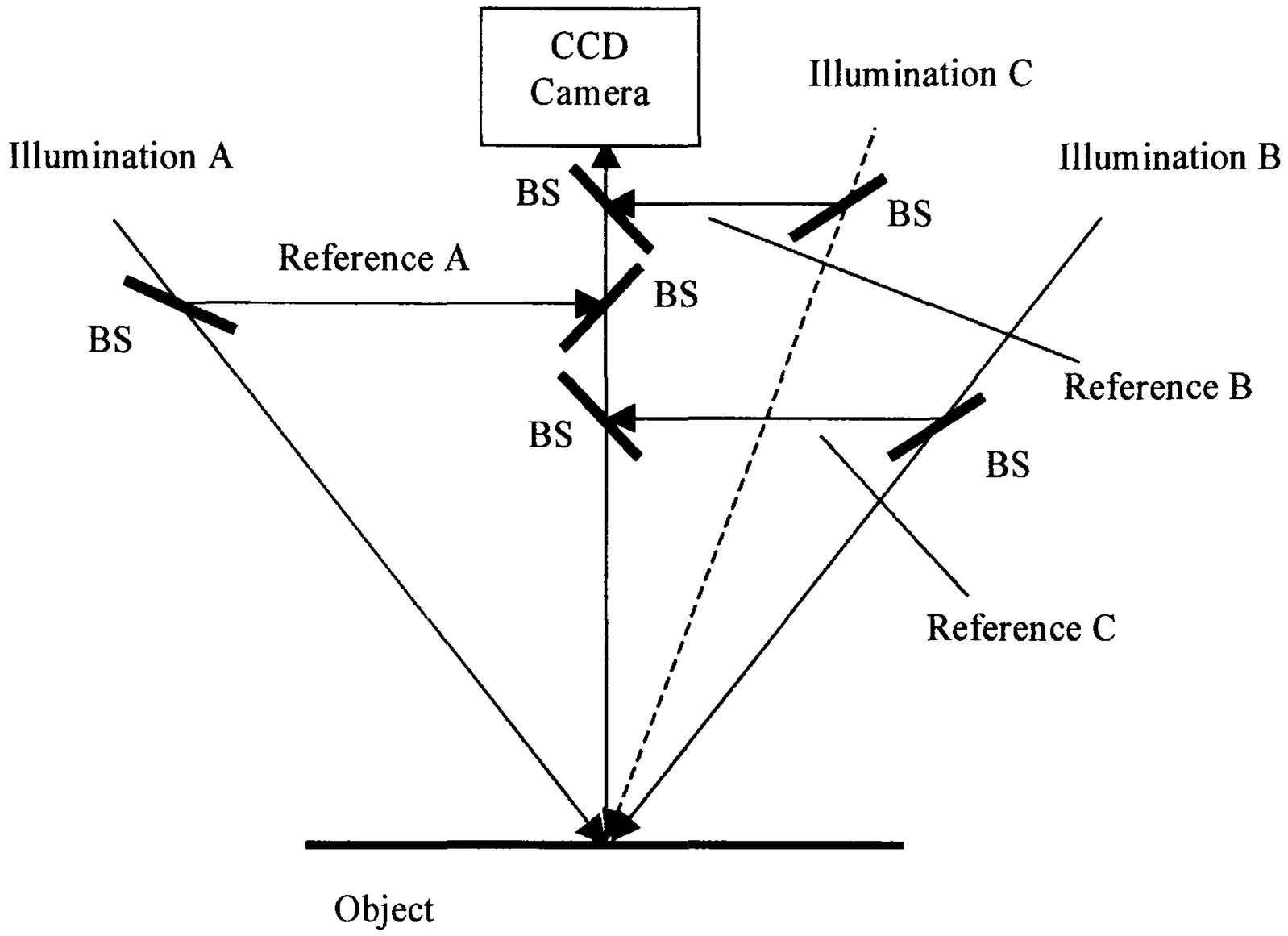

Figure 2.8 This is the ESPI configuration for simultaneous measurement of the in-plane and out-of-plane displacements. BS is a beamsplitter.

manipulation. The optical phase changes , for each channel, due to displacement are:

$$\begin{pmatrix} \phi_{dq1} \\ \phi_{dq2} \\ \phi_{dq3} \end{pmatrix} = \begin{pmatrix} k_{x1} & k_{x2} & k_{x3} \\ k_{y1} & k_{y2} & k_{y3} \\ k_{z1} & k_{z2} & k_{z3} \end{pmatrix} \begin{pmatrix} u \\ v \\ w \end{pmatrix} = M \begin{pmatrix} u \\ v \\ w \end{pmatrix} \tag{2.53}$$

To obtain the u, v and w components of displacement:

$$\begin{pmatrix} u \\ v \\ w \end{pmatrix} = M^{-1} \begin{pmatrix} \phi_{dq1} \\ \phi_{dq2} \\ \phi_{dq3} \end{pmatrix} \tag{2.54}$$

2.4.4. Shape Measurement using ESPI

To perform shape measurement using ESPI correlation fringes sensitive to the object contours are generated. This can be done in a number of ways including two wavelength contouring (Denby *et al* 1976), tilting the object (Jaisingh and Chiang 1981). In Section 6.2 an analysis of the slope and shape measurement techniques using shearography is presented. A theoretical analysis of the two wavelength technique shape measurement using ESPI is presented here.

The two wavelength technique may be performed by simultaneously illuminating the object with two optical wavelengths to form correlation fringes by addition. These correlation fringes can be seen 'live' with no image processing. Alternatively correlation fringes may be formed by subtraction. The object is sequentially illuminated by two optical wavelengths and a camera frame is recorded for each of the two illumination wavelengths. Subtraction of camera frames yields correlation fringes sensitive to the surface contours. A mathematical analysis of this technique is presented

here for illuminating and imaging directions collinear and normal to the object surface. For the reference frame (frame *A*), referring to equations 2.43 to 2.46, the optical phase, ϕ_A, is:

$$\phi_A = \left[SP_{AZ} + PC_{AZ} - L\right]\frac{2\pi}{\lambda_1} + \phi_{noise} \tag{2.55}$$

where SP_{AZ}, PC_{AZ} and L are optical pathelengths, λ_1 is the first optical wavelength and ϕ_{noise} is speckle noise. For the signal frame (frame *B*) the optical phase , ϕ_B, is:

$$\phi_B = \left[SP_{BZ} + PC_{BZ} - L\right]\frac{2\pi}{\lambda_2} + \phi_{noise} \tag{2.56}$$

where SP_{BZ}, PC_{BZ} and L are optical pathelengths and λ_2 is the second optical wavelength. The optical pathlength difference contained within the square brackets in equations 2.55 and 2.56 is constant and may be represented by Δ.

Subtracting equation 2.55 from equation 2.56 yields the phase of the shape sensitive correlation fringes, ϕ_{SH}:

$$\phi_{SH} = \phi_B - \phi_A = \Delta 2\pi\left(\frac{1}{\lambda_1} - \frac{1}{\lambda_2}\right) \tag{2.57}$$

The speckle noise term in equations 2.55 and 2.56 is constant and cancels.

A change in the surface height, in the z direction, of Δz, across the field of view will generate a phase change across the field of view. The sensitivity is to $2\Delta z$ due to the illumination path changing by Δz and the viewing path changing by Δz.

$$\Delta\phi_{SH} = 4\pi\Delta z\left(\frac{1}{\lambda_1} - \frac{1}{\lambda_2}\right) \tag{2.58}$$

A knowledge of λ_1 and λ_2 will allow the sensitivity of the correlation fringes to shape to be determined. For the contours to be spaced at 1 mm intervals a wavelength shift of 0.3 nm is required for an initial illumination wavelength of 800 nm.

2.5. Phase Measurement Methods

The techniques described in this thesis use a temporal phase measurement method which is suitable for processes which are slow compared with the camera frame rate. Phase-stepping in interferometry was originally described by Carré (1966). A number of interferograms are recorded sequentially, with the phase-step introduced between the camera frames. The phase-stepped images are then processed using a mathematical algorithm to yield the phase at each point on the object surface. The final stage of the phase-stepping techniques is the unwrapping process where phase discontinuities, due to the phase of light having a bound between $+\pi$ and $-\pi$ radians, are removed.

The alternative techniques are the fringe analysis techniques such as computer processed fringe counting (Nakadate et al 1981) and the spatial phase measurement methods (Kujawinska 1993) where simultaneous phase-stepped images are recorded. The spatial fringe measurement technique is more suitable for high-speed processes but offers lower accuracy than temporal phase-stepping when used for static or slow processes.

2.5.1. Methods of Phase-Stepping

The phase-step is introduced by changing the optical pathlength in the interferometer by a fixed length so that the phase difference between the paths changes by a known distance. A review paper by Wyant and Shagman (1978) describes the methods of moving a mirror in the interferometer, rotating a half wave-plate, or quarter wave-plate, moving a grating, using a Bragg cell or using a two frequency laser. Martini (1987) reports a phase shifting technique by stretching an optical fibre with a piezoelectric transducer (PZT). In shearography phase-stepping has been performed by tuning the optical wavelength in conjunction with an imbalanced Michelson Interferometer (Huang *et al* 1996) and by polarisation modulation performed by stretching an optical fibre (Valera and Jones 1997). An alternative technique is to simultaneously record phase-stepped images using multiple cameras. This is described by Kujawinska (1993).

The approaches taken in the experimental sections of this thesis are changing the optical wavelength in Chapter 4 and moving a mirror with a PZT in Chapters 6 and 7.

2.5.2. Phase-Stepping Algorithms

There are a wide range of phase-stepping algorithms varying from algorithms with a few phase-steps to error correcting algorithms with more steps. In this section a simple three-step algorithm is derived then algorithms with higher frame numbers including some of the error correcting algorithms available are discussed.

Automatic phase stepped interferogram analysis can be performed using 'temporal phase stepping speckle correlation' (TPSSC) (Nakadate and Saito 1985) or 'digital

phase stepping speckle interferometry'(DiPSSI) (Creath 1985). TPSSC provides images showing the individual images at different phase steps. A reference frame is recorded before deformation of the object. Then the object is deformed and three, or more, phase-stepped interferograms are recorded. By subtracting each of these three phase-stepped interferograms individually from the reference frame, and taking the absolute value, individual phase-stepped images containing correlation fringes are obtained. As an alternative phase-stepped images of the reference frame may be recorded and a single signal image may be recorded. DiPSSI involves recording phase-stepped images of both the reference and signal images. At each pixel in the image the phase is calculated for both the reference and signal frames before the subtraction is performed.

2.5.2.1.Three-Frame Phase-Stepping Algorithm

The algorithm calculates the phase from three frames which have relative phases 0, $-2\pi/3$ and $+2\pi/3$ (ed. Robinson and Reid). This three-frame algorithm is used in the experimental chapters of this thesis. The intensities, I, for frames A to C are:

$$I_A = I_0\left[1+\gamma\cos\left(\phi-\frac{2\pi}{3}\right)\right] \tag{2.59}$$

$$I_B = I_0\left[1+\gamma\cos(\phi)\right] \tag{2.60}$$

$$I_C = I_0\left[1+\gamma\cos\left(\phi+\frac{2\pi}{3}\right)\right] \tag{2.61}$$

where I_0 is the maximum intensity, γ is the visibility and ϕ is the optical phase.

Expand the cos (A+B) terms:

$$I_A = I_0\left[1+\gamma\left\{\cos\phi\cos\left(\frac{-2\pi}{3}\right)-\sin\phi\sin\left(\frac{-2\pi}{3}\right)\right\}\right] \tag{2.62}$$

$$I_B = I_0[1+\gamma\cos(\phi)] \tag{2.63}$$

$$I_c = I_0\left[1+\gamma\left\{\cos\phi\cos\left(\frac{2\pi}{3}\right)-\sin\phi\sin\left(\frac{2\pi}{3}\right)\right\}\right] \tag{2.64}$$

Simplifying yields:

$$I_A = I_0\left[1+\gamma\left\{-0.5\cos\phi+\frac{\sqrt{3}}{2}\sin\phi\right\}\right] \tag{2.65}$$

$$I_B = I_0[1+\gamma\cos(\phi)] \tag{2.66}$$

$$I_c = I_0\left[1+\gamma\left\{-0.5\cos\phi-\frac{\sqrt{3}}{2}\sin\phi\right\}\right] \tag{2.67}$$

Linear combinations of these equations yield $sin\phi$ and $cos\phi$:

$$\sin\phi = \frac{(I_C - I_A)}{\sqrt{3}I_0\gamma} \tag{2.68}$$

$$\cos\phi = \frac{(2I_B - I_A - I_C)}{3I_o\gamma} \tag{2.69}$$

and tanϕ can be found by:

$$\tan\phi = \sqrt{3}\frac{(I_C - I_A)}{(2I_B - I_C - I_A)} \tag{2.70}$$

This function gives values of ϕ between -π/2 and +π/2. The range of this function can be extended by modifying the arctan function as described in section 2.5.2.2.

2.5.2.2.Modified Arctan Function

It is desirable to extend the arctan function to yield values between -π and +π to simplify and speed up the phase unwrapping process. This is achieved by considering the sign of the individual sine and cosine terms. The modified function is (Creath 1993):

$$\phi_E = \begin{cases} \phi & \sin\phi > 0, \cos\phi > 0 \\ \phi - \pi & \sin\phi > 0, \cos\phi < 0 \\ \phi + \pi & \sin\phi < 0, \cos\phi < 0 \\ \phi - 2\pi & \sin\phi < 0, \cos\phi > 0 \\ \pi/2 & \sin\phi > 0, \cos\phi = 0 \\ \pi & \sin\phi = 0, \cos\phi < 0 \\ 3\pi/2 & \sin\phi < 0, \cos\phi = 0 \\ 0 & \sin\phi = 0, \cos\phi \geq 0 \end{cases} \quad if \qquad (2.71)$$

where ϕ is determined from equation 2.70 and is bounded between -π/2 and +π/2 and ϕ_E is bounded between -π and +π.

2.5.2.3. *Further Phase-Stepping Algorithms*

A number of further phase-stepping algorithms are available and an increase in the number of phase-steps generally increases the complexity of the phase-stepping process but yields better quality results. The redundancy in the phase-stepping algorithms with more steps can allow correction for errors such as illumination intensity changes or phase angle errors.

Creath (1993) provides a detailed description of the available methods. Briefly the more important are given below. The 4-step Carré technique (1966) uses an arbitrary phase-step of α, where α is usually approximately π/2. This algorithm can self calibrate for the phase shift. The five frame technique (Hariharan et al 1987) also uses the π/2 phase-step and records a frame *both* at -π and +π radians. If the phase-step is exactly π/2 these two frames should be identical. A five frame phase-stepping technique that is immune to the variations in illumination intensity, when the phase-stepping is performed using a laser

diode in conjunction with an imbalanced interferometer, is described by Hariharan (1989).

2.5.3. Phase Unwrapping

Phase unwrapping is a technique that is used to remove the phase discontinuities in a wrapped phase map. The phase of light is bounded by $-\pi$ to $+\pi$ radians but when performing a measurement the actual optical pathlength difference in the interferometer is required to recover the measurand.

A number of techniques are available to unwrap phase maps of different image quality and at different speeds. In this thesis commercial software using the 'minimum spanning tree' principle (Ettemeyer 1989) is used. A detailed description of the various phase unwrapping techniques is given by Robinson (1993) and by Judge and Bryanston-Cross (1994).

2.6. Summary

This section contains a comparison of the shearography and the ESPI techniques and a brief summary of phase-stepping techniques.

Sensitivity to:	**Shearography**	**ESPI**
Displacement	No	Yes
Displacement Gradient	Yes	Yes, by differentiation
Out-of-plane Components	Yes	Yes
In-plane Components	Yes	Yes

Surface Strain Components	Yes	Yes, by differentiation
Bulk Strain Components	No	No
Flexural Strain Components	Yes, by differentiation	Yes, by double differentiation
Surface Slope	Yes	Yes, by differentiation
Object Shape	Yes, by integration	Yes
Qualitative Measurement	Yes	Yes
Quantitative Measurement	Yes, potentially with calibration	Yes, with calibration

Table 2.1 Summary of speckle interferometry techniques

Technique	**Comments**
PZT Controlled Mirror	With reference mirror in interferometer or as extra mirror in reference arm
PZT Controlled Fibre	Good in an in-fibre reference arm in ESPI
Wavelength Shifting	Satisfactory if laser wavelength changes are consistent
3 phase-step algorithms	Simple, minimum number of frames but less accurate
More than 3 phase-step algorithms	Allow error correction for either phase or intensity errors

Table 2.2 Summary of phase measurement techniques

2.7 References

Benamati B L, "In search of the Ultimate Image Sensor", pp. 132-136, *Photonics Spectra*, **35**:9, 2001.

Butterns J N and Leendertz J A, "Holographic and Video Techniques applied to Engineering Measurement", *J. Meas. Control*, **4**, pp. 349-354, 1971.

Carré P, "Installation et utilisation du comparateur photoélectric et interféréntiel du Bureau des Poids et Mesures", *Metrologia*, **2**:1, pp. 13-23, 1966.

Creath K, "Digital speckle pattern interferometry (DSPI) using a 100x100 imaging array", *Proc. SPIE* **501**, pp. 292-298, 1984.

Creath K, "Phase-shifting speckle interferometry", *Appl. Opt.*, **24**:18, pp. 3053-3058, 1985.

Creath K, "Temporal Phase Measurement Methods" in ed. Robinson D W and Reid G T, "*Interferogram Analysis Digital Fringe Pattern Measurement Techniques*", Institute of Physics Publishing, Bristol, 1993.

Denby D, Quintanilla G E and Butters J N, "Contouring by electronic speckle pattern interferometry", pp. 171-197, in ed. Robertson E R, "*The Engineering Uses of Coherent Optics*", Cambridge University Press, Cambridge, 1976.

Ettemeyer A, Neuport U, Rottenkolber H and Winter C, "Schnelle und robuste bildanalyse von streifenmustern – ein wichtiger schritt der automation von holografischen profprozessen", *Proc. 1st Int. Workshop on Automatic Processing of Fringe Patterns*, pp. 23-31, 1989.

Goodman J W, "Some fundamental properties of speckle", *J. Opt. Soc. Am.*, **66**:11, pp. 1145-1150, 1976.

Hariharan P, Oreb B F and Eiju T, "Digital phase-shifting interferometry: a simple error-compensating phase calculation algorithm", *Appl. Opt.*, **26**, pp. 2504-2505, 1987.

Hariharan P, "Phase-stepping interferometry with laser diodes: effect of changes in laser power with output wavelength", *Appl. Opt.*, **28**:1, pp. 27-29, 1989.

Huang J-R, Ford H D and Tatam R P, "Phase-stepped speckle shearing interferometer by source wavelength modulation, *Opt. Lett.*, 21, pp. 1421-1423, 1996.

Huang J-R, Ford H D and Tatam R P, "Slope Measurement by Two-wavelength Electronic Shearography", *Opt. Laser. Eng.*, **27**, pp. 321-333, 1997.

Hung Y Y, Turner J L, Tafralian M, Hovanesian J D and Taylor C E, "Optical method for measuring contour slopes of an object", *Appl. Opt.*, **17**:1, pp. 128-131, 1978.

Hung Y Y, "Shearography: a new optical method for strain measurement and nondestructive testing", *Opt. Eng.* **21** (3), pp. 391-395, 1982.

Jaisingh G K and Chiang F P, "Contouring by laser speckle", *Appl. Opt.*, **20**:19, pp. 3385-3387, 1981.

James S W and Tatam R P, "Time-Division-Multiplexed 3D Shearography", *Proc. SPIE* **3744**, pp. 394-403, 1999.

Jones R and Wykes C, "*Holographic and Speckle Interferometry*", p. 147, Cambridge University Press, Cambridge, 2nd edition, 1989.

Judge T R and Bryanston-Cross P J, "A Review of Phase Unwrapping Techniques in Fringe Analysis", *Opt. Laser. Eng.*, **21**, pp. 199-239, 1994.

Kujawinska M, "Spatial Phase Measurement methods", in ed. Robinson D W and Reid G T, "*Interferogram Analysis Digital Fringe Pattern Measurement Techniques*", Institute of Physics Publishing, Bristol, 1993.

Leendertz J A and Butters J N, "An image-shearing speckle pattern interferometer for measuring bending moments", *J. Phy. E.*, **6**, pp. 1107-1110, 1973.

Martini G, "Analysis of a single-mode optical fibre piezoceramic phase modulation", *Opt. Quantum Electron.*, **19**, pp. 179-190, 1987.

Nakadate S, Magome N, Honda T and Tsujiuchi J, "Hybrid holographic interferometer for measuring three-dimensional deformations", *Opt. Eng.*, **20**, pp. 246-252, 1981.

Nakadate S and Saito H, "Fringe scanning speckle-pattern interferometry", *Appl. Opt.*, **24**:14, pp. 2172-2180, 1985.

Parker R J, "Industrial application of holographic interferometry", in ed. Williams D C , "*Optical Methods in Engineering Metrology*", Chapmann and Hall, London, 1993.

Rastogi P K, "An Electronic Pattern Speckle Shearing Interferometer for the Measurement of Surface Slope Variations of Three-Dimensional Objects", *Opt. Laser. Eng.*, **26**, pp. 93-100, 1997.

Robinson D W, "Phase Unwrapping Methods" in ed. Robinson D W and Reid G T, "*Interferogram Analysis Digital Fringe Pattern Measurement Techniques*", Institute of Physics Publishing, Bristol, 1993.

ed. Robinson D W and Reid G T, "*Interferogram Analysis Digital Fringe Pattern Measurement Techniques*", Institute of Physics Publishing, Bristol, 1993.

Takezaki J and Hung Y Y, "Direct Measurement of Flexural Strains in Plates by Shearography", *J. Appl. Mech.*, **53**, pp. 125-129, 1986.

Tay C J, Chau F S, Shang H M, Shim V P W and Toh S L, "The measurement of slope using shearography", *Opt. Laser. Eng.*, **14**, pp. 13-24, 1991.

Valera J D R and Jones J D C, "Strain and Vibration Analysis by Fibre Based Speckle Shearing Interferometry", *Opt. Laser. Eng.*, **26**, pp. 361-376, 1997.

Wyant J C and Shagam R N, "Use of electronic phase measurement techniques in optical testing", *Proc.* **ICO-11**, Madrid, pp. 659-662, 1978.

3. LITERATURE REVIEW

3.1 Introduction

The technique of Electronic Speckle Pattern Interferometry (ESPI) dates from the early 1970s. In this Chapter the chronological development of ESPI and Shearography is detailed with emphasis on the modifications to the technique. This thesis is concerned with strain and shape measurement and in this Chapter defect location, displacement and strain measurement capabilities and the shape and strain measurement capabilities are reviewed.

3.2 Techniques: Early Developments, The 1970s

Leendertz in 1970 described a method of correlating two speckle patterns to yield correlation fringes sensitive to in-plane displacement. This technique used a photographic plate and illumination by a coherent source from two directions, as shown in Figure 3.1. Like the other initial speckle interferometry techniques this was a development of the holographic interferometry techniques already in use (Ennos 1968).

The Electronic Speckle Pattern Interferometry technique (ESPI) was initially demonstrated by Butters and Leendertz (1971), Macovski *et al* (1971), Schwomma (1972) and Köpf (1972). Butters and Leendertz described an ESPI system for in-plane displacement measurement, using illumination from two directions with the speckle interferogram recorded using a TV camera. The correlation fringes were formed by subtraction of speckle interferograms recorded by the camera at a resolution of 180 by

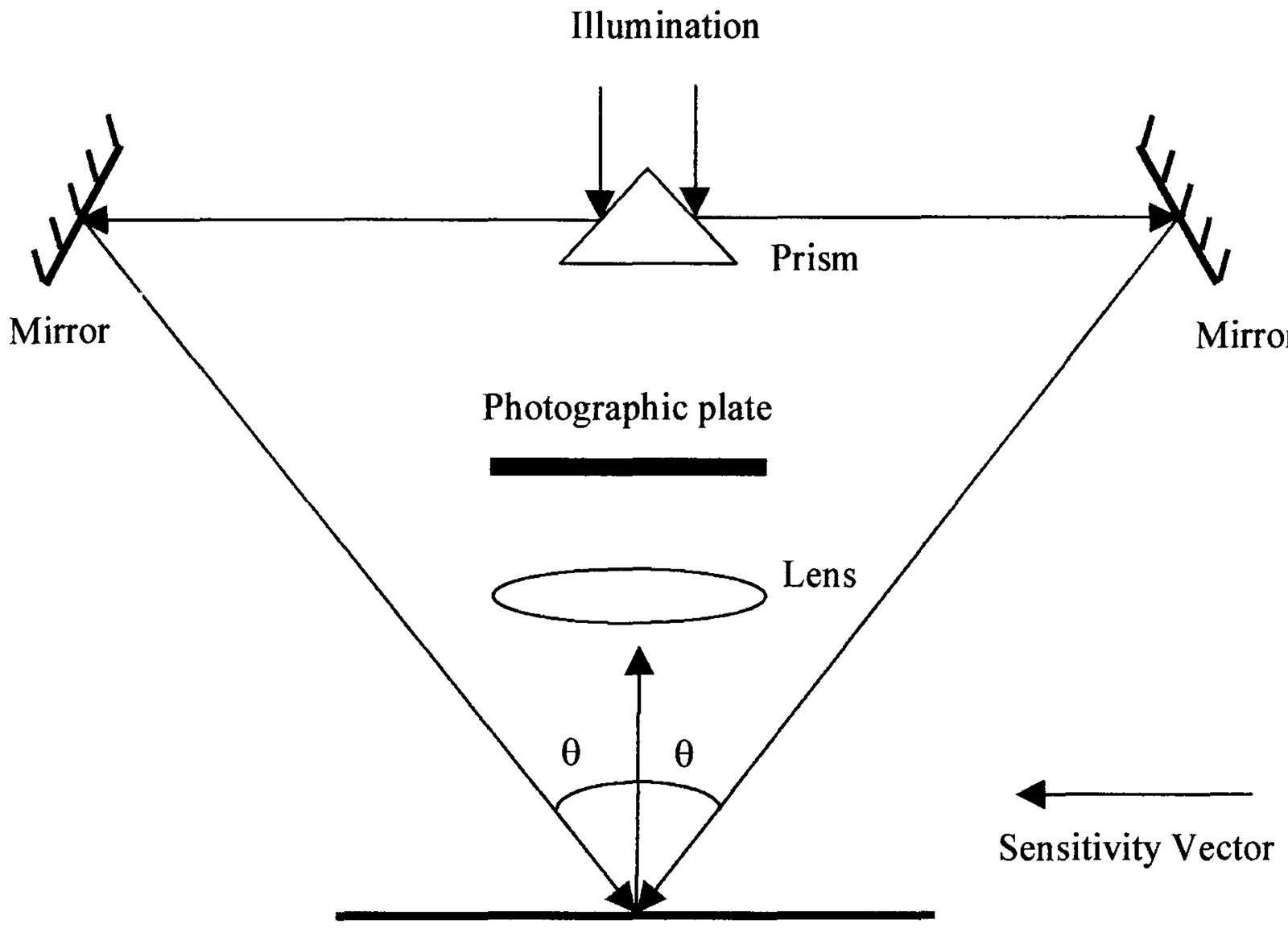

Figure 3.1 The figure shows the dual illumination configuration for the measurement of in-plane displacement using Speckle Pattern Correlation Interferometry (Leendertz 1970). The object is simultaneously illuminated at equal, but opposite angles, from two directions. The image is recorded on a photographic plate.

350 *pixels*. Macovski *et al* used two-beam illumination, a vidicon TV camera and image subtraction to form the correlation fringes. Configurations sensitive to stress and surface contours were presented. Schwomma described an ESPI system using a TV camera and correlation by addition to generate the fringes. Köpf used an ESPI system with a TV camera for vibration mode analysis. Also in 1972 a method of measuring the three components of the displacement and the strain was first described (Hung 1972). This technique used photographic plates and the superposition of photographic negatives.

Duffy (1972) described a two aperture method for measurement of in-plane displacement using Moiré. Subsequently an out-of-plane displacement measurement technique was described by Duffy (1974), again using a two aperture technique but incorporating spatial frequency filtering. Hung and Taylor (1973) applied the two aperture technique to form a shearing interferometer, the apertures incorporating glass wedges.

A speckle interferometry technique to measure displacement gradient, using a shearing interferometer, was first reported in 1973 by Butters and Leendertz. The shear was applied using a Michelson interferometer with a tilt applied to one of the mirrors and the speckle interferograms were recorded using photographic plates, although the possibility of using the electronic image storage techniques, which were under development at the time at Loughborough, UK, was alluded to. The wavefront shearing interferometer used had previously been described by Bates (1947). The speckle shearing interferometer was also described in papers by Hung and Taylor (1974) and

Hung (1974). The first of these papers used a two aperture lens as the shearing device and the second used the shearing Michelson interferometer. Photographic plates were used for both techniques.

The development of the ESPI technique continued through the mid 1970s with papers on in-plane strain measurement by Denby and Leendertz (1974) and a three illumination in-plane strain measurement system to measure the two components of in-plane strain by Jones and Leendertz (1974). Biedermann and Ek (1975) and Løkberg and Høgmoen (1976) continued the development of the ESPI technique by investigating vibration mode behaviour. Biedermann and Ek generated time-average vibration fringes using photographic film and Løkberg and Høgmoen generated time-average vibration fringes using a TV camera and incorporated vibration of a mirror in the reference arm at a fixed frequency to map contours of constant phase. Høgmoen and Løkberg (1977) described the application of this reference phase modulation at a fixed frequency to the measurement of the vibration modes of small objects, including an early biomedical application the analysis of the vibration modes of the malleus and incus of the inner ear. Pulsed ruby lasers were used to study vibration analysis using ESPI by Cookson *et al* (1978). Vibration analysis of unstably vibrating objects, using ESPI and chopped laser light, was reported by Løkberg (1979).

The development of shearography, or speckle shearing interferometry (SSI) as it was commonly known then, was continued by Hariharan (1975) who introduced the use of a diffraction grating as a shearing device and Boone (1975) who introduced a method of

generating slope and strain contours using SSI. Boone generated the slope sensitive fringes by object displacement and rotation.

The phenomena of laser speckle was described in a book by ed. Dainty (1975) which in particular contained an important chapter in the statistical properties of speckle patterns by Goodman (1975). Goodman (1976) continued to publish on the properties of speckle patterns investigating the random walk technique to explain the statistical properties of speckle patterns.

Towards the end of the 1970s the image shearing camera, developed by Hung *et al* (1978) was used to measure the surface slope of objects and to measure surface strains (Hung and Liang 1979). Hung and Durelli (1979) reported a multiple shearing device that could simultaneously record the $\delta w/\delta x$ and the $\delta w/\delta y$ components on a single photographic film.

In summary the early 1970s saw the first ESPI systems, the first shearography systems and further developments of speckle correlation interferometry. In the middle to late 1970s the development of ESPI applied to vibration analysis became one of the main research areas.

3.3 Techniques: Developments in the 1980s

The name 'TV-Holography', or TVH, for Electronic Speckle Pattern Interferometry was first used in 1980 in a paper by Gasvik (1980). This was the main term used for ESPI during the late 1980s and early 1990s although ESPI has reverted to be the more

commonly used term today. Also at the beginning of the 1980s the term 'shearography' for speckle shearing interferometry was coined (Hung 1982) and this is the dominant term in use today. The term shearography was initially applied to the SSI technique using an image shearing camera.

Wykes *et al* (1981) described three ways of improving the fringe contrast in correlation speckle patterns. These were matching the speckle size to the camera resolution, optimizing the ratio, *r*, of the reference to object beams, with *r* of 2 being optimum and *r* from 1 to 20 acceptable, and using the full modulation of the camera in recording speckles. A further paper, Varman and Wykes (1982) described a number of methods of smoothing speckle and Moiré patterns, with consideration given to the limited processing power available. A review of the general parameters for the design and optimization of ESPI systems was published by Jones and Wykes (1981) and the first edition of the reference book on speckle interferometry by Jones and Wykes followed in 1983.

In shearography various methods of generating sheared images were published. These were the use of a Fresnel Biprism (Nakadate *et al* 1980), a glass plate (Chao *et al* 1981), the split-lens (Krishna Murthy *et al* 1982) and the use of a glass wedge in the image-shearing camera (Hung 1982). The image-shearing camera technique is still used today but it has not replaced the original method of shearing the image using a shearing Michelson interfeometer (Butters and Leendertz 1973). The shearing Michelson interferometer is easily adjustable to vary the direction and the magnitude of applied shear but is light inefficient. In 1984 Krishna Murthy *et al* described a radial shearing

interferometer which was insensitive to rigid body motions. Ganeran *et al* (1988) described a universal shearing interferometer, which could apply lateral, radial, rotation and inversion shears. Slettemoen in 1980 described an ESPI system incorporating a speckle reference beam. Whilst the fringe quality was initially not comparable with conventional ESPI systems the speckle reduction system with rotating aperture technique, also described, was able to improve the fringe quality. A comparison between speckle reference ESPI and shearography fringe quality was made in a later paper by Slettemoen and Løkberg (1981). The fringe quality in the paper was comparable between the two techniques. A theoretical analysis of the speckle patterns was also published by Slettemoen (1981).

The first use of optical fibre illumination and imaging was performed by Løkberg and Krakhella (1981) applied to the time-average analysis of vibrating objects. Løkberg and Slettemoen (1981) also presented the addition-subtraction method for comparison of fringes from two vibrating objects. A review of ESPI for vibration analysis was published by Løkberg in 1984.

A more sophisticated technique for the analysis of the fringe patterns produced by ESPI and shearography was required by the mid 1980s. The use of computer processing to enhance the existing methods of fringe counting was described by Nakadate *et al* (1981) and by Nakadate *et al (*1983). This was followed by the introduction of the phase-stepping techniques in speckle interferometry by Nakadate and Saito (1985) and Creath (1985). The technique of phase-stepping in interferometry was originally described by Carré (1966) for interferometric testing. To perform phase-stepping in speckle

interferometry, Nakadate and Saito used a piezoelectric transducer (PZT) controlled mirror in reference arm of the ESPI system and Kreath used a PZT controlled mirror in the signal arm of the ESPI system between the object and the viewing optics. The issue of the difficulty of unwrapping 'noisy' wrapped phase maps is apparent. Spatial median filtering was used by Creath and spatial averaging was used by Nakadate and Saito to improve the quality of the wrapped phase maps before unwrapping. Cheng and Wyant (1985) described techniques for calibration of PZT phase shifters and discussed phase-shifting algorithms. An alternative technique for phase shifting was described by Kothiyal and Delisle (1985) using a rotating phase shifter and a cyclic (Sagnac) interferometer. The interferometer was able to apply either a lateral or radial shear. Phase-shifting, in interferometry, performed by tuning the wavelength of a laser diode in an unbalanced interferometer, was described by Hariharan (1989).

Hung *et al* (1988) described the carrier fringe technique as an alternative method of analysis of correlation fringes in shearography. Carrier fringes were generated by illumination from two source positions, at different distances along the axis of illumination. The deformation of the object distorts the carrier fringes and the phase change due to the carrier fringes can be subtracted to yield the phase of the distortion, without ambiguity.

Review papers of ESPI by Sharp (1989) and of Shearography by Hung (1989) described the developments in speckle interferometer up the end of the 1980s.

In summary the 1980s provided a major step in the evaluation of fringe patterns using the phase-stepping techniques. Also the shearography technique with the capability to generate fringes sensitive to displacement gradient and the range of shearing devices developed in the 1980s, made this technique more important for defect location.

3.4 Techniques: Recent Developments, the 1990s to the Present Day.

A further method of phase-stepping were described by Kadono *et al* (1991) using a liquid crystal cell phase shifter. Krishna Mohan *et al* (1994) described a method of phase-stepping vibration sensitive shearography fringes using a PZT controlled mirror. Bias vibrations, at the frequency of vibration of the object under investigation, are applied to the PZT for positive bias, zero bias and negative bias phase-steps, to obtain the vibration amplitude. Pang and Wu (1996) described the application of temporal phase unwrapping to an ESPI system. The images were processed using a quasi-real-time 2D Fast Fourier Transform (FFT) algorithm. The application of spatial phase-shifting to ESPI and an investigation into phase reconstruction errors is presented by Bothe *et al* (1997). An alternative is described by Huang *et al* (1996) who incorporated a glass block of high refractive index in the longer arm of unbalanced interferometer and used wavelength shifting to perform the phase-stepping. This glass block corrected for the magnification difference between the unbalanced arms of the interferometer. Polarization-multiplexing incorporating phase-stepping, by laser diode current modulation was later described by Groves *et al* (2000).

Joenathan and Torroba (1991) described an ESPI system employing an off-axis reference beam but measuring the out-of-plane displacement component. The other

developments in ESPI were in measuring in-plane displacement and the 3D displacement components. Moore and Tyrer (1996) described an ESPI system which was able to measure the two in-plane displacement components. Illumination was by s-polarisation from two opposing directions in a horizontal plane and by p- polarisation from two opposing directions in a vertical plane. Two cameras were used to measure the two components independently, with a polarisation sensitive beamsplitter cube in front of the cameras to separate the components of polarisation. An alternative method of determining the in-plane deformation was described by Hurtado-Ramos *et al* (2001) where a mirror perpendicular to the object surface and illumination from a single direction was used in conjunction with carrier fringes generated by a source displacement. Adams *et al* (1997) investigated the effect of polarisation on fringe contrast in ESPI. Sohmer and Joenathan (1996) described a method of doubling the sensitivity for in-plane ESPI by illuminating and viewing from the same direction. Tong *et al* (1996) described a conventional in-plane ESPI system but using pulsed lasers to measure in-plane deformation under impact loading. This technique was able to investigate in-plane strain over periods of the order of tens of microseconds.

In shearography, Qin and Dai (1994) described a method for investigating large deformations by recording a sequence of images and correlating pairs of successive images. A control of the fringe density was made by varying the time between pairs of images. Ng (1995) described a method of determining the magnitude of applied shear by digital correlation. Another important issue in shearography is image doubling generating a loss of spatial resolution. This was investigated by Waldner (1996) who reconstructed the displacement field from the displacement gradient field. Shearography

can directly measure in-plane displacement gradient using a dual illumination system, similar to the dual illumination in-plane ESPI technique. This was described initially by Hung and Wang (1996) and subsequently extended to in-plane and out-of-plane displacement gradient measurement by using addition and subtraction by Patorski and Olszak (1997). Aebischer and Waldner (1997) described a shearography system suitable for in-plane and out-of-plane displacement gradient measurement, which could be extended to the measurement of the six displacement gradient components. An interferometer head suitable either for shearography or ESPI was presented by Fomitchov and Krishnaswamy (1997), which has a sliding mirror acting as the switchable element. Sjödahl and Saldner (1997) measured the deformation field of a slot in a Perspex plate using ESPI (TV holography) to measure the out-of-plane deformation field and speckle pattern photography to measure the in-plane deformation field. The use of a diffraction grating as a shearing device for shearography was reported by Henao *et al* (1997). An investigation into the errors present in shearography was made by Abdullah *et al* (1999). A review of shearography applied to strain analysis was published by Steinchen *et al* (1998b).

An overview of the field of interferogram analysis was given by ed. Robinson and Reid (1993). One of the developments in image processing was in the improvement of contrast in addition ESPI fringes by Alcalá Ochoa *et al* (1997). Addition and subtraction were used to extract components in techniques such as those described by Løkberg and Slettemoen (1981), Chatters *et al* (1995), Wang and Krishnaswamy (1996) and Hack *et al* (1998). Another recent development is the use of Wavelet analysis of ESPI

correlation fringes (Li 2000). Andersson *et al* (2000) described the use of speckle pattern photography to correct for rigid body motion in shearography.

Optoelectronic developments in speckle interferometry were reviewed by Tatam (1996 and 1999). These highlighted the increasing use of optical fibres and laser diodes in speckle interferometry and the developments in camera and computer technology.

The measurement of 3D components is an important area for recent developments. 3D shearography systems were reported by Kästle *et al* (1999), Waldner and Brem (1999) and James and Tatam (1999). Kästle *et al* described a multi-wavelength shearography system using three cameras, with wavelength selective filters in front of the camera face. Waldner and Brem described a shearography system which can measure the six components of displacement gradient by sequentially illuminating from 3 directions and with a servomotor attached to the shearing mirror to allow adjustment of the direction and magnitude of applied shear. James and Tatam described a shearography system using time-division-multiplexing, three illumination directions and a single camera. A technique for simultaneously measuring using two shear directions in shearography was described by Siebert and Schmitz (1999). This used polarisation sensitive components in the interferometer head and two cameras. Groves *et al* (2000) described a method of multiplexing the direction of applied shear using laser diode injection current modulation and polarisation sensitive components.

Ettemeyer (2000) described a commercially available ESPI system with a capability to measure 3D deformation components and object shape. This used multiple illumination

directions to measure the 3D components and measures object shape by source displacement (Siebert 2001). Krishna Mohan *et al* (2000) described a number of configurations for shearography for in-plane and out-of-plane displacement gradient measurement and for shape measurement by object rotation.

In summary the main developments over this period are the development of phase-stepping and image processing techniques to extract the phase data and the multi-component deformation and deformation gradient measuring instruments, some incorporating shape measurement.

3.5 Applications: Defect Identification, Displacement and Strain Measurement

The application of speckle interferometry techniques to the identification of defects and the measurement of displacement, displacement gradient and strain is covered in this section.

Speckle techniques are applied to defect location and strain measurement in a wide range for applications, including composite analysis, analysis of material properties, residual stress measurement, weld analysis, high temperature measurements, structural analysis of bridges and packaging seal testing, and in fields as diverse as automotive, aerospace, art conservation, medical, and other general industrial applications. Also pulsed lasers are used to study transient phenomena.

The qualitative analysis of composites is one of the major applications for speckle interferometry due to the anisiotropic behavior of the materials. Shearography has been

used to identify disbonds by Shang *et al* (1991), Hung (1996), Maji and Satpathi (1997), Steinchen *et al* (1998a) and Lanza di Scalea *et al* (2000). Similarly ESPI has also been used to identify disbonds, but also in some cases to perform measurements on composites by Paoletti *et al* (1994), Hertwig *et al* (1996), Zhang *et al* (1998) and Wang W-C *et al* (1998). Comparisons between shearography and ESPI in identifying defects in composites were made by Hung (1997) and Fomitchov *et al* (1997). A review of shearography applied to composite testing was made by Hung (1999). Picart *et al* (2001) described an in-plane ESPI system for measurement of the displacement field, using a Pockels cell to switch illumination polarisation, to perform phase shifting.

Materials properties have also been investigated using ESPI and shearography. Facchini and Zanetta (1995) described the use of ESPI to evaluate the mechanical characteristics of masonry. Moore and Tyrer (1990) described the use of ESPI for the measurement of the stress intensity factor, K_I, and the J-integral in aluminum alloy specimens. Schubach and Ettemeyer (1997) described the use of 3D ESPI for the determination of the strain field in aluminum alloy and Steinchen *et al* (1997) described the use of shearography to measure the 2D-straintensor. Read (1998) used ESPI to measure the Young's modulus of thin films.

Residual stress measurements have been made using shearography and ESPI. Hung (1997) used shearography to measure residual stress in a flat plate, recording interferograms before and after drilling a hole in the plate. For this application shearography has the advantage of insensitivity to rigid body motion. Lira *et al* (1997) describe the application of ESPI to determine the residual stress distribution, due to a

chemical etching process. Zhang and Change (1998) investigated the use of fibre ESPI in the measurement of residual stress due to hold drilling.

3D-ESPI has been applied to the quantitative measurement of welded joints in a T-branch pipe connection, Wang Z *et al* (1998), and in welded joints between plates, Wang and Ettemeyer (1998). The measurement of the six components of displacement gradient of a welded joint in a gas main pipe is the subject of Chapter 7 of this thesis.

Flexural strain analysis has been performed in shearography by Leendertz and Butters (1973) and Takezaki and Hung (1986). Quantitative measurements of flexural strain were performed by Owner-Peterson (1991). Tay *et al* (1994a) reported a multi-exposure technique for the direct determination of second order derivatives in plate bending, using shearography. A comparison between flexural strains determined by shearography and theoretical calculations was made by Yang et al (1996), with good agreement shown.

DSPI (ESPI) was used by Paoletti and Schirripa Spagnolo (1993) to diagnose defects in mural paintings. Shearography was applied to the structural inspection of bridges by Maji *et al* (1997). The rigid body motion of the bridge was sufficient to decorrelate the speckles necessitating the attachment of the shearography system to the bridge itself. The shearography technique was also too sensitive to crack formation for the bridge to be open to normal traffic during the testing. The measurement of the thermal expansion coefficients by ESPI at high temperature was reported by Kim *et al* (1997) and ESPI was applied to characterisation of alloys at temperatures of approximately 1000 °C by

Bhat (1998). Shearography has been applied to the detection of imperfect hermetical seals in microelectronic packages by Hung and Shi (1998).

An application of shearography in the automotive industry is in the non-destructive evaluation of tyres by Hung (1981). ESPI has also been used to investigate the vibration mode behaviour of turbine components by Løkberg and Svenke (1981). Current industrial applications of shearography in the aerospace industry include the non-destructive testing of the GLARE (GLAss REinforced) composite panels as used in the Airbus A380 (Steinchen *et al* 1998a) and for defect location in an on-line inspection system for the Eurocopter blades (Ettemeyer 1998). Steinbichler and Gehring (1996) review the industrial application of TV-holography and holographic interferometry, with an emphasis on vibration mode analysis, but with some discussion of strain field measurement for industrial components.

A medical application is the use of speckle inteferometry to determine the strain field of a canine pericardium membrane by Charette *et al* (1997a, 1997b). The experimental set-up uses transmission of light through the membrane.

Pulsed lasers were originally used to study vibration analysis using ESPI (Cookson *et al* 1978). Considering just the strain characterisation applications here, shearography with a pulsed Nd:YAG laser was used by Spooren *et al* (1993) to investigate deformation of an aluminium plate by a point impact. The pulse separation was varied between 200 μs and 200 ms. A pulsed Nd:YAG laser ESPI (TV holography) system was described by Fernández *et al* (1997) for crack detection in an aluminium beam. Subsequently

Fernández *et al* (2000) described the use of shearography for the measurement of transient out-of-plane displacement gradients in an aluminium plate deformed by a point impact. Davila *et al* (1996) described the use of carrier fringes in pulsed ESPI, which were processed using a Fourier transform technique, yielding a wrapped phase map of the displacement. The Fourier processing removed the constant frequency component of the carrier fringes.

In summary the speckle interferometry techniques of ESPI and shearography have already been demonstrated for a wide range of applications and are particularly important for the highly anisotropic mechanical behaviour of composite materials. Currently the shearography technique is limited to defect location and qualitative assessment of strain fields, whilst ESPI is used for quantitative measurements (Ettemeyer 2000). A future progression is to make quantitative measurements of strain fields using shearography and to consider errors in and calibration of the speckle interferometry techniques. This is necessary to obtain more widespread acceptance of the speckle interferometry techniques against the inertia of established strain measurement techniques, such as resistance strain gauges.

3.6 Applications: Shape and Slope Measurement

There are a number of techniques available to measure shape and slope using speckle interferometry. In this section a brief discussion is made of techniques using illumination by two laser emission lines, a change to the medium the light travels through, a change to the source position or orientation of the object, a change to the illumination conditions and other techniques.

The original speckle interferometry technique to measure shape was described by Denby *et al* (1976) using two of the emission lines of an Argon ion laser. Subsequently Zou *et al* (1996) have demonstrated the two-wavelength contouring technique using two emission lines from a ruby laser in an ESPI system. The emission lines were selected by control of the temperature of the etalons. Two-wavelength contouring using laser diodes has also been reported by Tatam *et al* (1990) in an ESPI system. The emission wavelength of the laser diodes was changed by modulation of the laser diode injection current. A calibration of the laser emission frequency shift, using a highly birefringent optical fibre, was described by Ford *et al* (1993) and applied to the calibration of a two-wavelength surface contouring ESPI system. Huang *et al* (1997) applied the technique of two-wavelength sequential illumination using a laser diode to shearography, generating slope sensitive correlation fringes. An alternative method of changing the emission wavelength is to use temperature modulation of the laser diode as described by Peng *et al* (1992a) for surface contouring using ESPI. A distributed Bragg-reflector (DBR) laser was used by Pfeifer *et al* (1998) to measure 3D topography using the two-wavelength ESPI technique. Simultaneous two-wavelength ESPI was used by Hack *et al* (1998) for surface contouring using the additive-subtractive method of combining interferograms. The additive-subtractive fringe formation method was previously described by Chatters *et al* (1995) for the reduction of noise in vibration analysis using shearography. In additive-subtractive speckle interferometry two images are recorded per camera frame (addition) for the signal frame. The reference frame undergoes continuous phase-shifting during recording to yield the background intensity. Subtracting the reference frame from the signal frame removes this background

intensity. As the addition fringes are recorded over a short period of time they are less sensitive to vibration than correlation by subtraction.

The change in the refractive index of the medium around the object as a method of slope contouring in shearography was described by Hung *et al* (1978).

To generate shape, or slope, sensitive correlation fringes the object has been rotated or tilted. Jaisingh and Chiang (1981) describe a method for surface contouring of 3D objects such as a *light bulb*, introducing an object tilt between camera frames. Subsequently shearography was used by Rastogi (1994) to determine the surface slope of a three-dimensional object by tilting the object. This technique was later modified to incorporate phase-stepping allowing quantitative measurement of slope (Rastogi 1997). An shearography system with a twofold increase in sensitivity to object slope, when the object is rotated, was described by Santhanakrishnan *et al* (1998), allowing the contouring of a more highly curved objects.

A further method of generating shape, or slope sensitive correlation fringes, is to change the illumination conditions. Winther and Slettemoen (1984) described an ESPI contouring technique by tilting the source position. Peng *et al* (1992b) described a dual-beam ESPI system incorporating object tilt to generate shape sensitive correlation fringes. Griffin *et al* (1995) describe a method of generating slope sensitive correlation fringes by tilting a mirror in the illumination path. The slope fringes were integrated to yield object shape.

In shearography Tay *et al* (1991) described a method for the measurement of slope by source displacement. Contouring by ESPI by displacing the illumination position was described by Rodríguez-Vera *et al* (1992). Subsequently, the contribution from the formation of carrier fringes was considered (Tay *et al* 1992), the sensitivity calculation was revised (Tay *et al* 1994b) and the influence of coordinate related fringes was considered (Tay *et al* 1997). Groves *et al* (2001) described the use of slope fringes generated by source displacement in shearography to obtain object shape using a mathematical model to determine measurement sensitivity.

Shape measurement using an ESPI system has been reported using a phase-stepped reference beam and the additive-subtractive method to process the interferograms (Wang and Krishnaswamy 1996). Shang *et al* (2000) applied a large shear in shearography to generate slope sensitive correlation fringes. Curvature can be measured in shearography using a Fourier processing method to extract the curvature measurement from correlation fringes sensitive both to curvature and displacement gradient (KrishnaKumar *et al* 2001).

In summary a number of techniques are in use for slope and shape measurement. Some of the techniques, such as changing the refractive index of the medium around the object, and object rotation for large objects are impractical. The two wavelength techniques and the techniques involving a change to the illumination conditions are useful and the choice depends on the laser stability requirements and whether a simple method for displacing, or tilting, the source can be implemented for that particular application.

3.7 Summary

In summary a wide range of speckle interferometry techniques and applications have been described since the original paper by Leendertz in 1970. In shearography the out-of-plane, in-plane and 3D displacement gradient components have been measured. Switching of the shear direction yields the other three displacement gradient components required to fully characterise the surface strain. Using either the source displacement technique or the two-wavelength technique, fringes sensitive to slope have been generated and these can be integrated to yield object shape. In ESPI, configurations for measurement of out-of-plane displacement, in-plane displacement and all three displacement components have been described. From these displacement measurements the strain fields have been calculated. Alternatively, shape measurement has been performed by ESPI using predominantly the two-wavelength technique.

The main developments of the 1970s were the introduction of the first ESPI and shearography systems and in applying these techniques to vibration analysis. In the 1980s the fringe analysis technique of phase-stepping was introduced and a wide range of shearing devices were introduced. During the 1990s phase-stepping, image processing techniques and multi-component systems were developed further.

The speckle interferometry techniques have been applied in a wide range of industries, but predominantly in the higher technology industries and usually at the development stage rather than for quality control. In particular composites, with their anisotropic behaviour, are widely investigated.

3.8 References

Adams M, Hinsch K D, Lange F and Wolff K, "Polarization effects in speckle correlation metrology", *Opt. Eng.*, **8**, pp. 2225-2228, 1997.

Aebischer H A and Waldner S, "Strain Distributions made Visible with Image-shearing Speckle Pattern Interferometry", *Opt. Laser. Eng.*, **26**, pp. 407-420,1997.

Alcalá Ochoa N, Mendoza Santoyo F, Moore A J and Pérez López C, "Contrast enhancement of electronic speckle pattern interferometry addition fringes", *Appl. Opt.*, **36**:13, pp. 2783-2787, 1997.

Andersson A, Krishna Mohan N, Sjödahl M and Molin N-E, "TV shearography: quantitative measurement of shear-magnitude fields by use of digital speckle photography", *Appl. Opt.*, **39**:16, pp. 2565-2568, 2000.

Bates W J, "A wavefront shearing interferometer", *Proc. Royal Soc.*, **59**, pp. 940-950, 1947.

Bhat G K, "Electronic Speckle Pattern Interferometry Applied to the Characterization of Materials at Elevated Temperature", *Mat. Eval.*, pp. 36-42, January 1998.

Biedermann K and Ek L, "A recording and display system for hologram interferometry with low resolution imaging devices", *J. Phy. E*, **8**, p. 571, 1975.

Boone P M, "Determination of Slope and Strain Contours by Double-exposure Shearing Interferometry", *Expt. Mech.*, pp. 295-302, 1975.

Bothe T, Burke J and Helmers H, "Spatial phase shifting in electronic speckle pattern interferometry: minimization of phase reconstruction errors", *Appl. Opt.*, **36**:22, pp. 5310-5316, 1997.

Butterns J N and Leendertz J A, "Holographic and Video Techniques applied to Engineering Measurement", *J. Meas. Control*, **4**, pp. 349-354, 1971.

Butters J N and Leendertz J A, "An image-shearing speckle-pattern interferometer for measuring bending moments", *J. Phy. E*, **6**, pp.1107-1110, 1973.

Carré P, "Installation et utilisation du comparateur photoélectric et interféréntiel du Bureau des Poids et Mesures", *Metrologia*, **2**:1, pp. 13-23, 1966.

Chao Y J, Sutton M A and Taylor C E, "A simple Tool for Speckle-shearing Interferometry", *Expt. Mech.*, pp. 436-440, 1981.

Charette P G, Hunter I W and Hunter P J, "Large deformation mechanical testing of biological membranes using speckle interferometry in transmission. 1: Experimental apparatus", *Appl. Opt.*, **36**:10, pp. 2238-2245, 1997a.

Charette P G, Hunter I W and Hunter P J, "Large deformation mechanical testing of biological membranes using speckle interferometry in transmission. 2: Finite element modeling", *Appl. Opt.*, **36**:10, pp. 2246-2251, 1997b.

Chatters T C, Pouet B F and Krishnaswamy S, "Additive-subtractive Phase-modulated Shearography with Synchronized Acoustic Stressing", *Expt. Mech.*, **35**, pp. 159-165, 1995.

Cheng Y-Y and Wyant J C, "Phase shifter calibration in phase-shifting interferometry", *Appl. Opt.*, **24**:18, pp. 3049-3052, 1985.

Cookson T J, Butters J N and Pollard H C, "Pulsed lasers in electronic speckle pattern interferometry", *Opt. Laser Technol.*, **10**, pp. 119-124, 1978.

Creath K, "Phase-shifting speckle interferometry", *Appl. Opt.*, **24**:18, pp. 3053-3058, 1985.

ed. Dainty J C, "*Laser Speckle and Related Phenomena*", Springer-Verlag, New York, 1975.

Dávila A, Kerr D and Kaufmann G H, "Fast electro-optical system for pulsed ESPI carrier fringe generation", *Opt. Comm.*, **123**, pp. 457-464, 1996.

Denby D and Leendertz J A, "Plane-surface strain examination by speckle-pattern interferometry using electronic processing", *J. Strain Analysis*, **9**:1, pp.17-25, 1974.

Denby D, Quintanilla G E and Butters J N, "Contouring by electronic speckle pattern interferometry", pp. 171-197, in ed. Robertson E R, "*The Engineering Uses of Coherent Optics*", Cambridge University Press, Cambridge, 1976.

Duffy D E, "Moiré Gauging of In-Plane Displacement Using Double Aperture Imaging", *Appl. Opt.*, **11**:8, pp. 1778-1781, 1972.

Duffy D E, "Measurement of Surface Displacement Normal to the Line of Sight", *Expt. Mech.*, **14**, pp. 378-384, 1974.

Ennos A E, "Measurement of in-plane surface strain by hologram interferometry", *J. Phy. E*, **1**, pp. 731-734, 1968.

Ettemeyer A, "Schnelle und sichere Werkstoff- und Bauteilentwicklung mit modernen Laser-Speckle-Meßtechniken", *Dr. Ettemeyer Applikationbericht, Nr.* **04-98**, 1998.

Ettemeyer A, "Combination of 3-D deformation and shape measurement by electronic speckle-pattern interferometry for quantitative strain-stress analysis", *Opt. Eng.*, **39**:1, pp. 212-215, 2000.

Facchini M and Zanetta P, "An electronic speckle pattern interferometry in-plane system applied to the evaluation of mechanical characteristics of masonry", *Meas. Sci. Technol.*, **6**, pp. 1260-1269, 1995.

Fernández A, Moore A J, Pérez-López C, Doval Á F and Blanco-García J, "Study of transient deformations with pulsed TV holography: application to crack detection", *Appl. Opt.*, **36**:10, pp. 2058-2065, 1997.

Fernández A, Doval Á F, Kaufmann G H, Dávila A, Blanco-García J, Pérez-López C and Fernández J L, "Measurement of transient out-of-plane displacement gradients in plates using double-pulsed subtraction TV shearography", *Opt. Eng.*, **39**:8, pp. 2106-2113, 2000.

Fomitchov P A and Krishnaswamy S, "A compact dual-purpose camera for shearography and electronic speckle pattern interferometry", *Meas. Sci. Technol.*, **8**, pp. 581-583, 1997.

Fomitchov P, Wang L-S and Krishnaswamy S, "Advanced Image-Processing Techniques for Automatic Nondestructive Evaluation of Adhesively-Bonded Structures Using Speckle Interferometry", *J. Nondestr. Eval.*, **16**:4, pp. 215-227, 1997.

Ford H D, Atcha H and Tatam R P, "Optical fibre technique for the measurement of small frequency separations: application to surface profile measurement using electronic speckle pattern interferometry", *Meas. Sci. Technol.*, **4**, pp. 601-607, 1993.

Ganesan A R, Sharma D K and Kothiyal M P, "Universal digital speckle shearing interferometer", *Appl. Opt.*, **27**:22, pp. 4731-4734, 1988.

Gasvik K, "Vibration analysis of a circular saw blade by means of Moiré technique and TV-Holography", *OSA Technical Digest of the Topical Meeting on Hologram Interferometry and Speckle Metrology*, **WA6-1**, 1980.

Goodman J W, "Statistical properties of laser speckle patterns", pp. 9-75, in ed. Dainty J C, "*Laser Speckle and Related Phenomena*", Springer-Verlag, New York, 1975.

Goodman J W, "Some fundamental properties of speckle", *J. Opt. Soc. Am.*, **66**:11, pp. 1145-1150, 1976.

Griffen C T, Hung Y Y and Chen F, "Three-dimensional shape measurement using digital shearography", *Proc. SPIE* **2545**, pp. 214-220, 1995.

Groves R M, James S W and Tatam R P, "Polarization multiplexed and phase-stepped fibre optic shearography using laser wavelength modulation", *Meas. Sci. Technol.*, **11**, pp. 1-7, 2000.

Groves R M, James S W and Tatam R P, "Shape measurement by source displacement in three-dimensional shearography", *Opt. Laser. Eng.*, (submitted), 2001.

Hack E, Frei B, Kästle R and Sennhauser U, "Additive-subtractive two-wavelength ESPI contouring by using a synthetic wavelength phase shift", *Appl. Opt.*, **37**:13, pp. 2591-2597, 1998.

Hariharan P, "Speckle-shearing interferometry: a simple optical system", *Appl. Opt.*, **14**:11, p. 2563, 1975.

Hariharan P, "High-precision, digital, phase-stepping interferometry with laser diodes", *Proc. SPIE* **1162**, pp. 86-91, 1989.

Henao R, Rabal H and Toroba R, "Dynamical digital speckle pattern shearing interferometry", *Optik*, **105**:1, pp. 13-15, 1997.

Hertwig M, Flemming T, Floureux T and Aebischer A, "Speckle Interferometric Damage Investigation of Fibre-reinforced Composites", *Opt. Laser. Eng.*, **24**, pp. 485-504, 1996.

Høgmoen K and Løkberg O J, "Detection and measurement of small vibrations using electronic speckle pattern interferometry", *Appl. Opt.*, **16**:7, pp. 1869-1875, 1977.

Huang J-R, Ford H D and Tatam R P, "Phase-stepped speckle shearing interferometer by source wavelength modulation", *Opt. Lett.*, **21**:18, pp. 1421-1423, 1996.

Huang J-R, Ford H D and Tatam R P, "Slope Measurement by Two-wavelength Electronic Shearography", *Opt. Laser. Eng.*, **27**, pp. 321-333, 1997.

Hung Y Y and Hovanesian J D, "Full-field Surface-strain and Displacement Analysis of Three-dimensional Objects by Speckle Interferometry", *Expt. Mech.*, pp. 454-460, 1972.

Hung Y Y and Taylor C E, "Speckle-shearing interferometric camera - - A tool for measurement of derivatives of surface displacement", *Proc. SPIE* **41**, pp. 169-175, 1973.

Hung Y Y, "A speckle-shearing interferometer: a tool for measuring derivatives of surface displacements", *Opt. Comm.*, **11**:2, pp. 132-135, 1974.

Hung Y Y and Taylor C E, "Measurement of Slopes of Structural Deflections by Speckle-shearing Interferometry", *Expt. Mech.*, pp. 281-285, 1974.

Hung Y Y, Turner J L, Tafralian M, Hovanesian J D and Taylor C E, "Optical method for measuring contour slopes of an object", *Appl. Opt.*, **17**:1, pp. 128-131, 1978.

Hung Y Y and Liang C Y, "Image-shearing camera for direct measurement of surface strains", *Appl. Opt.* **18**:7, pp. 1046-1050, 1979.

Hung Y Y and Durelli A J, "Simultaneous measurement of three displacement derivatives using a multiple image shearing camera", *J. Strain Anal.*, **14**:3, pp. 81-88, 1979.

Hung Y Y, "Shearography: A New Optical Method for Nondestructive Evaluation of Tyres", *Rubber Chem. Technol.*, **54**, pp. 1042-1050, 1981.

Hung Y Y, "Shearography: a new optical method for strain measurement and nondestructive testing", *Opt. Eng.*, **21**:3, pp. 391-395, 1982.

Hung Y Y, Hovanesian J D and Takezaki J, "A Fringe Carrier Technique for Unambiguous Determination of Fringe Orders in Shearography", *Opt. Laser. Eng.*, **8**, pp. 73-81, 1988.

Hung Y Y, "Shearography: A Novel and Practical Approach for Nondestructive Inspection", *J. Nondestructive Eval.*, **8**:2, pp. 55-67, 1989.

Hung Y Y and Wang J Q, "Dual-beam Shift Shearography for Measurement on In-plane Strains", *Opt. Laser. Eng.*, **24**, pp. 403-413, 1996.

Hung Y Y, "Shearography for Non-destructive Evaluation of Composite Structures", *Opt. Laser. Eng.*, **24**, pp. 161-182, 1996.

Hung Y Y, "Digital Shearography versus TV-Holography for Non-destructive Evaluation", *Opt. Laser. Eng.*, **26**, pp. 421-436, 1997.

Hung M Y Y, Long K W and Wang J Q, "Measurement of Residual Stress by Phase Shift shearography", *Opt. Laser. Eng.*, **27**, pp. 61-73, 1997.

Hung Y Y and Shi D H, "Technique for rapid inspection of hermetic seals of microelectronic packages using shearography", *Opt. Eng.*, **37**:5, pp. 1406-1409, 1998.

Hung Y Y, "Applications of digital shearography for testing of composite structures", *Composites B-Eng.*, **30**:7, pp. 765-773, 1999.

Hurtado-Ramos J B, Blanco-García J, Fernández A and Ribas F, "An ESPI system for determining in-plane deformations. Three-dimensional analysis of the carrier fringes and a proposal for analysis of transient in-plane deformations", *Meas. Sci. Technol.*, **12**, pp. 644-651, 2001.

James S W and Tatam R P, "Time-Division-Multiplexed 3D Shearography", *Proc. SPIE* **3744**, pp. 394-403, 1999.

Jaisingh G K and Chiang F P, "Contouring by laser speckle", *Appl. Opt.*, **20**:19, pp. 3385-3387, 1981.

Joenathan C and Torroba R, "Modified electronic speckle pattern interferometer employing an off-axis reference beam", *Appl. Opt.*, **30**:10, pp. 1169-1171, 1991.

Jones R and Leendertz J A, " Elastic constant and strain measurement using a three beam speckle interferometer", *J. Phy. E*, 7, pp. 653-657, 1974.

Jones R and Wykes C, "General parameters for the design and optimization of electronic speckle pattern interferometers", *Optica Acta*, **28**:7, pp. 949-972, 1981.

Jones R and Wykes C, "*Holographic and Speckle Interferometry*", Cambridge University Press, Cambridge, 1st edition, 1983.

Kadono, H, Toyooka S and Iwasaki Y, "Speckle-shearing interferometry using a liquid-crystal cell as a phase modulator", *J. Opt. Soc. Am.*, **8**:12, pp. 2001-2008, 1991.

Kästle R, Hack E and Sennhauser U, "Multiwavelength shearography for quantitative measurements of two-dimensional strain distributions", *Appl. Opt.*, **38**:1, pp. 96-100, 1999.

Kim K-S, Kim J-H, Lee J-K and Jarng S-S, "Measurement of thermal expansion coefficients by electronic speckle pattern interferometry at high temperature", *J. Mat. Sci. Lett.*, **16**, pp. 1753-1756, 1997.

Köpf U, "Der Einsatz von Fernsehanlagenbei der kohärent-optischen Messung mechanischer Schwingungen im µm-Bereich", *Meßtechnik*, **4**:72, pp. 10-108, 1972.

Kothiyal M P and Delisle C, "Shearing interferometer for phase shifting interferometry with polarization phase shifter", *Appl. Opt.*, **24**:24, pp. 4439-4442, 1985.

KrishnaKumar V, Murukeshan V M, Kishen A and Asundi A, "Opto-digital system for curvature measurement", *Opt. Eng.*, **40**:3, pp. 340-341, 2001.

Krishna Mohan N, Saldner H O, Molin N-E, "Electronic shearography applied to static and vibrating objects", *Opt. Comm.*, **108**, pp. 197-202, 1994.

Krishna Mohan N, Andersson A, Sjödahl M and Molin N-E, "Optical Configuration in TV holography for Deformation and Shape Measurement", *Opt. Laser. Eng.*, **10**, pp. 147-159, 2000.

Krishna Murthy R, Sirohi R S and Kothiyal M P, "Speckle shearing interferometry – a new method", *Appl. Opt.*, **21**:16, pp. 2865-2867, 1982.

Krishna Murthy R, Mohanty R K, Sirohi R S and Kothiyal M P, "Radial speckle shearing interferometer and its engineering applications", *Optik*, **61**:1, pp. 85-94, 1984.

Lanza di Scalea F, Spicer J B and Green Jr, R E, "Electronic Shearography with Thermal Loading for Detecting Debonds in Thick Polyurethane/Steel Panels for Marine Applications, *Res. Nondestr. Eval.*, **12**, pp. 43-51, 2000.

Leendertz J A, "Interferometric displacement measurement on scattering surfaces utilizing speckle effect", *J. Phy. E.*, **3**, pp. 214-218, 1970.

Li X, "Wavelet transform for detection of partial fringe patterns induced by defects in nondestructive testing of holographic interferometry and electronic speckle pattern interferometry", *Opt. Eng.*, **39**:10, pp. 2821-2827, 2000.

Lira I H, Vial C, Robinson K, "The ESPI measurement of the residual stress distribution in chemically etched cold-rolled metallic sheets", *Meas. Sci. Technol.*, **8**, pp. 1250-1257, 1997.

Løkberg O J and Høgmoen K , "Use of modulated reference wave in electronic speckle pattern interferometry", *Appl. Opt.*, **15**, pp. 2701-2704, 1976.

Løkberg O J, "Use of chopped laser light in electronic speckle pattern interferometry", *Appl. Opt.* **18**:14, pp. 2377-2384, 1979.

Løkberg O J and Svenke P, "Design and Use of an Electronic Speckle Pattern Interferometer for Testing of Turbine Parts", *Opt. Laser. Eng.*, **2**, pp. 1-12, 1981.

Løkberg O J and Krakhella K, "Electronic speckle pattern interferometry using optical fibres", *Opt. Comm.*, **38**:3, pp. 155-158, 1981.

Løkberg O J and Slettemoen G Å, " Interferometric comparison of displacements by electronic speckle pattern interferometry", *Appl. Opt.*, **20**:15, pp. 2630-2634, 1981.

Løkberg O J, "ESPI – The ultimate holographic tool for vibration analysis?", *J. Acoust. Soc. Am.*, **75**:6, pp. 1783-1791, 1984.

Macovvski A, Ramsey S D and Shaefer L F, "Time-lapse interferometry and contouring using television systems", *Appl. Opt.*, **10**, pp. 2722-2727, 1971.

Maji A K, "Satpathi D and Zawaydeh S, "Assessment of Electronic Shearography for Structural Inspection", *Expt. Mech.*, **37**:2, pp. 197-204, 1997.

Maji A K and Satpathi D, "Electronic Shearography for Detecting Disbonds in Lattice/Skin Structures", *Res. Nondestr. Eval.*, **9**, pp. 1-11, 1997.

Moore A J and Tyrer J R, "An electronic speckle pattern interferometer for complete in-plane displacement measurement", *Meas. Sci. Technol.*, **1**, pp. 1024-1030, 1990.

Moore A J and Tyrer J R, "Two-dimensional Strain Measurement with ESPI", *Opt. Laser. Eng.*, **24**, pp. 381-402, 1996.

Nakadate S, Yatagai T and Saito H, "Digital speckle-pattern shearing interferometry", *Appl. Opt.* **19**:24, pp. 4241-4246, 1980.

Nakadate S, Magome N, Honda T and Tsujiuchi J, "Hybrid holographic interferometer for measuring three-dimensional deformations", *Opt. Eng.*, **20**, pp. 246-252, 1981.

Nakadate S, Yatagai T and Saito H, "Computer-aided speckle pattern interferometry", *Appl. Opt.*, **22**:2, pp. 237-243, 1983.

Nakadate S and Saito H, "Fringe scanning speckle-pattern interferometry", *Appl. Opt.* **24**:14, pp. 2172-2180, 1985.

Ng T W, "Shear measurement in digital speckle shearing interferometry using digital correlation", *Opt. Comm.*, **115**, pp. 241-244, 1995.

Owner-Peterson M, "Digital speckle pattern shearing interferometry: limitations and prospects", *Appl. Opt.*, **30**:19, pp. 2730-2738, 1991.

Pang L and Wu X, "Nondestructive Testing by ESPI and Quasi Phase Shift Gradient Technique", *Opt. Laser. Eng.*, **25**, pp. 93-101, 1996.

Peng X, Zou Y L, Diao H Y and Tiziani H J, "A simplified multi-wavelength ESPI contouring technique based on a diode laser system", *Optik*, **91**, pp. 81-85, 1992a.

Peng X, Diao H Y, Zou Y L, Tiziani H J, "Contouring by modified dual-beam ESPI based on tilting illumination beams", *Optik*, **90**, pp. 61-64, 1992b.

Paoletti D and Schirripa Spagnolo G, "Application of fibre optic digital speckle interferometry to mural painting diagnostics", *Meas. Sci. Technol.*, **4**, pp. 614-618, 1993.

Paoletti D, Schirripa Spagnolo G, Zanettta P, Facchini M and Albrecht D, "Manipulation of speckle fringes for non-destructive testing of defects in composites", *Opt. Laser Technol.*, **26**:2, pp. 99-104, 1994.

Patorski K and Olszak A, "Digital in-plane electronic speckle pattern shearing interferometry", *Opt. Eng.*, **36**:7, pp. 2010-2015, 1997.

Pfeifer T, Wegner R and Mischo H, "Speckle-Interferometrie mit Diodenlasern zur Formprüfung", *Technisches Messen*, **65**, pp. 96-104, 1998.

Picart P, Lolive E and Berthelot J-M, "Characterization of composite materials using a polarizing speckle interferometer", *Opt. Eng.*, **40**:1, pp. 81-89, 2001.

Qin Y and Dai J, "Real-time Interval Technique for Electronic Shearing Speckle Pattern Interferometry", *Opt. Laser. Eng.*, **21**, pp. 241-248, 1994.

Rastogi P K, "Measurement of the derivatives of curved surfaces using speckle interferometry", *J. Mod. Opt.*, **41**:4, pp. 659-661, 1994.

Rastogi P K, "An Electronic Pattern Speckle Shearing Interferometer for the Measurement of Surface Slope Variations of Three-Dimensional Objects", *Opt. Laser. Eng.*, **26**, pp. 93-100, 1997.

Read D T, "Young's modulus of thin films by speckle interferometry", *Meas. Sci. Technol.*, **9**, pp. 676-685, 1998.

ed. Robinson D W and Reid G T, "*Interferogram Analysis Digital Fringe pattern Measurement Techniques*", Institute of Physics Publishing Ltd, Bristol, 1993.

Rodríguez-Vera R, Kerr D and Mendoza-Santoyo F, "Electronic speckle contouring", *J. Opt. Soc. Am. A*, 9, pp.2000-2008, 1992.

Santhanakrishnan T, Palanisamy P K and Sirohi R S, "Optical configuration in speckle shear interferometry for slope change contouring with a twofold increase in sensitivity", *Appl. Opt.*, **37**:16, pp. 3447-3449, 1998.

Schubach H R and Ettemeyer A, "Investigations on Aluminium Alloys with a 3D-ESPI-System", *Dr. Ettemeyer Application Report*, **01-97**, 1997.

Schwomma O, "Holographisch-interferometrishes oder moirémetrisches Verfahren", *Austrian Patent No.* **298 830**, 1972.

Shang H M, Toh S L, Chau F S, Shim V P W and Tay C J, "Locating and Sizing Disbonds in Glassfibre-Reinforced Plastic Plates Using Shearography", *J. Eng. Mat. Technol.*, **113**, pp. 99-103, 1991.

Shang H M, Hung Y Y, Luo W D and Chen F, "Surface profiling using shearography", *Opt. Eng.*, **39**:1, pp. 23-31, 2000.

Sharp B, "Electronic Speckle Pattern Interferometry (ESPI)", *Opt. Laser. Eng.*, **11**, pp. 241-255, 1989.

Siebert Th and Schmitz B, "A New Shearing Setup for Simultaneous Measurement of Two Shear Directions", *Proc. SPIE* **3637**, pp. 225-230, 1999.

Siebert Th, Ettemeyer AG, Germany, Private Communication, 2001.

Sjödahl M and Saldner H O, "Three-dimensional deformation field measurements with simultaneous TV holography and speckle pattern photography", *Appl. Opt.*, **36**:16, pp. 3645-3648, 1997.

Slettemoen G Å, "Electronic speckle pattern interferometric system based on a specular reference beam", *Appl. Opt.*, **19**:4, pp. 616-623, 1980.

Slettemoen G Å, "First-order statistics of displayed speckle patterns in electronic speckle pattern interferometry", *J. Opt. Soc. Am.*, **71**:4, pp. 474-482, 1981.

Slettemoen G Å and Løkberg O J, "Speckle reference ESPI: in practice", *Appl. Opt.* **20**:20, pp. 3467-3469, 1981.

Sohmer A and Jonathan C, "Twofold increase in sensitivity with a dual-beam illumination arrangement for electronic speckle pattern interferometry", *Opt. Eng.*, **35**:7, pp. 1943-1948, 1996.

Spooren R, Dyrseth A A and Vaz M, "Electronic shear interferometry: application of a (double-) pulsed laser", *Appl. Opt.*, **32**:25, pp. 4719-4727, 1993.

Steinbichler H and Gehring G, "TV-Holography and Holographic Interferometry: Industrial Applications", *Opt. Laser. Eng.*, **24**, pp. 111-127, 1996.

Steinchen W, Kupfer G and Lang L X, "Experimental Determination of the 2D-Straintensor by means of Digital Shearography", *Z. Angew. Math. Mech.*, **77**, pp. S493-S496, 1997.

Steinchen W, Yang L, Kupfer G and Mäckel P, "Non-destructive testing of aerospace composite materials using digital shearography", *Proc. Instn Mech, Engrs*, **212**:G, pp. 21-30, 1998a.

Steinchen W, Yang L X, Kupfer G, Mäckel P and Vössing F, "Strain analysis by means of digital shearography: potential, limitations and demonstration", *J. Strain Anal.*, **33**:2, pp. 171-182, 1998b.

Steinchen W, Yang L X, Kupfer G , and Mäckel P, "Non-destructive testing of aerospace composite materials using digital shearography", *Proc. Instn Mech. Engrs*, **212**:G, pp. 21-30, 1998.

Takezaki J and Hung Y Y, "Direct Measurement of Flexural Strains in Plates by Shearography", *J. Appl. Mech.*, **53**, pp. 125-129, 1986.

Tatam R P, Davies J C, Buckberry C H and Jones J D C, "Holographic surface contouring using wavelength modulation of laser diodes", *Opt. Laser Technol.*, **22**:5, pp. 317-321, 1990.

Tatam R P, "Optoelectronic developments in Speckle Interferometry", *Proc. SPIE* **2860**, pp. 194-212, 1996.

Tatam R P, "Speckle interferometry: Optoelectronic developments and applications", *Proc. SPIE* **3745**, pp. 114-133, 1999.

Tay C J, Chau F S, Shang H M, Shim V P W and Toh S L, "The measurement of slope using shearography", *Opt. Laser. Eng.*, 14, pp. 13-24, 1991.

Tay C J, Shang H M, Poo A N and Luo M, "Measurements of surface coordinates and slopes by shearography", *Opt. Laser Technol.*, **24**:4, pp. 209-213, 1992.

Tay C J, Toh S L, Shang H M and Lin Q Y, "Direct determination of second-order derivatives in plate bending using multiple-exposure shearography", *Opt. Laser Technol.*, **26**:2, pp. 91-98, 1994a.

Tay C J, Shang H M, Poo A N and Luo M, "On the Determination of Slope by Shearography", *Opt. Laser. Eng.*, **20**, pp. 207-217, 1994b.

Tay C J, Shang H M and Choong D, "Cross Influence of Coordinate and Slope Related Fringes during Shearographic Profiling", *Opt. Laser. Eng.*, **26**, pp. 259-278, 1997.

Tong J, Zhang D, Li H and Li L, "Study on in-plane displacement measurement under impact loading using digital speckle pattern interferometry", *Opt. Eng.*, **35**:4, pp. 1080-1083, 1996.

Varman P and Wykes C, "Smoothing of speckle and Moiré fringes by computer processing", *Opt. Laser. Eng.*, **3**, pp. 87-100, 1982.

Waldner S, "Removing the image-doubling in shearography by reconstruction of the displacement field", *Opt. Comm.*, **127**, pp. 117-126, 1996.

Waldner S and Brem S, "Compact shearography system for the measurement of 3D deformation", *Proc. SPIE* **3745**, pp. 141-148, 1999.

Wan Abdullah W S, Petzing J N and Tyrer J R, "Developing Accurate Quantified Speckle Shearing Data", *Proc. SPIE* **3744**, pp. 487-496, 1999.

Wang L-S and Krishnaswamy S, "Shape measurement using additive-subtractive phase shifting speckle interferometry", *Meas. Sci. Technol.*, **7**, pp. 1748-1754, 1996.

Wang W-C, Day C-H, Hwang C-H and Chiou T-B, "Nondestructive Evaluation of Composite Materials by ESPI", *Res. Nondestr. Eval.*, **10**, pp. 1-15, 1998.

Wang Z, Lemmens D, Keltjens J and Ettemeyer A, "Strain Analysis on a T-branch Pipe Connection with 3D-ESPI and FEA", *Dr. Ettemeyer Application Report*, **02-98**, 1998.

Wang Z and Ettemeyer A, "Verformungs- und Dehnungsfeld- ermittlung am Schweißpunkt mit 3D-Speckle-Meßverfahren", *Technisches Messen*, **65**, pp. 105-108, 1998.

Winther S and Slettemoen G Å, "An ESPI contouring technique in strain analysis", *Proc. SPIE* **473**, pp. 44-47, 1984.

Wykes C, Butters J N and Jones R, "Fringe contrast in electronic speckle pattern interferometry", *Appl. Opt.*, **20**:5, pp. 750-751, 1991.

Yang L X, Steinchen W and Kupfer G, "Digitale Shearographie für dir direkte Messung der Biege – und Scherdehnungen von dünnen Platten", *Forsch. im Ingenieurwesen – Eng. Res. Bd.*, **6**, pp. 168-174, 1996.

Zhang Z Y, Richardson M O W, Tyrer J R and Petzing J, "Application of phase stepping Electronic Speckle Pattern Interferometry (ESPI) to non-destructive testing of GRP composite materials", *Insight*, **40**:3, pp. 183-187, 1998.

Zhang J and Chong T C, "Fiber electronic speckle pattern interferometry and its applications in residual stress measurements", *Appl. Opt.*, **37**:28, pp. 6707-6715, 1998.

Zou Z-L, Pedrini G and Tiziani H, "Two-wavelength contouring with a pulsed ruby laser by employing TV-holography", *J. Mod. Opt.*, **43**:3, pp. 639-646, 1996.

4. SHEAR DIRECTION MULTIPLEXING IN SHEAROGRAPHY

4.1. Introduction

In a multi-component shearography system multiplexing is required to obtain the six individual components of displacement gradient. In this chapter the various methods of multiplexing the shear direction are discussed. A novel shear direction multiplexing technique, which was used to determine the $\delta w/\delta x$ and the $\delta w/\delta y$ out-of-plane components of displacement gradient, is presented. This technique uses wavelength tuning of a laser diode to perform both the shear direction multiplexing and the phase-stepping. The merits of this approach and issues involved in the implementation are discussed. Results are presented of phase-stepped correlation fringes, wrapped phase maps and unwrapped phase maps.

4.2. Shear Direction Multiplexing Techniques

Full characterisation of the surface strain requires information derived from the use of two orthogonal shear directions. Experimentally the problem is to multiplex between orthogonal shearing directions. This can be done by physically altering the tilt angle of a single shearing mirror, switching between two individual orthogonally tilted shearing mirrors or simultaneously measuring using two interferometers and two cameras. Simultaneous measurement, or measurement at a rate faster than the process under investigation, of two orthogonal displacement gradients is particularly important for objects that behave plastically or where a time history of the object behavior is of interest.

Recent publications have demonstrated a number of methods of multiplexing the shear direction for the measurement of displacement gradient. Kästle *et al* (1999) used a tilting mirror that could be switched between applying a horizontal shear and applying a vertical shear. The mirror was gimbal mounted allowing manual switching of the shear direction and enabling the six components of displacement gradient to be measured. Siebert and Schmitz (1999) described two methods of switching the shear direction. The first is the use of polarisation sensitive components in the interferometer head, recording two shear directions simultaneously using two CCD cameras. The second experimental set-up described in the paper by Siebert and Schmitz used a liquid crystal cell as a rotatable polarisation filter, and a single CCD camera, utilising polarisation division multiplexing to isolate the individual shearing components. Previously the method of polarisation switching described in the experimental part of this chapter had been demonstrated in a laser Doppler velocimeter, utilising the polarisation switching to measure two components of a flow velocity (Pannell *et al* 1988).

4.3. Phase-Stepping Techniques

The range of phase-stepping techniques available has been discussed previously in Chapter 2. Those which are directly relevant to the system described in this chapter are wavelength tuning to change the phase in a pathlength imbalanced interferometer (Ishii *et al* 1987 and Hariharan 1989) and in a speckle system using laser diode injection current modulation (Huang *et al* 1996).

4.4. Polarisation Multiplexed Shearography

In this chapter a shearography system that provides rapid sequential measurements using two orthogonal shear directions and performs phase-stepping using a single CCD camera and no moving mechanical components is described. The light exiting from a highly linearly birefringent optical fibre is switched between two orthogonal linearly polarised states by tuning the optical wavelength of a laser diode, via control of the injection current. A polarisation sensitive Michelson interferometer is used to shear the image in orthogonal directions for p- and s- polarised light. The change in the optical wavelength is also used to produce a phase-step in the pathlength imbalanced polarising Michelson interferometer. Wavelength modulation of a laser diode source is used to accomplish simultaneously the polarisation multiplexing and the phase-stepping in the shearing interferometer. By carefully matching the optical wavelength shift, the optical fibre length and the pathlength imbalance in the interferometer, the $\pi/2$ radians polarisation shift can be matched to the required phase-step.

4.5. Theory

4.5.1. Polarisation Multiplexing by Wavelength Tuning

In highly linearly birefringent fibres the fibre core is stressed to give a difference in refractive index, and hence a difference in the propagation vectors, between two normal modes of orthogonal polarisation (Kaminow 1981). The method of applying the stress to the core varies for different manufacturers. The techniques are either by asymmetry in the fibre or the introduction of stress lobes. Table 4.1 shows the details for different fibre types.

Optical Fibre	Technique of Applying Stress	Details	Beat Length (mm)
Corning PMF-38 Fibre	Asymmetry	Elliptical core	2.3 mm (experimentally determined at 800 nm)
3M PM Fibre	Asymmetry	Elliptical cladding (circular core)	0.9 mm (typical at 633 nm)
Fujikura Panda Fibre	Stress lobes	Circular stress lobes	1.2 mm (typical)
Fibrecore PM Fibre	Stress lobes	'Bow-tie' shaped stress lobes	< 2 mm (at 633 nm)

Table 4.1 Details of polarisation maintaining optical fibre from different manufacturers

For light coupled into a single normal mode the polarisation is maintained along the fibre (Rashleigh 1983). However when light is coupled into both normal modes, the phase difference between the modes varies along the length of the fibre. The phase difference, θ, after a length, L, along the fibre is:

$$\theta = \frac{2\pi\Delta nL}{\lambda} + \theta_0 \tag{4.1}$$

where Δn is the difference in the effective refractive index between the normal modes, λ is the optical wavelength and θ_0 is the initial phase. The beat length of the optical fibre, L_B, can be measured experimentally and is the length of fibre over which a 2π phase change occurs:

$$L_B = \frac{\lambda}{\Delta n} \tag{4.2}$$

The dependence of the phase on the optical wavelength can be used to form a polarisation switch. Differentiating Equation 4.1 and then combining with Equation 4.2 allows the expression for the phase change, $\Delta\theta$, due to a wavelength shift, $\Delta\lambda$, to be derived:

$$\Delta\theta = \frac{2\pi L}{L_B \lambda}\Delta\lambda \tag{4.3}$$

To perform polarisation-multiplexing by switching between orthogonal linear polarisation states requires a phase difference of $\pi/2$ radians between channels.

A Michelson interferometer is commonly used as the shearing device in speckle shearing interferometry (Leendertz and Butters 1973). The reference mirror is fixed and the shearing mirror is tilted to apply a lateral or vertical shear to the image. A polarisation sensitive shearing Michelson interferometer may be formed by the addition of a second shearing mirror and a polarising beamsplitter (PBS), as shown in Figure 4.1. The half-wave plate before the non-polarising beamsplitter (NPBS) is rotated to align the linear polarisation axes of the output from the fibre with that of the PBS.

The system consists of two interferometers, formed between mirrors M_{REF} and M_V, and between mirrors M_{REF} and M_H respectively. A PBS is used to multiplex between the interferometers. Consider p- polarised light first. At the NPBS 50% of the light is reflected to mirror M_{REF}, where it is reflected, passes undeflected through the NPBS and is imaged by the lens onto the camera. The other 50% passes undeflected through the NPBS, then passes undeflected through the PBS onto mirror M_H where a horizontal shear is applied. The reflected beam again passes through the PBS undeflected and is

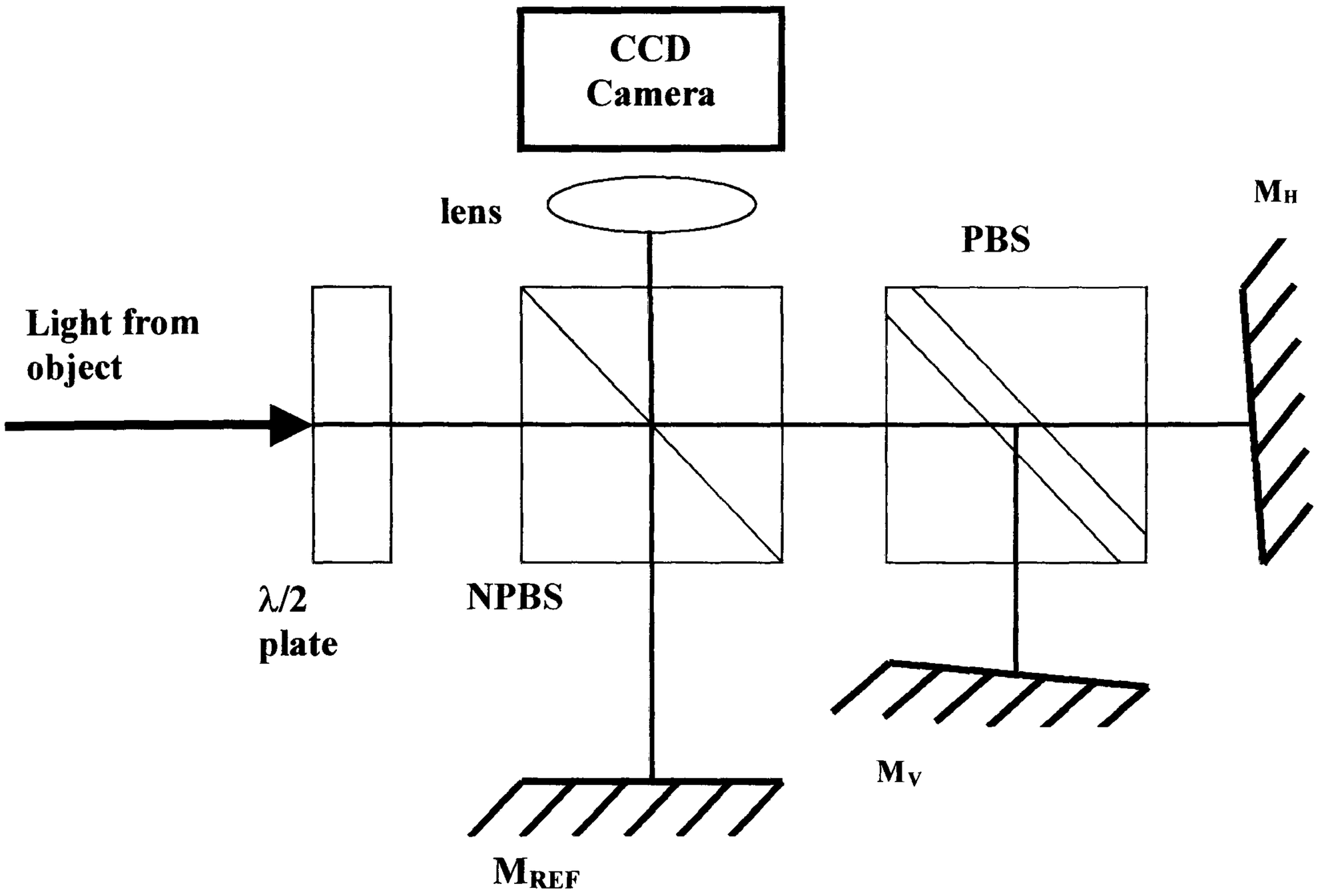

Figure 4.1 Experimental layout of the polarising shearing Michelson interferometer for the sequential measurement of the displacement gradient utilising polarisation division multiplexing and a single CCD camera. λ/2, half-wave plate; NPBS, non-polarising beamsplitter; M_{REF}, reference mirror; PBS, polarising beamsplitter; M_V, vertically shearing mirror; M_H, horizontally shearing mirror.

diverted by the NPBS to be imaged onto the camera. For s- polarised light 50% is also diverted to the reference arm. The light that passes straight through the NPBS is reflected onto mirror M_V by the PBS where a vertical shear is applied. The return path is by reflection at the PBS, then reflection at the NPBS to be imaged by the lens onto the camera. Thus two independently adjustable shears can be applied if two linear polarisations are used.

4.5.2. Phase-Stepping by Wavelength Tuning

Phase-stepping is a technique used in interferometry to recover the optical phase from the intensity. To determine the optical phase, the intensity is measured at three (or more) phase-steps (Creath 1993) and the individual intensities are combined using a phase-stepping algorithm to yield the wrapped phase (bounded between $-\pi$ and π radians).

In speckle interferometry, one or more speckle images are acquired of the object in an undeformed state. The object is then deformed and a number of speckle images are acquired, generally with a known phase-step between them. Subtraction of the images obtained before and after the deformation yields phase-stepped correlation fringes that can be combined using a phase-stepping algorithm to yield a map of the phase, wrapped modulo 2π, across the object surface. The 2π ambiguity is then removed using phase unwrapping techniques (Creath 1993) to obtain, in the case of shearography, the displacement gradient in the shear direction across the object surface.

Temporal phase-stepping speckle interferometry (TPSSC) (Nakadate and Saito 1985) is used in the experimental set-up in this paper. A reference frame is recorded before

deformation of the object. The object is deformed and three phase-stepped speckle images are recorded. Each of the phase-stepped images is subtracted from the reference image and the absolute value taken to yield correlation interferograms. These phase-stepped images are then combined using a phase-stepping algorithm to yield a wrapped phase map and the 2π ambiguity removed by unwrapping (Creath 1993).

The technique described uses injection current modulation to tune the optical wavelength of a laser diode. A change to the laser diode injection current will alter the temperature of the diode and the number of carriers. The variation in temperature changes the length of the cavity, and the number of carriers changes the refractive index of the cavity, the latter of which is the dominant effect (Tatsuno and Tsunoda 1987). The wavelength tuning range is limited by mode hops, which are discontinuous changes in optical frequency with injection current (Chinone *et al* 1985). In a pathlength imbalanced interferometer this wavelength shift is transduced to a phase shift, $\Delta\phi$, given by (Ishii *et al* 1987, Hariharan 1989):

$$\Delta\phi = \frac{2\pi\Delta D}{\lambda^2}\Delta\lambda \tag{4.4}$$

where ΔD is the optical pathlength imbalance, λ is the optical wavelength and $\Delta\lambda$ is the optical wavelength shift.

The pathlength imbalance results in a difference in magnification and focal distance between the two arms of the interferometer. This can be corrected by using a parallel sided glass block of high refractive index in the longer arm (Huang *et al* 1996). This is shown in Figure 4.2. To correct the magnification the required block thickness, t, is:

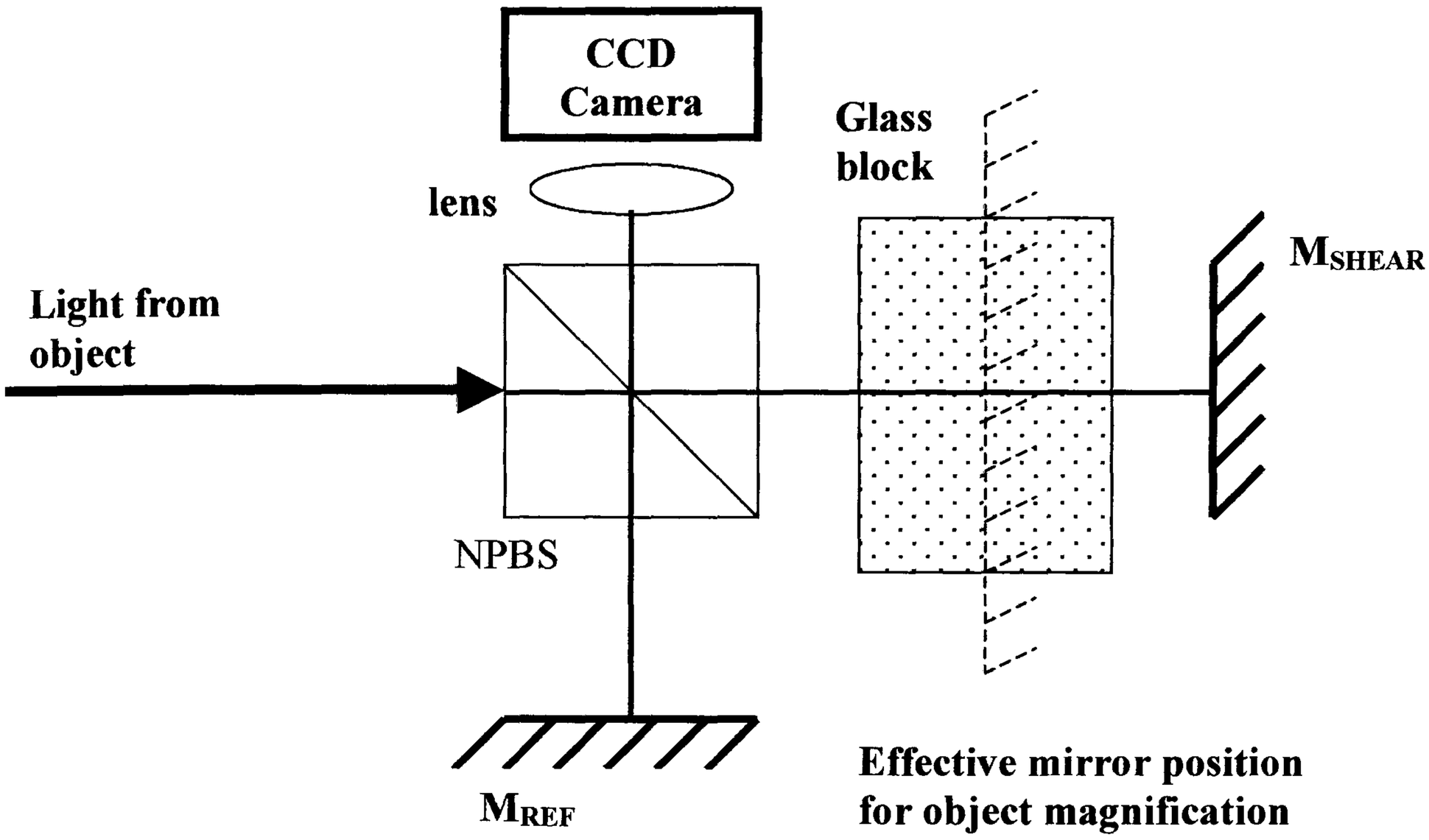

Figure 4.2 The use of a parallel sided block of high refractive index to correct for object magnification in a pathlength imbalanced Michelson interferometer (Huang *et al* 1996). NPBS, non-polarising beamsplitter; M_{REF}, reference mirror, M_{SHEAR}, shearing mirror.

$$t = \Delta d n_b (n_b - 1) \tag{4.5}$$

where Δd is the physical pathlength imbalance and n_b is the refractive index of the block. The use of a glass block also has the advantage of increasing the optical pathlength difference, so that the wavelength shift required to produce a given phase-step is reduced, thus avoiding mode hops. The total optical pathlength difference, ΔD, is:

$$\Delta D = 2\Delta d + 2(n_b - 1)t \tag{4.6}$$

Referring to Equation 4.4, by an appropriate choice of optical pathlength imbalance and wavelength shift, the phase-step required for the phase-stepping algorithm can be generated.

4.5.3. Combined Polarisation Multiplexing and Phase-Stepping

The system described in this chapter implements the polarisation-multiplexing and phase-stepping simultaneously. Combining Equations 4.3 and 4.4 leads to an overall expression for the parameters of the system, which is independent of the wavelength shift.

$$\frac{\Delta\theta}{\Delta\phi} = \frac{L\lambda}{\Delta D L_B} \tag{4.7}$$

To switch between linear polarisations requires a polarisation step, $\Delta\theta$, of $\pi/2$ radians. The phase-step, $\Delta\phi$, is specified by the phase-stepping algorithm used. The optical fibre length, L, optical wavelength, λ, optical fibre beat length, L_B, and optical pathlength difference, ΔD, are chosen to provide the correct ratio between the polarisation step and the phase-step.

4.6. Experimental

4.6.1. Source and Illumination Components

The experimental layout is shown in Figure 4.3. The optical source was a laser diode (SDL model 5411-G1, λ = 801 nm, optical power = 100 mW) powered by a laser diode driver (Seastar Model LD2000). The optical frequency/injection current ratio for the laser is 1.46 GHz mA^{-1}, measured using a Fabry-Perot interferometer (TecOptics model FPI-25 with MS-25 FP plates, 600-950 nm, Free spectral range 41.6 GHz, Finesse 30). The laser diode injection current was externally modulated by a personal computer via a D to A board. The laser was fitted with circular beam correction optics (Blue Sky Research) which produce a circular Gaussian intensity profile with a numerical aperture of 0.1, the same as that of a single mode optical fibre, allowing efficient coupling (>60%). An optical isolator (Optics for Research model 10-5-VIR, 5 mm aperture) was used to reduce feedback into the laser. A quarter-wave plate converts the linear polarisation from the laser diode to circular polarisation to permit equal population of both normal modes of the optical fibre, a 36.6 m length of highly-linearly-birefringent optical fibre (Corning PMF-38, elliptical core, cut-off wavelength 710 nm, beat length 2.3 mm). This fibre was available in sufficient length to limit the optical frequency shift required to switch between orthogonal polarisation states so the laser does not mode hop. The output from the fibre was expanded and used to illuminate the test object.

4.6.2. Image Capture and Processing Components

The object was imaged through a pathlength imbalanced polarising Michelson interferometer, which allows both polarisation multiplexing and phase-stepping. By matching the optical frequency shift, the length of optical fibre and the pathlength

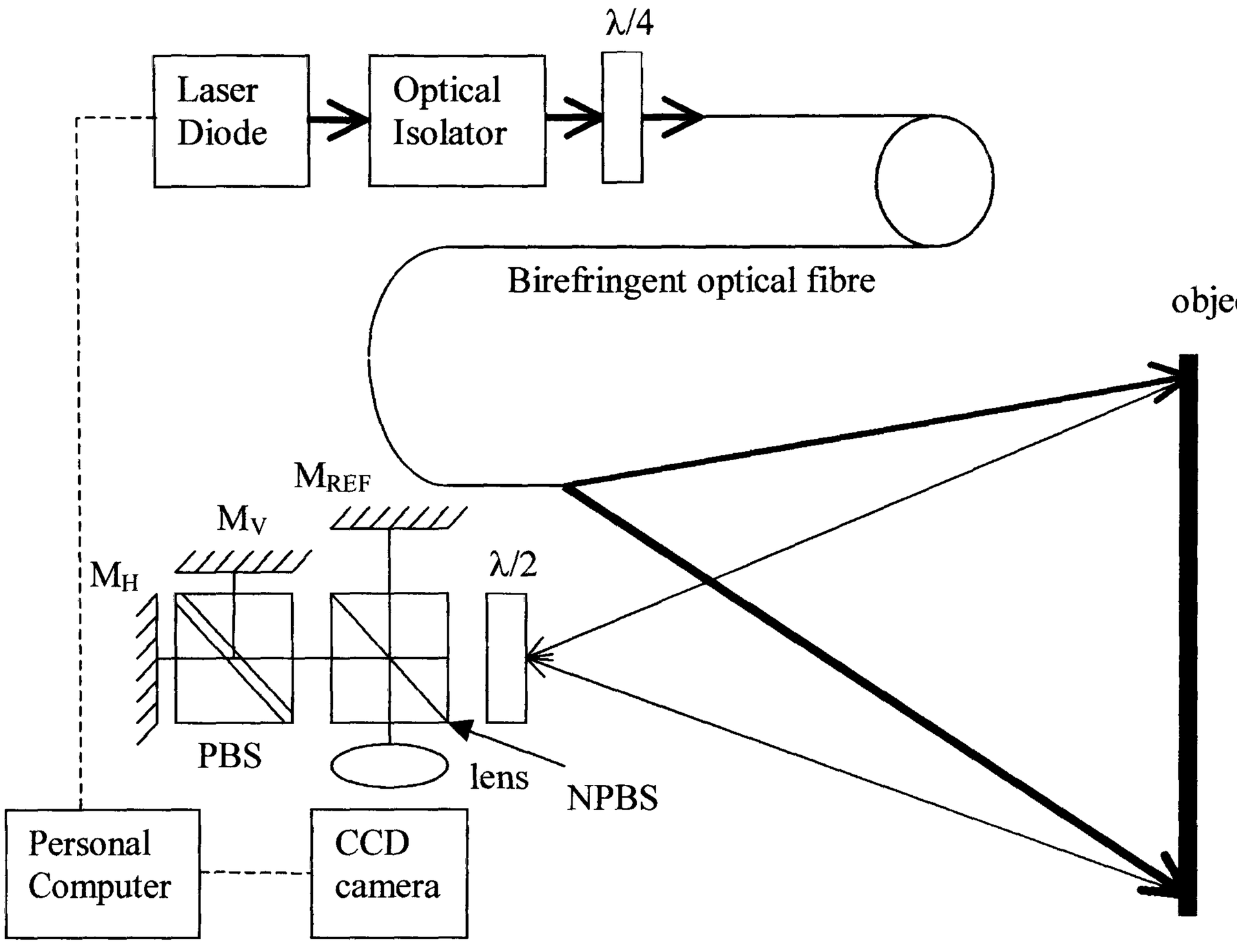

Figure 4.3 Experimental layout of the shearography system utilising wavelength tuning to perform the polarisation multiplexing of the shear direction and the phase-stepping. λ/4, quarter-wave plate; λ/2, half-wave plate; NPBS, non-polarising beamsplitter; M_{REF}, reference mirror; PBS, polarising beamsplitter; M_V, vertically shearing mirror; M_H, horizontally shearing mirror.

imbalance in the interferometer a change in the polarisation of π radians gave the phase-step of $2\pi/3$ radians which was required for the 3-step phase-stepping algorithm used. The physical pathlength imbalance in the interferometer arm, 7.5 ± 0.5 mm, was such that the thickness and refractive index of the PBS corrected the magnification difference between the arms of the interferometer, as described in Section 4.5.2, without additional optical components. The optical pathlength imbalance was 33.6 ± 0.5 mm.

An area scan 8-bit CCD camera (Dalsa CA-D4-0512A, 512 by 512 pixel array, frame rate 75 Hz) was used to record the speckle images, in conjunction with a PCI bus frame transfer card (Bitflow Roadrunner).

4.6.3. Image Acquisition, Timing and Image Processing

Laser diode injection current modulation and image frame capture were controlled by a PC (Pentium I) using a program written in Labview software by Dr S W James. For each of the 2 linear polarisations a reference frame of the object, before deformation, and three phase-stepped images of the object after deformation were captured. A three phase-step algorithm was chosen for simplicity and because the length of the optical fibre used was insufficient to allow for more polarisation steps to be made without the optical frequency shift required causing the laser to experience a mode hop. Four-step, five-step and six-step phase-stepping algorithms could be implemented by selection of suitable optical fibre length, beat length and optical wavelength shift. The laser diode injection current change, ΔI, required to change the polarisation by π radians (and the

phase by $2\pi/3$ radians) is 8.06 mA (equivalent to an optical frequency shift of 11.8 GHz).

A reference frame was recorded with a current of $I_B+\Delta I$ applied, corresponding to s-polarisation and zero phase. Then the object was deformed and three phase-stepped images (all with s- polarisation) were recorded with the injection current at I_B, $I_B+\Delta I$ and $I_B+2\Delta I$. To record frames with p- polarisation the sequence was repeated but with $+^1/_2\ \Delta I$ added to the bias current. In practice the current steps were arranged such that both reference frames were recorded before the object was deformed and the six image frames were recorded after. The waveform applied to the laser diode's injection current to achieve this and the resulting polarisation state and optical phase are shown in Figure 4.4(a).

4.6.4. Laser Diode Characteristics

To permit the necessary injection current steps without the laser mode hopping the stable operating regime, for laser diode injection current and temperature, was determined for the SDL Model 5411-G1 laser diode. Laser diode temperatures between 15.0 °C and 25.0 °C were investigated for mode hop instability using a flat plate Fabry-Perot interferometer (TecOptics model FPI-25, Free spectral range 41.6 GHz). The mode hops discontinuities for increasing and decreasing laser diode injection current displayed hysterisis. The slope of the lines of mode hop discontinuity was determined to be –19.3 mA/°C, between 106.0 and 97.1 mA, by keeping the optical wavelength fixed, using the flat plate Fabry-Perot interferometer. Further, by keeping the optical

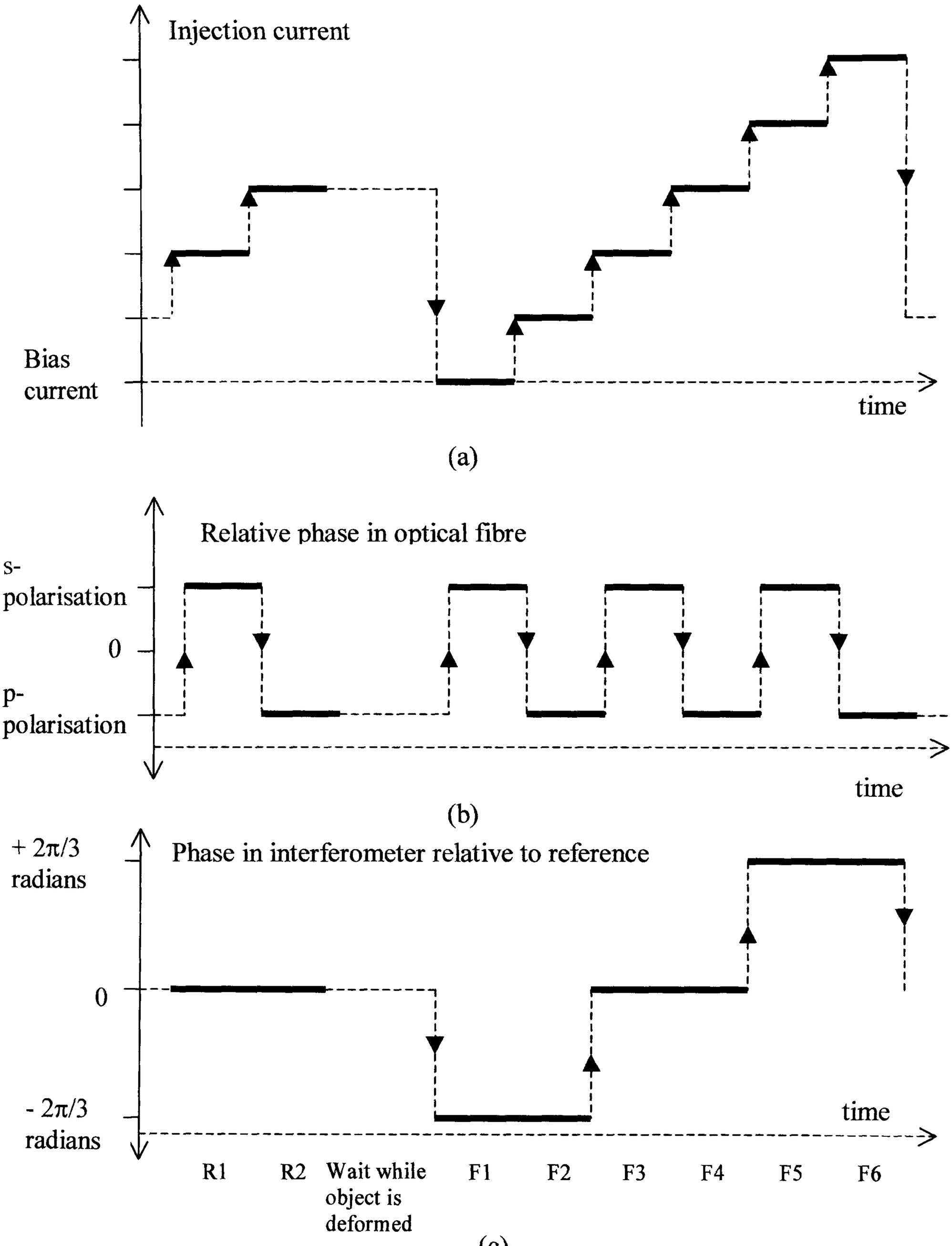

Figure 4.4 (a) waveform applied to laser diode injection current, (b) the polarisation state of the light exiting the distal end of the fibre against time and (c) the relative phase of light in the interferometer, compared with the reference frame of the same polarisation, against time. R1, R2, reference frames; F1 to F6, signal frames.

wavelength fixed, by small adjustments to both the injection current and the temperature, it was possible to follow a path from 105 to 30 mA without experiencing a mode hop. The temperature was adjusted between 15.5 and 18.9 °C to achieve this. This injection current and temperature information was used to select a stable operating region to operate the laser diode for the shearography experimental layout.

The laser diode was operated close to its' maximum output power (100 mW, coupling efficiency, η, of 0.35) and at a temperature where the diode operation was stable in a single longitudinal mode. An operating temperature in the range 16.02 to 16.26 °C was required to operate the laser diode with a stable longitudinal, single mode spectrum, close to its' maximum output power. The diode operated without mode hopping between injection currents of 89.4 mA and 108.6 mA when the injection current was increased and between 104.9 mA and 85.7 mA when the injection current was reduced. Stepping the diode through the required 6 current steps required a total current range of 20.1 mA which was greater than the 19.2 mA range between mode hops. Exploiting the hysterisis in the diode behaviour allowed a stable region between 85.7 mA and 108.6 mA (22.9 mA) to be used.

The injection current waveform which exploits this hysterisis in the laser performance is shown in Figure 4.4(a). The sequence in which the reference frames were recorded required that the injection current steps were positive. Following the loading of the object, the injection current was reduced to the lower limit of stable operation current range, and subsequent steps used positive changes in injection current. This allowed full exploitation of the hysterisis cycle. An injection current step frequency of 1 Hz was

chosen to allow the output wavelength to stabilise, although this parameter was not optimised.

4.6.5. Phase-Stepping

The images were processed using a 3 step, $2\pi/3$ phase step TPSSC algorithm (Creath 1993).

$$\phi = \tan^{-1}\left[\frac{\sqrt{3}(I_1 - I_3)}{(2I_2 - I_1 - I_3)}\right] \tag{4.8}$$

where ϕ is the phase and I_1, I_2 and I_3 are the images containing phase-stepped correlation fringes. An arctan function bounded between $-\pi$ and π radians was used to generate the wrapped phase maps. The wrapped phase map for s- polarisation state contains fringes that contour the deformation gradients in the vertical direction, Equation 4.9. For p- polarisation state the wrapped phase map contains fringes that contour the deformation gradients in the horizontal direction, Equation 4.10.

$$M_V = \tan^{-1}\left[\frac{\sqrt{3}\left(|F_1 - R_1| - |F_5 - R_1|\right)}{2|F_3 - R_1| - |F_1 - R_1| - |F_5 - R_1|}\right] \tag{4.9}$$

$$M_H = \tan^{-1}\left[\frac{\sqrt{3}\left(|F_2 - R_2| - |F_6 - R_2|\right)}{2|F_4 - R_2| - |F_2 - R_2| - |F_6 - R_2|}\right] \tag{4.10}$$

Both wrapped phase maps, M_V and M_H were unwrapped using ISTRA software (Ettemeyer AG) which uses the minimum spanning tree technique (Ettemeyer *et al* 1989).

4.7. Results and Discussion

A flat aluminium plate (150 mm x 180 mm), clamped around the perimeter was used as the test object. The centre of the plate was subjected to a point out-of-plane displacement, of a few μm, using a micrometer. The plate was coated with Scotchlite 7210 Silver Reflective Liquid which was found not to significantly depolarise the light reflected from the surface. Polarisation issues are discussed in Section 4.7.1.

Image acquisition followed the sequence described in section 4.6.3. Figure 4.5(a, b, c) show the 3 phase-stepped images obtained from s- polarised light. The applied shear was 10 mm, in the vertical direction, and the phase-step was $2\pi/3$ radians. Similarly Figure 4.5(d, e, f) show the 3 phase-stepped images from p- polarised light, with a horizontal shear of 10 mm and a phase-step of $2\pi/3$ radians. The fringes were combined to produce two wrapped phase maps using Equations 4.9 and 4.10; these are shown in Figure 4.6(a and b). In all these figures the correlation fringes can be clearly seen demonstrating the operation of the polarisation-multiplexing regime. Figure 4.6(c and d) shows the unwrapped phase maps for vertical and horizontal shear.

4.7.1. Polarisation Issues

Systems using polarisation as a multiplexing parameter must ensure that the polarisation is sufficiently maintained for demultiplexing. In the system presented here, the polarisation of the illumination must be maintained when scattered at the object surface (Moore and Tyrer 1990) so that the linear polarisations can be separated in the interferometer. In this system, with near to normal illumination and detection, various

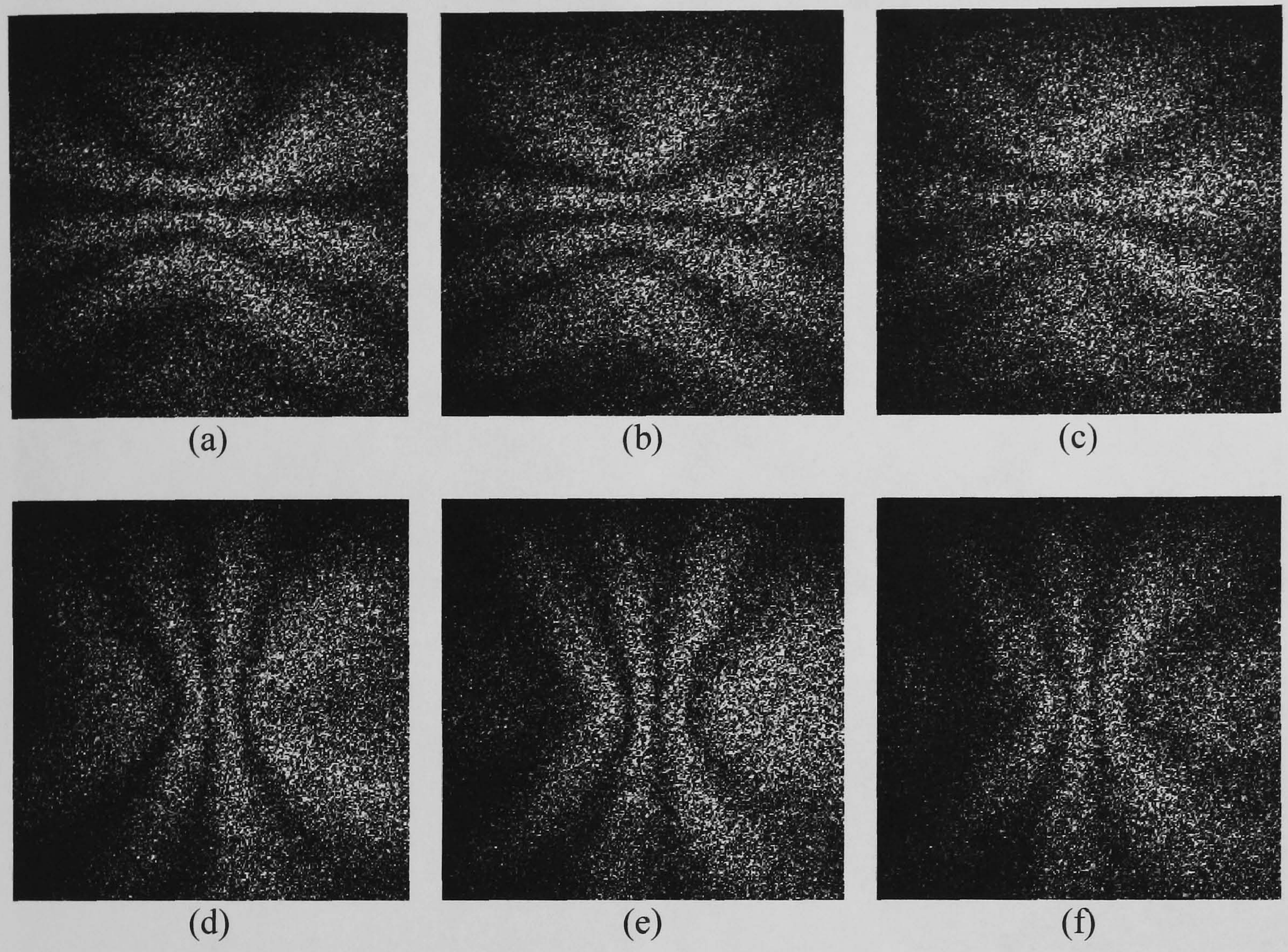

Figure 4.5 (a), (b) and (c) are phase-stepped images with a vertical shear of 10 mm applied. (d), (e) and (f) are phase-stepped images with a horizontal shear of 10 mm applied. The deformation applied to the object is a point deformation, out-of-plane, approximately at the centre of the field of view. To improve image quality the contrast of the images presented here was increased using Paintshop Pro software.

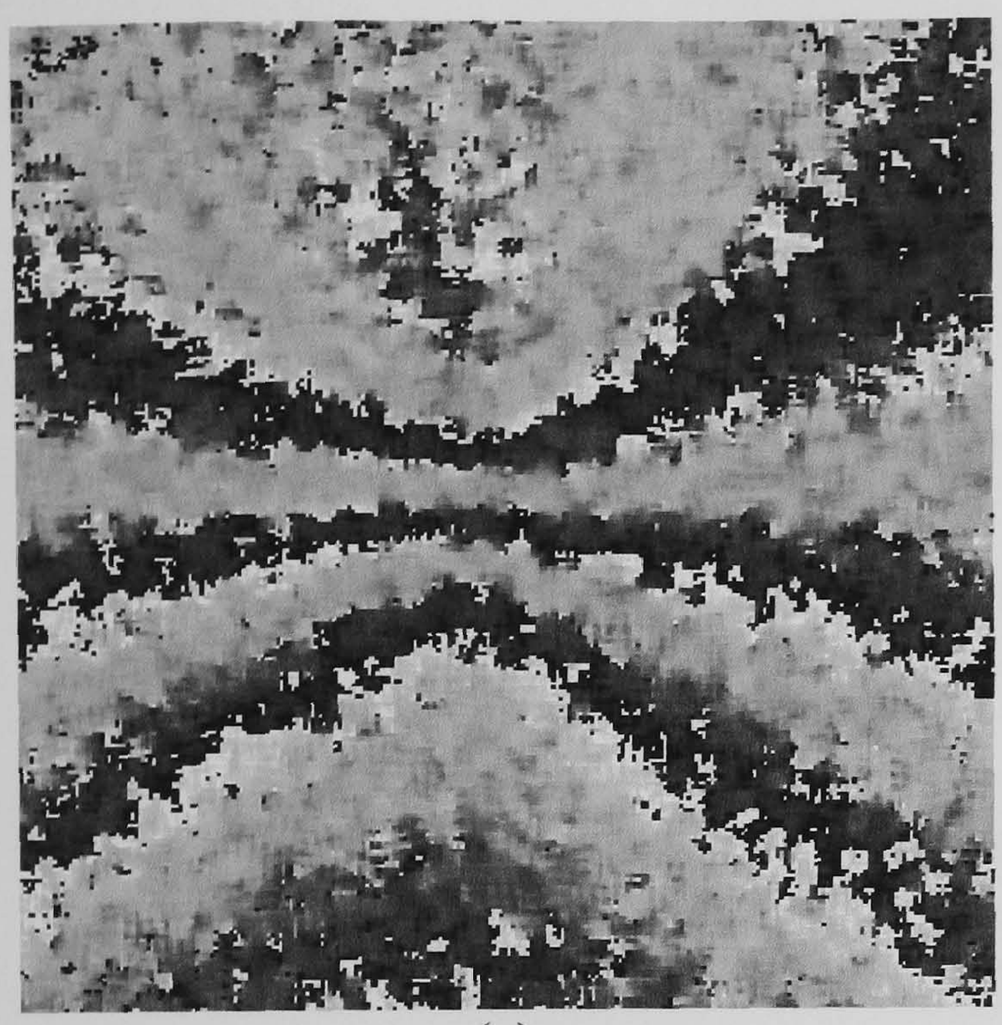

(a)

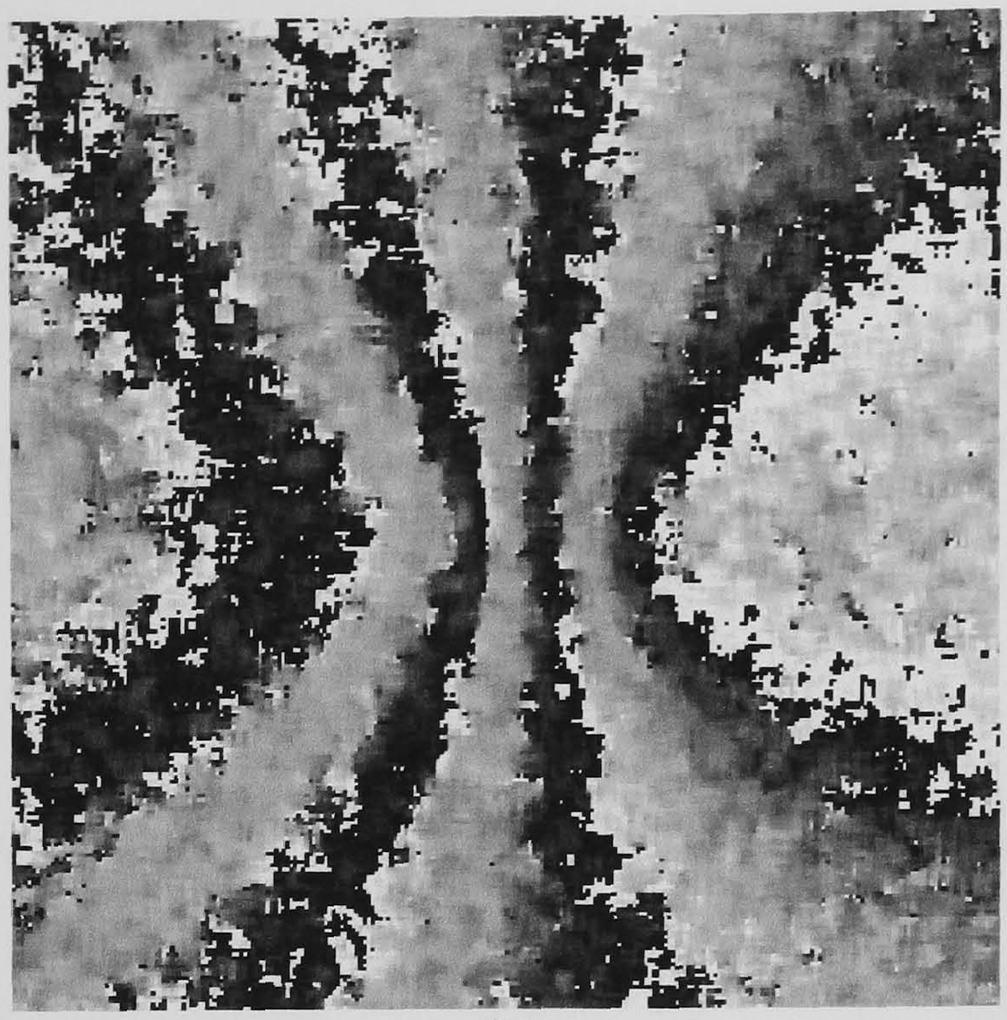

(b)

(c)

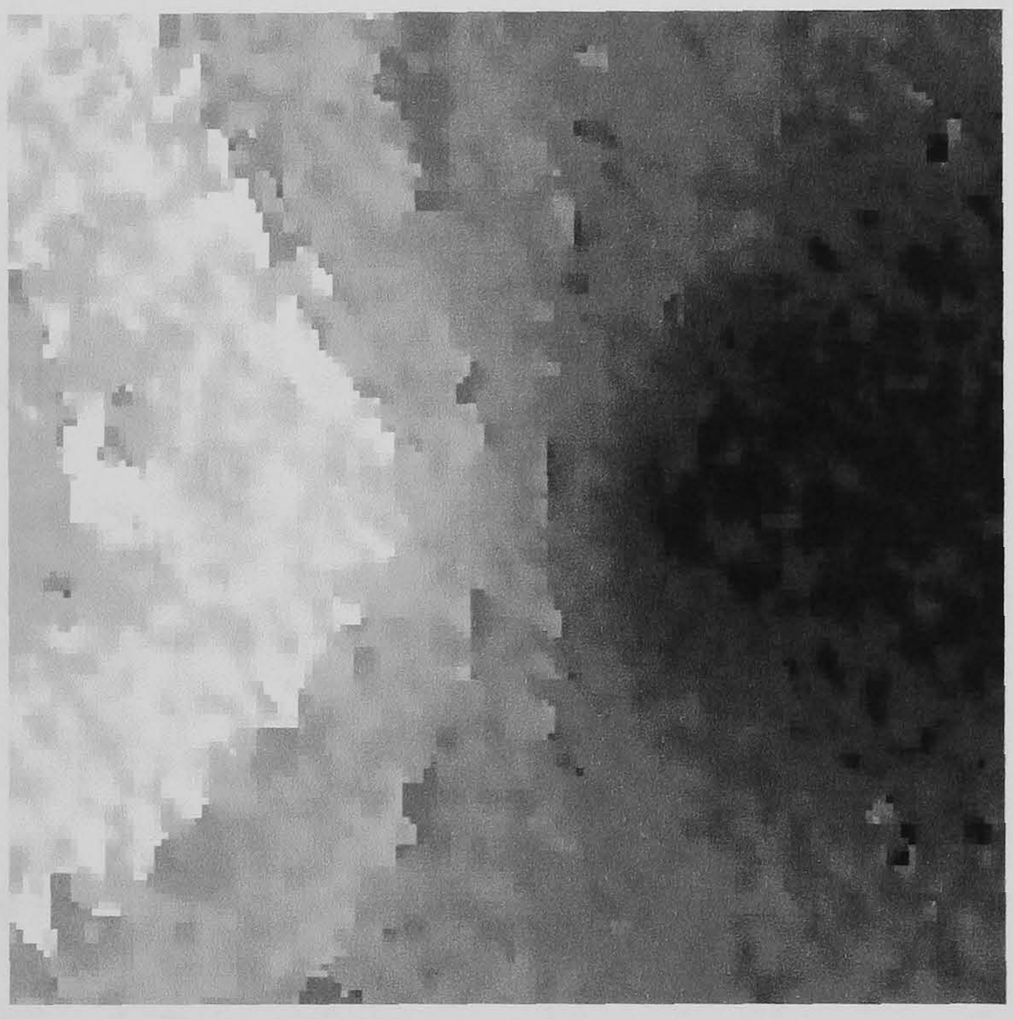

(d)

Figure 4.6 (a) and (b) are wrapped phase maps with a 10 mm shear applied in the vertical and horizontal directions respectively. (c) and (d) are the unwrapped phase maps showing displacement gradient for an point displacement, out-of-plane. For presentation here the intensities of the unwrapped phase maps were expanded to the full greyscale range using Paintshop Pro software.

painted surfaces were tested and 3M Scotchlite Silver Reflective Liquid was found to give the best performance.

Polarisation discrimination throughout the system, including the test object, was measured. This was measured by removing the camera and replacing with a polariser and optical power meter. A measurement of the s- and p- polarisation optical powers was made for incident s- and p- polarisation, set by adjusting the laser diode injection current, and the ratio measured was 7 dB.

An optical fibre with a shorter beatlength ideally with less sensitivity to temperature variations could be used to reduce polarisation drift. Polarisation drift due to changes in the fibre temperature can be corrected by applying a voltage to a fibre wrapped PZT (Jackson *et al* 1980) before starting the image capture sequence. To reduce the sensitivity of the polarisation to temperature fluctuations the main length of fibre could be placed in a temperature controlled box. Input and output fibres to the main length may be made temperature insensitive by coupling light along a single normal mode, and rotating the input and output leads by 45° before fusion splicing to the main fibre length (Ford and Tatam 1993). Additionally, active stabilisation by monitoring the state of polarisation of the Fresnel reflection from the distal end of the fibre can be used (Pannell *et al* 1988).

4.7.2. Phase Errors

Phase errors, which distort the wrapped phase map, arise from two sources in the experiment; inaccuracy in the pathlength imbalance in the interferometer and amplitude

modulation of the source. Knowledge of the laser behaviour and tolerances reduced pathlength imbalance error to 2.2 %. This error is composed of errors in setting the laser diode injection current (0.6 %), and errors in matching the pathlength imbalance between the s- polarisation and p- polarisation arms in the interferometer (2.1 %). It is assumed that the phase-step can be optimised for a single interferometer by reviewing the quality of the phase maps produced. This phase error due to matching pathlengths in the interferometer could be reduced further by mounting the shearing mirrors on a linear translation stage so that fine adjustment of pathlength imbalance may be made. A phase-stepping algorithm that corrects for small errors in the phase could also be used (Carré 1966).

The phase errors across the object due to the tilt of the mirror were found to be negligible (0.05 %). This value was calculated using typical system parameters of an applied shear of 10 mm and the test object at a distance of 300 mm from the shearing Michelson interferometer.

The output power of the laser diode is dependent on injection current. To obtain phase-stepped images containing correlation fringes, whilst minimising intensity differences between images, the reference frame was recorded with the same injection current as the middle image frame. The maximum intensity change relative to the reference frame is 12 %. For the algorithm used the resulting phase error is 12.2 %. This can be reduced to 2.4 % by phase-stepping both the reference frames and the frames recorded after deformation (Creath 1985) and phase errors due to a linear intensity change can be removed using a 6-step algorithm (Ishii and Onodera 1995).

To determine the values of phase error due to intensity variation a mathematical model was generated using Mathcad software. The phase error for signal phase, ϕ, and reference phase, θ, for all values of ϕ and θ between $-\pi$ and $+\pi$ radians, was calculated by considering $\phi+\theta$. The error for each individual phase-stepping algorithm was calculated. Figure 4.7 shows the mathematically calculated phase maps for (a) the 3-step phase-stepping algorithm used experimentally and (b) a 3-step phase stepping algorithm additionally incorporating 3 phase steps for the reference frames. Further calculation, using the same program, showed that the 6-step algorithm proposed by Ishii and Ondera (1995) was successful in correcting for phase errors due the intensity.

Alternatively the intensity can be normalised by monitoring the intensity at the laser diode monitor photodiode or by monitoring the intensity of light reflected from the distal face of the optical fibre using a photodiode and applying a correction (Tatsuno and Tsunoda 1987). To increase the number of phase-steps, longer optical fibre, fibre with a shorter beatlength or the use of a source tunable over a larger optical frequency is required. External cavity diode lasers, using the Littrow design, are currently available with up to 120 mW optical power, and tuneable between 810 and 825 nm (Toptica Photonics). This compares with the 200 mW optical power single-mode laser diodes currently available (SDL 5430 series).

4.7.3. Summary

The magnitude of the orthogonal shears and thus the measurement sensitivity are independently adjustable in this system to allow measurement of differing magnitudes of displacement gradient in the different shear directions. The implementation described

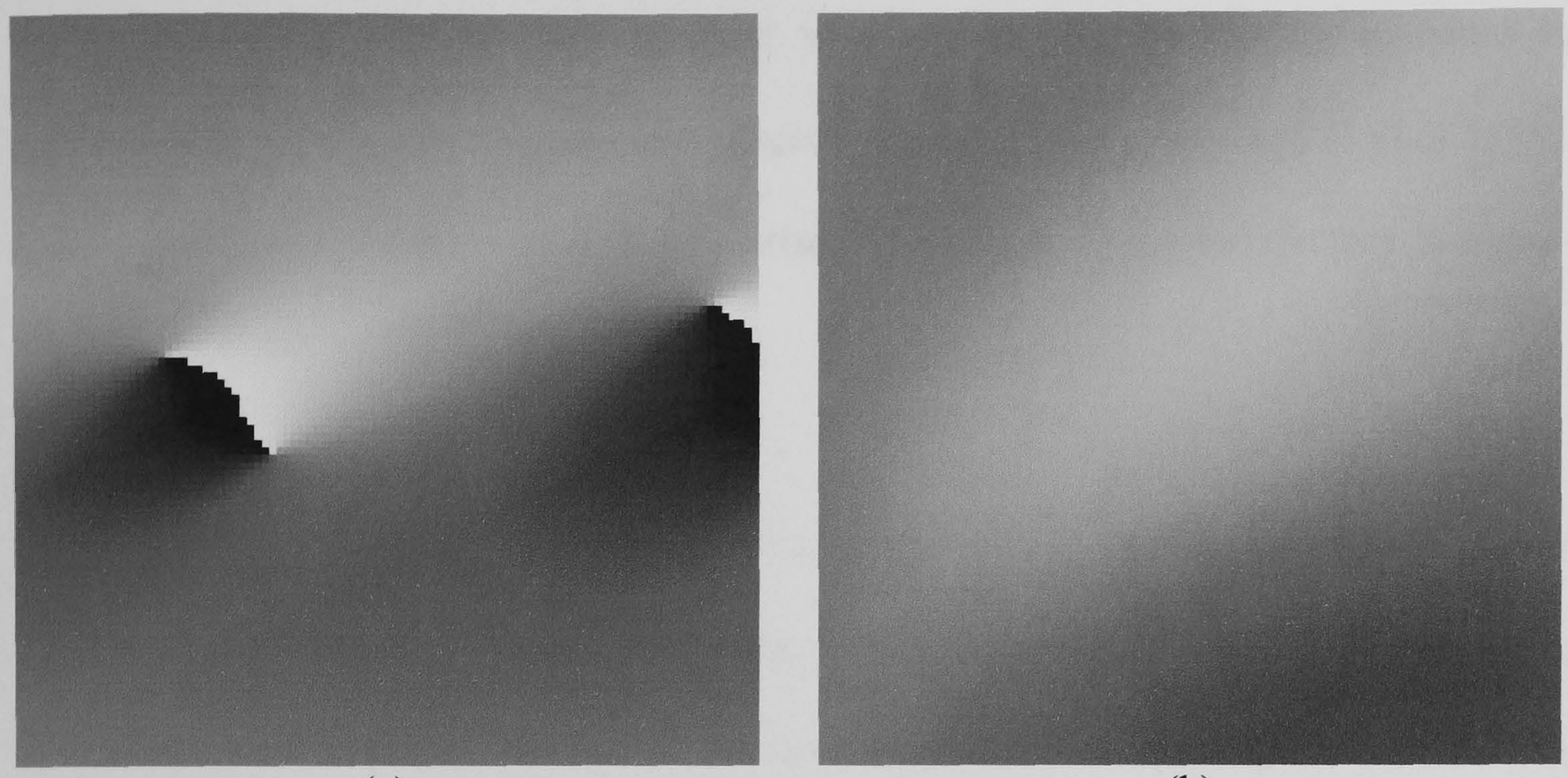

(a) (b)

Figure 4.7 These are greyscale plots of phase error for signal phase from 0 to 2π radians (horizontal) and reference phase from 0 to 2π radians (vertical). (a) shows the 3 phase-step signal, 1 phase-step reference algorithm, greyscale -π to +π and contains two phase discontinuities. White and black indicate phase errors of π radians. (b) shows the 3 phase-step signal, 3 phase-step reference algorithm, greyscale -π to +π and whilst the lighter grey region indicates a phase error, the phase error map does not contain a phase discontinuity.

is for out-of-plane displacement gradient measurement but the technique could be applied to the measurement of in-plane displacement gradient (Jones and Wykes 1989). Moore and Tyrer (1990) showed that polarisation multiplexing is satisfactory in a two-component in-plane ESPI system.

The technique could be extended to the multi-component shearography system described in Chapter 7 using polarisation-multiplexing to switch between shear directions. All six of the surface displacement gradient components could then be measured without manually adjusting the shear direction.

4.8. Conclusions

A shearography system measuring two orthogonal displacement gradient directions sequentially has been demonstrated. A change to the laser diode emission wavelength controls both the polarisation switching and the phase-stepping. This has been achieved by careful matching of the length and birefringence of the optical fibre to the pathlength imbalance in the interferometer. The polarising beamsplitter in the interferometer head performed a dual role, as a polarisation sensitive component to switch the path of the light; and as a block of high refractive index, correcting for magnification difference in the unbalanced interferometer. No moving components were contained within the interferometer head and only a single camera was required.

4.9. References

Carré P, "Installation et utilisation du comparateur photoélectrique et interférentiel du Bureau International des Poids et Mesures", *Metrologia*, **2**, pp. 13-23, 1966.

Chinone N, Kuroda T, Ohtoshi T, Takahashi T and Kajimura T, "Mode-Hopping Noise in Index-Guided Semiconductor Lasers and Its Reduction by Saturable Absorbers", *J. Quant. Electron.*, **QE-21**:8, pp. 1264-1270, 1985.

Creath K, "Phase-shifting speckle interferometry", *Appl. Opt.*, **24**:18, pp. 3053-3058, 1985.

Creath K, "Temporal Phase Measurement Methods" in ed. Robinson D W and Reid G T, "*Interferogram Analysis, Digital Fringe Measurement Techniques*", Institute of Physics, Bristol, 1993.

Ettemeyer A, Neuport U, Rottenkolber H and Winter C, "Schnelle und robuste bildanalyse von streifenmustern – ein wichtiger schritt der automation on holografichen profprozessen", *Proc. 1st Int. Workshop on Automatic Processing of Fringe Patterns*, pp. 23-31, 1989.

Ford H D and Tatam R P, "Narrow-band, wavelength-division multiplexers using birefringent optical fibre", *Opt. Comm.*, **98**, pp. 151-158, 1993.

Hariharan P, "High-precision, digital, phase-stepping interferometry with laser diodes", *Proc. SPIE* **1162**, pp. 86-91, 1989.

Huang J-R, Ford H D and Tatam R P, "Phase-stepped speckle shearing interferometer by source wavelength modulation", *Opt. Lett.*, **21**:18, pp. 1421-1423, 1996.

Ishii Y, Chen J and Murata K, "Digital phase-measuring interferometry with a tuneable laser diode", *Opt. Lett.*, **12**:4, pp. 233-235, 1987.

Ishii Y and Onodera R, "Laser-diode phase-shifting interferometer insensitive to the changes in laser power", *Proc. SPIE* **2544**, pp. 173-176, 1995.

Jackson D A, Priest R, Dandridge A and Tveten A B, "Elimination of drift in a single-mode optical fiber interferometer using a piezoelectrically stretched coiled fiber", *Appl. Opt.*, **19**:17, pp. 2926-2929, 1980.

Jones R and Wykes C, "*Holographic and Speckle Interferometry*", Cambridge University Press, Cambridge, 1989.

Kaminow I P, "Polarization in Optical Fibres", *J. Quant. Electron.*, **QE-17**:1, pp. 15-22, 1981.

Kästle R, Hack E and Sennhauser U, "Multiwavelength shearography for quantitative measurements of two-dimensional strain distributions", *Appl. Opt.*, **38**:1, pp. 96-100, 1999.

Leendertz J A and Butters J N, "An image-shearing speckle-pattern interferometer for measuring bending moments", *J. Phys. E*, **6**, pp. 1107-1110, 1973.

Moore A J and Tyrer J R, "An electronic speckle pattern interferometer for complete in-plane measurement", *Meas. Sci. Technol.*, **1**, pp. 1024-1030, 1990.

Nakadate S and Saito H, "Fringe scanning speckle-pattern interferometry", *Appl. Opt.*, **24**:14, pp. 2172-2180, 1985.

Pannell C N, Tatam R P, Jones J D C and Jackson D A, "Two dimensional fibre-optic laser velocimetry using polarisation state control", *J. Phys. E*, **21**, pp. 103-107, 1988.

Rashleigh S C, "Origins and Control of Polarization Effects in Single-Mode Fibers", *J. Lightwave Technol.*, **LT-1**:2, pp. 312-331, 1983.

Siebert Th and Schmitz B, "A New Shearing Setup for Simultaneous Measurement of Two Shear Directions", *Proc. SPIE* **3637**, pp. 225-230, 1999.

Tatsuno K and Tsunoda Y, "Diode laser direct modulation heterodyne interferometer", *Appl. Opt.*, **26**:1, pp. 37-40, 1987.

5. SOURCE POSITION MEASUREMENT USING SHADOW MOIRÉ

5.1. Introduction

The sensitivity of a shearography system to in-plane and out-of-plane displacement gradient components depends on the illumination and imaging directions. The direction of the displacement gradient component measured is given by the sensitivity vector, which is the bisector of the illumination and the viewing directions (Jones and Wykes 1989). To measure the out-of plane displacement gradient components normal illumination and normal viewing directions are used (Jones and Wykes 1989). To measure the in-plane displacement gradient components requires the measurement of displacement gradient from two illumination directions (Patorski and Olszak 1997). A multiple illumination geometry can be used to measure mixed in-plane and out-of-plane displacement gradient components (James and Tatam 1999, Kästle *et al* Sennhauser 1999, Aebishcher and Waldner 1997, Waldner and Bren 1999). These measured displacement gradient components are then transformed into an orthogonal coordinate system using a knowledge of the source positions, a process that is highly sensitive to errors in the knowledge of the source position (James and Tatam 1999). These errors are discussed further in Section 5.2

For multi-component shearography three possible techniques were considered for the measurement of the source position; these were (a) shadow Moiré, (b) a beam profile technique and (c) a shearography carrier fringe technique. Each of these techniques will

be discussed in this chapter and for the shadow Moiré technique the technique will be discussed in detail and results will be presented.

In this chapter the shadow Moiré technique combining linear and circular gratings is extended from one dimension to two dimensions. Two angles of illumination are measured using two orthogonal linear gratings and a circular grating. This has been applied to the measurement of the position of the optical source in shearography. The viewing direction is normal to the plane containing the grating, resulting in shadow Moiré fringe formation due only to the illumination direction. The circular grating is used to measure coarsely the source position by fringe counting and the symmetry of the fringe pattern is used to determine the horizontal and vertical components. The vertical and horizontal linear gratings are used to improve the measurement accuracy of the elevation and azmuthial angles of illumination respectively.

5.2. Coordinate Transformation Errors in Multi-Component Shearography

In multi-component shearography the in-plane and out-of-plane displacement gradient components are determined by a coordinate transformation of, a minimum of three, measured displacement gradient components. For the case where the source and object and imaging positions are known exactly this process is described in Section 2.3.4. The measurement of these parameters is subject to error and in Section 7.2.3. an analysis of the optimum illumination geometry is given using the determination of the conditioning number of the coordinate transformation matrix. A *well conditioned* matrix has a conditioning number, κ, of the order of unity (Goult *et al* 1974). A higher conditioning

number denotes a less well conditioned matrix and more susceptibility to error in the coordinate transformation.

The source position is defined using a right-handed orthogonal coordinate system, from which the azmuithal and elevation angles are defined, as shown in Figure 5.1. The object lies in the *x-y* plane with the centre of the front surface of the object at the origin. The *z* direction is from the object to the camera. The azmuithal angle, θ_A, is defined as the angle between the *z* axis and the object-illumination direction projected onto the *x-z* plane. The elevation angle, θ_E, is defined as the angle between the projection of the object-illumination direction onto the *x-z* plane and the object-illumination direction.

For optical sources located at 1. [0.2 m, -0.2 m, 0.5 m], 2. [0.2 m, 0.2 m, 0.5 m] and 3. [-0.2 m, 0.2 m, 0.5 m], and the principal plane of the imaging system at [0 m, 0 m, 0.5 m], an error of ± 5 mm in the *x* and *y* components of the source positions generates a maximum error of 3.8 % in the transformed displacement gradient components. It is assumed that the $\delta u/\delta x$, $\delta v/\delta x$ and $\delta w/\delta x$ displacement gradient components are of similar magnitude for this calculation.

5.3. Shadow Moiré

5.3.1. Introduction

Moiré is a full-field optical technique that can use either laser illumination or incoherent white-light illumination. The technique measures the relative displacement between two gratings and can be applied to displacement, shape, strain and angle of illumination measurement (Forno 1993). In shadow Moiré a single physical grating is used and the

optical source projects a shadow of the grating onto a surface behind the grating. Viewing the interaction between the grating and the shadow of the grating generates the Moiré intensity fringes.

To perform an angle of illumination measurement a grating is illuminated by an off-axis optical source projecting a shadow from the grating onto a diffusely reflecting surface at a fixed difference behind the grating. The grating has a transmission profile that varies ideally between 0 and 100 % and commonly has either a square wave profile, with 50 % duty cycle, or a sinusoidal profile. The fringe formation is dependent on the illumination direction and the viewing direction, and is simplified for normal viewing. The geometry of a linear grating shadow Moiré system is shown in Figure 5.2.

Shadow Moiré (Kafri and Glatt 1985) is an established method of measuring the angle of illumination. A linear grating can be used (Forno 1993), with fringe analysis by sub-fringe processing, to measure the angle of illumination in a direction orthogonal to the orientation of the grating. The unambiguous measurement range and sensitivity are determined by the pitch of the grating. Alternatively, the angle of illumination, from any angle which illuminates the front face of the grating, can be measured using a circular grating, using multiple fringe analysis and the determination of the angle of symmetry in the fringe pattern. The measurement range is limited by the maximum number of radial fringes in a quadrant that can be counted (Ng and Chau 1994). The linear and circular gratings have different measurement ranges because, for a given grating pitch, the linear grating measures the angle of illumination using fringe orders of less than one and the circular grating measures the angle of illumination using integer fringe orders.

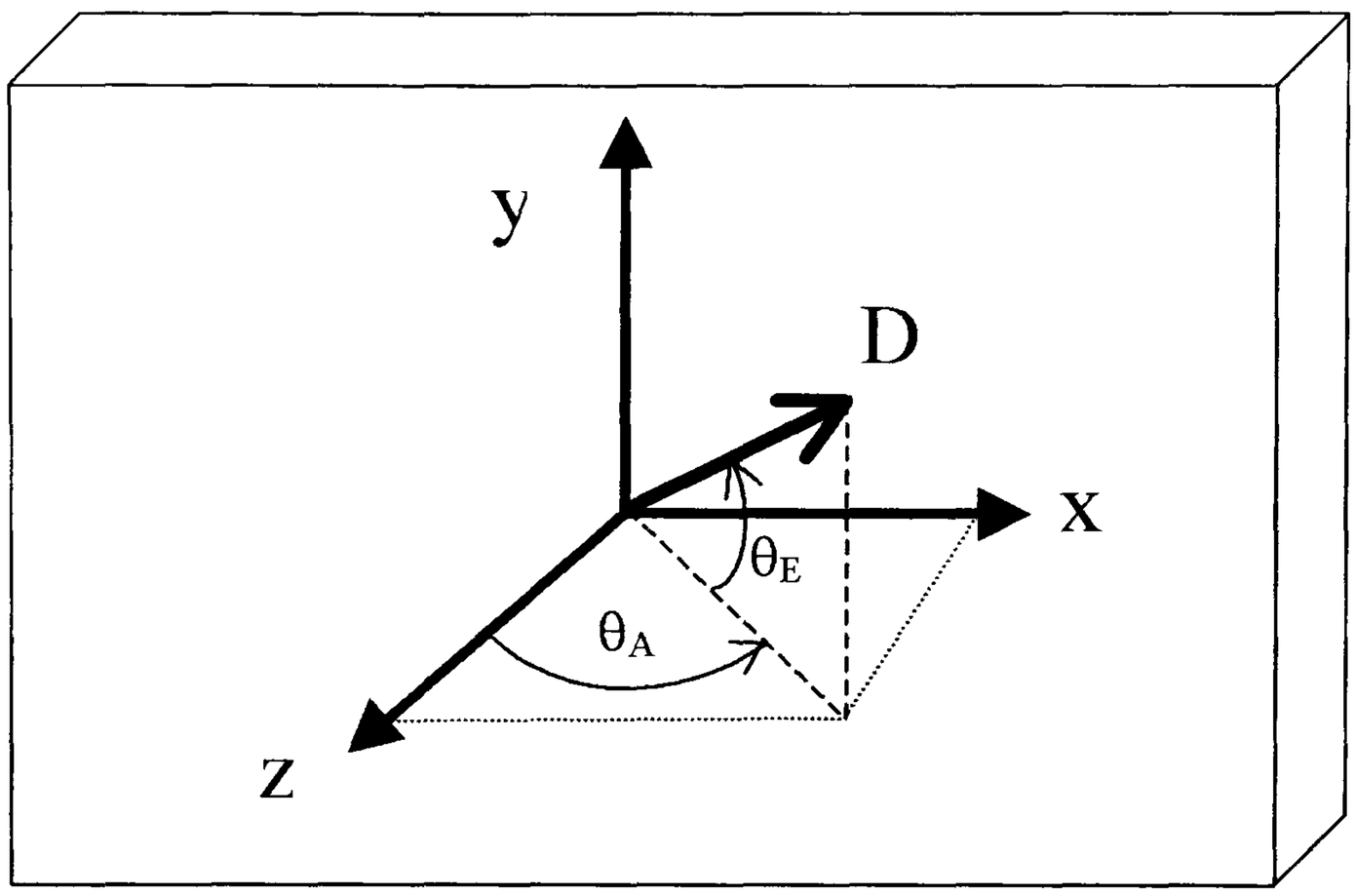

Figure 5.1 The right-handed coordinate system and the elevation, θ_E, and azmuithal, θ_A, angles of illumination. D is the object to illumination direction.

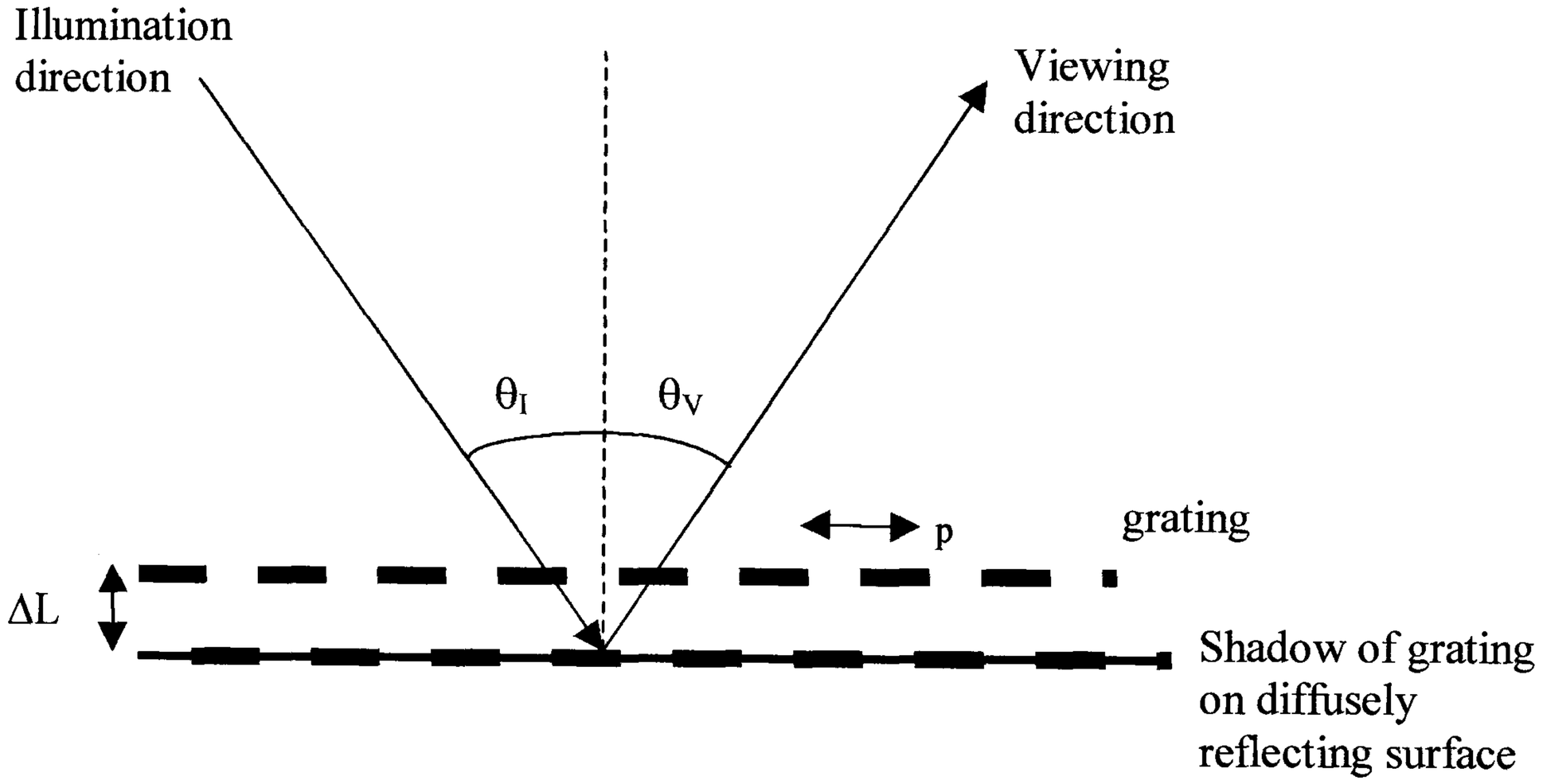

Figure 5.2 Diagram of a simple shadow Moiré system. The position of the shadow is dependent on the illumination and viewing directions, θ_I and θ_V respectively, the grating pitch, p, and the distance between the grating and the shadow, ΔL.

The linear and circular gratings are combined in the *athletic track grating* (Song *et al* 1998) to increase the measurement accuracy in one direction. Alternatively, the angles of the zeroth and first order radial fringes, produced by a circular grating, have been measured (Ng 1996) to increase measurement accuracy using only the circular grating.

5.3.2. Linear Grating Shadow Moiré

For a linear grating, with a 50 % duty cycle square wave and transmission varying between 0 and 100 %, the angle of illumination, θ_I, for a fringe of order one is given by (Forno 1993):

$$\tan\theta_I = \frac{p_I}{\Delta L} - \tan\theta_V \tag{5.1}$$

where p_I is the pitch of the linear grating, ΔL, is the grating to diffuse surface distance and θ_V is the viewing angle. For normal viewing, i.e. $\theta_V = 0^\circ$, the equation simplifies to:

$$\tan\theta_I = \frac{p_I}{\Delta L} \tag{5.2}$$

For normal viewing and illumination the shadow is directly behind the grating so the average intensity across the grating is 50 % of the illumination intensity. As the illumination angle is increased the average intensity reduces until the average intensity is 0 %, this is when the shadow is directly behind the spaces in the grating. Further increasing the angle of illumination increases the intensity until it is 50 % of the illumination intensity, this is when a line in the grating is in front of the shadow of the adjacent line, as viewed from the viewing direction. Continuing to increase the angle of illumination repeats this intensity variation. The intensity fringe formation on increasing the angle of illumination is shown in Figure 5.3. This repetition of the fringe pattern

introduces ambiguity for large angles of illumination and limits the range of the technique. The 0 % intensity of the fringe pattern is at angles of θ_N, where N = 0, 1, 2, 3,...:

$$\theta_N = \tan^{-1}\left(\frac{Np_l}{\Delta L}\right) \tag{5.3}$$

The accuracy of this technique is typically 10 % of the measurement range (Song *et al* 1998), limited by the measurement of the average intensity across the grating. The sensitivity of the grating is to the azimuthal angle of illumination for a vertical grating and the elevation angle of illumination for a horizontal grating.

5.3.3. Circular Grating Shadow Moiré

For a circular grating, with a 50 % duty cycle square wave and transmission varying between 0 % and 100 %, the number of radial fringes in a quadrant, *N*, for normal viewing is (Song *et al* 1998):

$$N = \frac{\Delta L}{p_c}\sin\theta_I \tag{5.4}$$

where *N* has integer values only and p_c is the circular grating pitch. The range is limited by the maximum number of fringes that can be accurately counted in each quadrant.

The grating is sensitive to the resultant of the azmuithal and elevation angles of illumination. The angle of symmetry of the fringe pattern can be used to determine the component angles of the illumination. For example, if the azmuithal and elevation angles of illumination are equal the fringe pattern has a line of symmetry at

approximately 45° to the vertical. Figure 5.4 shows (a) a schematic of a circular grating and (b) an experimentally determined radial fringe pattern.

5.3.4. Combined Linear and Circular Grating Shadow Moiré

In the *athletic track grating* (Song *et al* 1998) linear and circular gratings of the same pitch are combined to provide increased measurement range in *one direction*. This direction of measurement is in the plane of the grating and orthogonal to the linear grating lines. The grating described in this chapter combines a circular grating with a vertical linear grating and a horizontal linear grating. This composite grating improves the measurement accuracy of the angle of illumination in the *two orthogonal directions*, which lie in the plane of the grating.

The circular grating can be used to determine the coarse angle of illumination. The fringe counting algorithm has a resolution of ± ½ fringe in a quadrant. The symmetry of the radial fringe pattern can be used to determine the horizontal and vertical components to give a range for both the elevation and the azmuithal angles of illumination. The linear vertical and horizontal gratings improve the measurement accuracy for both these angles of illumination if appropriate pitches are chosen for the ratio of the circular grating pitch to the linear grating pitch.

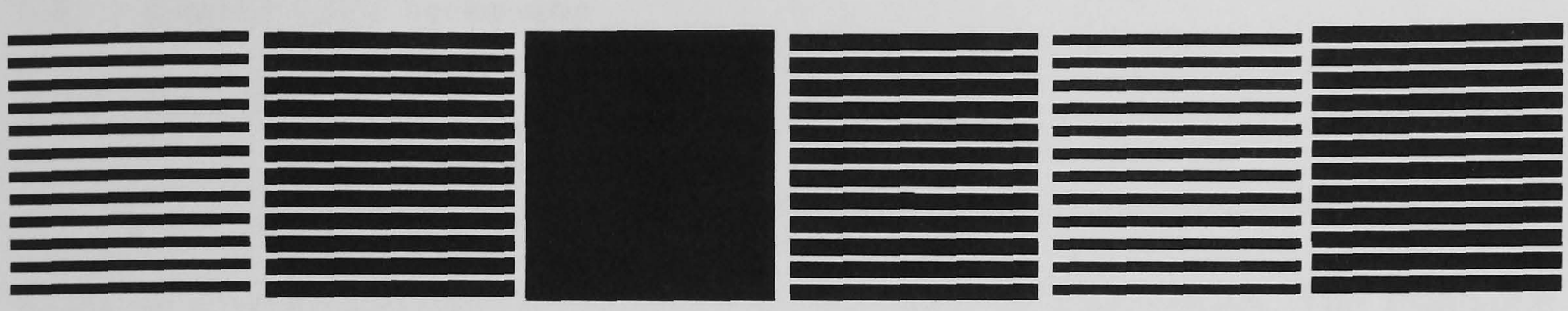

(a) (b) (c) (d) (e) (f)

Figure 5.3 Sequence of linear Moiré grating images obtained by increasing the angle of illumination

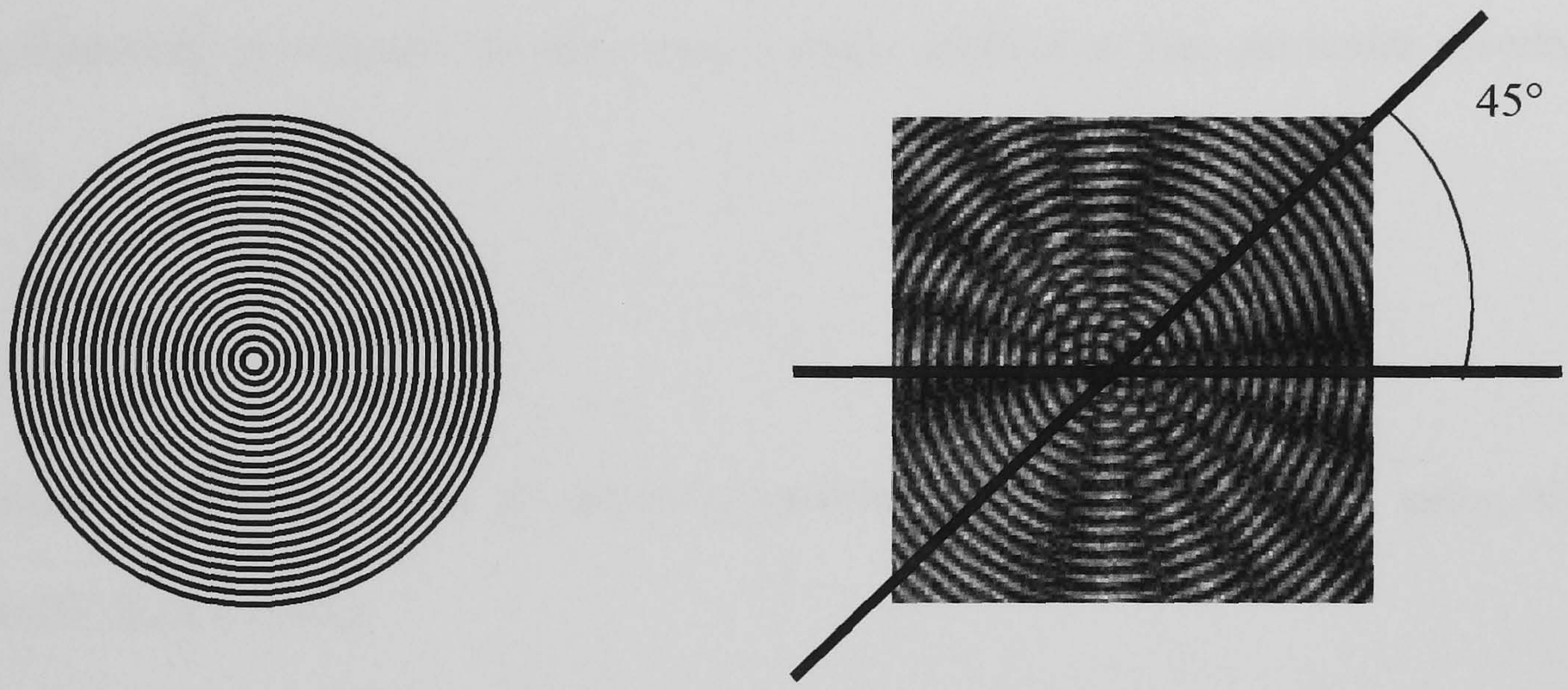

(a) (b)

Figure 5.4(a) Schematic of a circular grating and (b) an experimentally obtained radial fringe pattern with a line of symmetry at 45° to the horizontal. The grating pitch is 1.2 mm, and the angle of illumination is 19.5° from the normal, with equal horizontal and vertical components.

5.4. Beam Profile Technique

5.4.1 Introduction

The beam profile technique uses the deformation of the shape of an expanded laser beam on a reference surface to determine the angle of illumination. The technique requires the camera to be normal to a reference surface, which is placed at the object position, so this technique is most suited to multiple illumination and single viewing direction systems. If a single illumination direction and multiple viewing directions were to be used the reference object would need to be aligned individually, to each viewing direction, to measure the illumination angle relative to that particular viewing direction.

5.4.2. Theory

A Gaussian profile beam has an intensity profile that can be described using the equation (Williams 1993):

$$I(x,y) = \frac{2P}{\pi\omega_x\omega_y}\exp\left[-2\left\{\left(\frac{x}{\omega_x}\right)^2+\left(\frac{y}{\omega_y}\right)^2\right\}\right] \tag{5.5}$$

where $I(x,y)$ is the intensity at a point (x,y) on the surface of the object, P is the optical power and ω_x and ω_y are the Gaussian beam widths in the x and y directions respectively. The intensity is 13.5 % of the maximum intensity at the points ($x = 0, y = \pm\omega_y$) and ($x = \pm\omega_x, y = 0$).

For a Gaussian profile beam, which illuminates a surface from a non-normal direction, the beam profile will be distorted elliptical Gaussian. Figure 5.5 shows a schematic of

how the ellipticity of the beam varies for different angles of illumination. Additionally the elliptical beam profile is distorted, this is discussed in Section 5.4.3. A measurement of the distortion of the ellipticity of the beam on the object surface will allow determination of both the vertical and horizontal directions of illumination.

5.4.3. Accuracy of the Beam Profile Technique

An investigation into the theoretical accuracy of the technique was made. The shape of the Gaussian profile on the object surface was calculated for a number of illumination angles. The optical source was located at an angle of θ from the normal to the surface, with the centre of the illuminating beam at the centre of the object surface. For a beam expansion angle of α, the beam half-widths are:

$$\omega_{x1} = D[\tan(\theta+\alpha) - \tan(\theta)] \tag{5.6}$$

$$\omega_{x2} = D[-\tan(\theta-\alpha) + \tan(\theta)] \tag{5.7}$$

where D is the illumination to object distance and 2θ is the angular expansion of the beam. These equations were obtained by considering the angle of illumination at the beam half-widths and its' projection onto a flat surface.

Typical experimental values are $D = 0.5$ m, $\alpha = 30°$ and θ between $0°$ and $30°$, and $\omega_{x1} + \omega_{x2}$ covering a distance 500 camera pixels wide on the CCD chip. Figure 5.6 shows the difference in the number of pixels between ω_{x1} and ω_{x2} against the angle of illumination.

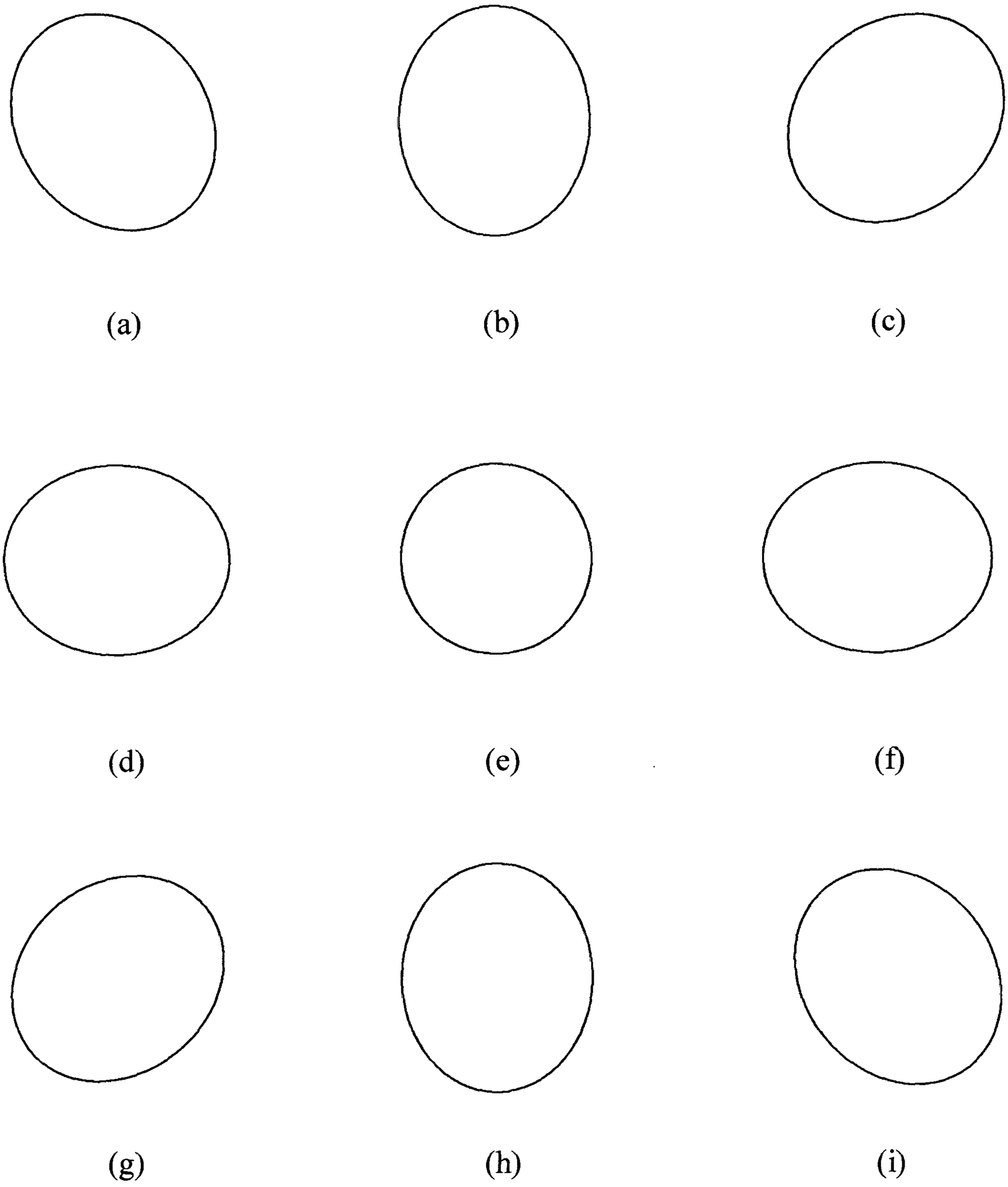

Figure 5.5 Schematic showing how the beam half-width of a Gaussian beam changes from circular to elliptical, depending on the angle of illumination of a flat plate. The illumination is from (a) [-a, a, D], (b) [0, a, D], (c) [a, a, D], (d) [-a, 0, D], (e) [0, 0, D], (f) [a, 0, D], (g) [-a, -a, D], (h) [0, -a, D] and (i) [a, -a, D]. The object is located at [0, 0, 0], a is an arbitrary distance and D is the source to object distance along the z direction.

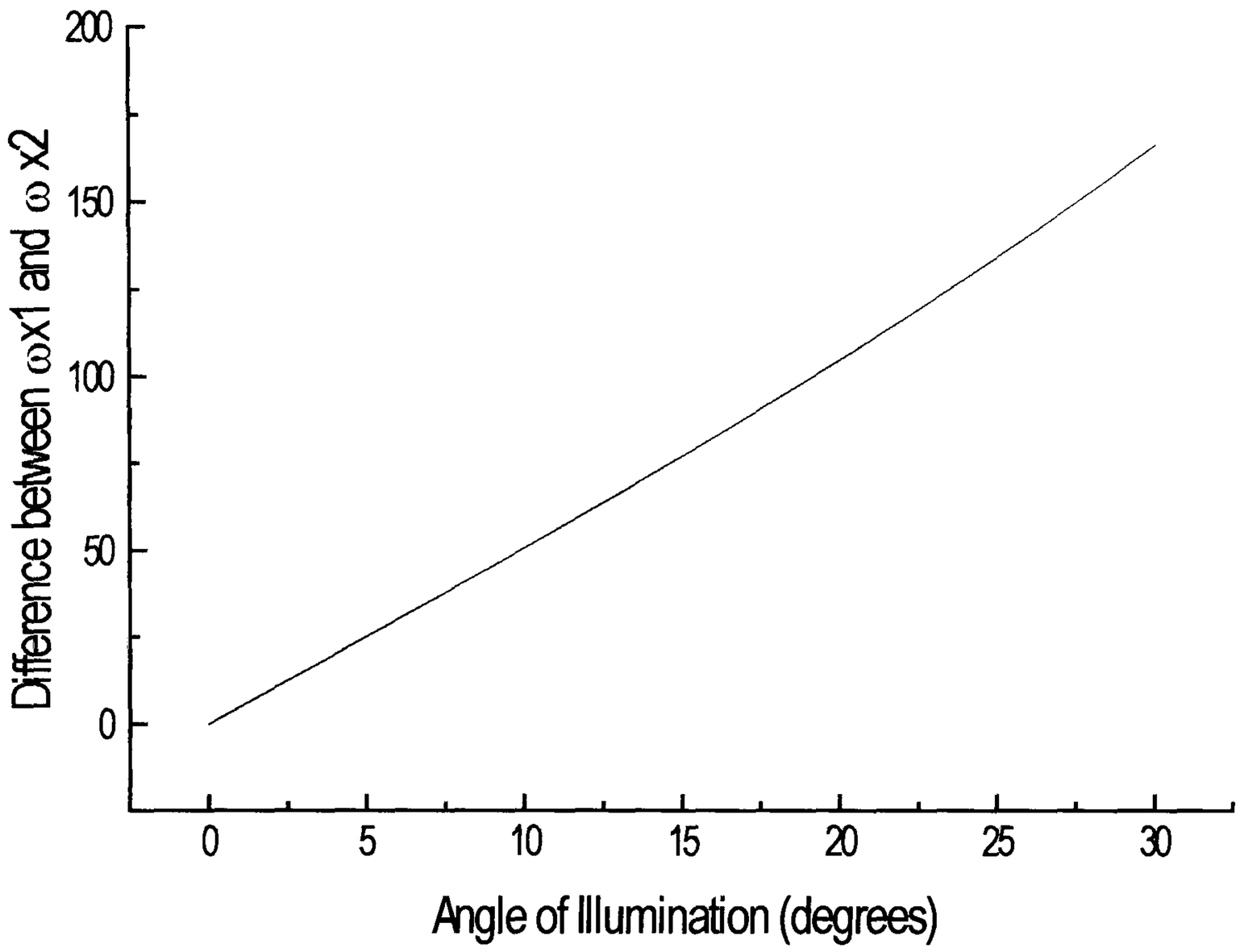

Figure 5.6 The graph show the relationship between the number of camera pixels difference between the ω_{x1} and ω_{x2} beam half-widths and the angle of illumination. ω_{x1} and ω_{x2} are the two beam half-widths on opposite sides of the beam centre, in the *x* direction.

A theoretical accuracy of ± 5 pixels is required in measuring the difference between ω_{x1} and ω_{x2} to give ± 1 ° accuracy in measuring θ. This equates to a error in x, or y distance, of ± 10 mm over a 200 mm distance. To measure to this accuracy requires an accuracy of ± 3 pixels in determining the centre of the beam and the position of the edges of the beam widths, from the camera pixel intensities. This has not been verified experimentally. The specular nature of the beam will reduce measurement accuracy, due to the lack of definition of the beam half-width. The possibility of performing sub-pixel interpolation may assist in improving the measurement accuracy.

5.5 Shearography Carrier Fringe Technique

5.5.1. Introduction

Displacement of the optical source by a distance of the order of 1 mm generates correlation fringes which are composed of a carrier fringe component and a slope fringe component, when speckle interferograms recorded before and after the source displacement are subtracted. The theory for this correlation fringe generation is discussed in detail in Section 6.3. In this section the key feature of the correlation fringe generation is that displacement of the optical source along the illumination optical axis generates carrier fringes and that displacement of the optical source in any other direction generates slope fringes or a mixture of slope and carrier fringes. On a flat object surface carrier fringes are identifiable as they are linear and are oriented in a direction orthogonal to the direction of applied shear.

5.5.2. Experimental

A simple experiment was performed to verify that this technique could be used for determination of angle of illumination. The experimental layout is shown in Figure 5.7. A diode-pumped frequency-doubled Nd:YAG laser (100 mW optical power) was used to illuminate a flat test object at a distance of 0.54 m from the laser and from an illumination angle of 23.6 °. The shearing head, with CCD camera, was located 0.5 m from the normal to the object surface and the applied shear was 10 mm. The coordinate system used has the z direction from the object to the shearing head and the x direction orthogonal to this direction in the plane of the optical table.

5.5.3 Results and Discussion

A source displacement of -0.2 mm in the z direction generated mixed slope and carrier fringes on subtracting the reference speckle interferograms. After a second subsequent source displacement of 0.1 mm in the x direction and subtraction of the original reference frame pure carrier fringes were generated. The second source displacement removes the slope fringe contribution to the correlation fringes as the resultant direction of the two displacements is along the axis of illumination. The angle of illumination was measured as 30°.

The technique could easily be extended to a 3-dimensional coordinate system by incorporating a method of source displacement in a third orthogonal direction. However the location of the displacements to generate pure carrier fringes would be more complicated because of the extra degree of freedom. Also the exact location of the displacements which yield pure carrier fringes was difficult to identify visually and

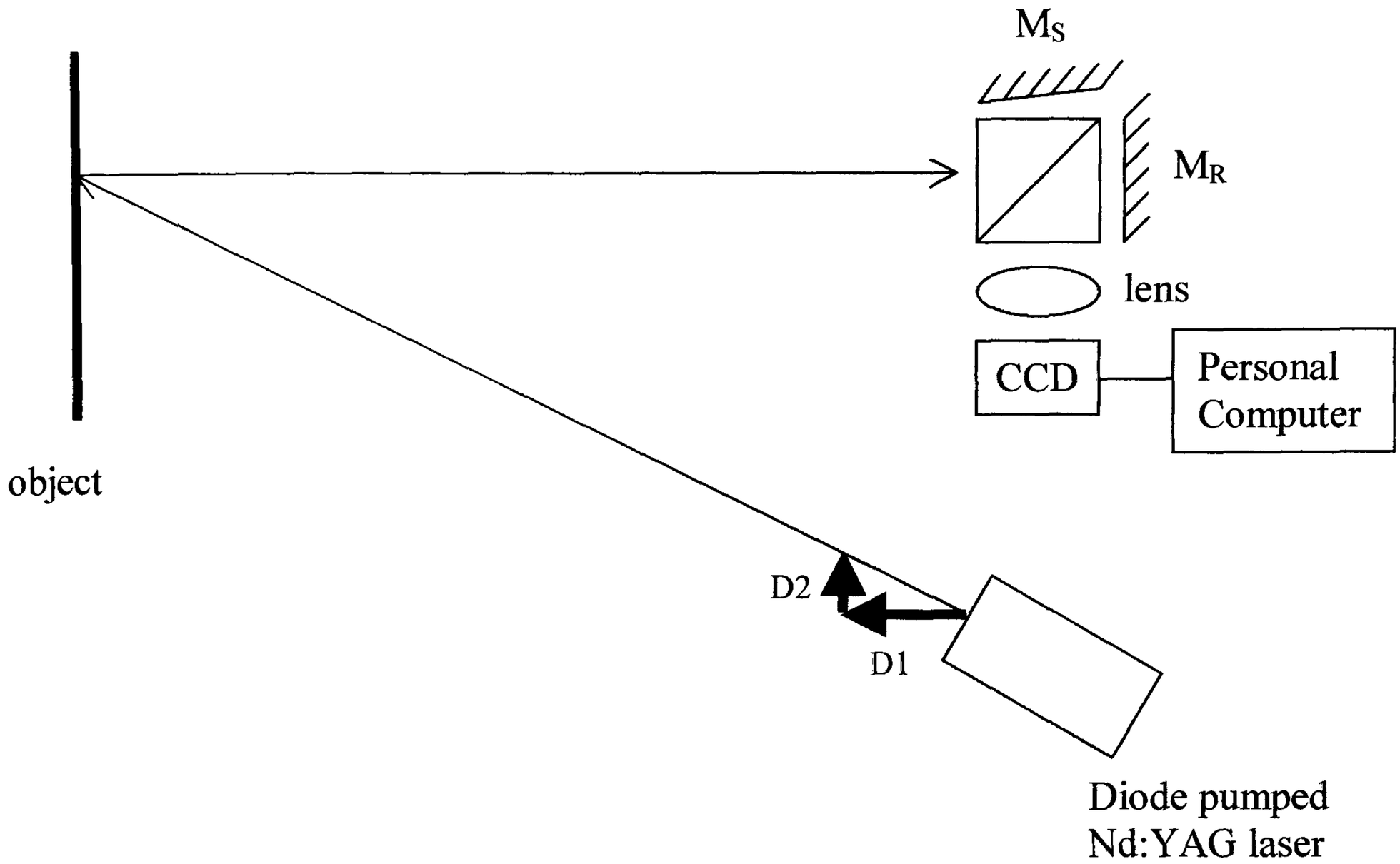

Figure 5.7 Experimental layout for verification of shearography carrier fringe technique. A source displacement D1 in the *z* direction generates a mixture of carrier and slope fringes. A second source displacement D2 in the *x* direction removes the slope fringe contribution leaving pure carrier fringes. M_S, shearing mirror; M_R, reference mirror.

would also be difficult when using automated fringe analysis techniques. Due to this difficulty the accuracy of the technique, with visual identification of carrier fringes, is ± 7° or ± 70 mm over a 200 mm distance. It may be possible to improve on the accuracy of this technique although the error was so large compared with the other two techniques investigated this technique was not investigated further.

5.6. Summary of Techniques

The shearography carrier fringe technique has a limitation in the accuracy of measurement, ± 70 mm over a 200 mm distance, although a sophisticated image processing algorithm may be able to improve this. The other two techniques, the beam profile technique and the shadow Moiré technique have better accuracies. The accuracy is calculated as ± 10 mm over a 200 mm distance for the beam profile technique and was experimentally determined ± 6 mm over a 200 mm distance for the shadow Moiré technique. The accuracy of both techniques is limited by speckle noise. The beam profile technique has the additional limitation that the orientation of the reference object is more critical than the shadow Moiré technique. Therefore the shadow Moiré technique was investigated further. Table 5.1 summarises the accuracies of the three techniques.

Technique	**Accuracy over a 200 mm *x* distance**
Carrier fringe technique	± 70 mm (experimentally determined)
Beam profile technique	± 10 mm (theoretical calculation)
Shadow Moiré technique	± 6 mm (experimentally determined)

Table 5.1 Summary of the accuracies of the three techniques for source position measurement

5.7. Shadow Moiré Experimental

5.7.1. Experimental System

The experimental layout for the shadow Moiré technique is shown in Figure 5.8. The shadow Moiré measurements were performed using the multi-component shearography system described in Chapter 7. The object under investigation was replaced by the composite circular/linear Moiré grating to perform the measurements of angles of illumination.

The multi-component shearography system used three optical fibre coupled laser diode sources (810 nm, 100 mW), to illuminate the object with an expanded beam from different directions. The shearing element, to optically process the image, was a Michelson interferometer, consisting of a reference mirror and a shearing mirror. For this shadow Moiré technique the shearing mirror was physically blocked to prevent the formation of interferometric speckles. The grating was viewed through the modified Michelson interferometer using a camera lens with images recorded by an 8-bit area scan camera (Dalsa CA-D4-0512A, 512 x 512 pixels, 75 Hz frame rate), in conjunction

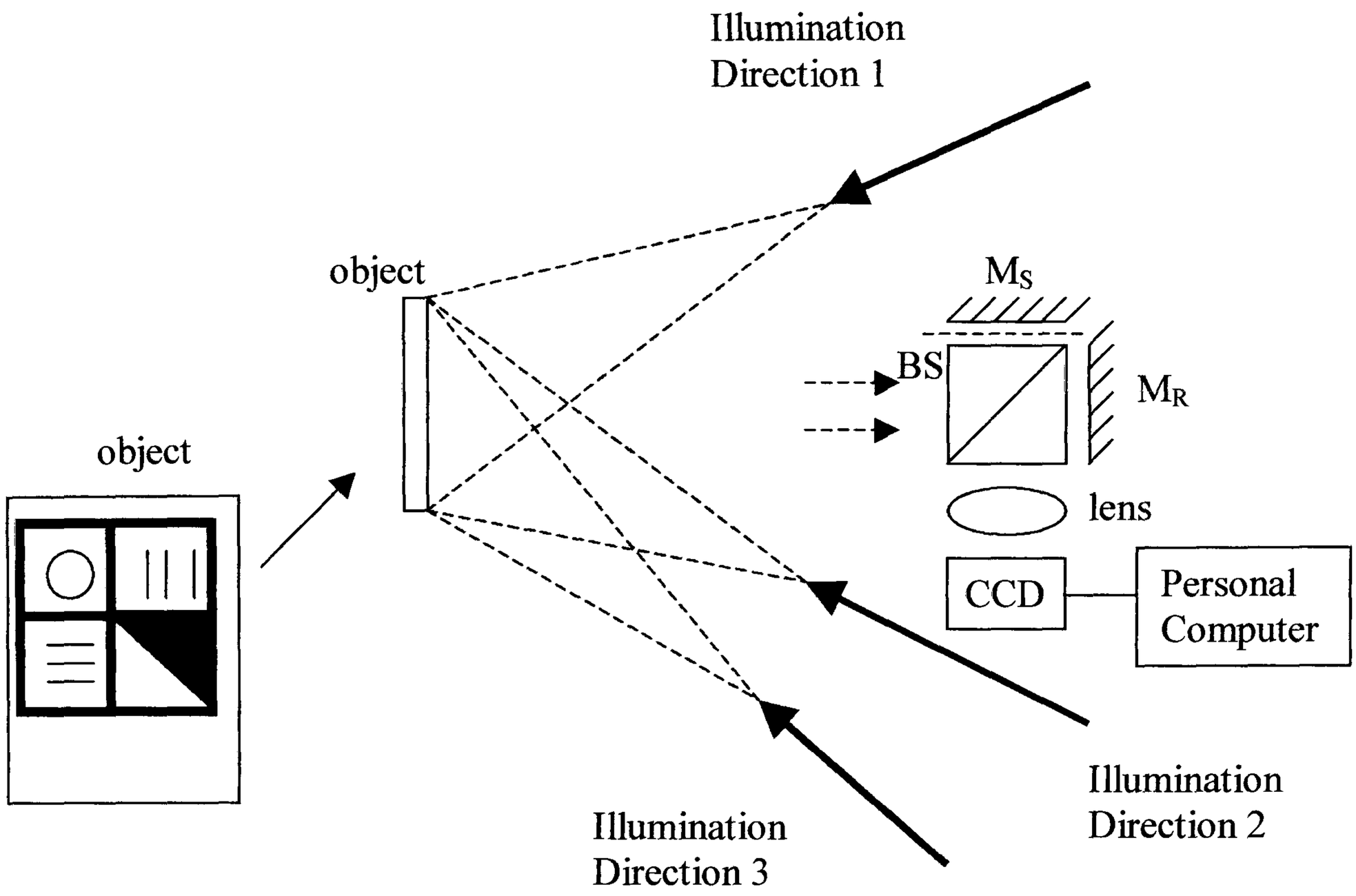

Figure 5.8 Experimental layout of the multi-component shearography system. BS, beamsplitter; M_R, reference mirror; M_S, physically blocked shearing mirror; CCD, camera. The object is a perspex block of thickness 11.8 mm with a grating attached to the front face, and with the rear surface painted white.

with a PCI bus frame transfer card (Bitflow Roadrunner). Image capture was controlled by a program written using Labview software.

A schematic of the composite grating is shown in Figure 5.9. The composite grating was composed of a circular grating region, used to measure coarsely the source position, a horizontal linear grating region and a vertical linear grating region used to refine the measurement of the source position in two directions, in the plane of the grating, and two triangular reference regions, one black and one transparent, which were used to define 0 % and 100 % transmission respectively.

For optimum performance of the source position determination, the system parameters are determined from an a priori knowledge of the approximate illumination geometry. The circular grating pitch was determined using the maximum number of radial fringes that the fringe counting algorithm could accurately count. The angles of the radial fringes are given by (Ng and Chau 1994):

$$\sin \varepsilon_N = \frac{Np_c}{d} \tag{5.8}$$

where ε is the angle of the radial fringe of order N, p_c is the pitch of the circular grating and d is the displacement between the grating and the shadow of the grating, in the grating plane. The fringe counting algorithm could distinguish fringes with a spacing of 10° and this corresponded to a maximum fringe order of 5 per quadrant. The circular grating pitch of 1.2 mm was determined using equation 5.4. For a maximum fringe order, that can be accurately counted, of 5 the maximum angle of illumination that could

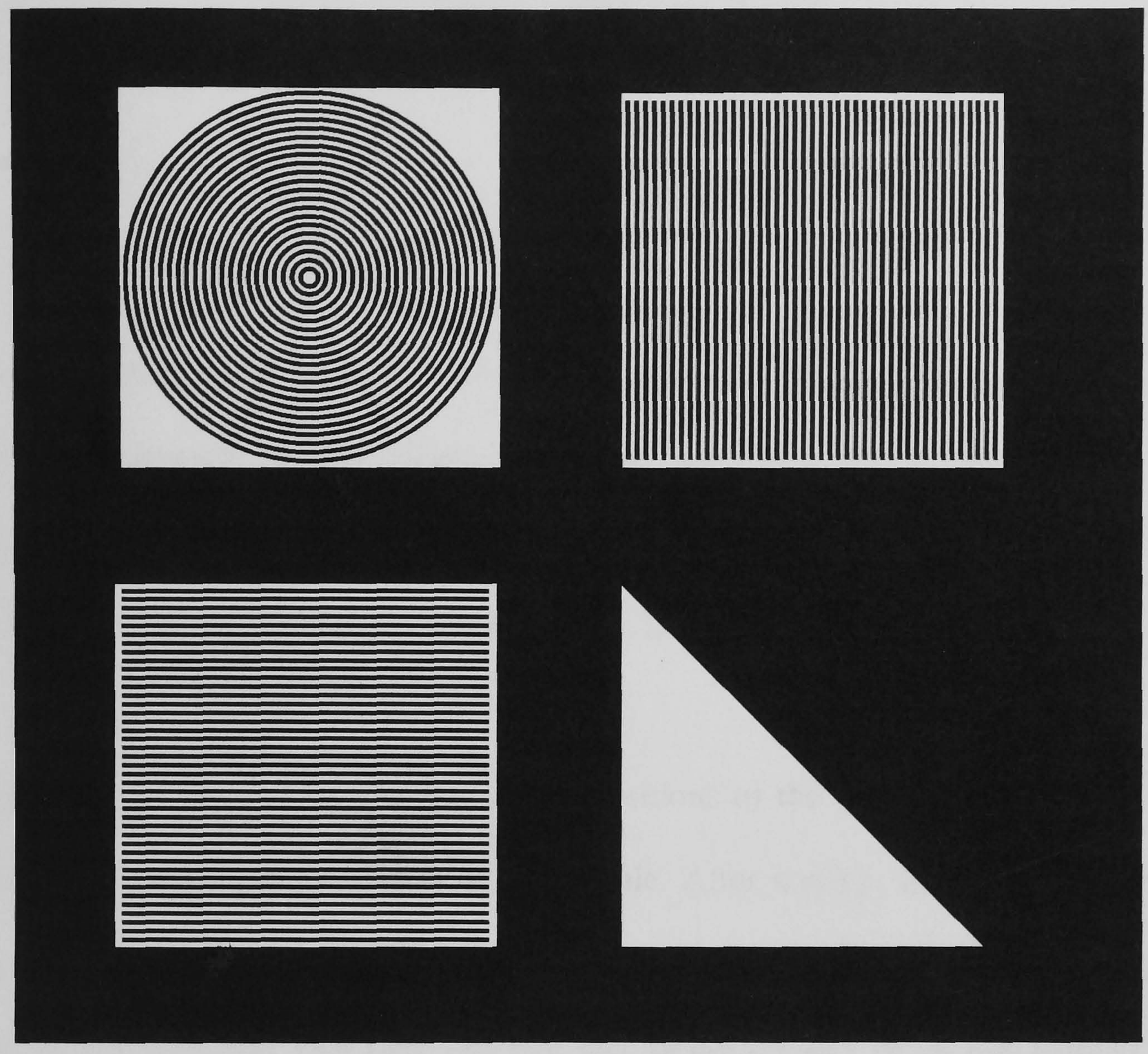

Figure 5.9 Schematic of the composite grating containing a vertical linear grating, a horizontal linear, a circular grating and two triangular reference intensity regions. The actual grating used had a circular grating pitch of 1.2 mm and a linear grating pitch of 0.84 mm.

be measured was 30.6°. For equal horizontal and vertical angles of illumination the linear grating pitch, p_l, was calculated using:

$$p_l = \frac{p_c}{\sqrt{2}} \tag{5.9}$$

The linear grating pitch used was 0.84 mm, calculated using equation 5.9. The reference region was triangular so that regions of 'black' and 'white' were sampled across the profile of the illuminating beam and also so that large intensity variations did not occur on a horizontal or vertical axis as this confused the edge detection algorithm.

The grating was formed by calculating the positions of the grating lines using Matlab software and saving the grating as an image file. After scaling, the image was printed using a laser printer onto an acetate sheet and affixed to the front face of a clear perspex block, optical thickness 17.6 mm. The rear face of the perspex block was painted white to provide a diffusely reflecting surface. A reference perspex block, of the same thickness and with the rear surface also painted white, was used to record the intensity profile of the beam at the grating position.

5.7.2. Fringe Analysis

Fringe analysis was performed using a program written in Matlab software. The fringe analysis program is summarised below, then the individual parts of the program are described in detail.

Summary of fringe analysis program

1. Locate individual linear and circular gratings, and reference intensity region, within the composite grating.
2. For the circular grating, count radial fringes and determine the line of symmetry of the fringe pattern. From these calculate the approximate position of the optical source.
3. For the linear gratings, calculate the average intensity across the gratings. The intensity is corrected for the Gaussian profile of the beam by dividing by a reference image of the beam.
4. The average intensity of a linear grating is used to determine a number of possible source positions by comparing with 0 % to 50 % intensity as discussed in Section 5.3.2. The 0 % and 100 % intensities are determined from two triangular reference regions within the composite grating. This is repeated for the second linear grating.
5. Use the possible source positions determined from the linear grating to refine the approximate source position measurement from the circular grating.

The program located the individual parts of the composite grating from the images captured by the CCD camera. For the circular grating the number of fringes in each quadrant and the symmetry of the fringe pattern were then determined. For the vertical linear and the horizontal linear gratings the average intensity across the grating was calculated, using the reference region to correct for intensity variations, caused by the use of an expanded Gaussian beam.

The position of the individual gratings in the composite grating was determined by locating the edge of the black border that surrounds the gratings. Pixel intensities for each line and column of the image were summed and the position of the black grating perimeter against the white background was identified by the maximum intensity change. The image was then cropped to remove parts of the image outside the grating. It was assumed that the edges of the grating were parallel with the edges of the image. The relative proportions of the sizes of the individual gratings to the size of the composite grating was used to separate the composite grating into the individual gratings. Subsequent processing of the individual gratings was performed on the central region of the individual gratings so that pixels near to the edge would be excluded to reduce processing errors.

For the circular grating, the number of radial fringes was counted and the axis of symmetry of the fringe pattern was identified. To do this the image was divided into three hundred and sixty 1° segments and the average intensity in each segment was calculated. To locate the peaks and troughs in the intensity pattern, a zero crossing algorithm was applied to the differential of the intensity pattern of the segments. To eliminate false zero crossings, gradients close to zero were set to zero. The zero crossings were counted to give the total number of fringes in each quadrant. Using this the line of symmenty could be determined to an accuracy of $\pm^1/_2$ fringe.

The symmetry of the radial fringe pattern obtained from the circular grating was determined by testing possible lines of symmetry in the intensity pattern. A symmetry number for each of the 180 possible radial lines of symmetry was determined by

multiplying the intensity of each segment by the intensity of the reflection of that segment in the possible line of symmetry and summing the multiplied intensities from all the segments. The actual line of symmetry was identified as the possible line of symmetry with the largest symmetry number. The fringe pattern has two lines of symmetry 90° apart so the correct line of symmetry was identified by an approximate knowledge of the source position. This method could determine the line of symmetry to ± 1°.

The fringe patterns from the vertical and horizontal linear gratings were analysed by measuring the average intensity. Using the magnification that would be employed in operating the shearography system, the grating pitch is relatively large compared with the camera pixel size (approximately 3:1). This ratio of grating pitch to camera pixel size generates intensity fringes due to the Moiré effect (Jähne 1995). The grating pitch remains unchanged when the angle of illumination is varied, only the duty cycle changes, so frequency based methods are not suitable. The gratings were illuminated by an expanded laser beam with circular Gaussian intensity profile, with beam expansion such that intensity variations across the grating were minimised, but still allowing sufficient illumination. The camera frame containing Moiré fringes was recorded with the perspex object, with the grating, in the object position, using the laser illumination. Intensity correction was performed by recording a reference image of the diffuse reflective surface of the perspex object illuminated by the source, but without the grating in place, using identical laser illumination and correcting the intensity at each pixel in the image. $I_{CORRECTED}$ was calculated using:

$$I_{CORRECTED} = \frac{I_{MOIRÉFRINGE}}{I_{REFERENCE}} \tag{5.10}$$

where $I_{MOIRÉFRINGE}$ and $I_{REFERENCE}$ were the pixel intensities for the Moiré fringe and reference frames respectively. For the reference intensity region of the composite grating, the corrected intensity values for 100 % intensity from the transparent area and for 0 % intensity from the black area were determined. The average intensities across the vertical and horizontal gratings were scaled to the 0 to 100 % range from the reference regions. The intensity of the linear grating region varies between 0 % and 50 % depending on the relative displacement between the grating and its' shadow. Equation 5.2 is used to calculate possible source positions along the axis which is both orthogonal to the grating and orthogonal to the *z* axis.

The measurements made with the circular grating give a small region, in the *x*-*y* plane, where the source may be located. The measurements made using the linear gratings provide the position, within this region, where the source is located.

In summary the determination of the source position used the circular grating to provide the coarse measurement, and the symmetry of the radial fringe pattern to separate this angle into two orthogonal components. The relative displacement of the linear gratings relative to their shadow was then used to increase the accuracy of the measurement by measuring the angle of illumination more accurately, but with ambiguity. The information provided by the circular grating was used to identify the correct source position from the possible source positions given by the linear grating measurements.

5.8. Results and Discussion

The shadow Moiré technique was used to measure a number of typical source positions that are used by the multi-component shearography system. A reference square grid, centred nominally at [0.20 m, 0.20 m, 0.00 m], was located in a plane parallel with the front surface of the object and at a distance of 0.5 m from the camera. Source positions were measured with x values of 0.15 m, 0.20 m and 0.25 m and y values of 0.15 m, 0.20 m and 0.25 m. The optical source was fitted to a translation stage which allowed movement of the source in this plane and accurate measurement of the source displacement. A typical image from the camera is shown in Figure 5.10. The presence of both the grating and the shadow can be seen in the figure. The results are given in Figure 5.11. Good agreement, to within ± 6 mm, is achieved between the shadow Moiré technique and the translation stage.

The uncertainty in the fringe analysis is ± $^1/_2$ fringe, over a 0 to 5 fringe range, for the circular grating and ± 10 % for the linear gratings. The uncertainty of the measurement of the angle of symmetry is ± 1°, measured experimentally. The error due to locating the grating away from the centre of the object position, when illuminated by an expanded beam, is 1.8 %. The error due to the increased size of the shadow, compared with the grating line, is 0.5 %. These uncertainties combine to give an error of 3 %, which is equivalent to ± 6 mm over a 200 mm distance, in either the x or y directions.

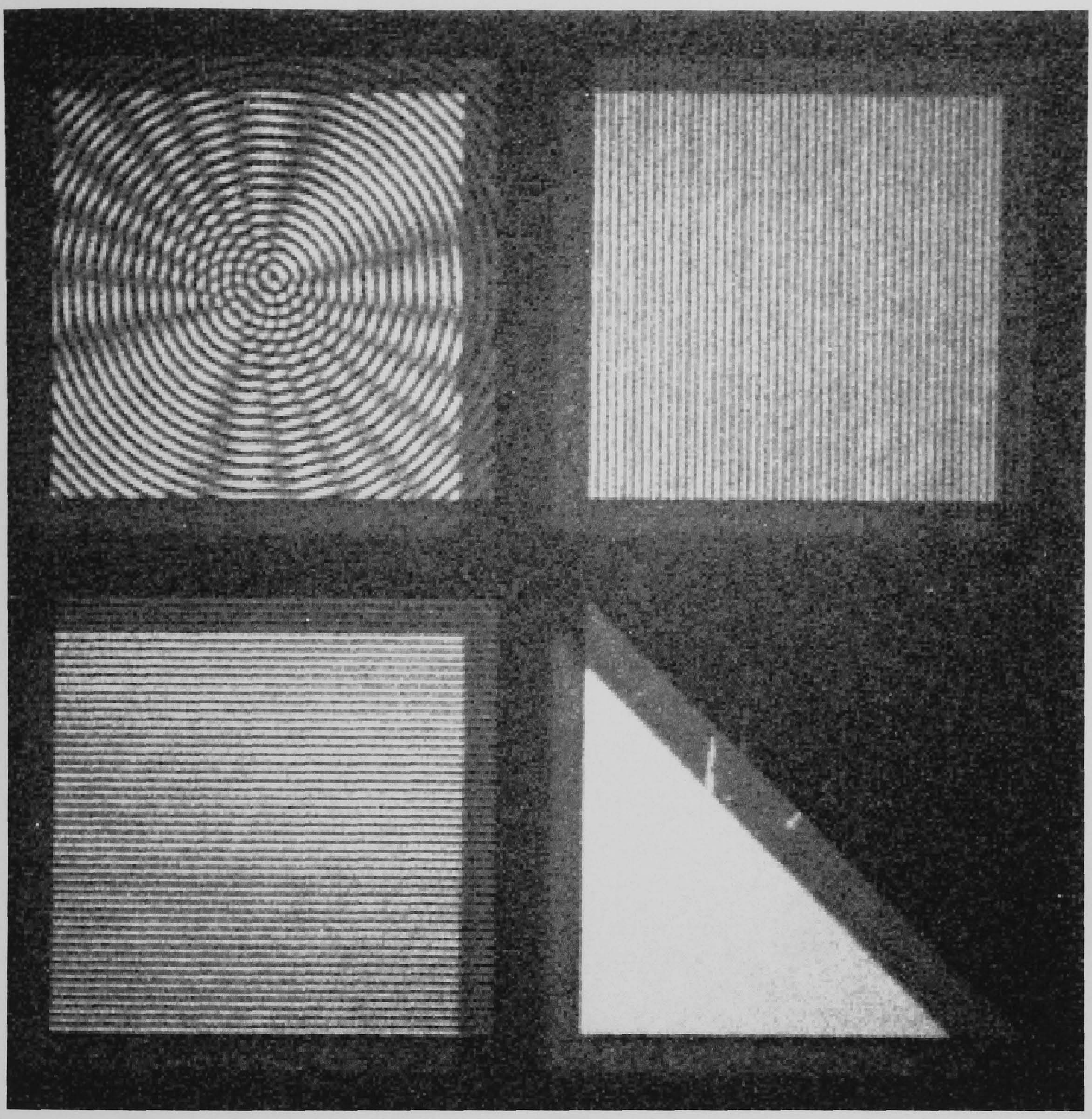

Figure 5.10 Image of the shadow Moiré grating, with normal imaging, and illumination by an expanded beam from a source at [0.2 m, 0.2 m, 0.5 m]. The uneven illumination is illustrated and this is corrected by using the reference image.

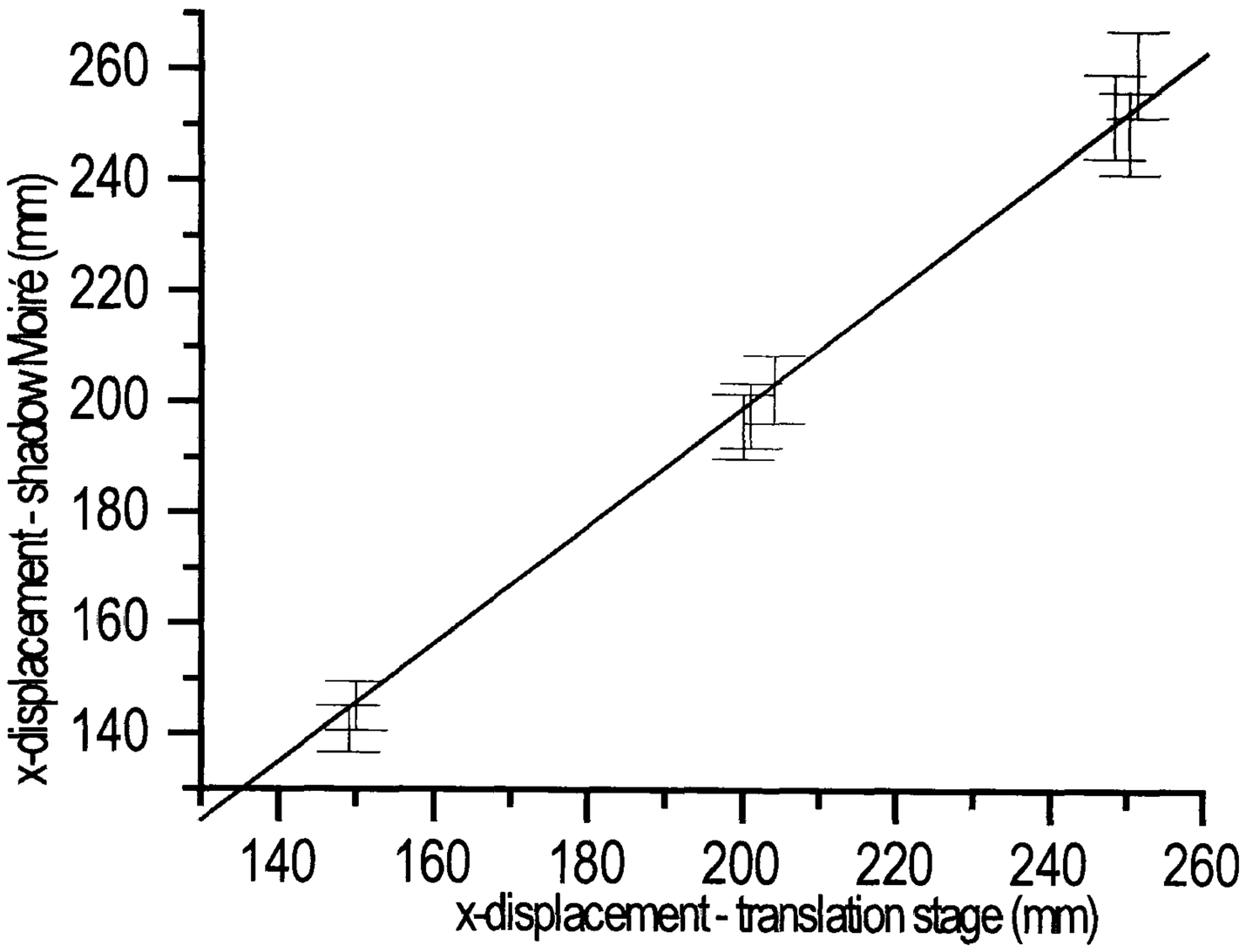

(a)

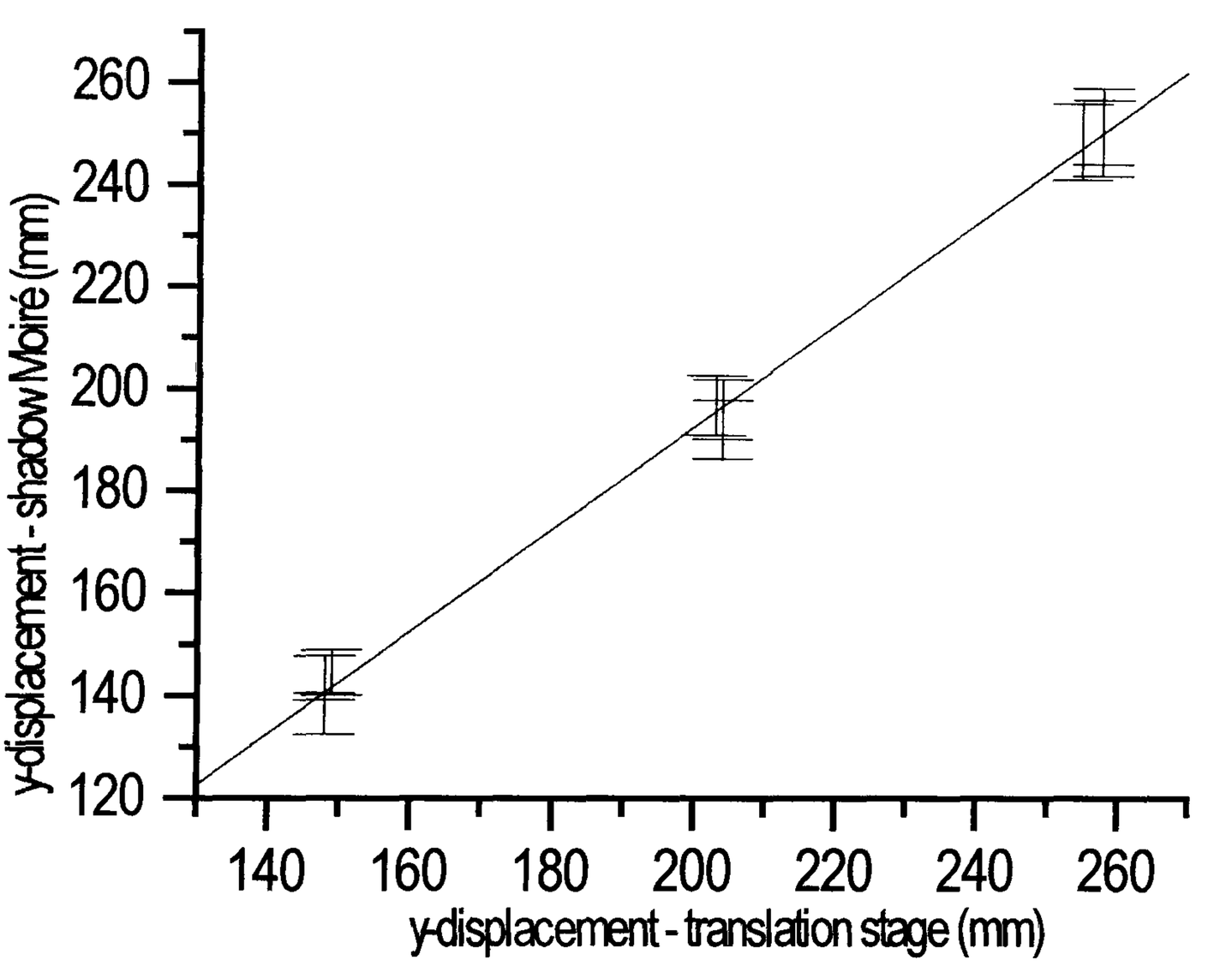

(b)

Figure 5.11 (a) The graph of x position measured using shadow Moiré against the x position measured from the stage position and (b) the graph of y position measured using shadow Moiré against the y position measured from the stage position.

The principal sources of error result from the illumination and imaging constraints of the shearography system. The analysis of the linear gratings used an intensity based method, because the pitch of the grating was close to the pitch of the CCD camera pixel spacing. The grating was illuminated by the expanded Gaussian intensity profile beam used for the shearography system. This intensity profile was corrected by dividing by the reference intensity profile of the beam, recorded using the reference perspex block. This greatly improved the linearity across the linear grating regions but left a residual intensity profile which is the principal source of error in the measurement. A more sophisticated intensity correction algorithm, such as fitting the recorded reference beam intensity to a Gaussian profile may increase measurement accuracy. The speckle noise in the Moiré fringe images could be removed by replacing the laser source with an incoherent light source. For the multi-component shearography system, with optical fibre illumination, this is a relatively simple modification as the incoherent light could be also be delivered to the illumination position using a optical fibre.

The determination of the fringe order of the linear grating fringes from the circular grating measurement can be ambiguous for some measurements as only the approximate source location is given. In this case, for the circular and linear grating pitches used, two possible source positions are suggested by the program with a maximum error of ± 11 mm if the incorrect one is chosen. This error can be reduced by decreasing the ratio of the circular to linear grating pitch, although this change increases the error when no ambiguity is present.

A further source of error resulting from the illumination and imaging geometry is that the distance to different parts of the gratings from the object centre varies when using illumination from a diverging beam rather than plane wave illumination. To reduce these errors the size of the grating could be reduced or the linear gratings could be located closer to the centre of the grating. For the experimental parameters used in the source position determination in this chapter the error due to the size of the grating is ± 1.8 %. The measurement accuracy may also be improved by using commercially produced gratings with a more accurate square wave intensity profile and pitch.

5.9. Conclusions

After reviewing the shadow Moiré method, the beam profile method and the shearography carrier fringe method the shadow Moiré method was chosen to measure the angle of illumination. Shadow Moiré has been successfully used to measure the source position in a multi-component shearography system. A grating containing circular, horizontal linear and vertical linear gratings has been used to measure the source position in two orthogonal directions with extended measurement range. The measurement is performed by replacing the object under investigation by the grating, blocking the shearing mirror in the interferometer and sequentially illuminating from the three illumination directions and recording the shadow Moiré fringe patterns obtained. Image processing of the fringe patterns yields the source position, in either the x or y directions, with an accuracy of ± 6 mm or ± 3 % for a typical source position of 200 mm, along either the x, or y, axis from the camera position..

5.10. References

Aebishcher H A and Waldner S, "Strain distributions made visible with image shearing interferometry", *Opt. Laser. Eng.*, **26**, pp. 407-420, 1997.

Forno C, "Moiré methods in strain measurement", in ed. Williams D C, "*Optical methods in engineering metrology*", Chapman and Hall, London, 1993.

Goult R J, Hoskins R F, Milner J A and Pratt A J, "*Computational Methods in Linear Algebra*", Stanley Thorne (Publishers) Ltd, London, 1974.

Jähne B, "*Digital Image Processing, Concepts, Algorithms and Scientific Applications*", Springer Verlag, Berlin Heidelberg, 1995.

James S W and Tatam R P, "Time-division-multiplexed 3D shearography", *Proc SPIE* **3744**, pp. 394-403, 1999.

Jones R and Wykes C, "*Holographic and Speckle Interferometry*", Chapter 3, Cambridge University Press, Cambridge, 1989.

Kafri O and Glatt I, "Moiré deflectometry – a ray deflection approach to optical testing", *Opt. Eng.*, **24,** pp. 944-960, 1985.

Kästle R, Hack E and Sennhauser U, "Multiwavelength shearography for quantitative measurements of 2D strain distributions", *Appl. Opt.*, **38**, pp. 96-100, 1999.

Ng T W and Chau F S, "Object illumination angle measurement in speckle interferometry", *Appl. Opt.*, **33**, pp. 5959-5961, 1994.

Ng T W, "Circular grating Moiré deflectometry analysis by zeroth and first order radial fringe order angle measurement", *Opt. Comm.*, **129**, pp. 344-346, 1996.

Patorski K and Olszak A, "Digital in-plane electronic speckle pattern shearing interferometry", *Opt. Eng.*, **36**:20, pp. 1007-2015, 1997.

Song J S, Lee Y H, Jo J H, Chang S and Yuk K C, "Moiré patterns of two different elongated circular gratings for the fine visual measurement of linear displacements", *Opt. Comm.*, **154**, pp. 100-108, 1998.

Waldner S and Bren S, "Compact shearography system for the measurement of 3D deformation", *Proc SPIE* **3745**, pp. 141-148, 1999.

Williams D C, "Laser beam geometry and its applications", in ed. Williams D C, "Optical Methods in Engineering Metrology", Chapman & Hall, London, 1993.

6. SHAPE AND SLOPE MEASUREMENT BY SOURCE DISPLACEMENT IN SHEAROGRAPHY

6.1 Introduction

To fully characterise the surface strain requires the measurement of the in-plane and the out-of-plane contributions to the strain field. Shearography can be used to measure surface deformation gradients and from these the surface strain components can be determined. However shearography measurements of the displacement gradient for non-planar objects contain errors due to the magnitude of the applied shear and the direction of the sensitivity vector varying across the surface of the object. A measurement of the object slope and shape allows a correction to be made for both of these errors.

Shearography with a sensitivity to *the derivative* can be used to generate correlation fringes sensitive to object slope. The slope determined in this way may be integrated numerically to yield the object shape. This sensitivity to slope of shearography is in contrast to the sensitivity to surface contours for the ESPI shape measurement techniques.

Slope measurement using shearography has been previously been demonstrated using wavelength contouring (Huang *et al* 1997), object rotation (Rastogi 1997 and Santhanakrishnan *et al* 1998), tilting a mirror in the illumination path (Griffin *et al* 1995) and by source displacement (Tay *et al* 1991, 1992, 1994 and 1997). Speckle interferograms are correlated before and after a change in the illumination conditions, or a change in the object position, in a procedure similar to that used for displacement gradient measurements yielding correlation fringes sensitive to the object slope. The

object rotation technique is unsuitable for large objects and the wavelength contouring technique relies on good laser stability when tuning the optical wavelength. The source displacement technique requires a method of displacing the optical source over a range of up to 1 mm and this can easily be implemented using fibre optic beam delivery and a translation stage.

In shearography source displacement will, in general, generate correlation fringes which are a mixture of slope and carrier fringes. A source displacement in a direction orthogonal to the axis of illumination generates slope fringes (Tay *et al* 1992). Carrier fringes are generated by changing the source to object distance (Takezaki and Hung 1986) and the carrier fringes distort the slope fringes when both are present.

In this chapter the source displacement method for determination of the object slope is investigated numerically. This provided information on the sensitivity to surface slope of the system as system parameters were changed. Relationships between surface slope and optical phase and, keeping the surface slope fixed, the relationship between system parameters and optical phase and between the magnitude and direction of source displacement and optical phase, are investigated. A shearography system that can measure object slope is described. Source displacement in a direction which minimises carrier fringe formation is used and a correction is made for the distortion in the slope fringes due to the necessary off-axis illumination required to give a sensitivity to slope. The measured slope is scaled using a slope sensitivity constant. The slope sensitivity constant is calculated using the numerical model using system parameters. The object slope is integrated along the shear direction to recover the object shape.

6.2. Slope and Shape Measurement Techniques in Shearography

This section covers the alternatives to the source displacement technique which may be used for the measurement of the slope using shearography. Section 6.3 describes the source displacement technique in detail.

6.2.1. Two-Wavelength Technique

The two-wavelength technique may be performed by sequentially illuminating the object with two optical wavelengths (Griffen *et al* 1995). Sequentially illuminating the object with first wavelength one then wavelength two and subtracting the interferometric speckle patterns obtained yields slope fringes. These slope fringes have a sensitivity that is determined by the wavelength shift, $\Delta\lambda$, and the magnitude of applied shear, dx. The optical phase of the slope fringes, $\Delta\phi_{SL}$, is:

$$\Delta\phi_{SL} = 4\pi \frac{\delta z}{\delta x}\left(\frac{1}{\lambda_1} - \frac{1}{\lambda_2}\right)dx \tag{6.1}$$

where $\delta z/\delta x$ is the object slope and λ_1 and λ_2 are the two optical wavelengths.

6.2.2. Object Rotation Technique

A description of this technique for shearography is given by Rastogi (1997). A small rotation of the object, by θ_r, generates a phase change sensitive to object slope, $\Delta\phi_{SL}$ (Rastogi 1997):

$$\Delta\phi_{SL} = \frac{2\pi}{\lambda} dx \frac{\delta z}{\delta x} \sin\theta \sin\theta_r \tag{6.2}$$

where λ is the optical wavelength, dx is the applied shear in the x-direction, $\delta z/\delta x$ is the slope and θ is the angle between the illumination direction and the z axis.

The magnitude of the illumination angle, θ, gives a sensitivity to slope. For typical experimental values of $\Delta\phi_{SL}$ = 62.8 radians, dx = 5 mm, θ = 30 ° and λ = 800 nm a rotation of the object by an angle of the order of 0.1 ° is required.

6.2.3. Changing the Illumination Path Technique

Hung *et al* (1978) described a method of measuring the object slope, by changing the refractive index of the medium around the object. The object was immersed in water in a rectangular glass tank. A reference frame was recorded of the interferometric speckle pattern and methanol was added to the water to change the refractive index. A second frame was recorded and the images were correlated, by subtraction, to obtain slope sensitive correlation fringes. The sensitivity of this method is (Hung *et al* 1978):

$$\Delta\phi_{SL} = \frac{2\pi}{\lambda} C \frac{\delta z}{\delta x} dx \tag{6.3}$$

where $\Delta\phi_{SL}$ is the phase of the slope fringes, λ is the optical wavelength, $\delta z/\delta x$ is the object slope and dx is the applied shear in the x direction. C is a constant given by:

$$C = n_1(1+\cos r_1) - n_2(1+\cos r_2) \tag{6.4}$$

where n_1 and n_2 are the refractive indices of the medium before and after the addition of methanol respectively. r_1 and r_2 are, respectively, the associated angles of refraction, given by:

$$r_1 = \arcsin\left(\frac{\sin\theta}{n_1}\right) \tag{6.5}$$

and

$$r_2 = \arcsin\left(\frac{\sin\theta}{n_2}\right) \tag{6.6}$$

For typical experimental parameters of $\Delta\phi_{SL}$ = 62.8 radians, λ = 800 nm, dx = 5 mm, n_1 = 1.5 and θ = 30 ° a refractive index change, Δn, of 1.5 x 10^{-3} is required. To generate this refractive index change by the addition of methanol to water would require a final methanol concentration of 5 mol dm^{-3}.

6.3. Source Displacement Technique Theory

6.3.1. Introduction

Correlation fringes sensitive to slope can also be generated by optical source displacement in shearography. Subtracting the speckle interferograms recorded before and after source displacement yields correlation fringes. In general the correlation fringes formed in this way are a mixture of slope and carrier fringes.

6.3.2. Carrier Fringe Formation

Carrier fringes are formed by moving the source along the source to object direction (Takezaki and Hung 1986). When carrier fringes and slope fringes are present together the slope fringes are dominant but are distorted by the carrier fringes. For this reason the formation of carrier fringes should be minimised when measuring object slope and shape. Carrier fringes have also been used to determine fringe order in shearography (Hung et al 1988).

A translation of the optical source along the source to object direction generates a quadratic variation in the phase of the wavefront across the object surface (Takezaki and Hung 1986). As the shearing interferometer is sensitive to the gradient of the phase change, this quadratic phase change results in the formation of linear correlation fringes

in a direction orthogonal to the shearing direction, if the illumination and viewing are normal to the object surface. The phase, $\phi_C(x)$, of the carrier fringes across a flat plate in the x-direction when normal illumination and viewing is employed, by an expanded beam, is given by (Takezaki and Hung 1986):

$$\phi_C(x) = \frac{2\pi}{\lambda}\left(\frac{DW}{W(W+DW)}\right)xdx \tag{6.7}$$

where λ is the optical wavelength, DW is the source displacement in the source-object direction, W is the source to object distance, x is a distance along the x axis and dx is the applied shear in the x direction. The pitch of the carrier fringes, Δ_C, generated in this way is given by:

$$\Delta_C = \frac{W(W+DW)\lambda}{DWdx} \tag{6.8}$$

For illumination of the object at an angle to the z axis, the carrier fringes are distorted. Figure 6.1 shows mathematically modelled undistorted and distorted carrier fringes generated for two angles of illumination, 0 ° and 20 °, of a flat plate. The carrier fringes are linear for illumination normal to the object surface and curved for illumination from an angle of 20 °.

6.3.3. Slope Fringe Formation

Slope fringes can be generated by displacement of the optical source when illumination at an angle to the z axis is employed (Tay *et al* 1992). The sensitivity of the correlation fringes to slope is dependent on the angle between the illumination and the imaging directions and the magnitude of the applied shear. Carrier fringe formation is minimised by moving the source in a direction orthogonal to the illumination direction.

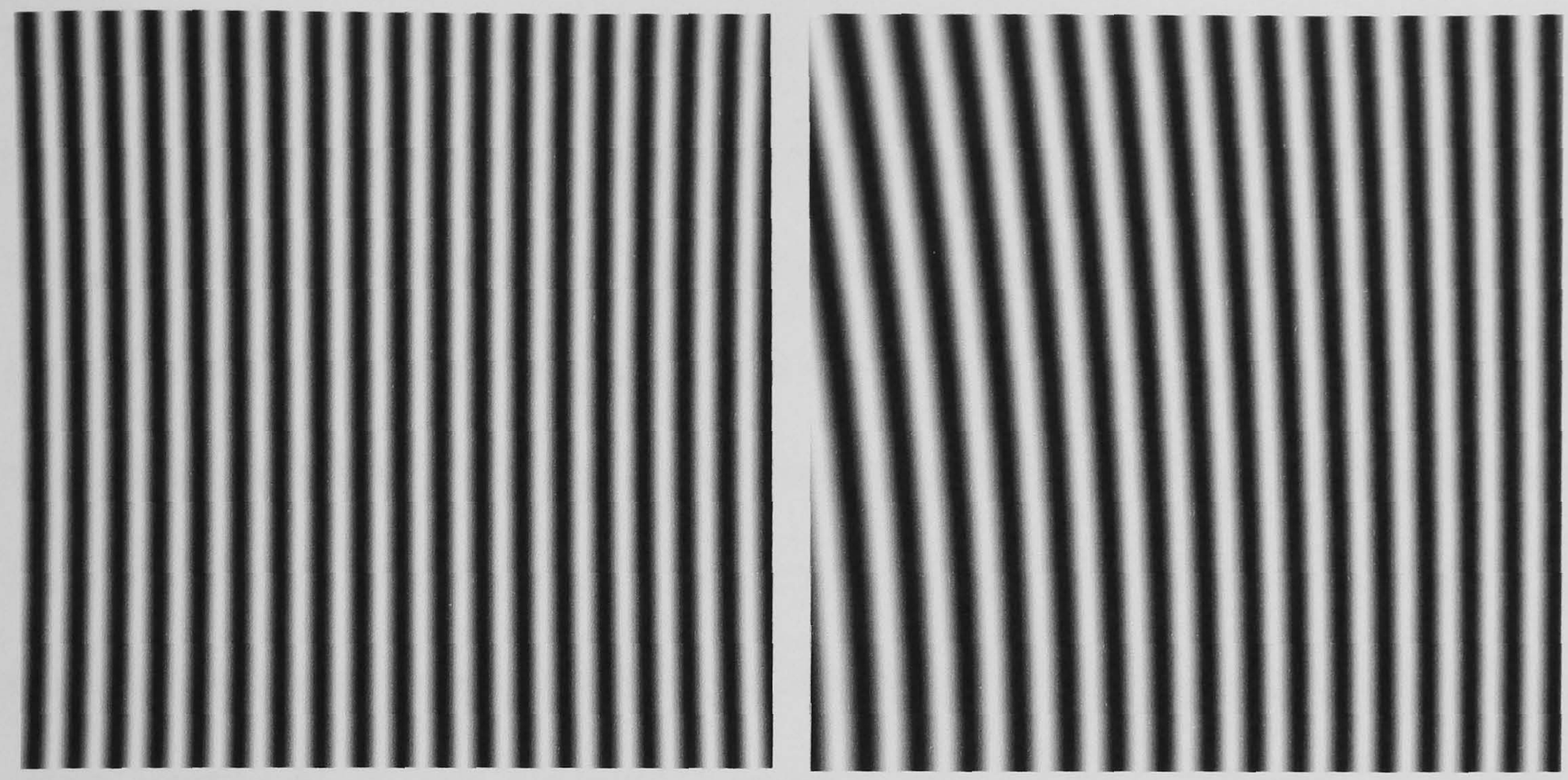

(a) (b)

Figure 6.1 Mathematically generated carrier fringes on a flat plate object for (a) illumination normal to the object surface and (b) illumination at 20° to z axis. In both cases the optical wavelength is 800 nm, the object to source distance is 0.5 m, the source displacement is 2 mm in the object to source direction and the applied shear is 5 mm in the x direction.

The relationship between the surface slope, $\delta z/\delta x$, the applied shear, dx, and the optical phase, ϕ_S, has previously been approximated using a binomial expansion (Tay et al 1991, 1994). The treatments involved calculations of terms of order one and two. In the $(1+x)^{1/2}$ term if x is much less than 1 then the $(1+1/2x)$ expansion may be used as an approximation (Jeffrey 1985) and for the expansion to be finite then x must be less than 1 (Jeffrey 1985). As subsequent steps in the calculation of the optical phase in the source displacement technique require calculation of differences in optical pathlengths, errors introduced in the binomial expansion are quickly magnified. A binomial expansion using further terms is possible depending on the illumination geometry but approximately ten, or more, terms are required, to achieve a comparable accuracy to the numerical method described in this chapter and this would result in an equation that is unwieldy.

In this chapter a numerical approach to the calculation of the relationship between the surface slope, applied shear, optical phase and source displacement is taken. The method of calculating the phase is described in Section 6.3.4. Section 6.3.5. describes the determination of the relationship between optical phase and surface slope. Subsequent sections describe individual calculations of the relationship between the optical phase and various system parameters.

6.3.4. Optical Phase Calculation

The optical phase is calculated numerically. The pathlength difference between the two paths through the shearing interferometer is calculated before and after the source

displacement. Subtracting the optical pathlength differences and converting to optical phase gives the phase of the correlation fringes.

To describe the slope fringe formation two orthogonal coordinate systems, *XYZ* and *UVW* have been defined, as shown in Figure 6.2. Both coordinate systems have their origin at the geometric centre of the object. The *XYZ* coordinate system has *Z*, object to imaging direction; *X*, orthogonal horizontally and *Y*, orthogonal vertically. The *UVW* coordinate system has *W*, object to initial optical source direction and two orthogonal directions *U* and *V*. The *XYZ* coordinate system can be transformed into the *UVW* coordinate system by a rotation of θ_1 in the *x-y* plane followed by a rotation of θ_2 in the *w-y* plane. The transformation is given by:

$$\begin{pmatrix} U \\ V \\ W \end{pmatrix} = \begin{pmatrix} \cos\theta_1 \cos\theta_2 & \sin\theta_2 & \sin\theta_1 \cos\theta_2 \\ -\cos\theta_1 \sin\theta_2 & \cos\theta_2 & -\sin\theta_1 \cos\theta_2 \\ -\sin\theta_1 & 0 & -\cos\theta_1 \end{pmatrix} \begin{pmatrix} X \\ Y \\ Z \end{pmatrix} \tag{6.9}$$

The source is initially located at $\boldsymbol{S_1}$ *[Sx₁, Sy₁, Sz₁]* and is used to illuminate an object, with the geometric centre of the object at ***O*** *[0, 0, 0]*. Point $\boldsymbol{P_1}$ *[Px₁, Py₁, Pz₁]* on the object surface is optically mixed with Point $\boldsymbol{P_2}$ *[Px₂, Py₂, Pz₂]* by the shearing Michelson interferometer. The principal plane of the imaging plane is at ***H*** and the applied shear is ***ds*** *[dx, dy, 0]*.

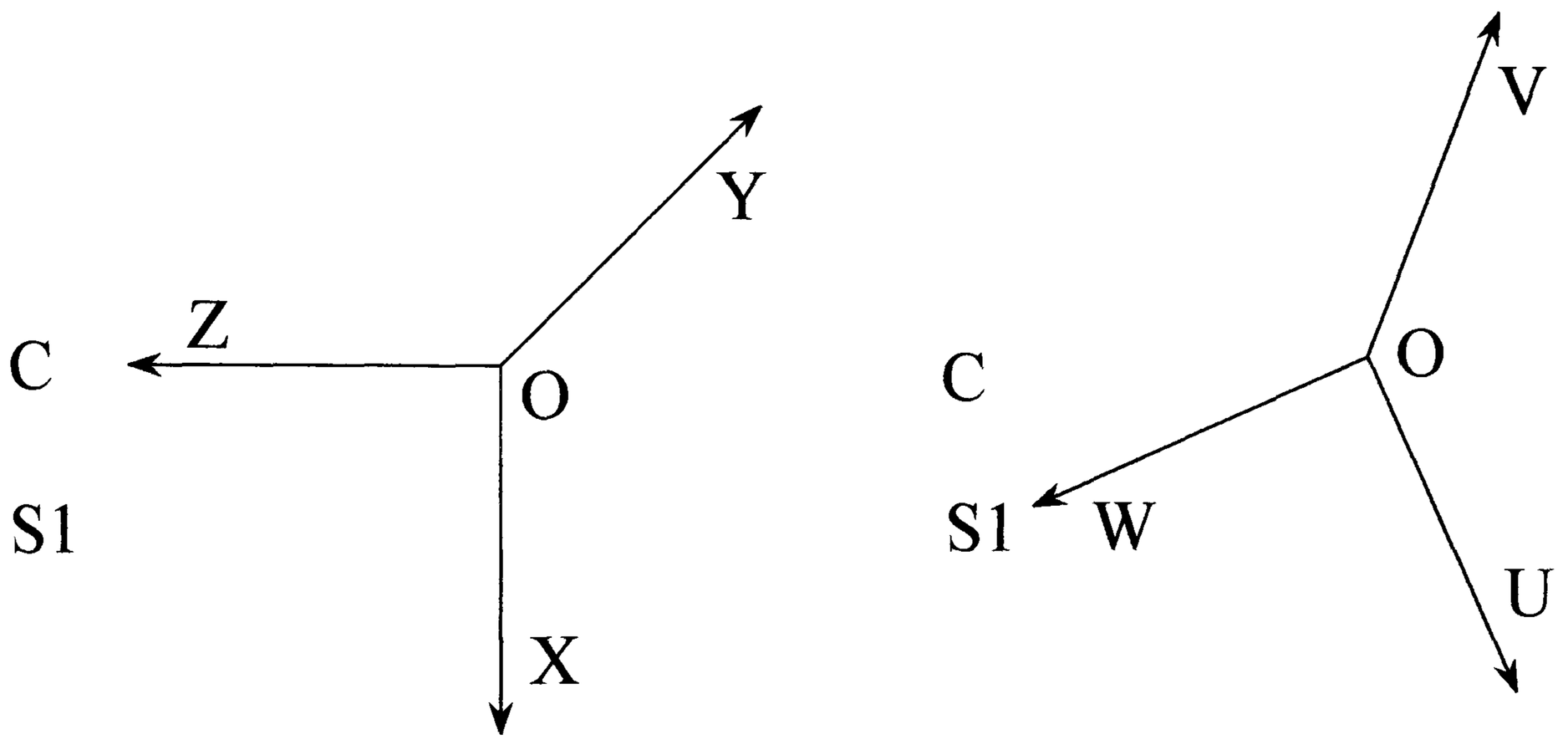

Figure 6.2 The location of the camera, C, object, O, and the initial optical source position, S1, in (a) the *XYZ* coordinate system and (b) the *UVW* coordinate system. O is the origin of the coordinate system and is at the centre of symmetry of the object.

The source is displaced by ***DD*** *[DX, DY, DZ]* to position $\boldsymbol{S_2}$ *[Sx_2, Sy_2, Sz_2]*.

$$\mathbf{S}_2\left[Sx_2, Sy_2, Sz_2\right] = \left[Sx_1 + DX, Sy_1 + DY, Sz_1 + DZ\right] \tag{6.10}$$

An interferometric speckle pattern with phase information on the optical pathlength difference between the two sheared images, Λ_{REF}, is recorded when the source is at $\boldsymbol{S_1}$:

$$\Lambda_{REF} = \left(S_1P_1 - P_1H\right) - \left(S_1P_2 - P_2H\right) \tag{6.11}$$

After displacement of the source to $\boldsymbol{S_2}$, a second interferometric speckle pattern is recorded, with phase information on the optical pathlength difference between the two sheared images, Λ_2, when the source is at $\boldsymbol{S_2}$:

$$\Lambda_2 = \left(S_2P_1 - P_1H\right) - \left(S_2P_2 - P_2H\right) \tag{6.12}$$

Subtracting the second image from the reference image yields the overall optical pathlength difference, Λ_Δ:

$$\Lambda_\Delta = \Lambda_2 - \Lambda_{REF} = S_2P_1 - S_2P_2 - S_1P_1 + S_1P_2 \tag{6.13}$$

The optical pathlengths P_1H and P_2H are constant in equations 6.11 and 6.12 and cancel.

In the mathematical model the terms S_2P_1, S_2P_2, S_1P_1 and S_1P_2 are expanded using the position vectors for the points, $\boldsymbol{S_1}$, $\boldsymbol{S_2}$, $\boldsymbol{P_1}$ and $\boldsymbol{P_2}$. These are:

$$S_2P_1 = \left\{\left(Sx_2 - Px_1\right)^2 + \left(Sy_2 - Py_1\right)^2 + \left(Sz_2 - Pz_1\right)^2\right\}^{1/2} \tag{6.14}$$

$$S_2P_2 = \left\{\left(Sx_2 - Px_2\right)^2 + \left(Sy_2 - Py_2\right)^2 + \left(Sz_2 - Pz_2\right)^2\right\}^{1/2} \tag{6.15}$$

$$S_1P_1 = \left\{\left(Sx_1 - Px_1\right)^2 + \left(Sy_1 - Py_1\right)^2 + \left(Sz_1 - Pz_1\right)^2\right\}^{1/2} \tag{6.16}$$

$$S_1P_2 = \left\{\left(Sx_1 - Px_2\right)^2 + \left(Sy_1 - Py_2\right)^2 + \left(Sz_1 - Pz_2\right)^2\right\}^{1/2} \tag{6.17}$$

Similar expressions can be obtained in the *UVW* coordinate system. In this model the shape of the object is used to calculate the z coordinate of $\boldsymbol{P_1}$ from the x and y coordinates. The x, y and z coordinates of $\boldsymbol{P_2}$ are calculated from the shape of the object and a knowledge of the applied shear $\boldsymbol{ds}$ and $\boldsymbol{P_1}$. $\boldsymbol{S_1}$ is calculated from the illumination geometry and $\boldsymbol{S_2}$ is calculated from $\boldsymbol{S_1}$ and the source displacement $\boldsymbol{DD}$.

The optical pathlength difference, Λ_Δ, is converted to optical phase, $\Delta\phi$, using:

$$\Delta\phi = \frac{2\pi\Lambda_\Delta}{\lambda} \tag{6.18}$$

where λ is the optical wavelength.

This intensity, I, of the correlation fringes is modelled using:

$$I = I_0(1+\cos(\Delta\phi + d\phi)) \tag{6.19}$$

where I_0 is the maximum intensity which occurs when $\Delta\phi+d\phi=0$ and $d\phi$ is a phase offset. Speckle noise cancels completely in the correlation process in this model.

The wrapped phase change, $\Delta\phi_W$, can also be modelled using:

$$\Delta\phi_W = \Delta\phi - 2\pi m \tag{6.20}$$

where m is an integer. This model is used to investigate the relationship between the optical phase and the object slope whilst varying system parameters.

6.3.5. Relationship Between the Optical Phase and the Surface Slope

The relationship between the optical phase and the surface slope is investigated by considering typical parameters for the system geometry and for the source displacement

direction and magnitude. The optical pathlength differences, and hence optical phase change, are calculated for various surface slopes. The typical system parameters used in the model are $\boldsymbol{S_1}$ *[0.2 m, 0.2 m, 1.0 m]*, ***ds*** *[5 mm, 0 mm, 0 mm]* and ***DD*** *[1 mm, 0 mm, 0 mm]*. For a range of surface slopes, $\delta z/\delta x$, between –5 and +5, the optical phase shows a linear dependence on the surface slope. This is shown in Figure 6.3. This is slightly larger than a practical range of surface slopes as a slope of 5 corresponds to an angle of illumination of 78°. The relationship between optical phase and surface slope for an angle of illumination of 35.8 ° to the *z* axis is also shown in Figure 6.3. In Section 6.3.6. the angle of illumination of 35.8 ° is determined as the angle of illumination for maximum sensitivity. For practical purposes, the surface slope is proportional to the optical phase and this linear relationship can be used to determine the change in surface slope from the optical phase change.

6.3.6. Relationship Between the Optical Phase and the System Geometry

The sensitivity is also determined by the angle between the illumination and imaging directions. The relationship between optical phase and the angle of illumination for surface slopes of +1 and –1 is shown in Figure 6.4. In the calculation, the angle of illumination has equal components in the *x*-*z* and the *y*-*z* directions. The relationship is non-linear and has zero slope when the angle of illumination is 35.8 °. At 35.8 ° the sensitivity of optical phase to surface slope is at a maximum. The non-linear nature of the graph makes the determination of the sensitivity to surface slope more complicated but does allow operation at an optimum angle of illumination.

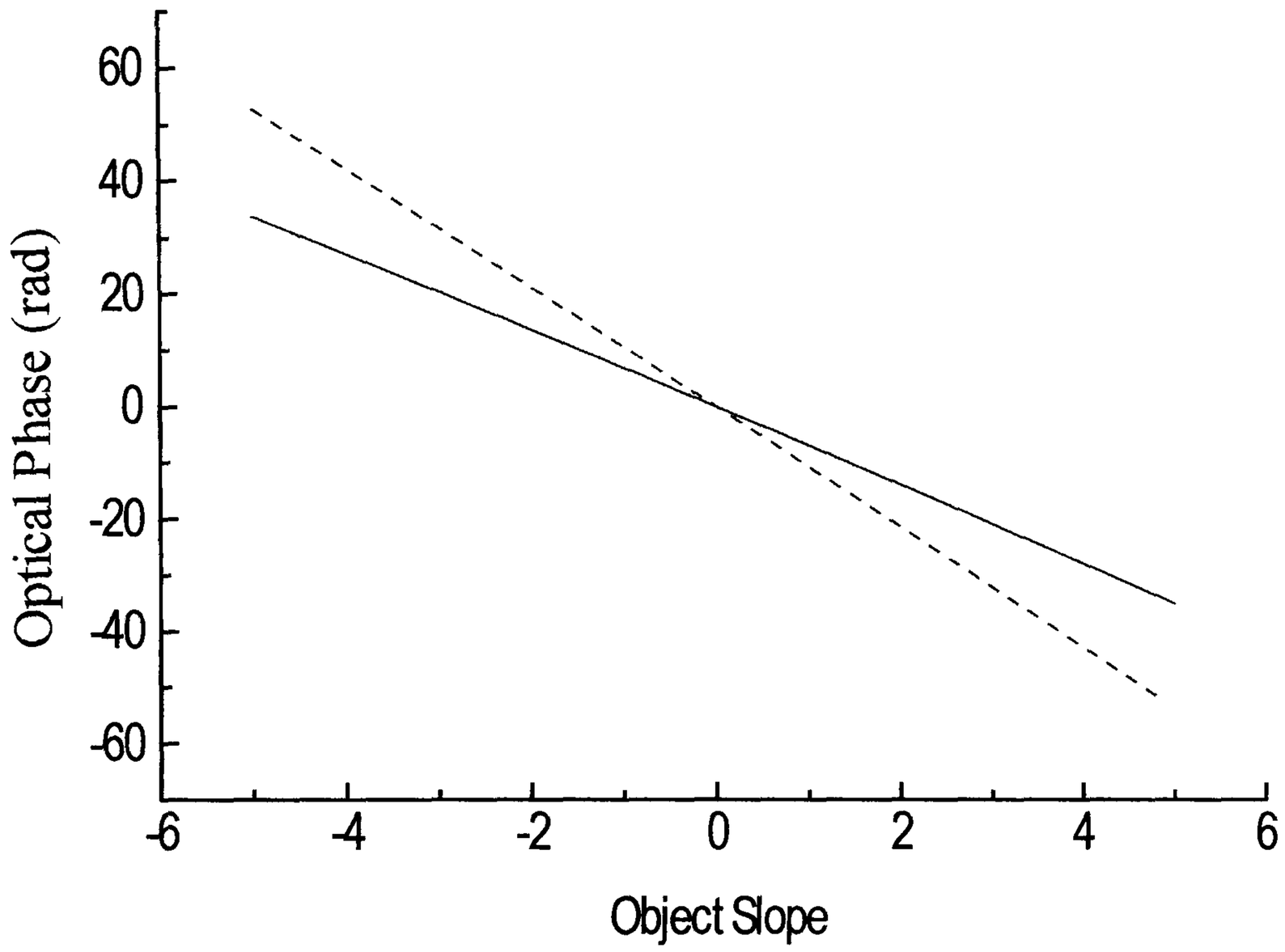

Figure 6.3 Relationship between the optical phase and the surface slope over a range of surface slopes, $\delta z/\delta x$, between –5 and +5. For (a) *solid line,* typical source position, $\boldsymbol{S}_1$ *[0.2 m, 0.2 m, 1.0 m]*, and (b) *dashed line,* source position for maximum sensitivity, $\boldsymbol{S}_1$ *[0.6 m, 0.6 m, 1.0 m]*, the angle of illumination is 35.8° as determined in Section 6.3.6. ***ds*** *[5 mm, 0 mm, 0mm]*, ***DD*** *[1 mm, 0 mm, 0 mm]*.

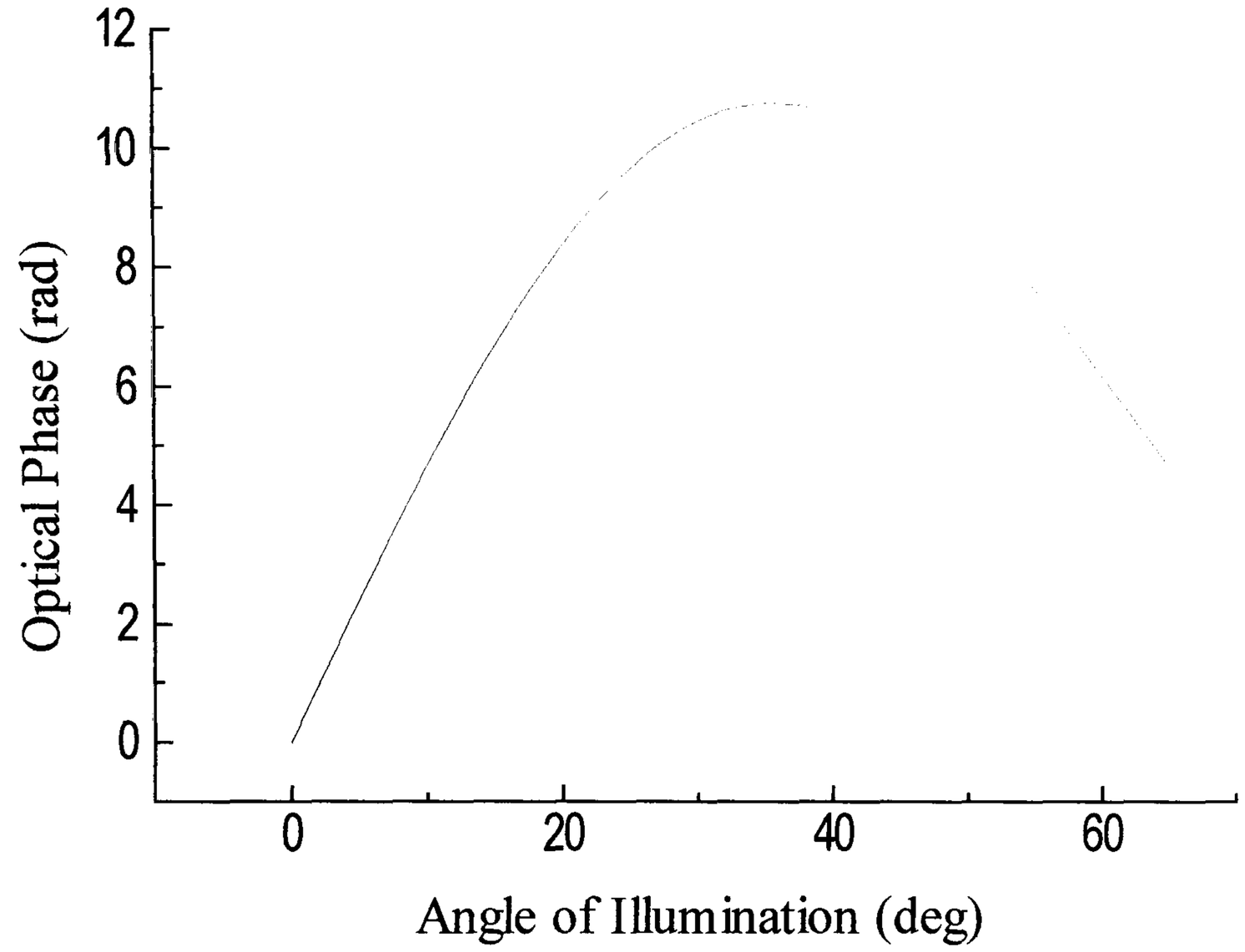

(a)

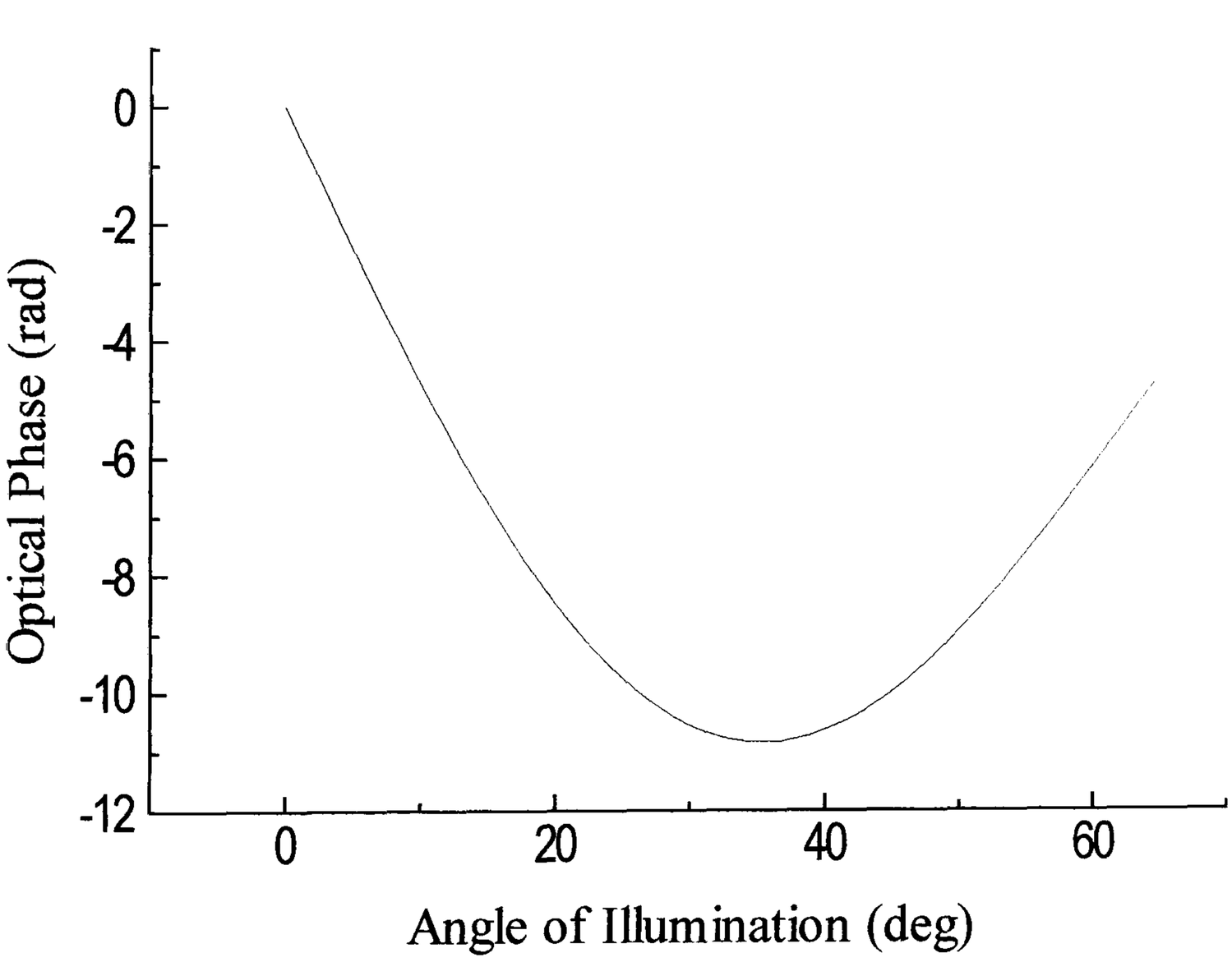

(b)

Figure 6.4 Relationship between the optical phase and the angle of illumination for surface slopes, $\delta z/\delta x$, of (a) –1 and (b) +1. ***ds*** *(5 mm, 0 mm, 0mm)*, ***DD*** *(1 mm, 0 mm, 0 mm)*. $\boldsymbol{S}_1$*[a, b, 1.0 m]* where $a=b$ and the angle of illumination is $sin^{-1}(a\sqrt{2})$

6.3.7. *Relationship Between the Optical Phase and the Magnitude and the Direction of the Source Displacement*

The relationship between the magnitude of source displacement in the x direction and the optical phase is investigated for surface slopes of –1 and +1. For typical source displacement magnitudes ***DD*** *[DX, 0, 0]* between 100 μm and 2 mm the relationship is linear as shown in Figure 6.5. A source displacement in the z direction would produce carrier fringes as this source displacement direction includes a large component of displacement in the w direction, as discussed in Section 6.3.2.

The optical source may also be moved in the *UVW* coordinate system as discussed previously. Movement of the optical source in the w direction generates carrier fringes. Movement of the optical source in the u direction, or the v direction, generates correlation fringes sensitive to surface slope, with a small contribution from a carrier fringe component.

6.3.8. *Calculation of the Slope Sensitivity Constant*

For most practical experimental conditions the optical wavelength, the magnitude of the source displacement and the magnitude of applied shear have a linear relationship to the sensitivity of the slope sensitive fringes. It can be shown that the phase change, $\phi_S(x,y)$, at a point (x,y) within the field of view is given by:

$$\phi_S(x,y) = \frac{DVdx}{\lambda}\left(K\frac{\delta z}{\delta x}(x,y) + C(x,y)\right) \tag{6.21}$$

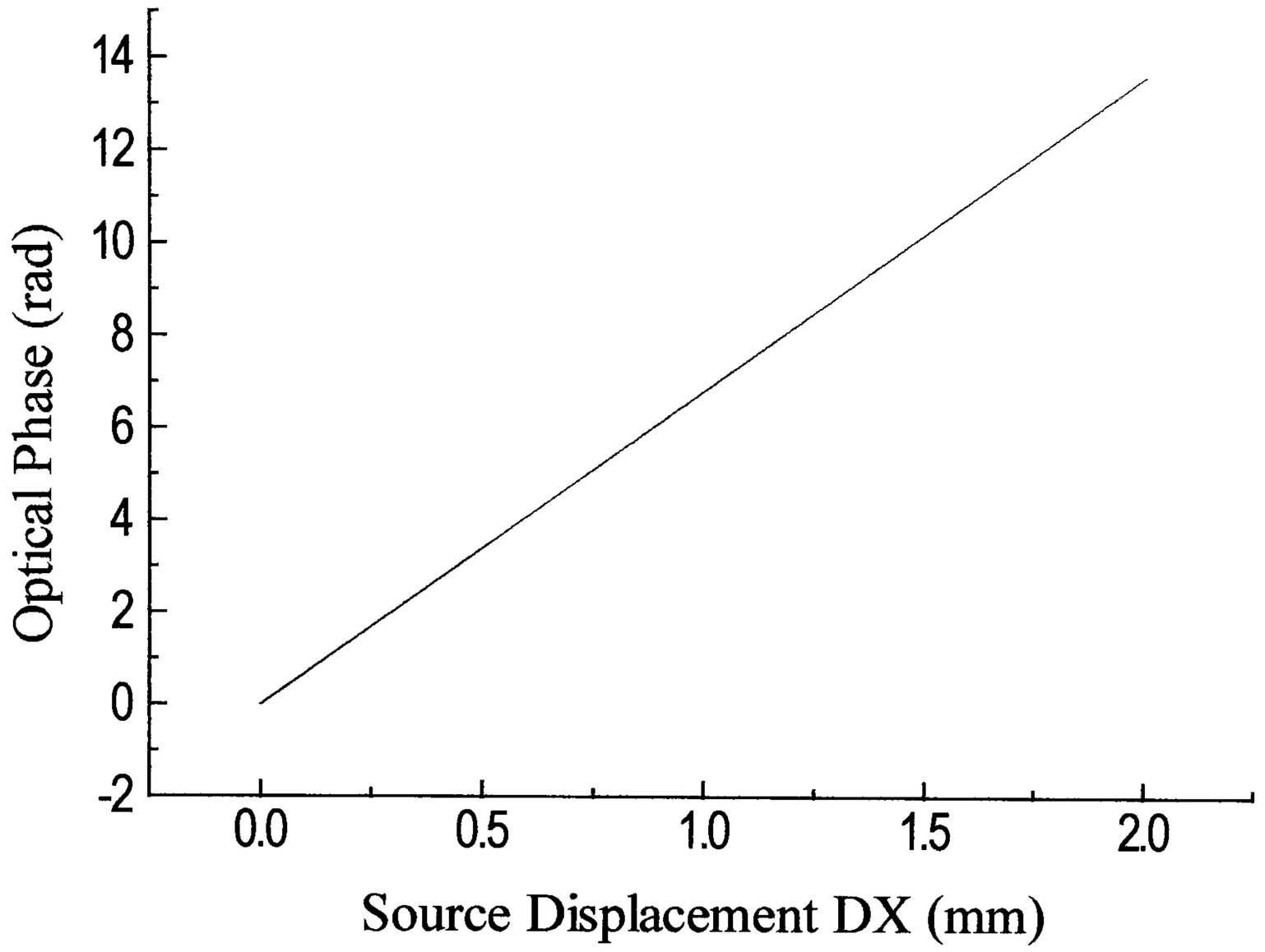

(a)

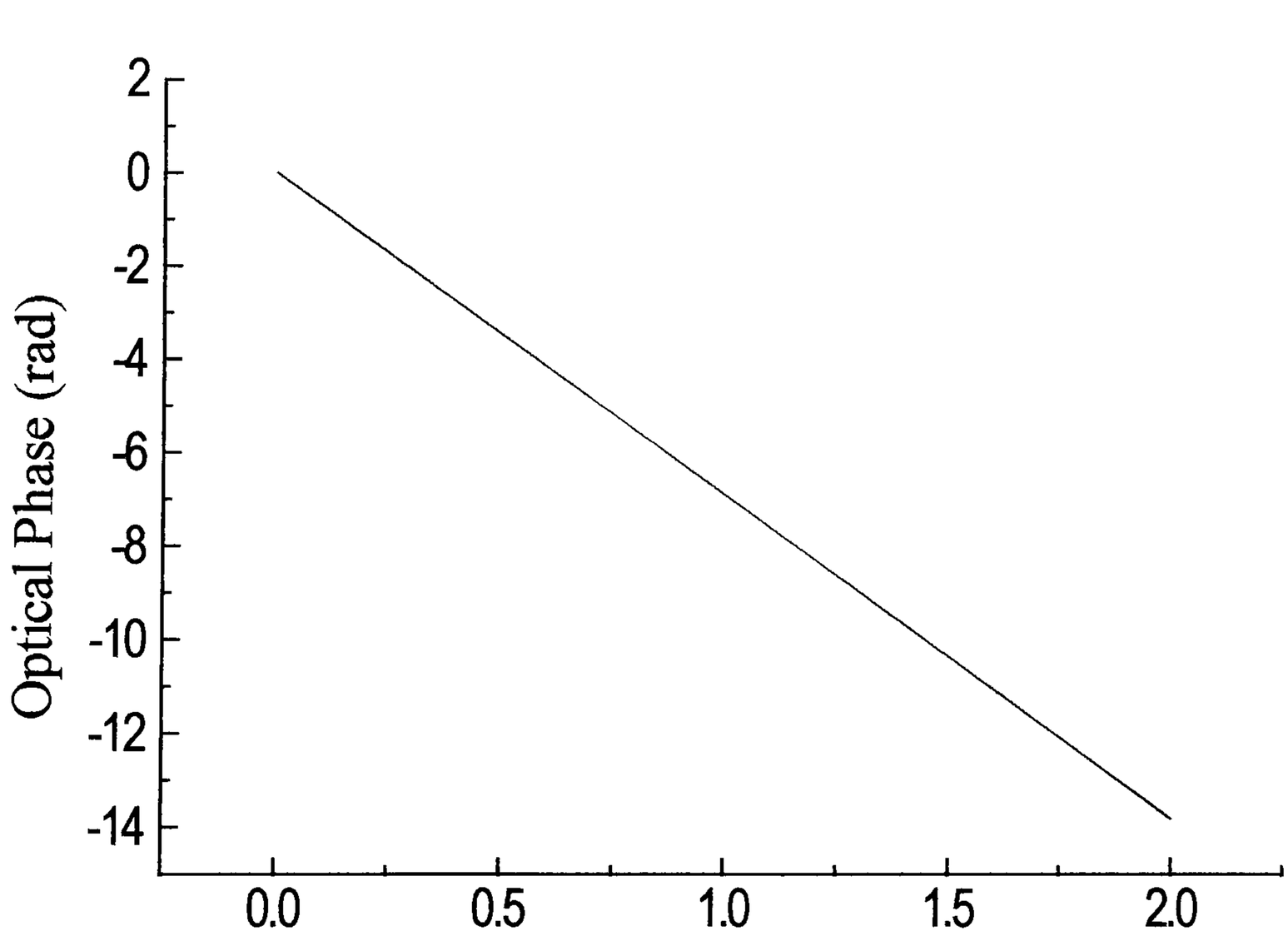

(b)

Figure 6.5 Relationship between the optical phase and the magnitude of source displacement, ***DD****[DX, 0, 0]*, between 0 mm and 2 mm, for a slope of (a) – 1 and (b) +1. $\boldsymbol{S_1}$ *[0.2 m, 0.2 m, 1.0 m]*, ***ds*** *[5 mm, 0 mm, 0mm]*.

where DV is the magnitude of a source displacement, in the v direction, dx is the applied shear, λ is the optical wavelength, K is the slope sensitivity constant, $\delta z/\delta x(x,y)$ is the surface slope at (x,y) and $C(x,y)$ is the zero slope constant at (x,y). The linear relationship between optical phase and surface slope, and between optical phase and the magnitude of source displacement have been shown previously. A linear relationship is assumed between optical phase and optical wavelength and between optical phase and the magnitude of applied shear. The introduction of the zero slope constant is to isolate the phase change across the object surface that is not due to surface slope changes.

The slope sensitivity constant, K, is calculated by the numerical model using the actual experimental parameters for the source and object positions, the direction and magnitude of source displacement, the direction and magnitude of applied shear and the optical wavelength.

The zero slope constant, $C(x,y)$, is determined experimentally using a flat plate test object. The flat plate object replaces the object under investigation, with the orientation of the flat plate defining the plane of zero slope. The slope fringe formation procedure is repeated for the flat plate, using an identical direction and magnitude of source displacement, and after image processing a value for $C(x,y)$ is determined across the field of view. These values of $C(x,y)$ can be subtracted from the measured slope of the object under investigation, to remove the influence of the change in optical phase across the field of view.

6.4. Experimental

The slope measurement technique described was incorporated in the multi-component shearography system described in Chapter 7. The shape measurement part of the system consisted of a fibre Bragg grating (FBG) stabilised laser diode (SDL model 5410 series, 810 nm, 100 mW) with light coupled via an optical fibre to the illumination position. Further details of the FBG stabilisation are contained within Section 7.3. The laser was fitted with circular beam correction optics (Blue Sky Research, San Jose, California, USA) so the laser produces a circular profile Gaussian beam. The optical power at the distal end of the fibre was 35 mW. Light exiting the fibre was expanded using a lens. The distal end of the fibre and the lens were located on a translation stage allowing source displacement in the *U*, *V* and *W* directions as defined in the *UVW* coordinate system. The illumination position was nominally located at $\boldsymbol{S}_1[-0.2\ m,\ 0.2\ m,\ 0.3\ \ m]$, in the *XYZ* coordinate system and is existing source location 3 in the multi-component shearography system.

The object was imaged through a Michelson interferometer consisting of a reference mirror, a shearing mirror and a non-polarising beamsplitter. The shearing mirror can apply shears in the *x* direction, the *y* direction or any direction in the *x*-*y* plane. The reference mirror was fitted with a piezoelectric transducer to allow phase-stepping. An 8-bit 75 Hz frame rate area scan camera (Dalsa Model CA-D4-0512A, 512 by 512 pixels) was used to record the speckle images, in conjunction with a PCI bus frame transfer card (Bitflow Roadrunner). Image capture and phase-stepping were synchronised using a program written using Labview software by Dr S W James. The experimental layout is shown in Figure 6.6.

To perform a measurement of surface slope and shape a reference frame of the speckle interferogram of the object was recorded. The source was subsequently displaced in a direction orthogonal to the axis of illumination. To recover the phase information lost in the correlation process, phase-stepping was implemented. Following the source displacement three phase-stepped frames were recorded with a $2\pi/3$ radians phase-step between them. These were combined using the 3-step "Temporal Phase Stepping Speckle Correlation" algorithm (Nakadate *et al* 1985) to calculate a wrapped phase map. The wrapped phase map was unwrapped using ISTRA software (Ettemeyer AG) which uses the minimum spanning tree technique (Ettemeyer *et al* 1989). The measurements were repeated for a flat plate test object, using the same magnitude and direction of source displacement to determine the zero slope constant, $C(x,y)$. The position of the flat plate in the z direction determines the point defined as zero slope on the object. The point defined as zero slope should also be used as the starting point for the ISTRA phase unwrapping software (Ettemeyer AG). The zero slope constant was subtracted from the unwrapped phase map of the object and the calculated slope was scaled using the slope sensitivity constant, K. The corrected unwrapped phase map of slope was integrated along the shear direction to determine the object shape. The integration was performed in Matlab software using the *cumulative trapezoidal numerical integration* function.

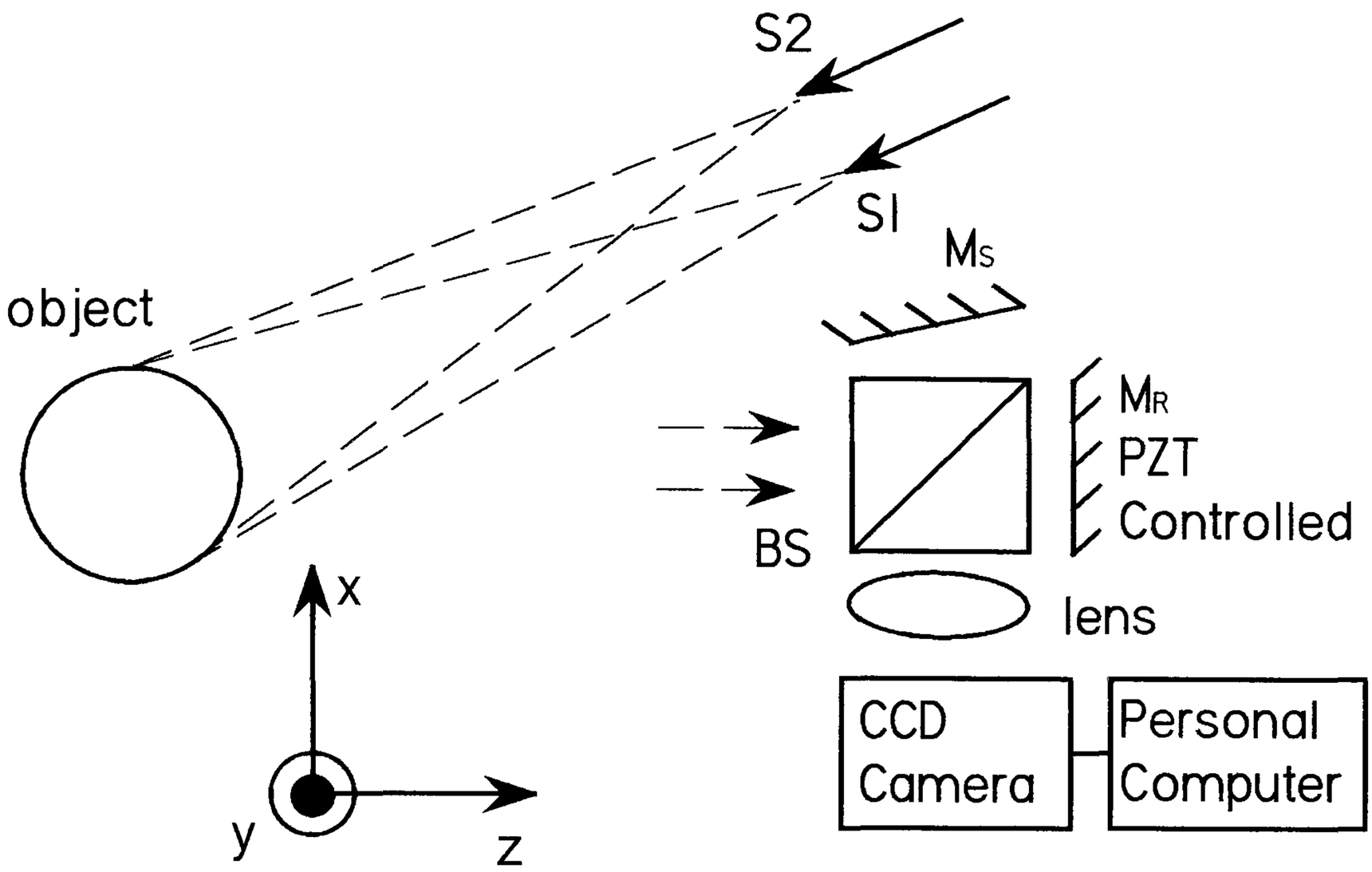

Figure 6.6 Experimental Layout. S1 and S2, source positions; BS, beamsplitter; M_S, shearing mirror; M_R, reference mirror.

6.5. Results and Discussion

The test object was a cylindrical gas main pipe, of length 900 mm and diameter 90 mm, coated with reflective paint. The applied shear was 10 mm in the x direction. Slope fringes were generated by a source displacement of 300 μm in the DV direction. Figure 6.7 shows experimentally determined wrapped phase maps of slope of the pipe and of a flat plate test object. Figure 6.8 shows the recovered object shape, with and without performing a correction using the zero slope constant. Both figures show a region of 40 by 55 mm on the surface of the pipe. The slope was scaled using a calculated slope sensitivity constant, K, of 11 m^{-1}, and a calculated zero slope constant, $C(x,y)$, as described in Section 6.3.8. If the correction is not performed the shape of the cylinder is distorted along both the length and around the circumference. The slope sensitivity constant cannot be used to scale the uncorrected shape so the uncorrected object shape in Figure 6.8 is scaled manually to enable comparison with the corrected shape.

Figure 6.9 shows sections through the measured shape at both ends of the field of view and, for comparison, a section through an ideal cylinder. The maximum error is ± 2 mm, or ± 10 % between the corrected experimentally determined shape and the actual shape of the object. This is determined by comparing the sections through each end of the cylinder with the theoretical shape.

To generate slope fringes the optimum direction of source displacement is orthogonal to the axis of illumination. Illumination at an angle to the z axis is required for the fringes to have a sensitivity to surface slope but the direction of applied shear may be in any direction in the x-y plane. The relationship between the magnitude of source

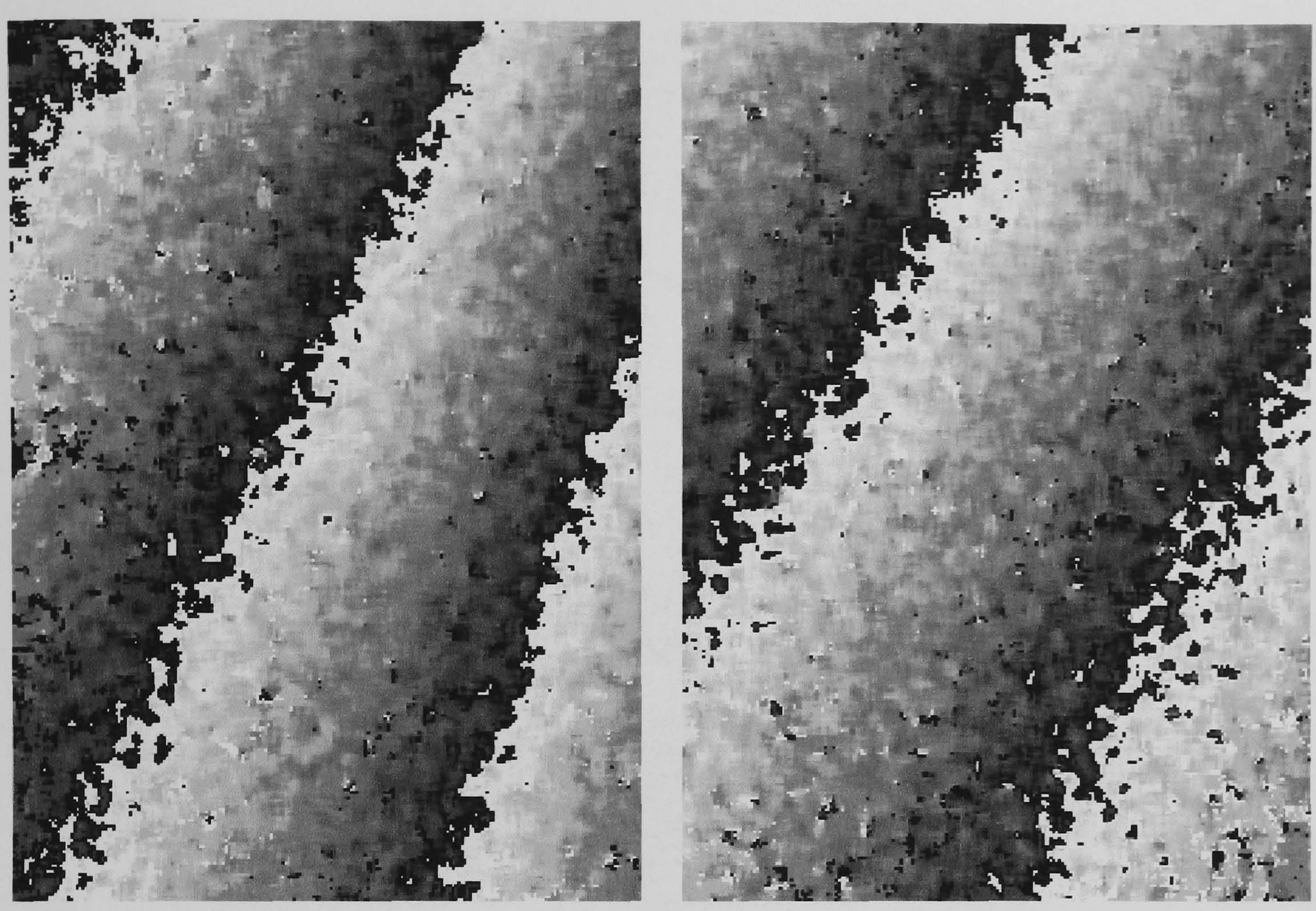

(a) (b)

Figure 6.7 Experimental slope fringes of a region 40 mm by 55 mm (a) on the cylindrical test object of diameter 90 mm and (b) on the flat plate test object, of size 200 mm square. $\mathbf{S_1}$[-0.2 m, 0.2 m, 0.3 m], **ds**[10 mm, 0 mm, 0mm] and in the UVW coordinate system **DD**[0 μm,300 μm, 0 μm].

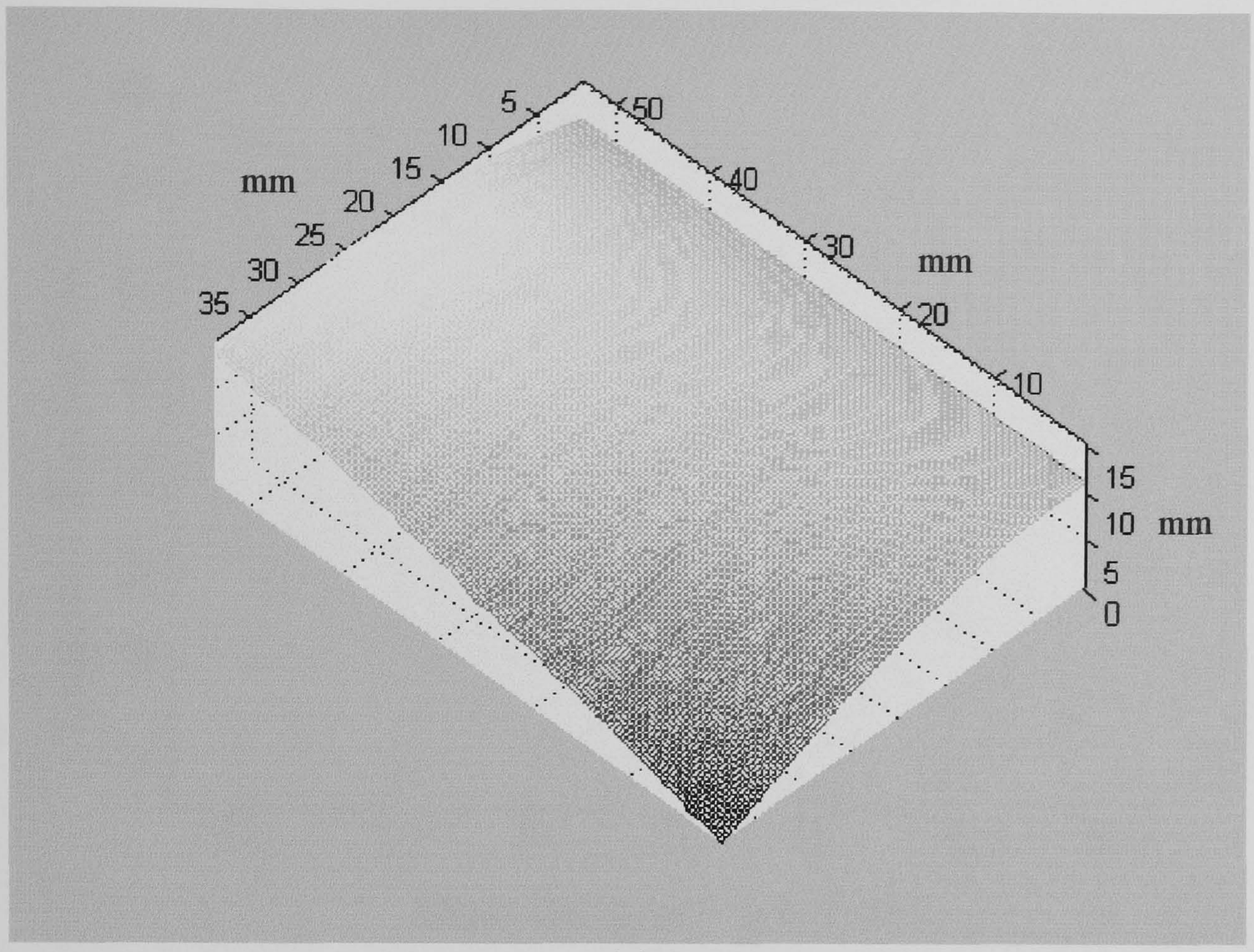

(a)

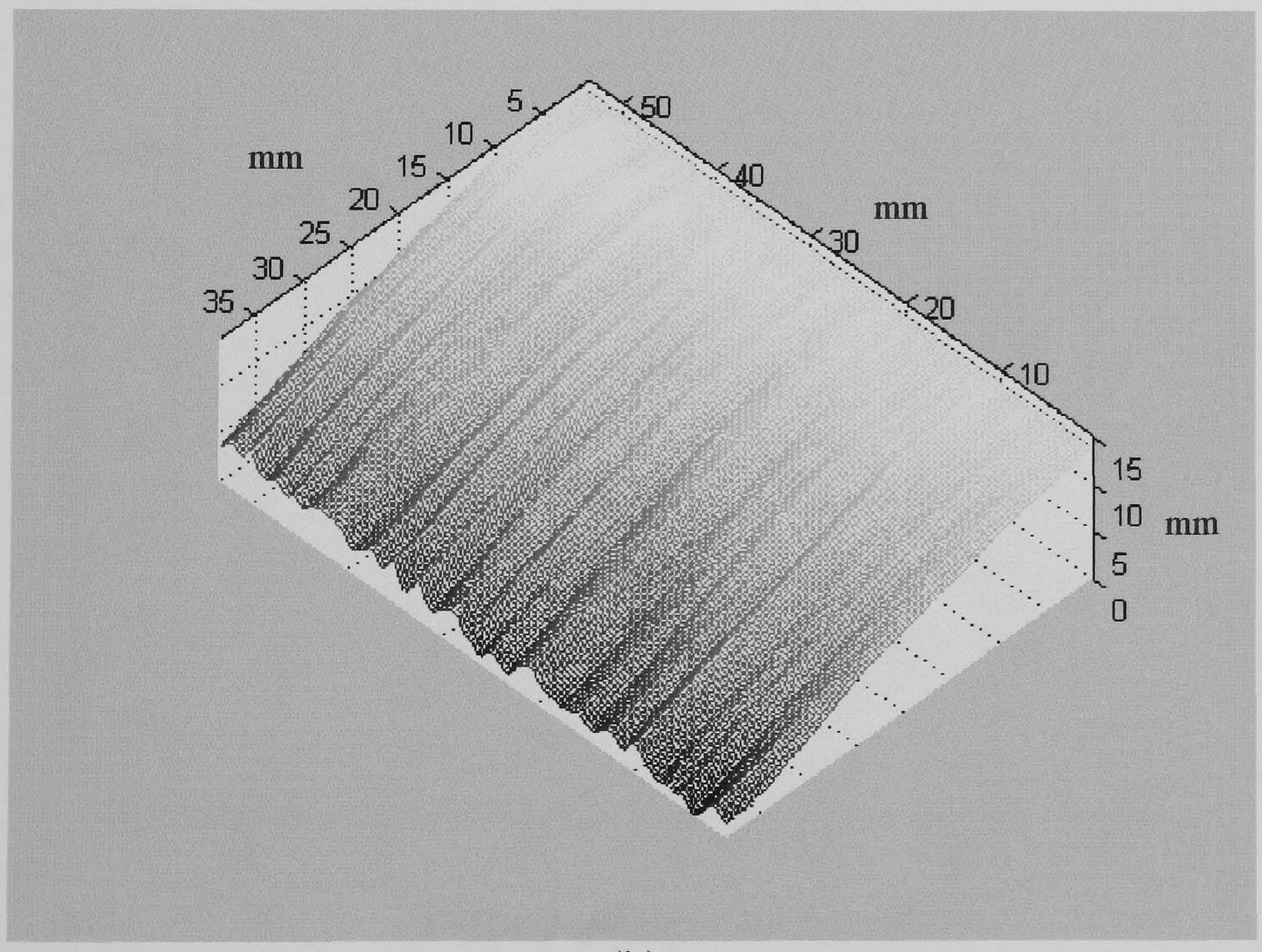

(b)

Figure 6.8 Experimentally determined shape of the cylindrical test object (a) without correction, and (b) with correction using the phase change across the flat plate.

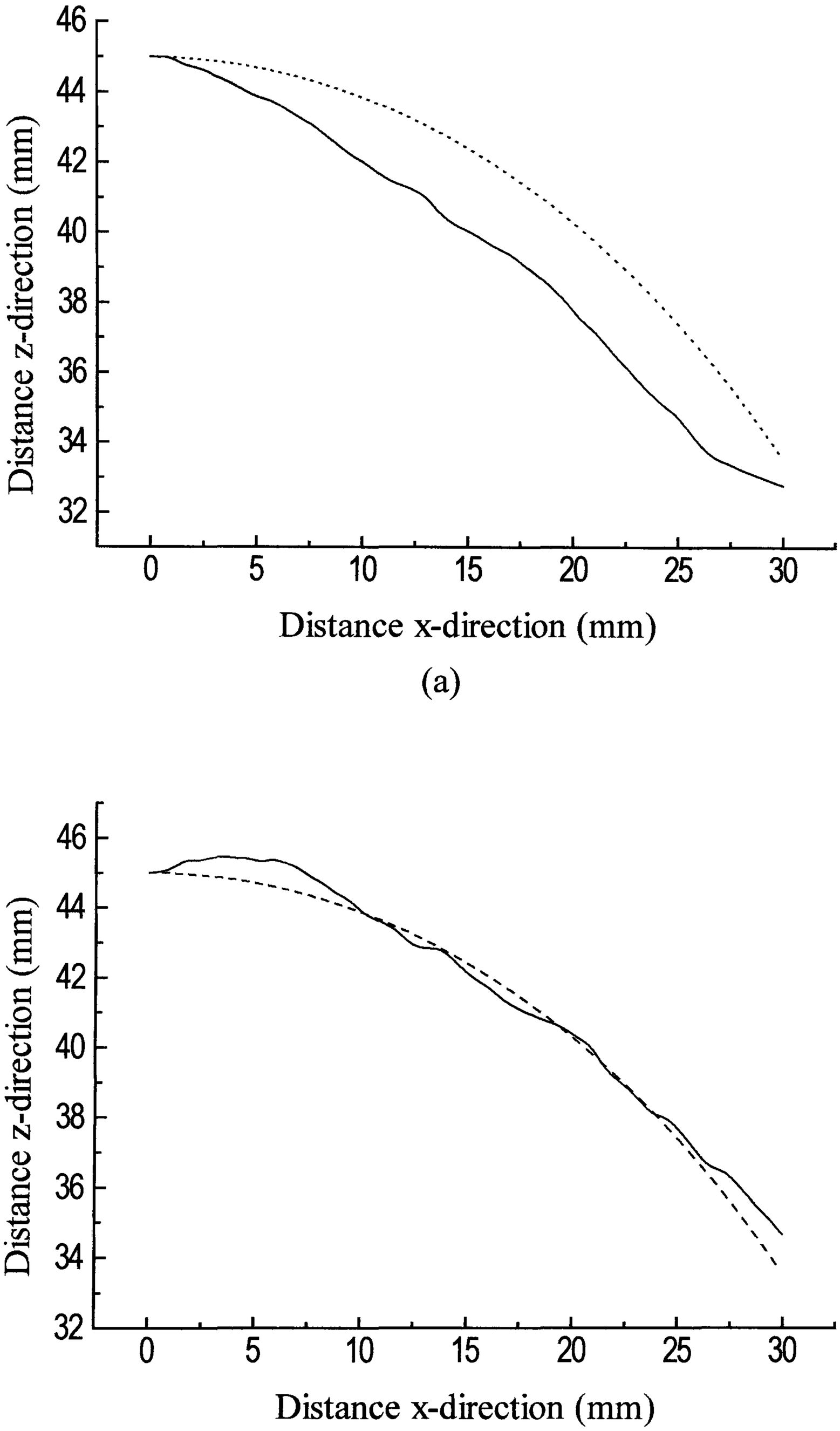

Figure 6.9 Sections through the object shape for (a) nearest end of the object in Figure 6.8(b) and (b) the farthest end of the object in Figure 6.8(b). (i) measured shape, *solid line*, (ii) theoretical shape, *dashed line*.

displacement and the optical phase has been shown to be sufficiently close to linear that a full numerical recalculation of K is not required when the magnitude of the source displacement is changed. However a full numerical recalculation of K is required when the angle of illumination is changed.

6.6. Summary

This chapter contains a full theoretical treatment of the measurement of surface slope and shape using source displacement in shearography. The influence of system geometry and the magnitude and direction of the source displacement on the sensitivity to surface slope were investigated. Numerically determining the relationship between surface slope and the optical phase, individually calculated for a set of system parameters, was shown to be more accurate than previous techniques involving simplification of equations.

The correction of the distortion of the slope fringes by subtraction of the unwrapped phase map of slope of a flat plate is important to improve the accuracy of the measurement of slope and, more importantly, the shape measurement. The slope sensitivity constant, K, can be calculated using the numerical model.

The generation of slope fringes by source displacement in shearography is complex. This chapter has shown how by considering typical experimental parameters the linear and non-linear parameters can be determined and the object shape can be determined to within $\pm$ 10 %.

A knowledge of the object shape and slope allows a correction to displacement gradient measurements in multi-component shearography and the determination of the surface strain in-plane and out-of-plane components relative to the local profile of the object surface. The shape and slope measurements of the cylinder made in this chapter are used in Chapter 7 to perform these corrections to the surface strain and to determine the surface strain components relative to the object surface. The choice of shearography for shape measurement is not ideal but does allow both the slope and shape to be determined using the same equipment that is used for surface strain measurement.

6.7. References

Ettemeyer A, Neuport U, Rottenkolber H and Winter C, "Schnelle und robuste bildanalyse von streifenmustern – ein wichtiger schritt der automation on holografichen profprozessen", *Proc. 1st Int. Workshop on Automatic Processing of Fringe Patterns*, pp. 23-31, 1989.

Griffen C T, Hung Y Y and Chen F, "Three-dimensional shape measurement using digital shearography", *Proc. SPIE* **2545**, pp. 214-220, 1995.

Huang J-R, Ford H D and Tatam R P, "Slope Measurement by Two-wavelength Electronic Shearography", *Opt. Laser. Eng.*, **27**, pp. 321-333, 1997.

Hung Y Y, Turner J L, Tafralian M, Hovanesian J D and Taylor C E, "Optical method for measuring contour slopes of an object", *Appl. Opt.*, **17**:1, pp. 128-131, 1978.

Hung Y Y, Hovanesian J D and Takezaki J, "A Fringe Carrier Technique for Unambiguous Determination of Fringe Orders in Shearography", *Opt. Laser. Eng.*, **8**, pp. 73-81, 1988.

Jeffrey A, "*Mathematics for Engineers and Scientists*", Van Nostrand Reinhold (UK) Co. Ltd, Wokingham, 1985.

Nakadate S and Saito H, "Fringe scanning speckle-pattern interferometry", *Appl. Opt.* **24**:14, pp. 2172-2180, 1985.

Rastogi P K, "An Electronic Pattern Speckle Shearing Interferometer for the Measurement of Surface Slope Variations of Three-Dimensional Objects", *Opt. Laser. Eng.*, **26**, pp. 93-100, 1997.

Santhanakrishnan T, Palanisamy P K and Sirohi R S, "Optical configuration in speckle shear interferometry for slope change contouring with a twofold increase in sensitivity", *Appl. Opt.*, **37**:16, pp. 3447-3449, 1998.

Takezaki J and Hung Y Y, "Direct Measurement of Flexural Strains in Plates by Shearography", *J. Appl. Mech.*, **53**, pp. 125-129, 1986.

Tay C J, Chau F S, Shang H M, Shim V P W and Toh S L, "The measurement of slope using shearography", *Opt. Laser. Eng.*, 14, pp. 13-24, 1991.

Tay C J, Shang H M, Poo A N and Luo M, "Measurements of surface coordinates and slopes by shearography", *Opt. Laser Technol.*, **24**:4, pp. 209-213, 1992.

Tay C J, Shang H M, Poo A N and Luo M, "On the Determination of Slope by Shearography", *Opt. Laser. Eng.*, **20**, pp. 207-217, 1994.

Tay C J, Shang H M and Choong D, "Cross Influence of Coordinate and Slope Related Fringes during Shearographic Profiling", *Opt. Laser. Eng.*, **26**, pp. 259-278, 1997.

7. SURFACE STRAIN MEASUREMENT OF NON-PLANAR OBJECTS USING SHEAROGRAPHY

7.1 Introduction

Shearography can be used to fully characterise the surface strain of an object, undergoing deformation. Six components of displacement gradient comprising three orthogonal components for *x* applied shear and three orthogonal components for *y* applied shear are measured to obtain the surface strain. To determine these six components, measurements are performed with three different directions of sensitivity vector, and with two orthogonal directions of applied shear. The magnitude of the applied shear controls the sensitivity of the displacement gradient measurement. The measured components of displacement gradient are non-orthogonal and the orthogonal in-plane and out-of-plane displacement gradient components are determined by a coordinate transformation.

An object that is non-planar, or that is tilted relative to the plane of the camera image, has a different magnitude of applied shear to that which is measured in the image plane. This variation in the applied shear relative to the measured magnitude of applied shear may be corrected by considering the surface slope of the object in the shear direction. Additionally a knowledge of the object shape allows the sensitivity vector to be locally determined across the object surface when performing the coordinate transformation allowing for any variation due to the object shape to be corrected. It is desirable to calculate the displacement gradient components, relative to the object surface profile, and this may also be performed using a knowledge of the object shape. The surface

slope and shape measurements may be performed using the source displacement technique in shearography as described in Chapter 6.

The experimental part of this chapter describes the investigation of a welded joint in a gas main pipe using shearography. A full surface strain determination is performed, with a correction to the data using the surface slope and the shape information. Six components of displacement gradient are measured using three illumination directions, multiplexed in the time domain, a single camera and shearing head, and two orthogonal directions of applied shear. A correction to the variation in applied shear across the object surface is made using surface slope information and the object shape is used to calculate local sensitivity vectors across the object surface, for each measurement channel. A coordinate transformation, using object shape information, is performed on the measured displacement gradient components to obtain the in-plane and out-of-plane displacement gradients relative to the local profile of the object surface.

7.2 Theory

7.2.1. Multi-Component Strain Measurement using Shearography

The component of displacement gradient measured by shearography is determined by the sensitivity vector and by the direction of the applied shear. A measurement of the two in-plane and one out-of-plane displacement gradient components, for a particular direction of applied shear, may be made in two ways.

The components may be measured directly by using dual illumination for each in-plane component and collinear illumination and viewing for the out-of-plane component. This technique, whilst providing independent measurements of the in-plane and out-of-plane displacement gradient components, requires the use of five illumination, or viewing, directions and does not allow for a correction for the error due to the slope and shape of the object.

The alternative is to use a minimum of three illumination, or viewing, directions and perform a coordinate transformation to obtain the in-plane and out-of-plane displacement gradient components. The location of the source positions is important to minimise the errors introduced in the coordinate transformation. This is discussed in Section 7.2.3. This technique, as the in-plane and the out-of-plane components are not measured directly, allows additional error correction to be performed within the calculations. This makes this technique particularly suitable for non-planar objects as an error correction may be incorporated to take account of varying shear magnitude and varying sensitivity vector across the object surface.

A measurement of all the three displacement gradient components, the out-of-plane and two in-plane components, can be performed using either a single illumination direction and three, or more, viewing directions or a single viewing direction and three, or more, illumination directions. The latter is employed in the experimental system described in this thesis. This approach removes the need to correct for perspective distortion due to different viewing directions and to match the magnitudes and directions of shear in the

multiple interferometers. The cost of multiple interferometers would also be greater and the bulkiness of the system would be increased. For illumination, via optical fibres, from laser diode sources there is only a small increase in complexity. A coordinate transformation is used to transform from the measured displacement gradient components to the out-of-plane and two in-plane components.

The applied shear is determined by the direction and magnitude of the tilt applied to the shearing mirror in the shearing interferometer. Two orthogonal directions of applied shear, in conjunction with the three different illumination directions, are required to obtain the six components of displacement gradient required to fully characterise the surface strain. The magnitude of applied shear controls the measurement sensitivity and is typically of the order of 5 to 10 mm.

The surface strain is determined from the six components of displacement gradient. Shearography is able to measure all the surface strain components, shown in bold in equation 7.1, but is not able to measure the bulk strain components, $\delta u/\delta z$, $\delta v/\delta z$ and $\delta w/\delta z$. A measurement of the bulk strain components using shearography would require the applied shear to be in a direction into the object. The strain tensor, S, is given by:

$$S = \begin{pmatrix} \dfrac{\delta u}{\delta x} & \dfrac{1}{2}\left(\dfrac{\delta u}{\delta y}+\dfrac{\delta v}{\delta x}\right) & \dfrac{1}{2}\left(\dfrac{\delta u}{\delta z}+\dfrac{\delta w}{\delta x}\right) \\ \dfrac{1}{2}\left(\dfrac{\delta v}{\delta x}+\dfrac{\delta u}{\delta y}\right) & \dfrac{\delta v}{\delta y} & \dfrac{1}{2}\left(\dfrac{\delta v}{\delta z}+\dfrac{\delta w}{\delta y}\right) \\ \dfrac{1}{2}\left(\dfrac{\delta w}{\delta x}+\dfrac{\delta u}{\delta z}\right) & \dfrac{1}{2}\left(\dfrac{\delta w}{\delta y}+\dfrac{\delta v}{\delta z}\right) & \dfrac{\delta w}{\delta z} \end{pmatrix} \tag{7.1}$$

7.2.2. Laser Sources

A range of laser sources have been used for speckle interferometry including gas lasers (Davies and Buckberry 1986), ruby lasers (Zou *et al* 1996) and solid state diode lasers (Wykes and Flannagan 1987, Tatam *et al* 1990). For this application the flexibility of use of the diode lasers is important. The output power of laser diodes may be modulated by modulation of the injection current. Single mode laser diodes offer spectral characteristics suitable for interferometry when the injection current is modulated and the optical power currently available is sufficient to illuminate objects of area 0.25 m^2.

7.2.3. Optimum Illumination Geometry

Ideally the illumination geometry would be arranged such that the direction of each sensitivity vector results in the production of correlation fringes that are sensitive to only one of the displacement gradient components. For the measurement of the in-plane displacement gradient a calculation is usually used to obtain the in-plane component from two measured displacement gradient components. In a full surface strain measuring system separation of the in-plane and out-of-plane contributions to the deformation of an object's surface generally requires the illumination, or viewing, of the object from a minimum of three directions. The measured phases from the three viewing directions, $\Delta\phi_1$, $\Delta\phi_2$ and $\Delta\phi_3$, may be described by the matrix operation given in equation 7.2.

$$\begin{pmatrix} \Delta\phi_1 \\ \Delta\phi_2 \\ \Delta\phi_3 \end{pmatrix} = \begin{pmatrix} k_{x1} & k_{y1} & k_{z1} \\ k_{x2} & k_{y2} & k_{z2} \\ k_{x3} & k_{y3} & k_{z3} \end{pmatrix} \begin{pmatrix} \frac{\partial u}{\partial x} \\ \frac{\partial v}{\partial x} \\ \frac{\partial w}{\partial x} \end{pmatrix} dx = M \begin{pmatrix} \frac{\partial u}{\partial x} \\ \frac{\partial v}{\partial x} \\ \frac{\partial w}{\partial x} \end{pmatrix} dx \tag{7.2}$$

where k_{xi}, k_{yi}, k_{zi} are components of the sensitivity vector, k_i pertaining to illumination directions $i=1,2,3$, $\delta u/\delta x$, $\delta v/\delta x$ and $\delta w/\delta x$ are the displacement gradient components in the strain tensor, dx is the applied shear and M is the coordinate transformation matrix. Extraction of the orthogonal displacement gradient components from the three fringe maps requires a coordinate transformation from the non-orthogonal measurement co-ordinate system to the orthogonal system.

$$\begin{pmatrix} \frac{\partial u}{\partial x} \\ \frac{\partial v}{\partial x} \\ \frac{\partial w}{\partial x} \end{pmatrix} dx = M^{-1} \begin{pmatrix} \Delta\phi_1 \\ \Delta\phi_2 \\ \Delta\phi_3 \end{pmatrix} \tag{7.3}$$

The coordinate transformation, by matrix multiplication, in shearography may be analysed by calculation of the condition number of the matrix (James and Tatam 1999). In the paper by James and Tatam the optimum practical illumination geometry for multi-component geometry was determined. This is sources located at 1. [a, -a, D], 2. [a, a, D] and 3. [-a, a, D], the principal plane of the imaging system located at [0, 0, D] and a ratio a/D of greater than 0.2. Figure 7.1 shows this ideal practical illumination geometry.

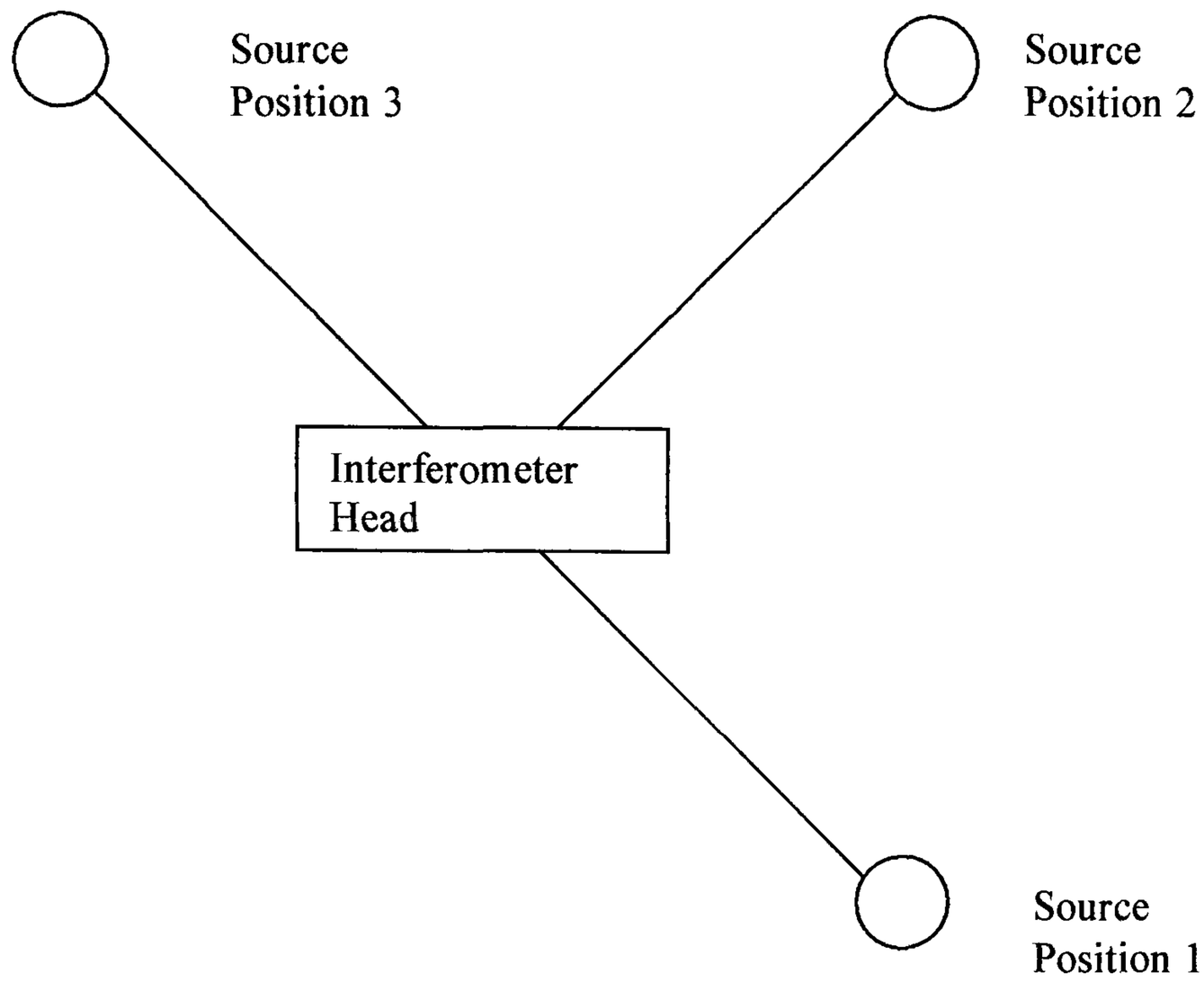

Figure 7.1 Ideal practical illumination geometry for multi-component shearography, as viewed from the object

The performance of matrix operations were considered by calculating the condition number of the transformation matrix. The system $Ax = b$ is said to be well conditioned if small errors in the coefficients of the transformation matrix A have a small effect on the solution, and is said to be ill conditioned if the effect is large. For a full surface strain measurement system the solution may be thought of in terms of the intersection of three planes. If the planes are orthogonal, then the intersection point is well defined, and small errors in the inclination of the planes have little effect upon the location of the intersection. This corresponds to the transformation being well conditioned, and the matrix has a condition number of unity. However, as the relative inclination of the planes is reduced any uncertainties in the geometry may result in large inaccuracies in the calculated intersection point and the condition number increases.

In general, a matrix transformation is well conditioned if the conditioning number, κ, is of the order of unity (Goult *et al* 1974). Matrix transformations with higher conditioning numbers are less well conditioned. The conditioning number may be calculated using the *cond(x)* function using Matlab software. For a typical experimental shearography system with sources positioned at 1. [0.2 m, -0.2 m, 1.0 m], 2. [0.2 m, 0.2 m, 1.0 m] and 3. [-0.2 m, 0.2 m, 1.0 m], the object at [0.0 m, 0.0 m, 0.0 m] and the principal plane of the imaging system at [0.0 m, 0.0 m, 1.0 m] the conditioning number, κ, would be 20.

The transformation matrix required to calculate the orthogonal deformation gradient components from measurements of displacement gradient components for these typical source positions is (Aerbischer and Waldner 1997):

$$\begin{pmatrix} \frac{\partial u}{\partial x} \\ \frac{\partial v}{\partial x} \\ \frac{\partial w}{\partial x} \end{pmatrix} = \frac{1}{dx} \begin{pmatrix} 0 & \frac{1}{2k_x} & -\frac{1}{2k_x} \\ \frac{1}{2k_y} & -\frac{1}{2k_y} & 0 \\ \frac{1}{2k_z} & 0 & \frac{1}{2k_z} \end{pmatrix} \begin{pmatrix} \Delta\phi_1 \\ \Delta\phi_2 \\ \Delta\phi_3 \end{pmatrix} \tag{7.4}$$

where the sources are located such that the sensitivity vectors for the three channels are: (k_x, k_y, k_z), $(-k_x, k_y, k_z)$, and $(-k_x, -k_y, k_z)$ respectively. This matrix for typical ideal source positions requires the addition or subtraction of appropriate pairs of images.

In a practical system the sources will not be exactly in the nominal positions. In this case the inverse matrix is calculated from the actual source positions. For example for the source positions used in the experimental determination in this chapter with source 1 at [0.220 m, -0.173 m, 0.270 m], source 2 at [0.224 m, 0.176 m, 0.265 m] and source 3 at [-0.177 m, 0.187 m, 0.265 m] the inverse matrix is:

$$M^{-1} = \begin{pmatrix} -0.379 & 2.615 & -2.812 \\ -2.879 & 2.831 & 0.066 \\ 2.200 & -0.317 & 2.333 \end{pmatrix} \tag{7.5}$$

where all the matrix components are in metres. This matrix has a conditioning number, κ, of 4.3. This experimental geometry was used to increase optical power at the object surface, but it also had the advantage of reducing the conditioning number of the transformation matrix, reducing coordinate transformation errors.

7.2.4. Multiplexing Techniques

A number of options exist for multiplexing the three measurement channels. Spatial-division-multiplexing (SDM) may be performed, where the object is illuminated from a single direction, and is simultaneously viewed from three different directions through three shearing interferometers. As discussed earlier, this approach has a number of complications associated with the alignment of the three views of the object with sub-pixel accuracy. A wavelength-division-multiplexed (WDM) scheme has been reported (Kästle *et al* 1999), in which the object was simultaneously illuminated from three separate directions by three sources operating at three different wavelengths. The object was viewed through a single shearing interferometer, and imaged onto three CCD chips via a complex arrangement of wavelength and polarisation selective optical elements. The third option, exploited here, employs time-division-multiplexing (TDM), in which the object is sequentially illuminated from three directions.

The object is imaged through a single shearing interferometer onto a single CCD camera using a simple optical arrangement. The illumination is synchronised with the frame rate of the CCD camera, such that each frame contains an image of the object viewed from one of the three illumination directions. The TDM approach does not suffer from the image registration requirements associated with the SDM and WDM schemes. However, SDM and WDM techniques allow the three channels to be monitored simultaneously at the camera frame rate, while the TDM approach requires that three sequential frames be recorded, which can increase the measurement time by a factor of three. To maintain the same data rate a higher speed camera may be used. In

shearography TDM has be performed using mechanical shutters (Waldner and Brem 1999) and may be performed by injection current modulation of laser diodes.

7.2.5. Phase-Stepping Techniques

In order to obtain quantitative strain data from shearography fringe maps, an unwrapped phase map must be generated, which requires the acquisition of at least three phase-stepped images of the object in a deformed, or undeformed, state. In a single image containing correlation fringes the fringes can represent either a positive or a negative phase change so the phase information has been lost. The phase can be determined by using three, or more, speckle images with a known phase-step between them. A number of phase stepping techniques for shearography have been proposed and demonstrated for this purpose, using polarisation (Kothiyal and Diesle 1985), liquid crystal (Kadano *et al* 1991), piezo-electric phase shifters (Valera and Jones 1994, Mohan *et al* 1994) and laser diode wavelength modulation (Huang *et al* 1996, Groves *et al* 2000) combined with algorithms employing 3, 4 and 5 phase steps (Creath 1993). The time taken to acquire the phase-stepped images defines the duration of the measurements, and thus the stability requirements of the object under investigation.

The multi-component shearography system described in this thesis uses a piezo electric transducer (PZT) controlled reference mirror to perform the phase-stepping. This method of phase-stepping is suitable for the severe environments found when testing industrial components.

To perform the phase-stepping using a PZT phase shifter the reference mirror in the interferometer head is fitted with a PZT allowing displacement of the mirror on applying a voltage with the magnitude of the displacement determined by the magnitude of applied voltage. Control of the PZT voltage, in synchronisation with the recording of camera frames allows the appropriate phase-stepped images to be recorded to generate the wrapped phase map using the phase-stepping algorithm. The wrapped phase maps are processed using phase unwrapping software, such as ISTRA (Ettemeyer AG), to remove the discontinuities in the wrapped phase map. The three frame technique with a $2\pi/3$ phase-step used in the experimental section of this chapter uses the minimum number of frames required to determine the phase. An analysis of the errors when using this algorithm is given in Section 4.7.2.

7.2.6. Strain Measurement Utilising Slope and Shape Information

The slope and shape information can be used to correct the displacement gradient measurements for slope and shape dependent measurement errors and can also provide a surface onto which the strain measurements can be mapped. Corrections are made for the applied shear, and therefore the displacement gradient sensitivity, varying across a curved surface and for the change in sensitivity vector across the object surface. A summary of the process is given in a flow chart in Figure 7.2.

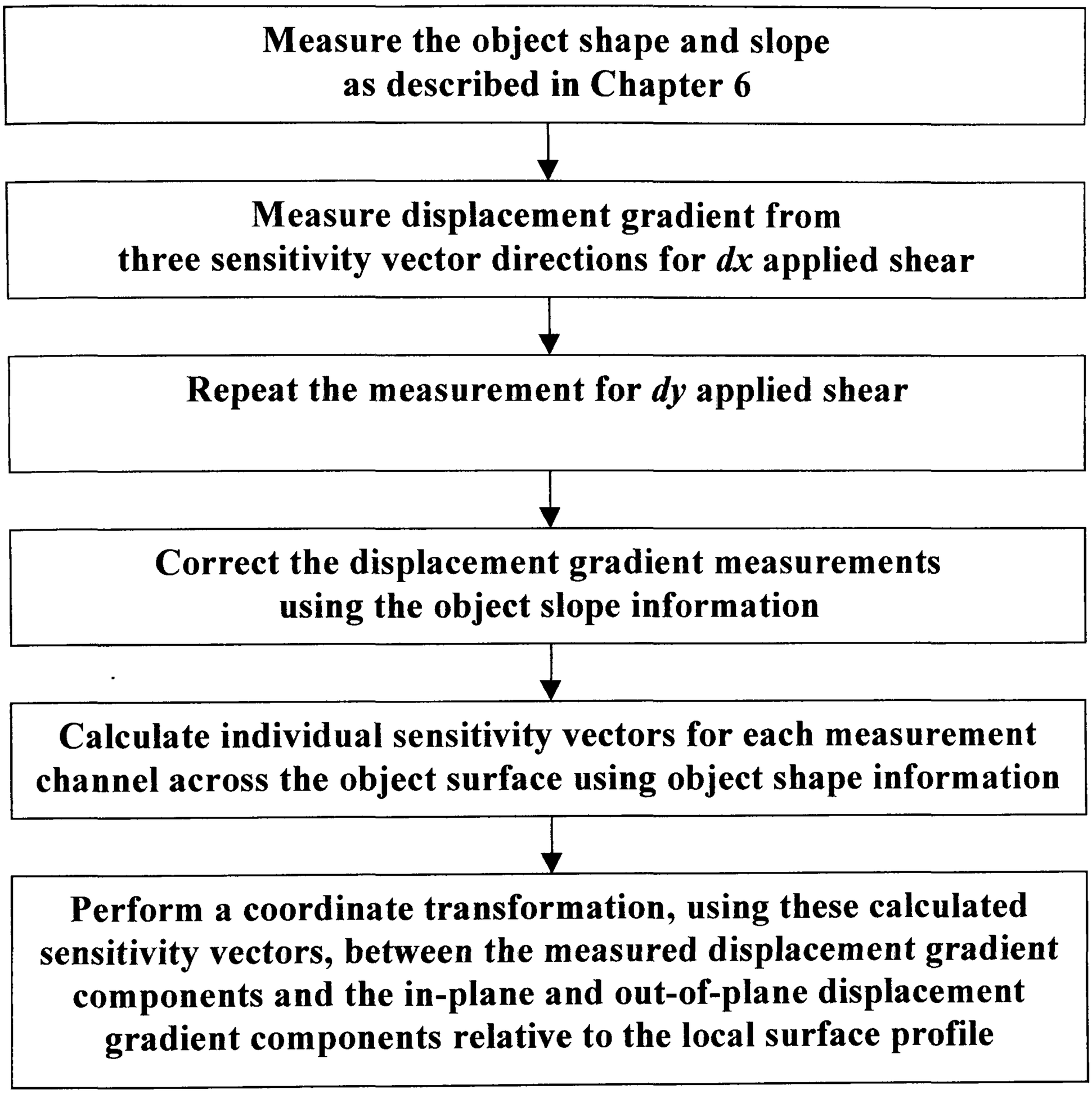

Figure 7.2 Flow chart of the strain measurement process using the multi-component shearography system

The applied shear is usually measured in the plane of the camera image. For a curved surface, or surface inclined with respect to the plane of the camera image, the applied shear on the object surface is larger, as the measured applied shear is stretched over a larger distance on the object surface. This error can be corrected using a knowledge of the object slope and geometry. The corrected shear, dx_C, is calculated using:

$$dx_C = dx_M \sqrt{\left(\left(\frac{\delta z}{\delta x}\right)^2 + 1^2\right)} \tag{7.6}$$

where dx_M is the measured applied shear and $\delta z/\delta x$ is the surface slope in the x direction. Equation 7.6 is obtained by considering an applied shear of dx, in the plane of the camera image, and projecting this distance onto the sloping surface of the object. Figure 7.3 shows the variation in applied shear for various slopes of object surface.

The error due to the variation in the sensitivity vector across the object surface can be corrected by calculating individual sensitivity vectors across the object surface using a knowledge of system geometry. The calculation involves, for each pixel in the camera image, a calculation of illumination and imaging directions, and from these the sensitivity vectors for each measurement channel. This is performed using a knowledge of the three source positions, the position of the principal plane of the imaging system, the field of view and the object shape. From these, the three sensitivity vectors of the measurement channels are calculated. The shape of the object also provides the orientation of the surface, and hence the directions of the in-plane and out-of-plane directions. A coordinate transformation is performed between the measured coordinate

systems and the local coordinate system of the object surface. At the edge of the field of view the angle of the sensitivity vector is modified most, compared with the centre of the field of view. Figure 7.4 shows a schematic of how the sensitivity vector changes across the field of view, for normal viewing and illumination.

7.3 Experimental

The multi-component TDM shearography system with phase-stepping and coordinate transformation software was developed by Dr S W James under the EU funded MuWaS project. The modifications made to the system were the addition of the shape measurement channel, as described in Chapter 6, utilising source displacement, and software was written using Matlab to process the unwrapped phase map of slope to obtain the object shape. The coordinate transformation software was modified to incorporate corrections for the object slope and shape by Dr S W James. The multi-component TDM shearography system is now able to measure the six displacement gradient components and perform the surface slope and shape measurement.

The shearography system utilised three illumination directions and one interferometer head to perform the measurements. Three fibre Bragg grating stabilised laser diodes (SDL Model 5410 series, 810 nm, 100 mW optical power), with fibre optic beam delivery to the source position were used to illuminate the object. The Bragg gratings were formed at the laser diode end of a 1 m length of optical fibre (Spectron, single-mode photosensitive, cut-off wavelength 780 nm, reflectivity 40 %) by illumination of the fibre core with a high power pulsed UV laser under controlled conditions (Dockney

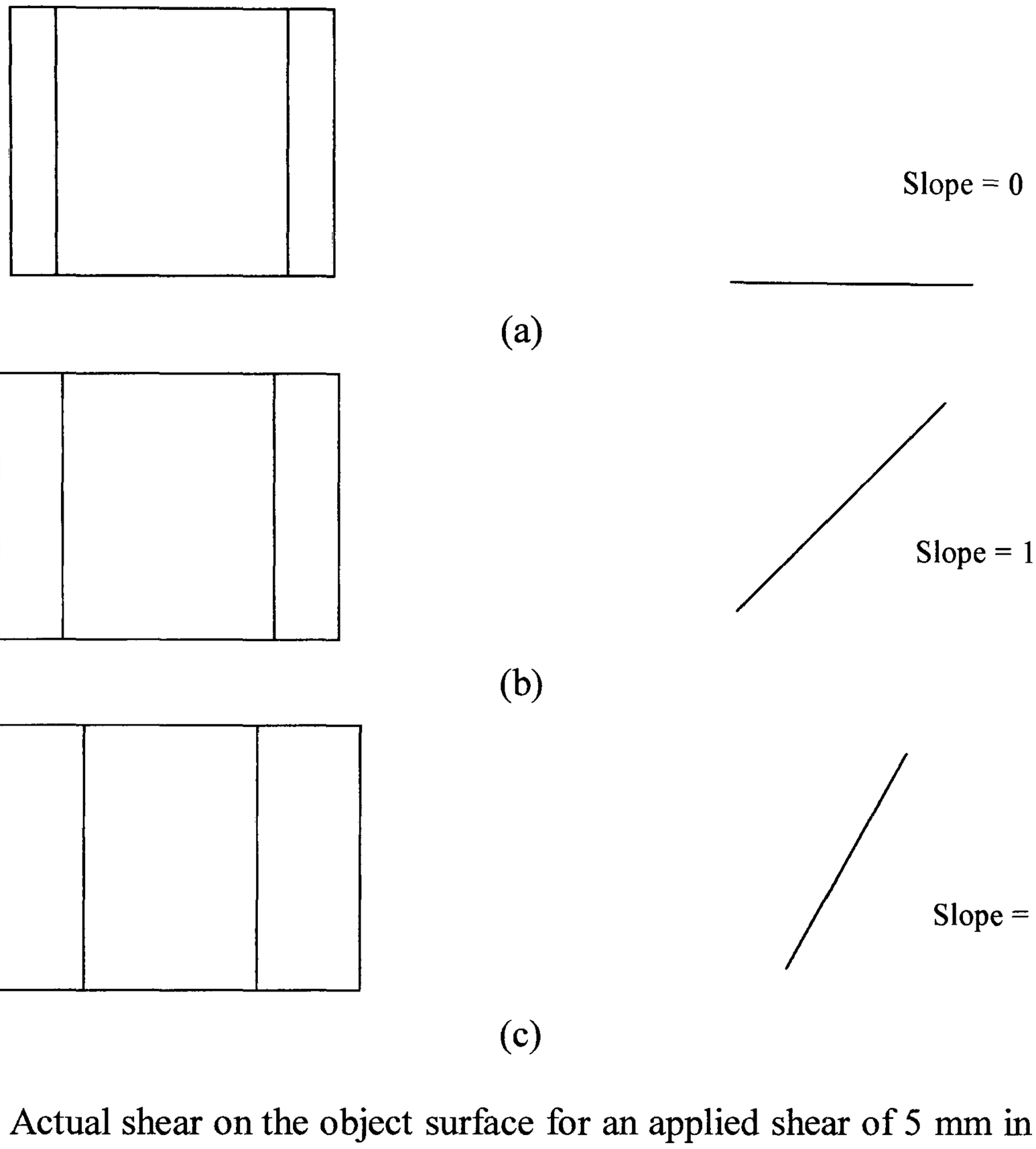

Figure 7.3 Actual shear on the object surface for an applied shear of 5 mm in the image plane. The sheared image is shown on the left and the slope is shown on the right. (a) dx = 5 mm, slope = 0, (b) dx = 7 mm, slope = 1 and (c) dx = 11 mm, slope = 2.

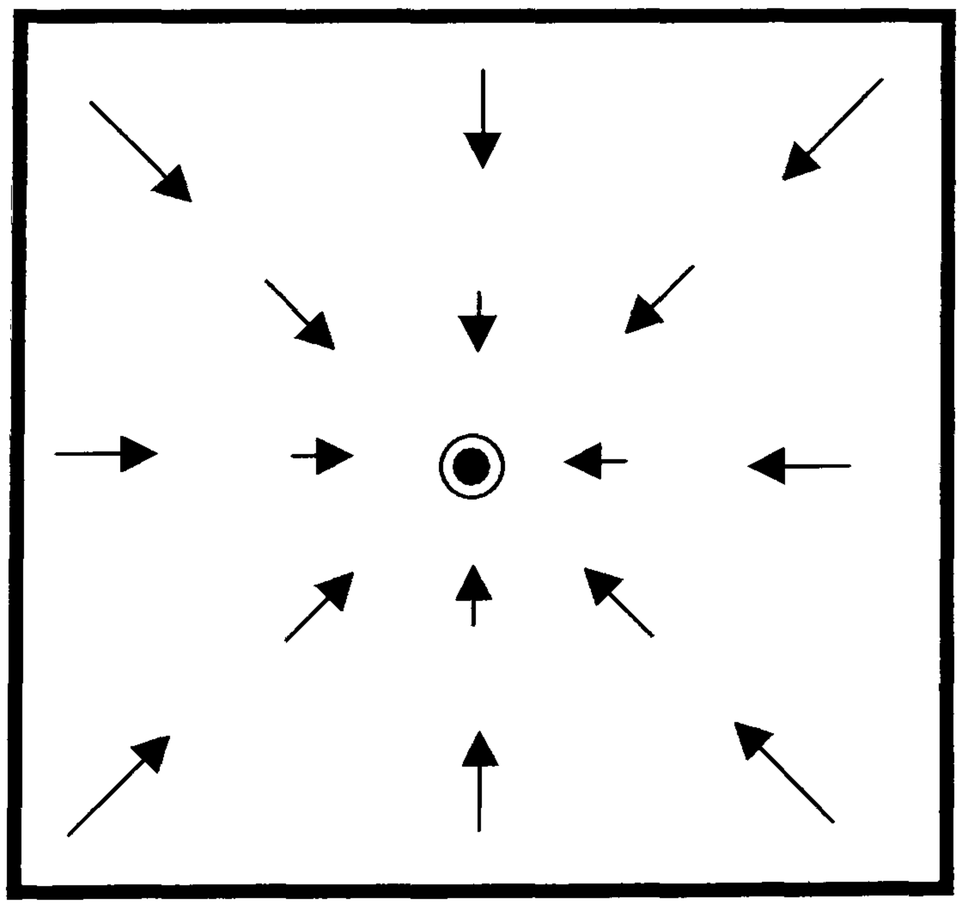

Figure 7.4 Schematic of the variation in sensitivity vector across the field of view for collinear illumination and viewing. The length of the vector shows the component of the vector in the plane of the image

et al 1996). The fibre Bragg gratings were fabricated by Dr S W James. The fibre Bragg gratings selectively reflect a single wavelength, typical bandwidth 0.2 nm, which is returned to the laser diode cavity and acts as a seed wavelength. The fibre optic beam delivery provided spatial filtering and a flexible beam delivery to the source position for the surface slope measurement channel. Lenses at the distal end of the fibres allowed an adjustment to the expansion of the beams illuminating the object. The object was illuminated by an optical power of 30 mW. The source positions were nominally located at 1. [0.2 m, -0.2 m, 0.3 m], 2. [0.2 m, 0.2 m, 0.3 m] and 3. [-0.2 m, 0.2 m, 0.3 m], measured from the centre of the field on the object surface. These source positions are located at three of the four corners of a square as discussed previously in Section 7.2.3. Source position 3 was fitted with a translation stage at the end of the fibre allowing source displacement in three orthogonal directions. This channel was used to perform the surface slope and shape measurements.

The interferometer head was composed of a shearing Michelson interferometer, a camera lens and a camera. The shearing Michelson interferometer comprised a beamsplitter (75 mm diameter), a shearing mirror (50 mm diameter) that could be adjusted to give different magnitudes and directions of applied shear and a reference mirror (50 mm diameter), that was fitted with a PZT allowing phase-stepping to be performed. The optical components in the interferometer head were suitable for an optical wavelength of 810 nm. The camera, an area scan CCD camera (Dalsa CA-D4-0512A, 75 Hz frame rate, 8-bit, 512 by 512 pixels), in conjunction with a PCI bus frame transfer card (Bitflow Roadrunner) was used to record the speckle interferograms. A PC

controlled the modulation of the laser diode injection currents, the phase-stepping and the image capture using a program written using Labview software by Dr S W James.

Figure 7.5 shows a photo of the multi-component shearography system and Figure 7.6 shows a close-up photo of the interferometer head.

7.3.1 *Multi-Component Displacement Gradient Measurement*

To fully characterise the surface strain required the measurement of six components of displacement gradient. The six components were measured using three illumination directions and two orthogonal directions of applied shear. Figure 7.7 shows the experimental layout.

Initially the shear was applied in the x direction. The object was sequentially illuminated from the three illumination directions by modulating the Bragg grating stabilised laser diode injection currents between below threshold and the operating current, in synchronisation with the recording of reference camera frames. After deformation of the object the laser diode pulsing sequence was repeated, but with three phase-stepped signal frames recorded from each channel. The camera frames from an individual channel were processed using a phase-stepping algorithm to yield an unwrapped phase map and unwrapped using ISTRA phase unwrapping software (Ettemeyer AG). The shear was then applied in the y direction and the recording of reference and phase-stepped signal frames before and after object deformation, respectively, was repeated to yield the other three displacement gradient components.

Figure 7.5 The multi-component shearography system. The object is illuminated from source positions S1, S2 and S3, using fibre optic beam delivery by fibre Bragg grating stabilised laser diodes (not shown). The images are optically processed and recorded by a camera in the Interferometer Head. The PC performs laser diode pulsing and image capture and processing.

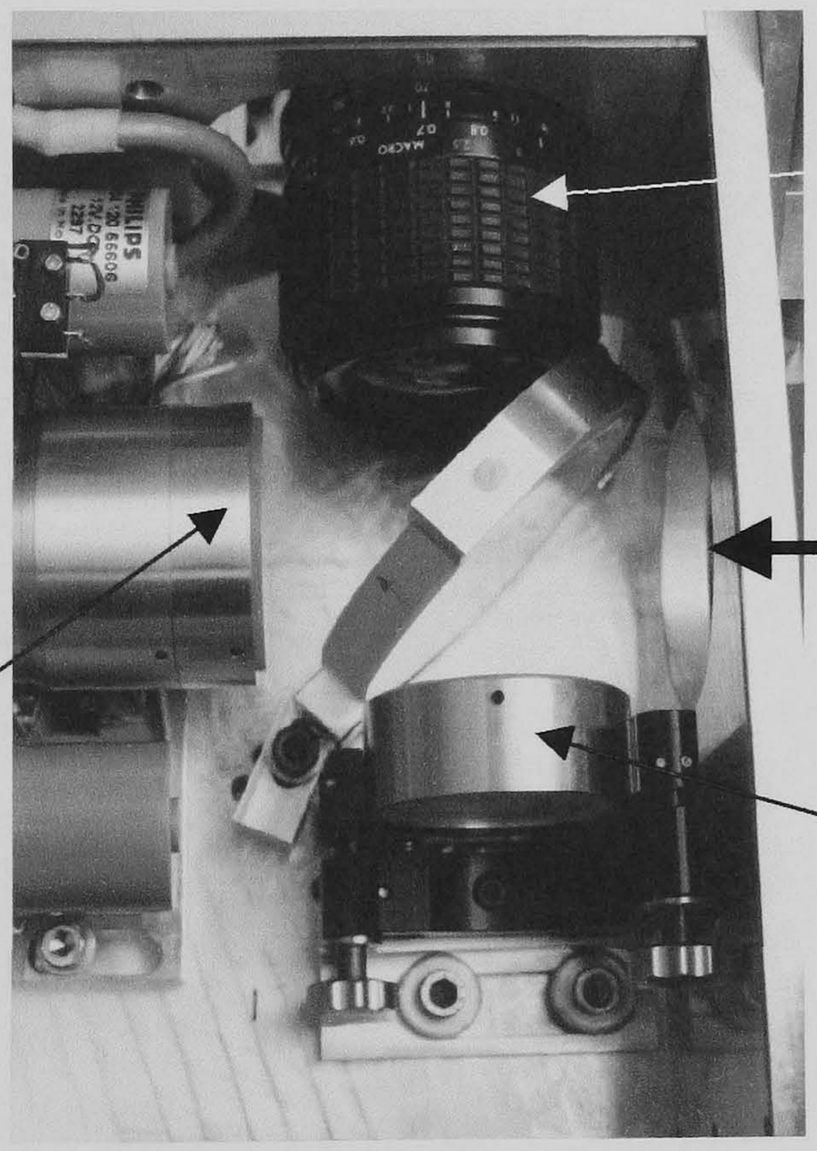

Figure 7.6 Close-up of the shearing Michelson interferometer head in the multi-component shearography system

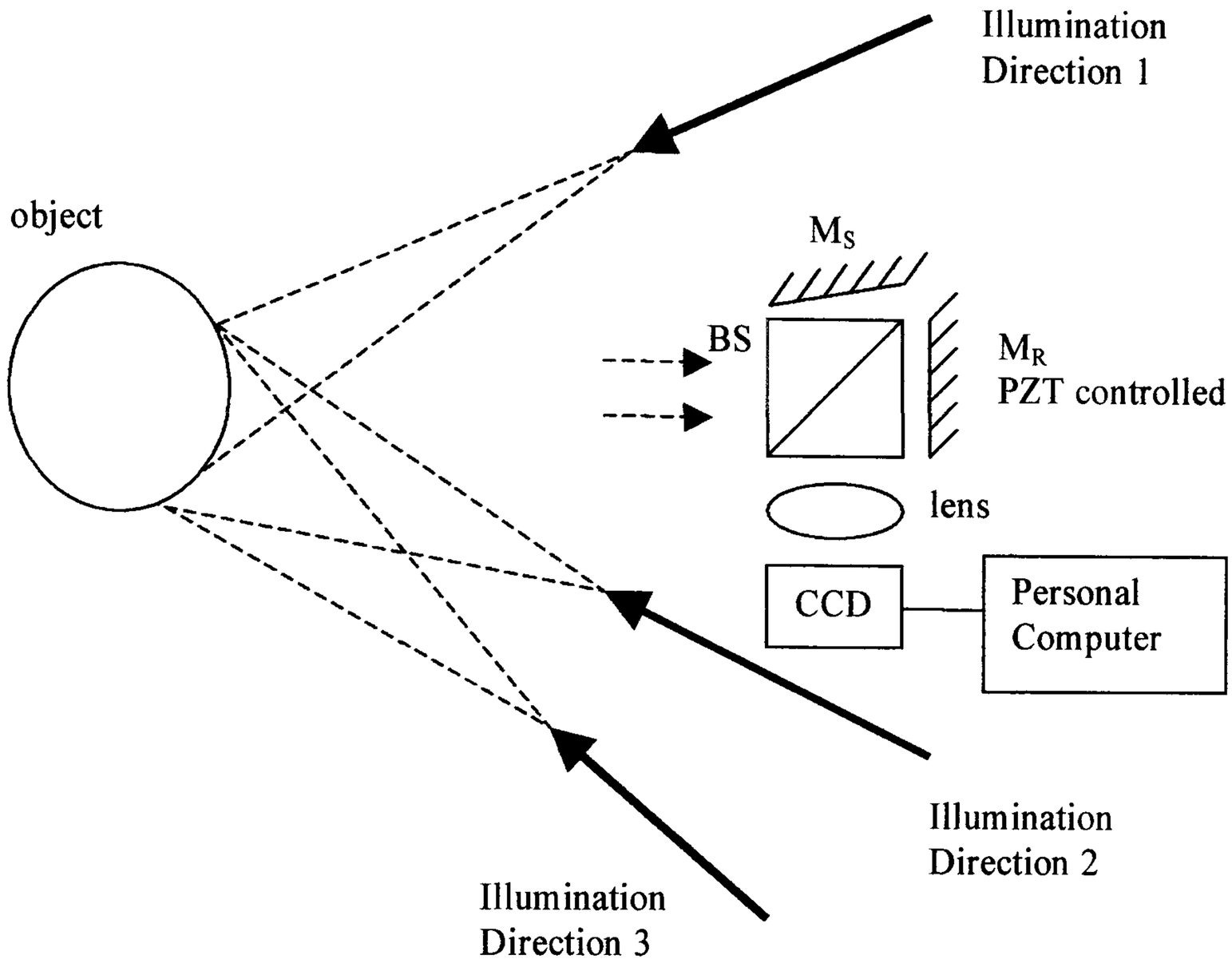

Figure 7.7 Experimental layout for displacement gradient measurement. Laser diodes, using single mode optical fibres for beam delivery, are used to illuminate the object from three directions, using TDM. The shearing head, consists of beamsplitter, BS; reference mirror controlled by a piezoelectric transducer, M_R; Shearing mirror, M_S; a lens and a CCD camera.

7.3.2. Slope and Shape Measurement

The experimental layout to perform surface slope measurement is shown in Figure 7.8. Illumination of the object was from source position 3. A reference frame was recorded first. The source was then displaced in the *v* direction by a magnitude of *DV* of the order of hundreds of microns and three phase-stepped signal frames were recorded. The *v* direction is orthogonal to the source to object optical axis and is predominantly in the *y* (vertical) direction. The reference and signal frames were combined using a phase-stepping algorithm to yield an wrapped phase map. This was unwrapped using ISTRA software (Ettemeyer AG). The object was replaced by a flat plate located at the object position, with the normal to the surface of the plate in the direction of the interferometer head. The process of capturing a reference frame, displacing the source in the *DV* direction, recording three phase-stepped frames and the image processing was repeated. The magnitude and direction of the source displacement must be the same as used for the object under investigation. The phase change determined for the flat plate was subtracted from the measured phase change on the object under investigation, and scaled using the parameters given in equation 6.21, to yield the object slope. The object slope was integrated to obtain the object shape. This process is described in detail in Chapter 6.

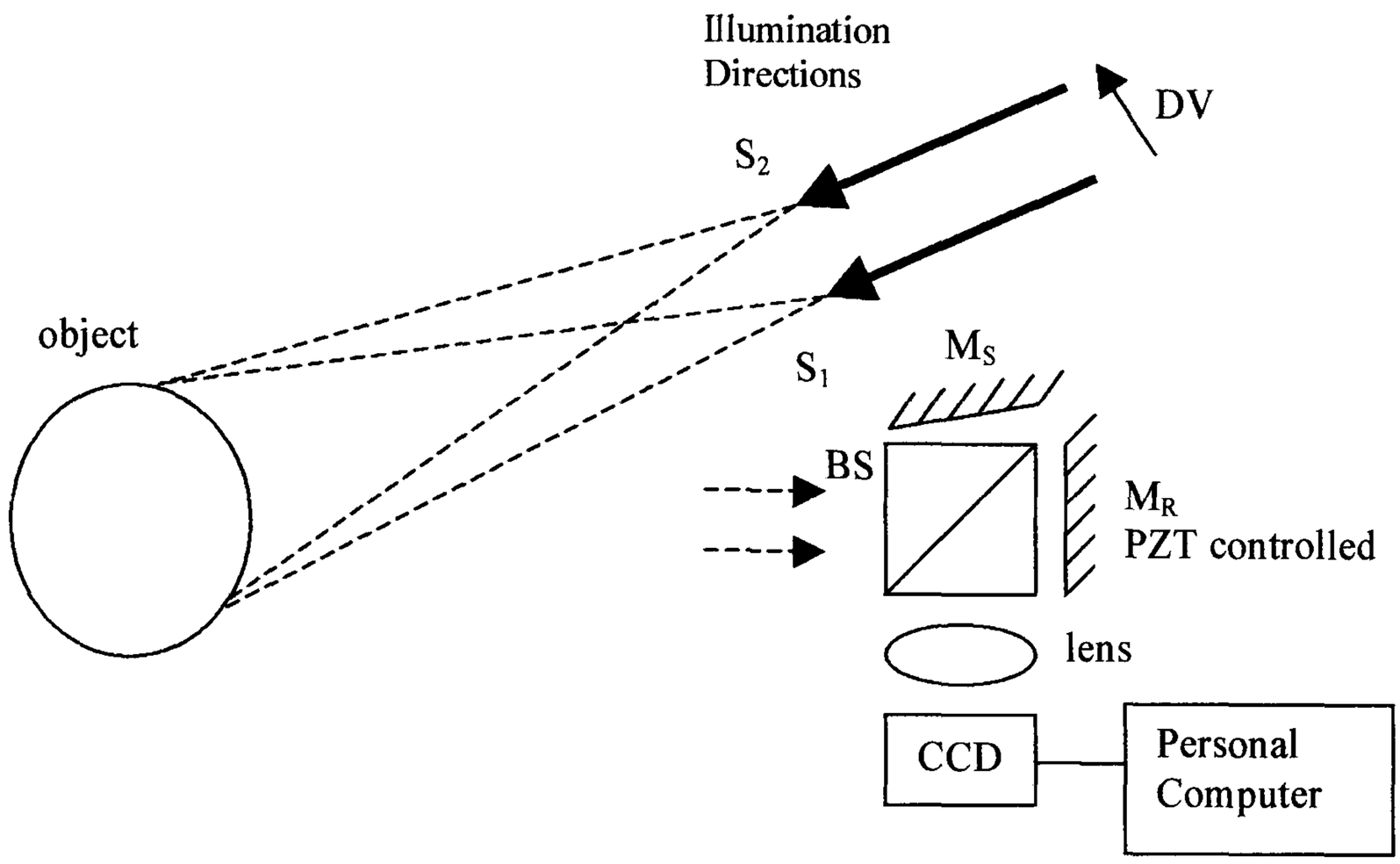

Figure 7.8 Experimental layout for slope and shape measurement. The source is displaced from S_1 to S_2 by a distance DV between camera frames. The shearing head consists of beamsplitter BS, shearing mirror M_S, reference mirror M_R, controlled by a piezoelectric transducer, a lens and a CCD camera.

7.3.3. Surface Strain Measurement Applying a Correction for Object Slope and Shape

The displacement gradient components were corrected for the change in applied shear and the variation in the sensitivity vector across the object and are mapped onto the object surface, as detailed in Section 7.2.6. The surface strain components can be calculated by referring to the strain tensor, given in Equation 7.1.

7.3.4. Surface Strain Measurements using Resistance Strain Gauges

A measurement of the hoop strain and axial strain of pipe sections in regions away from the welded joints, was performed using resistive strain gauges. These measurements were performed jointly with Mr D Furfari, a PhD student in the Damage Tolerance Group, headed by Professor P E Irving, School of Industrial and Manufacturing Science, Cranfield University. Two strain gauges (Tokyo Sokki Kenkyujo Co., Ltd, FLA-3-11; gauge length, 3 mm; Resistance, 120 ± 0.3 Ω) were glued to a 15 mm thick section of the pipe, approximately 50 mm away from the weld, and orientated to measure the axial strain and the hoop strain. A further two strain gauges were fitted to an 8 mm thickness section of pipe, again oriented to measure the axial strain and the hoop strain.

Measurements of strain were performed using a resistance box (RDP Group, Model modular 600), an interface box (Strawberry Tree Incorporated, Terminal Panel T31), and a 486 PC fitted with an A to D card (Strawberry Tree Incorporated) and running data acquisition software (Strawberry Tree Incorporated, Quicklog PC V 2.1.0).

To perform the measurements the pipe was pressurised using a hand pump (Rigid Model 1450), the Wheatstone bridge in the resistance box was balanced and the voltage zeroed. On depressurising the pipe the voltage was recorded and the strain, *S*, was calculated using:

$$S = \frac{4(V - V_0).\mu_F g_F}{V_B.G_F} \tag{7.7}$$

where V is the voltage across the strain gauge, V_0 is the initial voltage across the strain gauge, μF is the microstrain factor, g_F is the gauge factor, V_B is the bridge voltage and G_F is the gain factor. Equation 7.7 was given in the Signal Conditioning Amplifier Model 2311Manual (Vishay Measurements Group).

7.3.5. Theoretical Calculation of the Axial and the Hoop Strain

The thickness is 9 % of the overall diameter for the 8 mm thickness section and 17 % of the overall diameter for the 15 mm thickness section. Therefore the equations modelling a thick walled cylinder are appropriate as the thin wall cylinder approximation is only valid for cylinders of thickness of less than 5 % of the diameter (Hearn 1989).

The equations for axial stress, σ_A, radial stress, σ_R, and hoop stress, σ_H, are (Sinnott 1996):

$$\sigma_A = \frac{P_i D_i^2}{\left(D_0^2 - D_i^2\right)} \tag{7.8}$$

$$\sigma_R = P_i\left[\frac{D_i^2\left(D_0^2 - d^2\right)}{d^2\left(D_0^2 - D_i^2\right)}\right] \tag{7.9}$$

$$\sigma_H = P_i\left[\frac{D_i^2\left(D_0^2 + d^2\right)}{d^2\left(D_0^2 - D_i^2\right)}\right] \tag{7.10}$$

where P_i is the internal pressure. It is assumed that the external pressure, P_o, is negligible, so P_i - $P_o \approx P_i$. D_i is the internal diameter of the cylinder, D_o is the external diameter of the cylinder and d is the diameter at the point of interest.

At the surface of the cylinder $d = D_o$ so the equations for σ_R and σ_H simplify to:

$$\sigma_R = 0 \tag{7.11}$$

$$\sigma_H = P_i\left[\frac{2.D_i^2}{D_0^2 - D_i^2}\right] \tag{7.12}$$

The axial strain, ε_A, is given by (Sinnott 1996):

$$\varepsilon_A = \frac{1}{E}\left[\sigma_A - \nu\sigma_H\right] \tag{7.13}$$

where E is Young's modulus and γ is Poisson's ratio. The hoop strain, ε_H, is given by (Hearn 1989):

$$\varepsilon_H = \frac{1}{E}\left[\sigma_H - \nu\sigma_A\right] \tag{7.14}$$

7.4 Results

The test object was a section of stainless steel gas main pipe of length 900 mm and diameter 90 mm. This is shown in Figure 7.9. The pipe was constructed from two end plates and three pipe sections, joined by welds around the circumference of the pipe. The section of the pipe investigated using shearography contained a welded joint between a 15 mm and an 8 mm pipe section. The section of the pipe under investigation

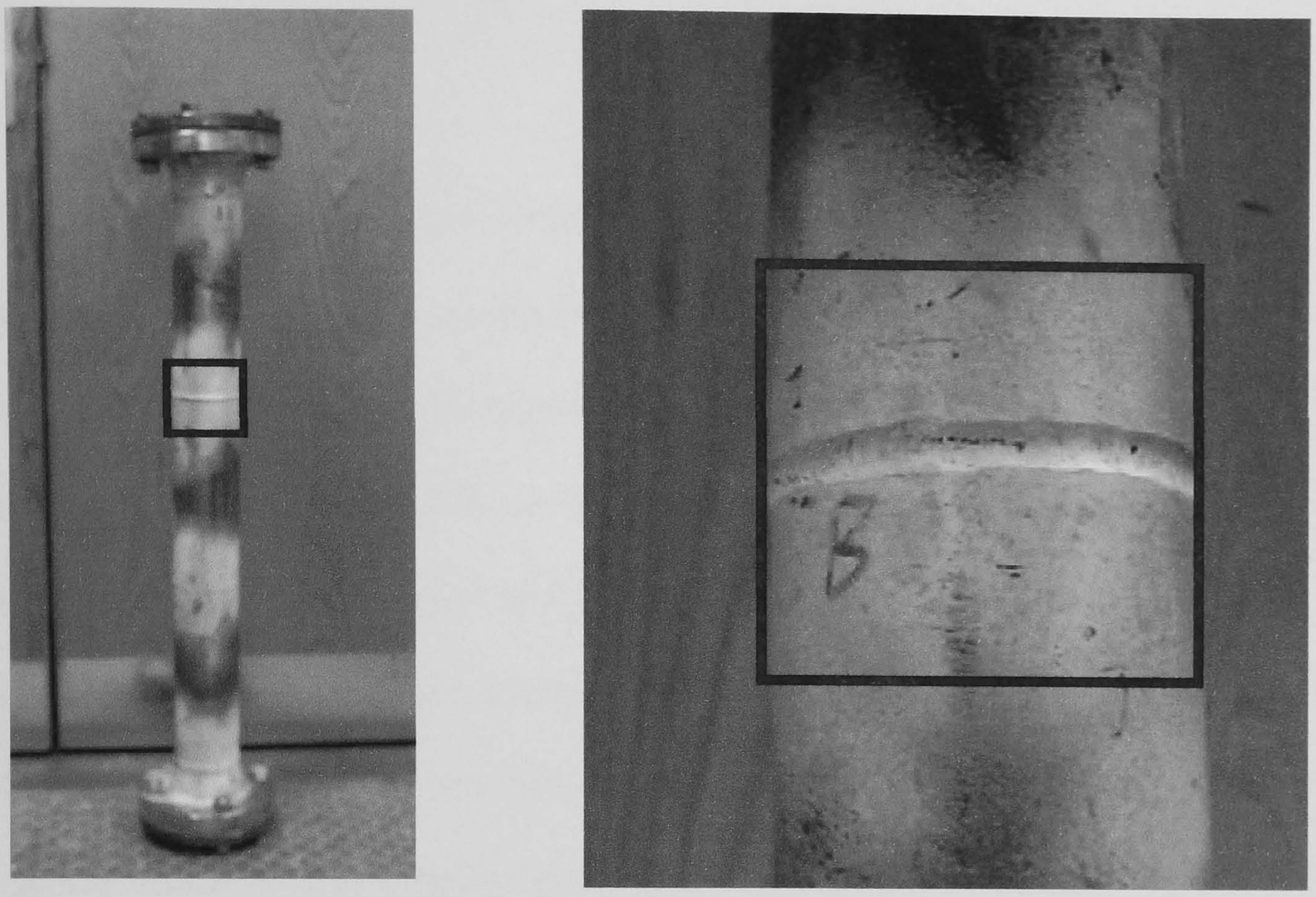

(a) (b)

Figure 7.9 Photograph of (a) the gas main pipe, of length 900 mm and diameter 90 mm, and (b) a close-up of the section of pipe investigated using the Shearography system. The black border in both pictures indicates the field of view of the camera, a region of approximately 90 mm by 90 mm

was coated with white paint.

7.4.1. Multi-Component Surface Displacement Gradient Measurement

Displacement gradient measurements were performed using three illumination positions and two shear directions. The illumination positions were situated at 1. (0.220 m, -0.173 m, 0.270 m), 2. (0.224 m, 0.176 m, 0.265 m) and 3. (-0.177 m, 0.187 m, 0.210 m). Shears of magnitude 10 mm were applied in the x and the y directions. This yielded six components of measured displacement gradient in total. The pipe was pressurised to 350 kPa before recording the reference frames, using a hand pump (Rigid Model 1450) and depressurised to 0 kPa before recording the phase-stepped signal frames. Figure 7.10 shows wrapped phase maps for the six measured displacement gradient components of a region of approximately 40 mm by 55 mm. The noise of the phase map in Figure 7.10(e) is greater, this is due to the wavelength of laser diode 2 being less stable during injection current modulation. The intensity of scattered light from other regions of the surface within the field of view was insufficient to generate a wrapped phase map, when illuminated from one or more of the illumination directions.

After the unwrapping procedure six unwrapped phase maps of the measured displacement gradient components are obtained, these are shown in Figure 7.11.

7.4.2. Slope and Shape Measurement

The object surface slope and shape were measured using the source displacement technique described in Chapter 6. For these measurements, channel 3 of the multi-

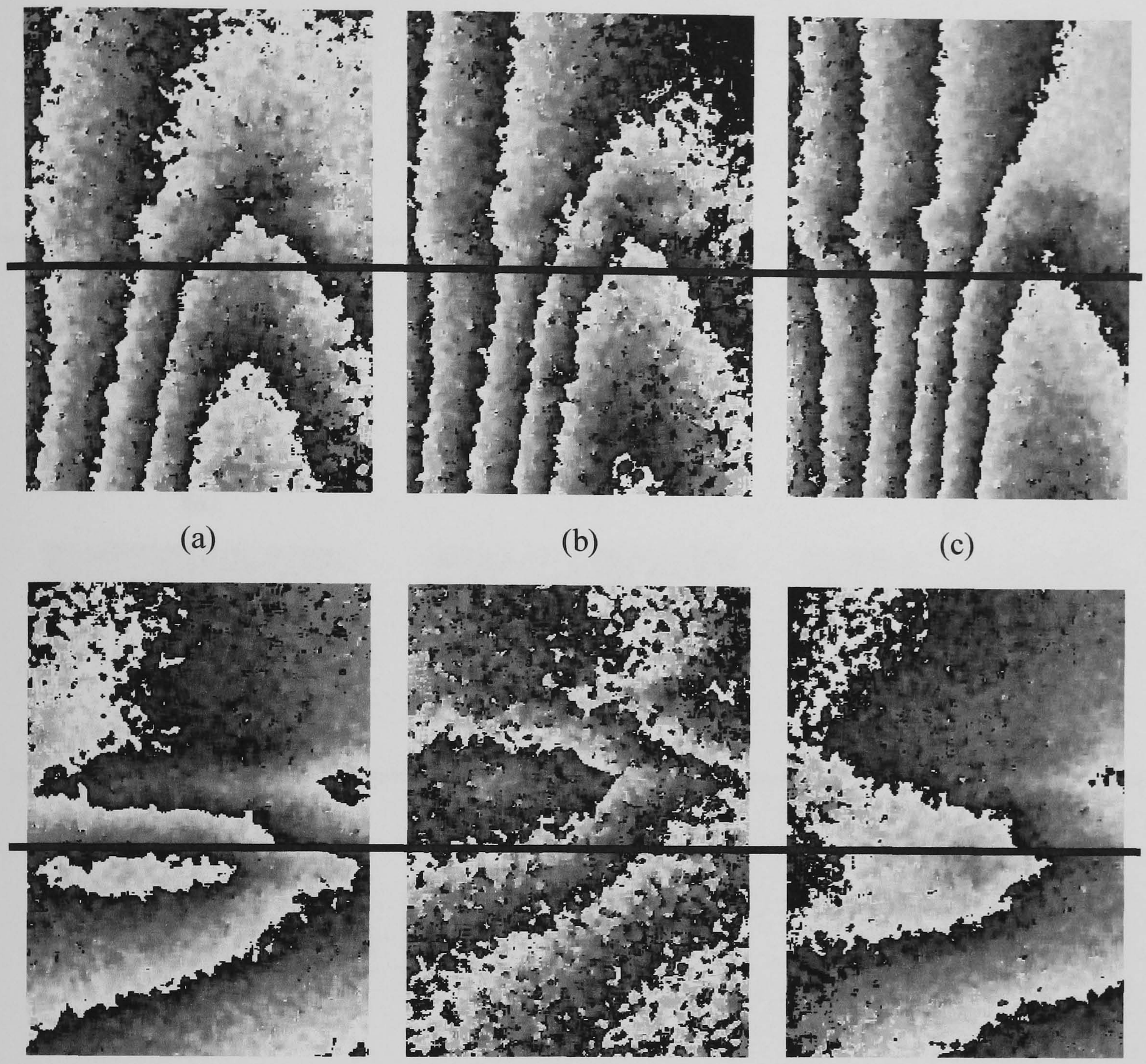

(a) (b) (c)

(d) (e) (f)

Figure 7.10 (a), (b) and (c) are respectively the wrapped phase maps of displacement gradient for applied shear in the x direction for illumination directions 1, 2 and 3. (d), (e) and (f) are respectively the wrapped phase maps of displacement gradient for applied shear in the y direction for illumination directions 1, 2 and 3. In all pictures the weld is horizontally across the centre of the picture as indicated by the position of the black lines.

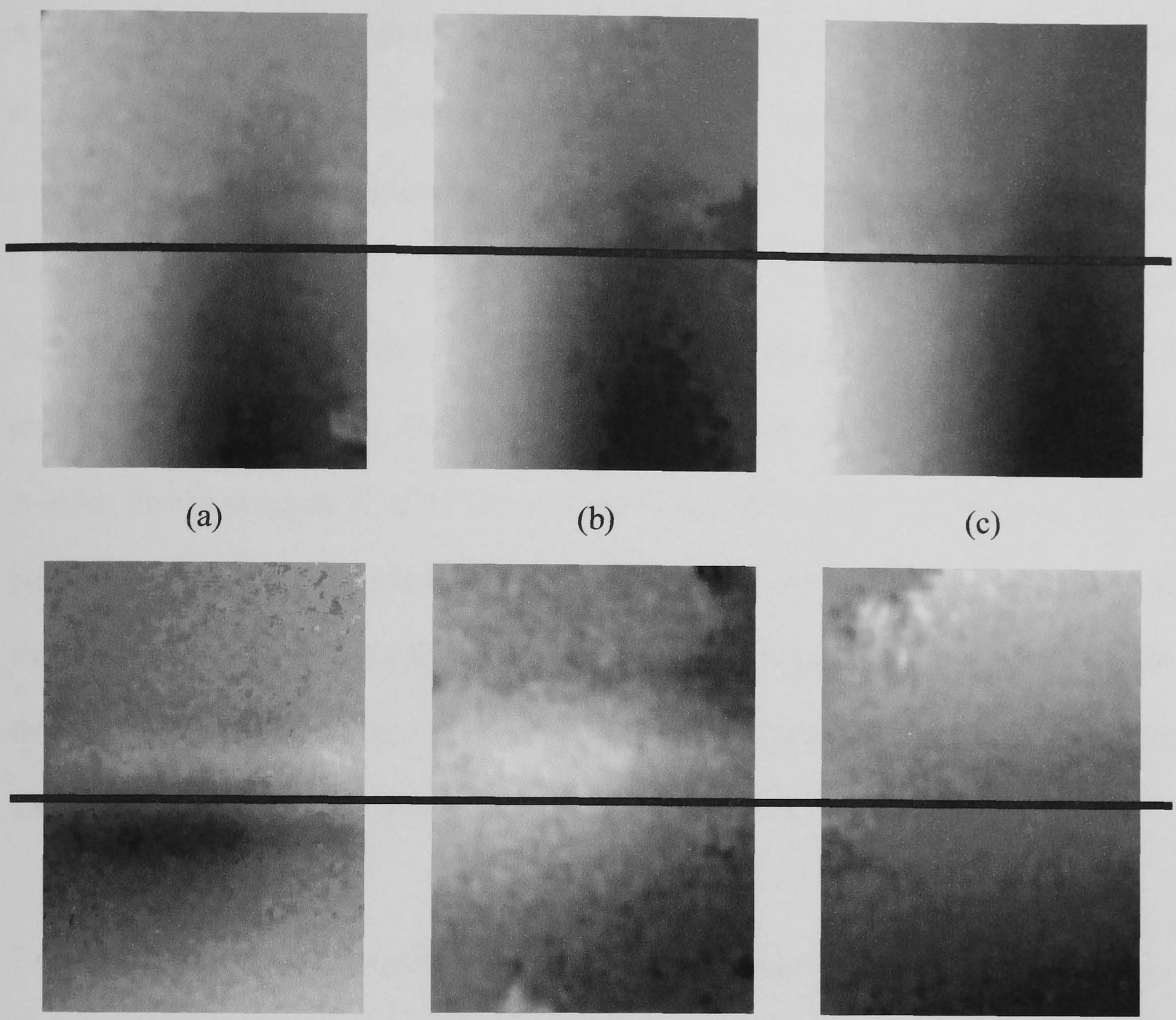

Figure 7.11 (a), (b) and (c) are respectively the unwrapped phase maps of displacement gradient for applied shear in the x direction for illumination directions 1, 2 and 3. (d), (e) and (f) are respectively the unwrapped phase maps of displacement gradient for applied shear in the y direction for illumination directions 1, 2 and 3. The white regions represent regions of maximum displacement gradient. In all pictures the weld is horizontally across the centre of the picture as indicated by the position of the black lines.

component shearography system was used, with the source position initially at (-0.177 m, 0.187 m, 0.210 m). The slope was measured using an applied shear of 10 mm in the x direction and a source displacement of 300 μm in the DV direction. A measurement of the phase change across a flat plate test object was also performed for a source displacement of 300 μm in the DV direction. This phase change was subtracted from the phase change on the pipe to obtain the surface slope, in the shear direction, for the pipe. A value for the constant K of 11 m^{-1} was calculated numerically and this was used to perform the scaling of the measured slope. The surface slope was integrated to recover the object shape. Figure 7.12 shows the recovered object shape using the correction for the phase change across the flat plate. The issues regarding this slope and shape measurement technique are discussed in detail in Chapter 6.

7.4.3. Surface Strain Measurement Applying a Correction for Object Slope and Shape

The measured displacement gradient components are corrected using the object slope and shape information and mapped onto the object surface using the coordinate transformation. Figure 7.13 shows the six components of displacement gradient relative to the local object surface. The range of the data is –32 με to +32 με. The images are of a region approximately 40 mm by 55 mm in size. Difference maps of corrected and uncorrected displacement gradient measurements are shown in Figure 7.14. From these results the difference in axial strain, $\Delta\varepsilon_{AS}$, between the 8 mm and the 15 mm thickness pipe, the $\Delta(\delta v/\delta y)$ component, is 8 ± 11 με. The difference in hoop strain, $\Delta\varepsilon_{HS}$, between the 8 mm and the 15 mm thickness pipe, the $\Delta(\delta u/\delta x)$ component, is 4 ± 11 με.

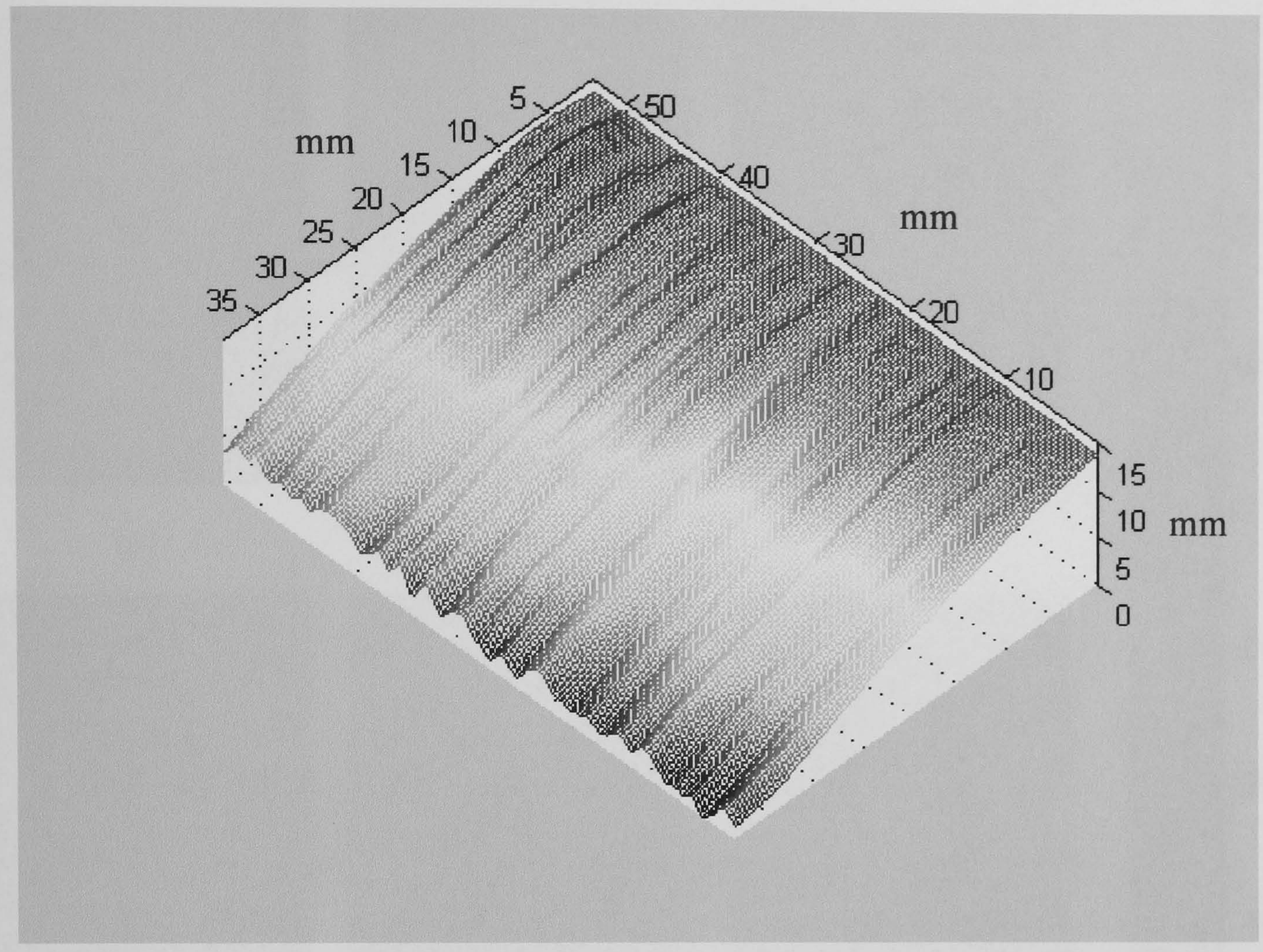

Figure 7.12 shows the object shape obtained using the source displacement in shearograpy technique.

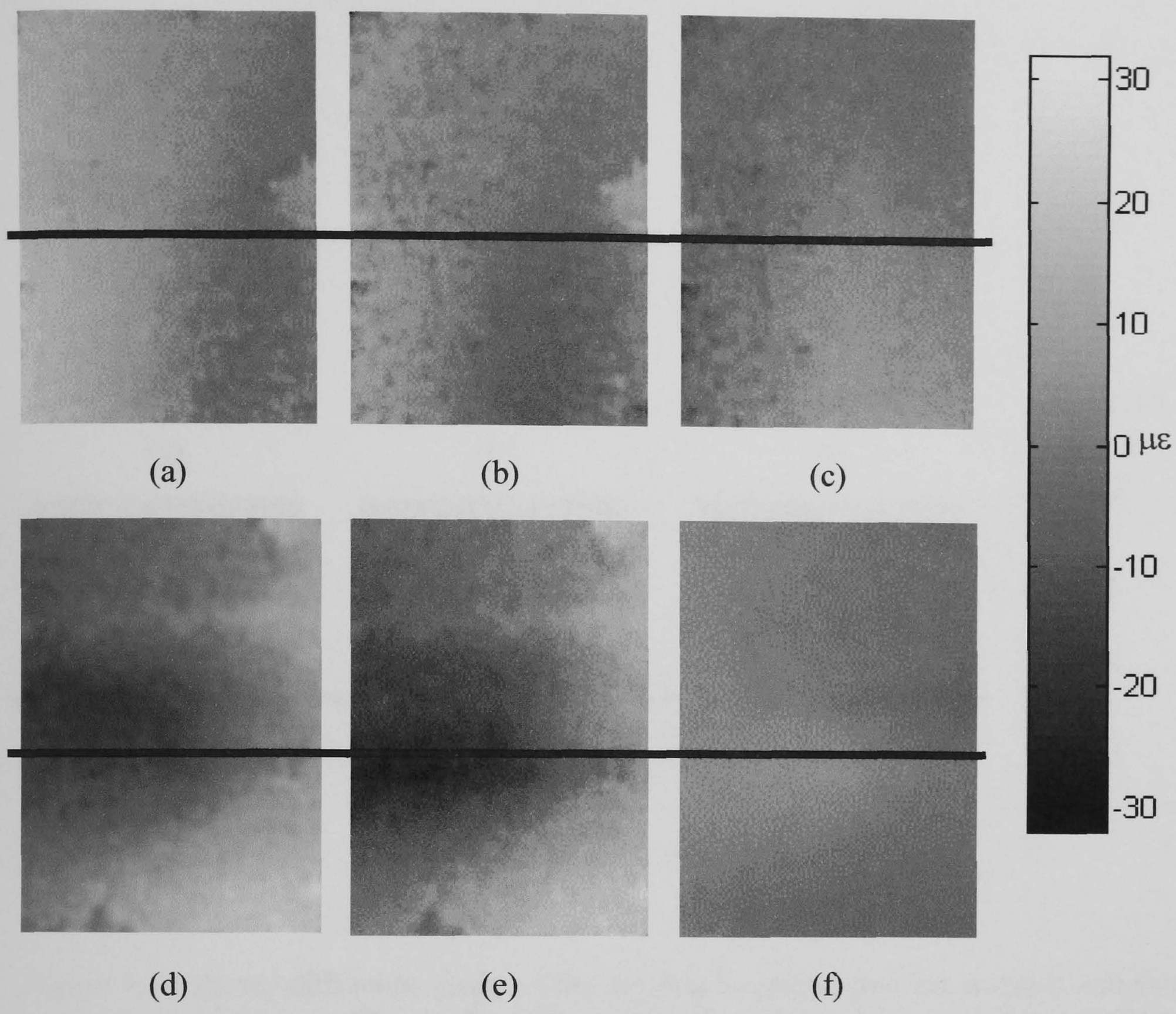

Figure 7.13 shows the six corrected displacement gradients mapped relative to the local surface profile. These are (a) $\delta u/\delta x$, (b) $\delta v/\delta x$, (c) $\delta w/\delta x$, (d) $\delta u/\delta y$, (e) $\delta v/\delta y$ and (f) $\delta w/\delta y$. (g) is the greyscale in micro strain. The images are of a region approximately 40 mm by 55 mm in size. The range of the data is –32 με (black) to +32 με (white). The black lines indicate the position of the weld.

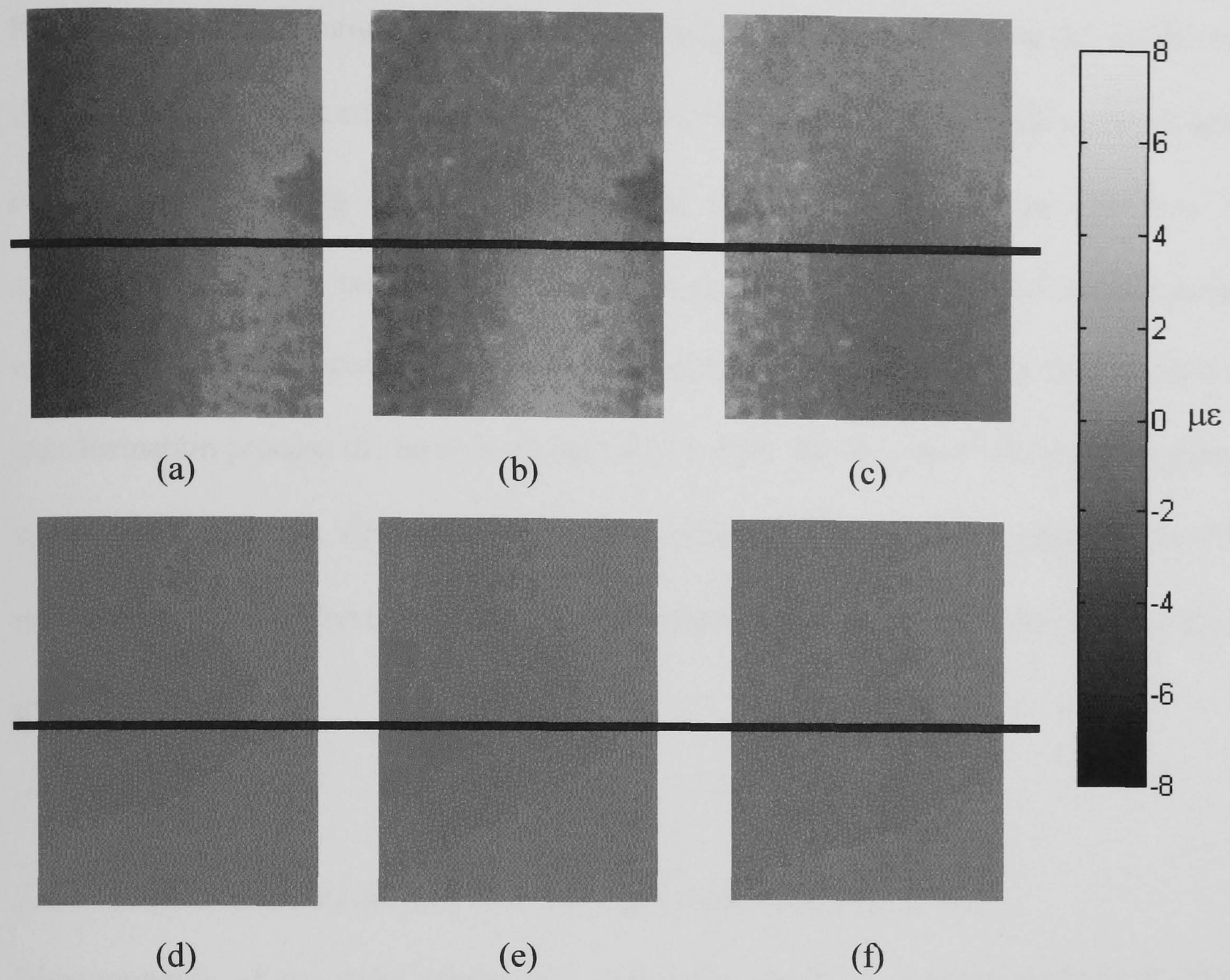

Figure 7.14 shows difference maps of the six displacement gradient mapped relative to the local surface profile, to show the effect of applying a correction for surface slope and shape. These are (a) $\delta u/\delta x$, (b) $\delta v/\delta x$, (c) $\delta w/\delta x$, (d) $\delta u/\delta y$, (e) $\delta v/\delta y$ and (f) $\delta w/\delta y$. (g) shows the relationship between greyscale and microstrain. The images are of a region approximately 40 mm by 55 mm in size. The black lines indicate the position of the weld.

For a single measurement channel with illumination geometry of [0.2 m, 0.2 m, 0.3 m] the accuracy of displacement gradient measurement is ± 4 με for an optical wavelength of 810 nm, measuring to ± 0.1 fringe from the phase map. As the geometry is symmetrical the other two measurement channels will have an identical measurement error. Taking into account the illumination geometry, and considering the coordinate transformation process the error is increased to ± 8 με, for the out-of-plane and in-plane components. For the determination of the $\Delta(\delta u/\delta x)$ and $\Delta(\delta v/\delta y)$ components the measurement is a difference of two measurements and therefore the error is now ± 11 με.

7.4.4. Measurement of Surface Strain using Resistance Strain Gauges

Measurements of the axial strain, ε_{AR}, and hoop strain, ε_{AR}, were performed using resistance strain gauges for both the 8 mm and 15 mm thickness sections of pipe. The pump was internally pressurised to 350 kPa using a hand pump (Rigid Model 1450) and the Wheatstone bridge was balanced. The internal pressure was released, to 0 Pa, and the measurements taken as described in Section 7.3.4. The results were:

ε_{AR} (8 mm) = 6.0 ± 5 με ε_{HR} (8 mm) = 19.2 ± 5 με

ε_{AR} (15 mm) = 2.8 ± 5 με ε_{HR} (15 mm) = 12.0 ± 5 με

The error is calculated by reference to Vishay Measurements Group, TN-506 (1988) and is ± 5 με. The difference between 8 mm and 15 mm sections of pipe for axial strain, $\Delta\varepsilon_{AR}$, and hoop strain, $\Delta\varepsilon_{HR}$ are:

$\Delta\varepsilon_{AR} = 3.2 \pm 7\ \mu\varepsilon$ $\Delta\varepsilon_{HR} = 7.2 \pm 7\ \mu\varepsilon$

7.4.5. Theoretical Axial Strain and Hoop Strain

The theoretical axial strain, ε_{AT}, and hoop strain, ε_{HT}, was calculated as described in Section 7.3.5. A typical value of Young's modulus, *E*, for steel is 200 x 10^9 Nm^{-2} (Hearn 1989) and a typical value of Poission's ratio, ν, for metals is 0.3 (Hearn 1989). The external pipe diameter, D_o, is 90 mm and the internal diameter, D_i, is 82 mm for the 8 mm thick pipe and 75 mm for the 15 mm thick pipe. The internal pressure, P_i, is 350 kPa. The calculated strains are:

ε_{AT} (8 mm) = 3.4 $\mu\varepsilon$ ε_{HT} (8 mm) = 14.5 $\mu\varepsilon$

ε_{AT} (15 mm) = 1.6 $\mu\varepsilon$ ε_{HT} (15 mm) = 4.0 $\mu\varepsilon$

Below is the difference between 8 mm and 15 mm sections of pipe for axial strain, $\Delta\varepsilon_{AT}$, and hoop strain, $\Delta\varepsilon_{HT}$:

$\Delta\varepsilon_{AT} = 1.8\ \mu\varepsilon$ $\Delta\varepsilon_{HT} = 10.5\ \mu\varepsilon$

7.4.6 Summary of Theoretical and Measured Strain Results

Technique	$\Delta\varepsilon_A$ (με)	$\Delta\varepsilon_H$ (με)
Shearography	8 ± 11	4 ± 11
Resistance Strain Gauges	3.2 ± 7	7.2 ± 7
Theoretical	1.8	10.5

Table 7.1 Summary of theoretical and measured strain results from Sections 7.4.3, 7.4.4. and 7.4.5.

7.5 Discussion

The shearography measurements are of the correct order of magnitude when compared with both the resistance strain gauge measurements and with theoretical values for axial strain and hoop strain. The measured strain is close to the limit of detection for both the shearography system and the resistance strain gauges. These initial measurements of the six components of displacement gradient allow full characterisation of the surface strain but only with an agreement to an order of magnitude. The next step would be to perform the same experimental measurements over a larger range of surface strain magnitudes to determine the operating range of the shearography system.

In this chapter errors in the measurement of displacement gradient, due to the surface slope and shape are investigated and corrected. For a curved object, or for an object tilted relative to the plane of the camera image, the applied shear measured in the plane of the camera image is smaller than the actual applied shear at the object surface. From the difference maps of displacement gradient, with the shear applied in the *y* direction the error is due to the change in direction of the sensitivity vector and is determined

experimentally for this test object as 2 to 3 %. From the difference maps of the displacement gradient applied in the *x* direction the error is determined experimentally as 5 to 10 %. This is due predominantly to the change in slope in the *x* direction. These corrections will become more important for objects which have surfaces of higher curvatures and when the magnitude of the surface strain is greater.

For both the displacement gradient and the slope measurements the slope of the surface relative to the illumination and imaging directions limits the regions on the pipe where satisfactory reading may be taken. This is because sufficient optical power is required at the camera to generate a satisfactory wrapped phase map from the set of images. It may be possible to change the surface coating or increase the laser power to perform measurements over a larger region of the surface of the pipe and at regions with greater surface slope.

7.6 Conclusions

Shearography has successfully been used to measure the six displacement gradient components, the object slope and the object shape in the region of a welded joint in a gas main pipe. This is the first time that *quantitative* surface strain measurements have been made with shearography. The slope and shape information has been used to correct the displacement gradient measurements. The difference between compensated and uncompensated strain is ± 3 % for the sensitivity vector direction variation and ± 10 % for the shear magnitude variation and the sensitivity vector direction variation combined. An agreement to within an order of magnitude was achieved compared with

resistance strain gauges and theoretical calculation of surface strain for surface strain levels of ± 30 με. This was achieved using a multi-component TDM shearography system, with a translation stage that was fitted to one of the source positions providing the surface slope and shape measurement capability. The displacement gradient was mapped onto the object surface to obtain in-plane and out-of-plane displacement gradient components relative to the local profile of the object surface.

7.7 References

Aerbischer H A and Waldner S, "Strain distributions made visible with image shearing speckle pattern interferometry", *Opt. Laser. Eng.*, **26**, pp. 407-420, 1997.

Creath K, "Temporal phase measurement methods" in "*Interferogram analysis, digital fringe measurement techniques*", ed. D. W. Robinson and G. T. Reid, Institute of Physics Publishing, Bristol, 1993.

Davies J C and Buckberry C H, "Application of electronic speckle pattern interferometry in automotive product development", *VDI Berichte*, **617**, pp. 279-293, 1986.

Dockney M L, James S W and Tatam R P, "Fibre Bragg gratings fabricated using a wavelength tuneable laser source and a phase mask based interferometer", *Meas. Sci. Technol.*, **7**, pp. 445-448, 1996.

Goult R J, Hoskins R F, Milner J A and Pratt A J, "*Computational Methods in Linear Algebra*", Stanley Thorne (Publishers) Ltd, London, 1974.

Groves R M, James S W and Tatam R P, "Polarization-multiplexed and phase-stepped fibre optic shearography using laser wavelength modulation", *Meas. Sci. Technol.*, **11**, pp. 1389-1395, 2000.

Hearn E J, "*Mechanics of Materials, Volume 1*", Permagon Press plc, Oxford, 1989.

Huang J-R, Ford H D and Tatam R P, "Phase stepping of speckle shearing interferometers using a wavelength modulated laser diode", *Opt. Lett.*, **21**, pp. 1421-1423, 1996.

James S W and Tatam R P, "Time-Division-Multiplexed 3D Shearography", *Proc. SPIE* **3744**, pp. 394-403, 1999.

Kadano H, Toyooka S and Iwasaki Y, "Speckle-shearing interferometry using a liquid-crystal cell as a phase modulator", *J. Opt. Soc. Am. A*, **8**, pp. 2001, 1991.

Kästle R, Hack E and Sennhauser U, "Multiwavelength shearography for quantitative measurements of two-dimensional strain distributions", *Appl. Opt.*, **38**, pp. 96-100, 1999.

Kothiyal M P and Diesle C, "Shearing interferometer for phase shifting interferometry with a polarisation phase shifter", *Appl. Opt.*, **24**, pp. 4439, 1985.

Mohan N K, Saldner H O and Molin N E, "Electronic shearography applied to static and vibrating objects", *Opt. Comm.*, **108**, pp. 197-202, 1994.

Sinnott R K, "*Coulson and Richardson's Chemical Engineering*", Butterworth-Heinemann, Oxford, 1996.

Tatam R P, Davies J C, Buckberry C H and Jones J D C, "Holographic surface contouring using wavelength modulation of laser diodes", *Opt. Laser Technol.*, **22**, pp. 317-321, 1990.

Valera J D and Jones J D C, "Phase-stepping in fibre-based speckle shearing interferometry", *Opt. Lett.*, **19**, pp. 1161-1163, 1994.

Vishay Measurements Group, Inc., "Shunt Calibration of Strain Gage Instrumentation", *Tech. Note* **TN-514**, 1988.

Waldner S and Brem S, "Compact shearography system for the measurement of 3D deformation", *Proc. SPIE* **3745,** pp. 141-148, 1999.

Wykes C and Flannagan M, "The use of a diode laser in an ESPI system", *Opt. Laser Technol.*, **19**, pp. 37-39, 1987.

Zou Y-L, Pedrini G and Tiziani H, "Two-wavelength contouring with a pulsed ruby laser by employing TV-holography", *J. Mod. Opt.*, **43**, pp. 639-646, 1996.

8. CONCLUSIONS AND FUTURE WORK

8.1 Introduction

In this thesis the speckle correlation technique of shearography has been investigated for the measurement of the surface strain of non-planar objects. The measurement of the full surface strain requires the measurement of the in-plane and the out-of-plane displacement gradient components using two orthogonal shear directions. The measurement of the in-plane and out-of-plane displacement gradient components was performed using a determination of displacement gradient using three illumination directions and a coordinate transformation. The position of the optical source relative to the position of the camera must be known accurately to perform the coordinate transformation. For non-planar objects a knowledge of the object shape allows a correction to be made for errors due to the shape of the object.

8.2 Polarisation-Multiplexing Applied to the Shear Direction

A method of switching the direction of applied shear was demonstrated in Chapter 4. The optical wavelength of a laser diode was tuned by injection current modulation. The variation in optical wavelength in conjunction with a highly-birefringent optical fibre provided an illumination beam that was switchable between s- and p- polarisation. A polarising Michelson interferometer was used to perform switching between orthogonal shearing mirrors *and* the Michelson interferometer was pathlength imbalanced to allow phase-stepping by the optical wavelength tuning. The crosstalk between the channels, 7 dB was satisfactory to separate the measurement channels. Outside the laboratory the

polarisation drift in the hi-bi optical fibre due ambient temperature changes would be a problem but this could be compensated for by active correction of the polarisation drift.

8.3 Source Position Measurement using Shadow Moiré

In Chapter 5 the issue of determining the relative positions of the optical source, object and camera were investigated. A shadow Moiré method incorporating circular, vertical linear and horizontal linear gratings was developed which could measure the source position with increased accuracy in two directions. This technique has increased accuracy compared with either a single circular grating or a single horizontal grating. A measurement accuracy of ± 3% over a 200 mm distance was achieved. One of the advantages of this technique was the simplicity. The grating target replaces the object at the object position and an image of the grating pattern was recorded. For illumination that was uneven across the object surface, such as that from a Gaussian profile beam, a reference image was required to perform a correction for this variation. In the technique a Moiré fringe pattern can be generated with incoherent light, and fringe formation can be demonstrated using a desk lamp. This approach of combining different types of gratings for metrology deserves some further thought and some ideas are given in Section 8.7.

8.4 Shape Measurement by Source Displacement

Chapter 6 described the use of source displacement in shearography to perform shape measurement. Correlation fringes sensitive to slope in the shear direction were generated and these were integrated to yield object shape. The illumination and imaging cannot be collinear for the fringes to be sensitive to slope, yet this angle between the

illumination and imaging directions created a distortion. Reference correlation fringes formed by an identical source displacement, with a flat plate located at the object position, were processed and subtracted to perform a correction. Also the scaling was difficult to calculate mathematically from the source, object and imaging positions and from the direction of source displacement. A numerical model was developed to calculate the scaling from these parameters. Finally an accuracy of ± 2 mm over a 15 mm distance on the object surface was achieved. This accuracy of measurement was sufficient to make an error correction of up to 10 % in the displacement gradient measurement and this was achieved with only the addition of a xyz translation stage to one of the illumination positions and some additional image processing. The complexity of this shape measurement technique lies within the software and performing a shape measurement experimentally is relatively simple. There are some further ideas in Section 8.7.

8.5 Full Surface Strain Measurement of Non-Planar Objects

Chapter 7 described a shearography system that incorporates three illumination directions and a single camera and is capable of the measuring the in-plane and out-of-plane surface strain components. The magnitude and direction of the applied shear were adjusted by tilting the shearing mirror. This system was used to measure the surface strain of a gas main pipe. The issues of choice of illumination geometry and phase-stepping techniques were discussed. Measurement of the six components of displacement gradient measurable by shearograpy, with correction for the slope and shape of the object, were made on a welded joint of a gas main pipe subjected to internal pressure. The results for regions of the pipe away from the weld were compared

with theoretical calculations and with measurements made using conventional resistance strain gauges. The agreement was to within an order of magnitude between the shearography measurements, the resistance strain gauge measurements and the theoretical calculation of the surface strain for strain levels of $\pm$ 30 $\mu\varepsilon$.

8.6 Conclusions

This thesis has demonstrated a number of novel techniques relevant to full surface strain measurement of non-planar objects using shearography. A novel method of switching the shear direction was presented in Chapter 4 using polarisation multiplexing. In Chapter 5 a shadow Moiré technique was presented for source position measurement that extends the conventional range of shadow Moiré in two directions. Chapter 6 presented a source displacement technique for slope and shape measurement that allowed a substantial error correction, for errors due to object shape, for non-planar objects. The complete six component shearography system was described in Chapter 7 and was used to perform full surface strain measurement, with error correction for slope and shape, of an industrial object, a gas main pipe.

8.7 Future Work

In this section firstly practical improvements to the measurement accuracy and ease of measurement of the six components of displacement gradient using shearography will be considered followed by some more general ideas and thoughts arising from work in this thesis.

Surface strain measurements using the two techniques, multi-component shearography and resistance strain gauges, need to be performed over a range of surface strain magnitudes from –75 με to +75 με, on a uniform section of pipe, to determine the operating range and accuracy of the shearography system. For large surface strains the shearography system may be made less sensitive by reducing the magnitude of applied shear.

One of the limiting factors in multi-component shearography systems and from sloping surfaces is the amount of scattered light reaching the camera. It is possible to increase the optical power using a higher power laser. An increase in optical power may also be achieved by placing the laser diodes directly at the illumination positions, although then it would not be possible to take advantage of the FBG stabilisation technique, when the laser diode injection current is modulated. Alternatively the camera integration time could be increased. The multi-component shearography system could be constructed with manual switching of a continuously operating laser, for example with shutters (Waldner and Brem 1999). This is less elegant but would avoid problems of instability on switching the laser diodes on and off.

The measurement of the position of the optical sources relative to the object and the camera could be simplified by design of the components in the shearography system that are used to adjust the source position. The importance of accurate knowledge of the source position, and the effect on the final displacement gradient measurement, was discussed in Chapter 5. Restricting the source position to a single linear axis with rotation about this axis to direct the beam would simplify the source position

measurement as the source position could be measured in a single direction. Figure 8.1 shows the degrees of freedom of movement of the source position required. No additional benefit is gained by allowing further degrees of freedom of movement of the optimum illumination geometry. The illumination head would be increased in complexity but this would be outweighed by the ease of performing accurate measurements.

An additional modification that can be made to the illumination is to increase the number of illumination directions from three to four. This is currently used in a commercially available ESPI system (Ettemeyer 2000) and further investigation of the merits of the use of redundant measurement channels is required either to perform more accurate measurements or to provide reassurance of the satisfactory operation of the system. For objects with a more complex shape, the region of interest on the object may be in shadow from one of the illumination directions, but with the addition of a redundant channel measurements could still be performed.

Redundant channels may also be employed when performing measurements from multiple shear directions. It is envisaged that performing measurements using three shear directions, two orthogonal and one at an angle of 45 °, would allow two ways of calculating each measurement with a particular direction of applied shear, directly and by calculation. The level of agreement between the two measurements would provide information on system performance.

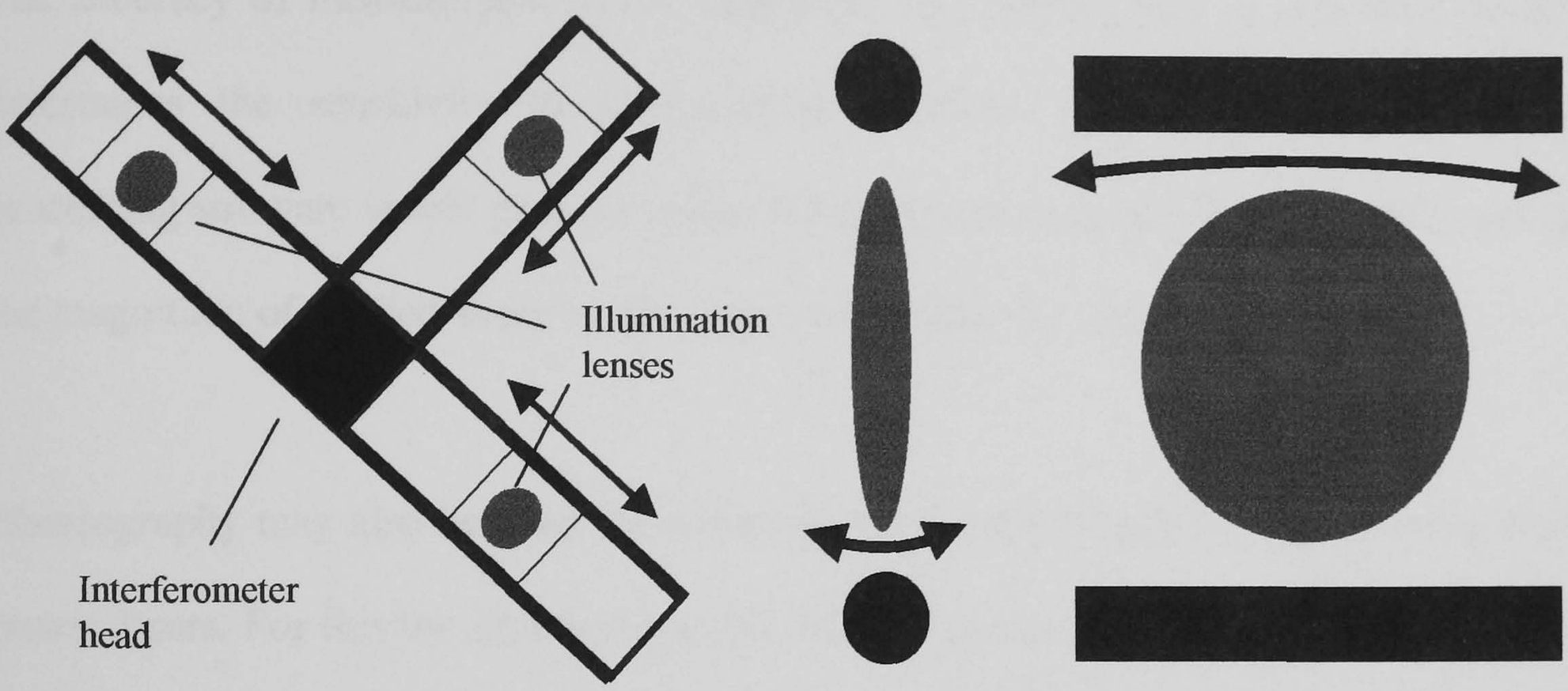

Figure 8.1 Schematic of the proposed magnitudes and directions of movement for the illumination lenses in multi-component shearography system. The magnitude and direction of movement is shown by the bold arrows.

The accuracy of measurement of the magnitude of applied shear is important as this determines the sensitivity to displacement gradient. Pixel, or sub-pixel, image processing software would provide higher measurement accuracy than manually setting the magnitude of applied shear by viewing a target with the camera.

Shearography may also be used for strain measurements in moving objects using high power lasers. For this the illumination and imaging geometry could be reversed to give a single illumination direction and multiple viewing directions. This then introduces the image registration requirements and control of the magnitudes and direction of the applied shear in multiple interferometers. However with multiple cameras measurements could be made simultaneously.

The shape measurement could be performed using a more conventional technique rather than shearography. The system complexity would increase but the slope and shape measurement would be improved. A suggested technique is ESPI. This would be particularly advantageous for repetitive measurements of a number of identical objects or for repeated measurements of a single object. Shape information that is available from original engineering drawing could also be used. The integration of a shearography system with commercial engineering modelling software would provide a method of importing shape data and of displaying strain data in a way the industrial user is familiar with.

The generation of different forms of Moiré fringes from different types of grating by displacements, rotations and, for shadow Moiré, from different viewing directions

implies a lot of information can be extracted from the fringe patterns. An approach which may be taken is to start with the form of the final fringe pattern and from this to calculate the form and position of the gratings. It may then be possible to perform a simple analysis of the fringe pattern to perform an accurate measurement.

Shearography can also be applied in more complex situations. In principle most of the six component shearography techniques could be applied to moving objects, rotating objects and objects of widely varying sizes, from a few micrometers (Aswendt *et al* 2001) to a few metres in size, and for viewing inside objects using endoscopes (Kemper *et al* 2001). The extension of the multi-component techniques to these areas will be the subject of future research.

An issue that is limiting shearography currently its acceptance as a strain measurement tool in industry. Performing quantitative measurements of surface strain with validated measurement accuracy will be key in achieving this goal of wider use of speckle techniques and in particular shearography for strain measurement in industry.

8.8 References

Aswendt P, Schmidt C-D, Zielke D and Schubert S, "Inspection system for MEMS characterization on wafer level using ESPI", *Proc. SPIE* **4400**, pp. 43-50, 2001.

Ettemeyer A, "Combination of 3-D deformation and shape measurement by electronic speckle-pattern interferometry for quantitative strain-stress analysis", *Opt. Eng.*, **39**:1, pp. 212-215, 2000.

Kemper B, Kandulla J, Knoche S, Dirksen D, von Bally G, "Endoscopic electronic-speckle-pattern interferometry – Application to non-destructive quality control in industry and medicine, *Proc. SPIE* **4398**, pp. 168-175, 2001.

Waldner S and Brem S, "Compact Shearography System for the Measurement of 3D Deformation", *Proc. SPIE* **3745**, pp. 141-148, 1999.

LIST OF PUBLICATIONS

1. Groves R M, James S W and Tatam R P, "Polarisation-multiplexed and phase-stepped fibre optic shearography using laser wavelength modulation", *Proc. SPIE* **3745**, pp. 149-157, *Presented at Interferometry99, Pułtusk, Poland*, 1999.

2. Groves R M, James S W and Tatam R P, "Polarization-multiplexed and phase-stepped fibre optic shearography using laser wavelength modulation", *Meas. Sci. Technol.*, **11**, pp. 1389-1395, 2000.

3. Groves R M, James S W and Tatam R P, "Shadow Moiré method for the measurement of the source position in three-dimensional shearography", *Proc. SPIE* **4101**, pp. 113-120, *Presented at Laser Interferometry X, San Diego, USA*, 2000.

4. Groves R M, James S W and Tatam R P, "Shape measurement by source displacement in three-dimensional shearography", *Proc. SPIE* **4101**, pp. 121-131, *Presented at Laser Interferometry X, San Diego, USA*, 2000.

5. James S W, Groves R M and Tatam R P, "Surface strain characterisation using time-division-multiplexed 3D shearography", *Proc. SPIE* **4101**, pp. 389-398, *Presented at Laser Interferometry X, San Diego, USA*, 2000.

6. Groves R M, James S W and Tatam R P, "Three-Dimensional Shearography for Shape and Strain Measurement", pp. 67-68, *Presented at Applied Optics and Opto-Electronics Conference, Loughborough, UK*, 2000.

7. Groves R M, James S W and Tatam R P, "Polarisation-multiplexed and phase-stepped fibre optic shearography using laser diode wavelength tuning", *Presented at 14th International Conference on Optical Fiber Sensors, Venice, Italy,* 2000.

8. Groves R M, James S W and Tatam R P, "Shadow Moiré method for the determination of the source position in three-dimensional shearography", *Opt. Laser. Eng.*, **36**, pp. 317-329, 2001.

9. Groves R M, James S W and Tatam R P, "Strain measurement in curved industrial components using three-dimensional shearography", *Proc. SPIE* **4398**, pp. 216-224, *Presented at Lasers in Metrology and Art Conservation, Munich, Germany,* 2001.

10. Groves R M, James S W and Tatam R P, "Full-surface strain measurement using shearography", *Proc. SPIE* **4448**, *Presented at Optical Diagnostics for Fluids, Solids, and Combustion, San Diego, USA*, (in press), 2001.

11. Groves R M, James S W and Tatam R P, "Shape and slope measurement by source displacement in shearography", *Optics and Lasers in Engineering*, (submitted), 2001.

LIST OF CONTENTS